

UNIVERSITÉ DU QUÉBEC

**ÉTUDE DU CYCLE DU CARBONE HIVERNAL  
EN RÉGIONS ARCTIQUES ET BORÉALES**

THÈSE PRÉSENTÉE  
COMME EXIGEANCE PARTIELLE DU

DOCTORAT EN SCIENCES DE L'ENVIRONNEMENT  
OFFERT PAR L'UNIVERSITÉ DU QUÉBEC À MONTRÉAL  
EN ASSOCIATION AVEC  
L'UNIVERSITÉ DU QUÉBEC À MONTRÉAL À TROIS-RIVIÈRES

PAR  
ALEX MAVROVIC

MAI 2024

Université du Québec à Trois-Rivières

Service de la bibliothèque

Avertissement

L'auteur de ce mémoire, de cette thèse ou de cet essai a autorisé l'Université du Québec à Trois-Rivières à diffuser, à des fins non lucratives, une copie de son mémoire, de sa thèse ou de son essai.

Cette diffusion n'entraîne pas une renonciation de la part de l'auteur à ses droits de propriété intellectuelle, incluant le droit d'auteur, sur ce mémoire, cette thèse ou cet essai. Notamment, la reproduction ou la publication de la totalité ou d'une partie importante de ce mémoire, de cette thèse et de son essai requiert son autorisation.

UNIVERSITÉ DU QUÉBEC À TROIS-RIVIÈRES  
DOCTORAT EN SCIENCES DE L'ENVIRONNEMENT (PH. D.)

**Direction de recherche :**

---

Prof. Alexandre Roy

Directeur de recherche

---

Dr. Juha Lemmetyinen

Codirecteur de recherche

**Jury d'évaluation**

---

Prof. Alexandre Roy

Directeur de recherche

---

Dr. Juha Lemmetyinen

Codirecteur de recherche

---

Prof. Esther Lévesque

Présidente de jury

---

Prof. Julien Fouché

Évaluateur externe

---

Prof. Vincent Maire

Évaluateur interne

## Résumé

Le climat de notre planète est étroitement lié aux concentrations atmosphériques de gaz à effet de serre (GES) tel que constitue le dioxyde de carbone ( $CO_2$ ) et le méthane ( $CH_4$ ), deux composés carbonés. Les modèles climatiques permettant de prédire l'évolution du climat planétaire requièrent une connaissance des écosystèmes afin de déterminer s'ils agissent comme des puits (séquestration) ou des sources (émission) de GES et de comprendre quels facteurs environnementaux influencent ces échanges. Les régions arctiques et boréales sont parmi les régions les moins bien comprises en raison de leur difficulté d'accès. Dans ces environnements, l'hiver est la saison la plus négligée en raison des défis techniques posés par les conditions hivernales rigoureuses. Le premier objectif de mon projet de thèse est de quantifier les échanges naturels de  $CO_2$  et  $CH_4$  en toundra arctique et forêt boréale en hiver. Le second objectif est de déterminer les principaux facteurs environnementaux influençant les échanges de carbone en hiver. Le troisième objectif est de déterminer la contribution des échanges de GES hivernale sur le bilan net annuel. Pour ce faire, nous avons mesuré le gradient de concentration de GES à travers le couvert neigeux afin de quantifier les échanges de carbone entre le sol et l'atmosphère sur plusieurs sites de recherche en Arctique (Inuvik, Territoires du Nord-Ouest et Cambridge Bay, Nunavut) et en forêt boréale (Forêt Montmorency, Québec et Sodankylä, Finlande). La base de données ainsi collectées est la plus vaste actuellement disponible sur la variabilité spatiale des échanges de GES en hiver dans les régions arctiques et boréales. Nous avons aussi utilisé un algorithme d'apprentissage automatique (Random Forest) pour démontrer que la température du sol est le principal facteur influençant les émissions de  $CO_2$  lorsque le sol est complètement gelé. Cependant, lorsque la température du sol est près de  $0^\circ C$ , c'est le taux d'humidité du sol qui devient le principal facteur influençant les échanges de carbone. Nous avons ainsi mis en évidence qu'en hiver, les forêts boréales agissent comme des puits de  $CH_4$ , retirant du  $CH_4$  de l'atmosphère, alors que les zones humides boréales et arctiques émettent d'importantes quantités de  $CH_4$ . Sur nos sites de recherche, les émissions hivernales de  $CO_2$  peuvent compenser jusqu'à 42% de la séquestration du  $CO_2$  durant la saison de croissance. Cette contribution non négligeable est mal prise en compte dans les modèles climatiques actuellement dus à la rareté des données hivernale par la végétation (échange net de l'écosystème). Cette étude démontre la grande variabilité des échanges de carbone en hiver et souligne l'importance de comprendre ces échanges afin d'améliorer notre capacité à prédire le rôle des régions arctiques et boréales dans le système climatique.

# Abstract

The Earth's climate is closely linked to the atmospheric concentrations of greenhouse gases (GHG) such as carbon compounds of carbon dioxide ( $CO_2$ ) and methane ( $CH_4$ ). Climate models predicting the evolution of the planetary climate require knowledge of ecosystem processes to determine whether they act as sinks (sequestration) or sources (emission) of GHG and to understand which environmental factors influence these exchanges. Arctic and boreal regions are among the least understood environments due to their challenging accessibility. In these environments, winter is the most neglected season due to technical challenges posed by harsh winter conditions. The first objective of my thesis project is to quantify natural carbon exchanges in the Arctic tundra and boreal forest during winter. The second objective is to determine the primary environmental factors influencing winter carbon exchanges. The third objective is to determine the contribution of winter GHG to the annual net balance. To achieve these objectives, we measured the  $CO_2$  and  $CH_4$  concentration gradient through the snow cover to quantify winter exchanges between the soil and the atmosphere at several research sites in the Arctic (Inuvik, Northwest Territories, and Cambridge Bay, Nunavut) and in the boreal forest (Montmorency Forest, Quebec, and Sodankylä, Finland). The database thus collected is the largest currently available on the spatial variability of GHG fluxes in winter over Arctic and boreal regions. We also used a machine learning algorithm (Random Forest) to demonstrate that soil temperature is the primary environmental control influencing  $CO_2$  emissions when the soil is completely frozen. However, when the soil temperature is near  $0^\circ C$ , soil water liquid content becomes the primary factor influencing carbon exchanges. We highlighted that boreal forest soils act as  $CH_4$  sinks, removing  $CH_4$  from the atmosphere, while boreal and Arctic wetlands emit significant amounts of  $CH_4$  during winter. For the annual budget, we show that winter  $CO_2$  emissions can offset up to 42% of  $CO_2$  sequestration during the growing season by the vegetation (net ecosystem exchange). This significant contribution is not well accounted for in current biosphere and climate models due to the scarcity of winter data. This study demonstrates the important variability of GHG exchanges in winter and emphasizes the importance of understanding these exchanges to improve our ability to predict the role of Arctic and boreal regions in the climate system.

## **Remerciements**

Je remercie d'abord Alexandre Roy, directeur de ma thèse, de m'avoir permis de travailler sur ce projet stimulant. J'ai eu la chance de bénéficier de son encadrement exceptionnel et de sa porte toujours ouverte à ses étudiants. Il m'a inspiré à continuellement chercher à m'améliorer dans les multiples facettes de la recherche scientifique. Surtout, il m'a accordé une grande confiance et un support inébranlable dans tous les projets que j'ai initiés au cours de ma thèse. Je remercie Juha Lemmetyinen d'avoir codirigé ma thèse et de m'avoir accueilli par deux fois en Finlande. Je remercie Oliver Sonnentag de m'avoir dédié autant de temps au cours des dernières années. Même si son support restera officieux, je considère son grand support comme une codirection de ma thèse.

Je tiens à remercier chaleureusement les communautés autochtones qui nous ont accueillis et qui ont partagé leur territoire avec nous au cours des multiples campagnes terrain des dernières années à Iqaluktuutiaq, Inuvik et Kangiqsualujjuaq. Je suis reconnaissant d'avoir eu la chance d'échanger avec les jeunes d'Iqaluktuutiaq et Inuvik, j'aurai appris beaucoup à leur contact. Je remercie le FQRNT (subvention DIALOGUE) et l'organisme Actua de m'avoir permis d'organiser ces échanges par leur financement.

Je remercie tous les gens qui ont contribué à la réussite de ce projet à travers les multiples collaborations et liens qui se sont créés au cours des dernières années, la liste est très longue. Bien avant les réalisations scientifiques et les apprentissages qui ont été réalisés dans le cadre de ma thèse, ce sont toutes ces personnes que j'aurais côtoyées et les moments privilégiés que nous avons partagé dans des endroits extraordinaires que je vais me remémorer avec nostalgie pour le reste de ma vie.

Je remercie l'Association of Polar Early Career Scientists de m'avoir choisi pour prendre part à l'expédition arctique MOSAiC en 2019, l'une des expériences les plus mémorable et unique de ma vie. Merci à Josefine Lenz d'avoir géré la logistique et les multiples défis d'une telle expédition d'une main de maître.

Sans le support financier qui nous a été octroyé, ce projet n'aurait jamais pu décoller. Je remercie le CRSNG (notamment pour ma bourse Graham-Bell et Michael-Smith), le FQRNT (notamment pour ma bourse doctorale), l'UQTR (notamment pour ma bourse Universalis Causa), le MEES, le Programme de formation scientifique dans le Nord et le Centre d'Études Nordiques.

# Table des matières

<b>1 Chapitre 1 : Introduction</b>	<b>1</b>
1.1 Mise en contexte . . . . .	1
1.2 Problématique . . . . .	1
1.3 Objectifs . . . . .	3
1.4 Structure de la thèse . . . . .	4
<b>2 Chapitre 2 : Cadre théorique</b>	<b>6</b>
2.1 Cycle du carbone . . . . .	6
2.1.1 Dioxyde de carbone . . . . .	6
2.1.2 Méthane . . . . .	7
2.2 Composantes des flux de carbone et modélisation écosystémique . . . . .	9
2.2.1 Photosynthèse . . . . .	9
2.2.2 Respiration autotrophe . . . . .	11
2.2.3 Respiration hétérotrophe . . . . .	11
2.2.4 Méthane . . . . .	13
2.3 Télédétection et science du carbone . . . . .	13
<b>3 Chapitre 3 : Flux hivernaux de <math>CO_2</math></b>	<b>16</b>
3.1 Présentation de l'article scientifique . . . . .	16
3.2 Résumé de l'article scientifique en français . . . . .	17
3.3 Article scientifique 1 . . . . .	18
3.3.1 Introduction . . . . .	18
3.3.2 Method . . . . .	20
3.3.3 Results . . . . .	24
3.3.4 Discussion . . . . .	26
3.3.5 Conclusion . . . . .	29
3.3.6 Appendix A . . . . .	30
3.3.7 References . . . . .	34
<b>4 Chapitre 4 : Flux hivernaux de <math>CH_4</math></b>	<b>40</b>
4.1 Présentation de l'article scientifique . . . . .	40
4.2 Résumé de l'article scientifique en français . . . . .	41
4.3 Article scientifique 2 . . . . .	42
4.3.1 Introduction . . . . .	43
4.3.2 Materials and Methods . . . . .	45
4.3.3 Results . . . . .	47
4.3.4 References . . . . .	53

4.3.5	Supporting Information	62
<b>5</b>	<b>Chapitre 5 : Impact des flux de carbone hivernaux sur le bilan annuel</b>	<b>69</b>
5.1	Présentation de l'article scientifique	69
5.2	Résumé de l'article scientifique en français	70
5.3	Article scientifique 3	71
5.3.1	Introduction	71
5.3.2	Method	72
5.3.3	Results	75
5.3.4	Discussion	79
<b>6</b>	<b>Chapitre 6 : Télédétection micro-onde pour la science du carbone</b>	<b>93</b>
6.1	Présentation de l'article scientifique	93
6.2	Résumé de l'article scientifique en français	94
6.3	Article scientifique 4	95
6.3.1	Introduction	95
6.3.2	Principles of microwave remote sensing	97
6.3.3	Microwave remote sensing for retrieval of surface variables	98
6.3.4	Assimilating microwave data in terrestrial biosphere models in Arctic-boreal regions	105
6.3.5	Challenges and opportunities in microwave remote sensing for supporting carbon cycle science	105
6.3.6	Conclusions	107
6.3.7	Appendix A	108
6.3.8	Appendix B : Acronyms and abbreviations	110
6.3.9	References	111
<b>7</b>	<b>Chapitre 7 : Validation du produit SMAP L4C en hiver</b>	<b>125</b>
7.1	Introduction	125
7.2	Modèle L4C	126
7.3	Résultats et discussion	127
7.4	Conclusion	130
<b>8</b>	<b>Chapitre 8 : Conclusion et perspectives futures</b>	<b>131</b>
<b>9</b>	<b>Financement</b>	<b>136</b>
<b>10</b>	<b>Bibliographie complémentaire aux articles</b>	<b>137</b>
<b>A</b>	<b>Annexe A - Protocole concentration de gaz</b>	<b>142</b>
A.1	Introduction	142

A.2	Collecte d'échantillons de gaz . . . . .	142
A.2.1	Procédure . . . . .	143
A.2.2	Liste du matériel nécessaire . . . . .	144
A.3	Transfert d'échantillons de gaz . . . . .	145
A.3.1	Procédure . . . . .	145
A.3.2	Liste du matériel nécessaire . . . . .	147
A.4	Concentration des échantillons de gaz . . . . .	148
A.4.1	Procédure . . . . .	149
A.4.2	Liste du matériel nécessaire . . . . .	151
A.5	Traitement des données . . . . .	152
A.5.1	Étalonnage . . . . .	152
A.5.2	Calcul concentration . . . . .	154
<b>B</b>	<b>Annexe B - Méthodes de mesure des flux de carbone</b>	<b>155</b>
B.1	Covariance des turbulences . . . . .	155
B.2	Chambre dynamique et statique . . . . .	157
<b>C</b>	<b>Annexe C - Publications à titre de premier auteur et coauteur</b>	<b>160</b>

# Liste des figures

Figure 1.1 Structure de la thèse . . . . .	4
Figure 2.1 Impact de la végétation sur les flux de $CH_4$ . . . . .	8
Figure 2.2 Modèle de dégradation en cascade pour estimer la respiration hétérotrophe . . . . .	12
Figure 3.1 Study site locations in Canada . . . . .	21
Figure 3.2 Gas sampling setup . . . . .	23
Figure 3.3 $CO_2$ uncertainty . . . . .	24
Figure 3.4 Random forest (RF) performance and variable relative importance	25
Figure 3.5 $CO_2$ flux as a function of surface soil temperature for $T_{soil} < 0^\circ C$	25
Figure 3.6 $CO_2$ flux as a function of soil temperature at the Montmorency Forest study sites . . . . .	27
Figure 3.7 $CO_2$ flux as a function of soil volumetric liquid water content (LWC)	27
Figure 3.8 Boxplot of $CO_2$ flux across 12 vegetation types and 4 sites. . . . .	28
Figure 3.A.1 $CO_2$ in relation to atmospheric pressure and wind speed . . . . .	30
Figure 3.A.2 Violin plot of the snow depth range . . . . .	31
Figure 3.A.3 Examples of snow diffusion coefficient . . . . .	32
Figure 3.A.4 Comparison of winter $CO_2$ flux from different gas analyzers . . . . .	33
Figure 3.A.5 Violin plot of the soil temperature range . . . . .	33
Figure 4.1 $CH_4$ flux across the study sites . . . . .	48
Figure 4.2 $CH_4$ flux as a function of soil LWC . . . . .	49
Figure 4.3 $CH_4$ flux as a function of soil temperature . . . . .	49
Figure 4.S1 Study site locations . . . . .	62
Figure 4.S2 $F_{CH_4}$ uncertainty relationship to $ F_{CH_4} $ . . . . .	64
Figure 4.S3 $CH_4$ flux across vegetation types at Trail Valley Creek . . . . .	65
Figure 4.S4 $CH_4$ flux spatial variability in the boreal wetland at the Sodankylä study site . . . . .	66
Figure 4.S5 $CH_4$ flux as function of snow density, snow density and water equivalent . . . . .	67
Figure 4.S6 $CH_4$ flux as a function of $CO_2$ flux at the Montmorency Forest and Sodankylä boreal forest uplands study sites. . . . .	68
Figure 4.S7 $CO_2$ flux at Montmorency Forest and Sodankylä . . . . .	68
Figure 5.1 Yearly $CO_2$ exchanges at a mesic tundra site in Cambridge Bay .	75
Figure 5.2 Yearly $CO_2$ and $CO_4$ exchanges at an erect shrub site in Trail Valley Creek . . . . .	77
Figure 5.3 Yearly $CO_2$ and $CO_4$ exchanges at a black spruce boreal forest site in Havikpak Creek . . . . .	78

Figure 5.4	Yearly $CO_2$ exchanges at a balsam fir boreal forest site in Montmorency Forest . . . . .	79
Figure 5.5	Comparison of NEE from EC and snowpack gradient measurements . . . . .	80
Figure 5.6	Winter $CO_2$ flux contribution to the annual budget in arctic and boreal environments . . . . .	81
Figure 5.7	Winter $CO_4$ flux contribution to the annual budget in arctic and boreal environments . . . . .	81
Figure 5.A1	Yearly soil respiration $CO_2$ exchanges at a balsam fir boreal forest site in Montmorency Forest . . . . .	91
Figure 5.A2	Winter soil respiration $CO_2$ exchanges as a function of DOY at a balsam fir boreal forest site in Montmorency Forest . . . . .	91
Figure 6.1	Permafrost extent and distribution of eddy covariance sites . . . . .	96
Figure 6.2	Microwave signal decoupling through electromagnetic wave interaction with matter . . . . .	99
Figure 6.3	Temporal coverage of spaceborne microwave instruments . . . . .	100
Figure 6.4	Key environmental variables relevant for $CO_2$ and $CH_4$ fluxes and derivable with microwave remote sensing . . . . .	101
Figure 6.5	Mean monthly net ecosystem exchange (NEE) from the SPL4CMDL product for July and August between 2015 and 2021 . . . . .	106
Figure 6.A1	Microwave radiometers in the 1-100 GHz frequency range on sun-synchronous nearly polar orbits . . . . .	108
Figure 6.A2	Microwave radar missions . . . . .	109
Figure 7.1	Schématisation du modèle L4C . . . . .	126
Figure 7.2	Comparaison des simulations de NEE L4C versus les données <i>in situ</i> de $F_{CO_2}$ hivernaux . . . . .	128
Figure 7.3	Biais entre NEE L4C et données <i>in situ</i> de $F_{CO_2}$ hivernaux . . . . .	128
Figure 8.1	Évolution anticipée des échanges de $CO_2$ en régions arctiques et boréales au cours de l'hiver . . . . .	132
Figure 8.2	Évolution anticipée des échanges de $CH_4$ en régions arctiques et boréales au cours de l'hiver . . . . .	133
Figure 8.3	Projets futurs et en cours découlant de cette thèse . . . . .	135
Figure A.1	Positionnement des valves à trois voix . . . . .	144
Figure A.2	Matériel nécessaire pour la collecte d'échantillons de gaz . . . . .	145
Figure A.3	Montage pour le transfert d'échantillons de gaz . . . . .	147
Figure A.4	Matériel nécessaire pour le transfert d'échantillons de gaz . . . . .	148
Figure A.5	Montage analyse d'échantillon de gaz . . . . .	150
Figure A.6	Concentration de $CH_4$ mesurée par l'analyseur de gaz . . . . .	151
Figure A.7	Aire des pics de concentration en fonction du volume de gaz d'éta- lonnage . . . . .	153

Figure A.8 Étallonnage de l'analyseur de gaz . . . . .	154
Figure B.1 Comparaison des méthodes de mesure des flux de carbone . . . . .	155
Figure B.2 Principe de la mesure des flux de carbone à partir de la covariance des turbulences . . . . .	156
Figure B.3 Systèmes de mesure des turbulences des flux . . . . .	157
Figure B.4 Schéma d'une chambre dynamique . . . . .	158
Figure B.5 Exemple d'une chambre dynamique . . . . .	159

## Liste des tableaux

Tableau 3.1	Study sites with the number of sampling locations . . . . .	21
Tableau 3.A.1	Uncertainty sources in $F_{CO_2}$ . . . . .	30
Tableau 4.S1	Study sites with the number of sampling locations . . . . .	63
Tableau 4.S2	Vegetation, soil, and climate properties of the study sites . . .	63
Tableau 4.S3	$F_{CH_4}$ uncertainty sources. . . . .	64
Tableau 5.A1	Winter $CO_2$ flux contribution to the annual budget in arctic and boreal environments . . . . .	92
Tableau 5.A2	Winter $CO_4$ flux contribution to the annual budget in arctic and boreal environments . . . . .	92
Tableau 6.1	Available soil moisture products from spaceborne microwave remote sensing . . . . .	102
Tableau 6.2	Available surface freeze-thaw state products from spaceborne mi- crowave remote sensing . . . . .	103
Tableau 6.3	Available vegetation optical depth products from spaceborne mi- crowave remote sensing . . . . .	104
Tableau 6.4	Available snow water equivalent products from spaceborne mi- crowave remote sensing . . . . .	105
Tableau 6.5	Overview of selected future microwave satellite missions with a polar or near-polar orbit . . . . .	107
Tableau 7.1	Plant functional type description . . . . .	127
Tableau 7.2	Comparaison des simulations de $NEE$ L4C versus les données <i>in situ</i> de $F_{CO_2}$ hivernaux . . . . .	129

## Liste des acronymes

<i>A</i>	Empreinte au sol (footprint)
ABR ou RAB	Arctic and Boreal Regions (Régions Arctiques et Boréales)
AGU	American Geophysical Union
ASAR	Advanced Synthetic Aperture Radar
ASCAT	Advanced SCATterometer
AGB	Above-Ground Biomass (biomasse au-dessus du sol)
AMSR	Advanced Microwave Scanning Radiometer
AMSR-E	AMSR for Earth Observing System
APAR	Absorbed Photosynthetically Active Radiation (rayonnement photosynthétiquement actif absorbé par la végétation)
<i>C<sub>in</sub></i>	Concentration de gaz à l'entrée (input gas concentration)
<i>C<sub>out</sub></i>	Concentration de gaz à la sortie (output gas concentration)
CAFF	Conservation of Arctic Flora and Fauna
CARDAMOM	Carbon data model framework
CB	Cambridge Bay
CB-mes	Cambridge Bay Mesic
CB-wet	Cambridge Bay Wetland
CCI	Climate Change Initiative
<i>CH<sub>4</sub></i>	Méthane (methane)
CIMR	Copernicus Imaging Microwave Radiometer
CLASSIC	Canadian Land Surface Scheme Including Biogeochemical Cycles
CLM	Community Land Model
CNES	Centre National d'Études Spatiales
<i>CO<sub>2</sub></i>	Dioxyde de carbone (carbone dioxide)
CRSNG ou NSERC	Conseil de Recherche en Sciences Naturelles et en Génie du Canada (Natural Sciences and Engineering Research Council of Canada)
CSA	Canadian Space Agency (Agence Spatiale Canadienne)
<i>D</i>	Coefficient de diffusion (Diffusion coefficient)
DLR	German Aerospace Center
<i>d<sub>g</sub></i>	Diamètre granulométrique géométrique moyen du sol (soil geometric mean particle-size diameter)
<i>d<sub>snow</sub></i>	Snow depth (profondeur de neige par rapport à l'interface neige-atmosphère)
$\frac{d}{dz}$	Gradient vertical (vertical gradient)
<i>e</i>	Émissivité du sol (Soil emissivity)

EC	Eddy Covariance (covariance des turbulences)
EGU	European Geosciences Union
ERS	European Remote Sensing Satellite
ESA	European Space Agency
EVI	Enhanced Vegetation Index
FAO	Food and Agriculture Organization of the United Nations
$f_{c/si/sa}$	Soil fraction of clay/silt/sand (Fraction du sol d'argile/sable/limon)
$F$	Flux
$F_{CH_4}$	Flux de $CH_4$ ( $CH_4$ flux)
$F_{CO_2}$	Flux de $CO_2$ ( $CO_2$ flux)
$F_{diff}$	Flux par gradient de diffusion à travers le couvert neigeux (flux by diffusive gradient through snowpack)
$F_{neige}$	Flux par chambre sur le couvert neigeux (flux by chamber over snowpack)
$F_{sol}$	Flux par chambre sur le sol (flux by chamber over soil)
FQRNT	Fonds de recherche du Québec – Nature et technologies
FMI	Finnish Meteorological Institute
FY-3	FenYun-3
FW	Freshwater (eau douce)
FPAR	Fraction of Photosynthetically Active Radiation (fraction du rayonnement photosynthétiquement actif)
$f(x_i)$	Fonction générale du stress environnemental (general environmental stress function)
GEOS-5	Goddard Earth Observing System, Version 5
GD	Gradient de Diffusion (diffusion gradient)
GNSS	Global Navigation Satellite System
GPP	Gross Primary Production (production primaire brute)
GS	Growing Season (saison de croissance)
$h_{snow}$	Snow height (hauteur de neige par rapport à l'interface sol-neige)
$H_2O$	Eau (Water)
HPC	Havikpak Creek
IFOV	Instantaneous Field Of View (champ de vue instantané)
IQR	Écart interquartile (interquartile range)
InSAR	SAR interferometry (interférométrie SAR)
ISRO	Indian Space Research Organization
$Q$	Débit (rate of flow)
LAI	Leaf Area Index (indice de surface foliaire)
LiDAR	Light Detection And Ranging (détection et estimation de la distance par laser)
LPJ-wsl	Lund–Potsdam–Jena dynamic global vegetation model - Wald

	Schnee und Landschaft version
LST	Land Surface Temperature (température de surface terrestre)
LUE	Light Use Efficiency (efficacité d'utilisation de la lumière)
LWC	Liquid Water content (contenu en eau liquide)
$M_{c/si/sa}$	Mean particle-size diameter of clay/silt/sand (diamètre moyen des particules d'argile/sable/limon)
MEaSUREs	Making Earth System data records for Use in Research Environments
MM	Montmorency Forest
MODIS	MODerate-resolution Imaging Spectroradiometer
MPI	Max Planck Institute
MWRI	Micro-Wave Radiation Imager
N ou n	Nombre de données (number of data points)
NASA	National Aeronautics and Administration
NDVI	Normalized difference vegetation index (indice de végétation par différence normalisée)
NEE	Net Ecosystem Exchange (échange net de l'écosystème)
NEP	Net Ecosystem Production (production nette de l'écosystème)
NISAR	NASA-ISRO SAR mission
NPP	Net Primary Production (production primaire nette)
NSCAT	NASA Scatterometer
NU	Northumbria University
PALSAR	Phased Array type L-band SAR
PAR	Photosynthetically Active Radiation (rayonnement photosynthétiquement actif)
PFSN	Programme de formation scientifique dans le Nord
PFT	Plant Functional Type (type fonctionnel de plante)
POLAR ou POLAIRE	Polar Knowledge Canada (Savoir Polaire Canada)
PolInSAR	Polarimetric InSAR
PRI	Photochemical Reflectance Index
QuickSCAT	Quick Scatterometer
Q3	Troisième quartile (third quartile)
Q10	Temperature coefficient
$R_a$	Respiration Autotrophe (autotrophic respiration)
$R_{eco}$	Respiration de l'écosystème (ecosystem respiration)
$R_h$	Respiration Hétérotrophe (heterotrophic respiration)
$R_{soil}$	Respiration du Sol (soil respiration)
$R^2$	Coefficient de détermination (coefficient of determination)
REP	Red Edge Position
RF	Random Forest

RMSE	Root Mean Square Error (racine de l'erreur quadratique moyenne)
ROS	Rain-On-Snow event (événement de pluie sur neige)
ROSE-L	Radar Observing System for Europe - L-Band
$S$	Nombre de sites d'échantillonnage (number of sampling location)
SAR	Synthetic Aperture Radars
$SF_{sol}$	Flux par chambre sur le sol en continu (flux by permanent chamber over soil)
SMAP	Soil Moisture Active Passive
SMAP L4C	SMAP Level 4 Carbon product
SMMR	Scanning Multichannel Microwave Radiometer
SMOS	Soil Moisture and Ocean Salinity
SMOS-HR	SMOS High-Resolution
SMRT	Snow Microwave Radiative Transfer model
SOC	Soil Organic Carbon (carbone organique du sol)
SOD	Sodankylä
SOD-bor	Sodankylä Boreal Forest
SOD-wet	Sodankylä Wetland
SSA	Specific Surface Area (surface spécifique)
SWE	Snow Water Equivalent (équivalent en eau de la neige)
SMM/I	Special Sensor Microwave/Imager
$T$	Température (temperature)
$T_B$	Température de brillance (brightness temperature)
$T_o$	Température du point de congélation (freezing point temperature)
TCF	Terrestrial Carbon Flux
TomoSAR	SAR tomography
TVC	Trail Valley Creek
UdeM	Université de Montréal
UdeS	Université de Sherbrooke
UK	United Kingdom
UNAVCO	University NAVstar COnsortium
UQTR	Université du Québec à Trois-Rivières
$V_{cal}$	Volume du gaz de calibration (calibration gas volume)
$V_{sample}$	Volume du gaz échantillonné (sample gas volume)
VOD	Vegetation Optical Depth (épaisseur optique de la végétation)
WLU	Wilfrid Laurier University
$\gamma$	Atténuation par la végétation (vegetation attenuation)
$\eta$	Efficacité de conversion de la lumière (light conversion efficiency)
$\eta_{max}$	Efficacité de conversion de la lumière dans des conditions optimales (light conversion efficiency maximum in optimal conditions)

$\delta$	Incertitude (uncertainty)
$\varepsilon$	Permittivité électrique relative (relative permittivity)
$\theta$	Angle d'incidence (incident angle)
$\rho$	Densité(density)
$\rho_b$	Bulk density(densité apparente)
$\rho_w$	Water density(densité de l'eau)
$\sigma$ (Chap. 3, 4 et 5)	Écart-type (standard deviation)
$\sigma$ (Chap. 6)	Coefficient de rétrodiffusion (backscattering coefficient)
$\tau$ (Chap. 3, 4 et 5)	Tortuosité (tortuosity)
$\tau$ (Chap. 6)	Épaisseur optique (optical depth)
$\phi$	Porosité (porosity)
$\Omega$	Vegetation single-scattering albedo
$[CH_4]$	Concentration de méthane (methane concentration)
$[CO_2]$	Concentration de dioxyde de carbone (carbon dioxide concentration)
$[ ]_{cal}$	Concentration du gaz de calibration (calibration gas concentration)
$[ ]_{base}$	Concentration du gaz de base (baseline gas concentration)

# Chapitre 1 : Introduction

## 1.1 Mise en contexte

Les régions nordiques abritent deux importants biomes terrestres, le biome boréal et le biome arctique. Les stocks de carbone du sol dans les régions arctiques et boréales représentent de 30 à 40 % du carbone terrestre planétaire, et par conséquent, la compréhension des processus du cycle du carbone dans ces vastes régions revêt d'une grande importance (Tarnocai *et al.*, 2009 ; van Huissteden and Dolman, 2012). En revanche, les stocks de carbone dans la biomasse au-dessus du sol dans les régions arctiques et boréales sont relativement faibles (Pan *et al.*, 2011). Le biome boréal constitue le deuxième plus grand biome terrestre avec un tiers de la superficie forestière mondiale et 32 % des stocks mondiaux de carbone forestier (Pan *et al.*, 2011). Cependant, le biome boréal ne représente qu'environ 15 % de la biomasse forestière mondiale au-dessus du sol (FAO, 2001 ; Pan *et al.*, 2011 et 2013 ; Carreiras *et al.*, 2017).

Les stocks de carbone des régions arctiques et boréales sont vulnérables aux changements climatiques (Grosse *et al.*, 2011). Les régions arctiques et boréales se réchauffent à un rythme disproportionné par rapport au reste de la planète, avec des rétroactions potentielles sur le système climatique mondial (Box *et al.*, 2019 ; Derksen *et al.*, 2019 ; GIEC, 2019 ; Rantanen *et al.*, 2022). Ces régions connaissent actuellement une modification de leur régime de précipitations (Callaghan *et al.*, 2011 ; Bokhorst *et al.*, 2016 ; Dolant *et al.*, 2018), le dégel du pergélisol (sol complètement gelé pendant au moins deux années consécutives) et l'approfondissement de la couche hydrologiquement et biogéochimiquement active (Liljedahl *et al.*, 2016 ; Miner *et al.*, 2022), une modification de la dynamique de la végétation associées au «verdissement» et au «brunissement» (c'est-à-dire, une augmentation et une diminution de la productivité de la végétation, respectivement ; Sulla-Menashe *et al.*, 2018 ; Myers-Smith *et al.*, 2020), des gels tardifs à l'automne, des dégels précoce au printemps et l'allongement de la saison de croissance (Kimball *et al.*, 2004a ; Euskirchen *et al.*, 2006 ; Kim *et al.*, 2012), des modifications de l'occupation du sol (Wang *et al.*, 2020) et une intensification des régimes de perturbation tels que les incendies, la sécheresse, les infestations d'insectes et les maladies (Peng *et al.*, 2011 ; Yi *et al.*, 2013 ; Foster *et al.*, 2022).

## 1.2 Problématique

Les stocks et les flux de carbone des régions arctiques et boréales constituent d'importantes composantes du bilan de carbone planétaire (Tarnocai *et al.*, 2009 ; van Huissteden et Dolman, 2012 ; Carreiras *et al.*, 2017). Ces régions contiennent des quantités

substantielles de carbone en raison de leur taux de décomposition intrinsèquement lent, largement attribuables à leurs températures froides (Ravn *et al.*, 2020). Cependant, les régions arctiques et boréales se réchauffent jusqu'à quatre fois plus rapidement que le reste de la planète ce qui pourrait entraîner des rétroactions significatives sur le système climatique mondial (Derksen *et al.*, 2019 ; Rantanen *et al.*, 2022). Bien que le réchauffement de ces régions ait le potentiel d'allonger la saison de croissance de la végétation, et ainsi d'augmenter le stockage du carbone en biomasse (Sturm *et al.*, 2005 ; McMahon *et al.*, 2010), le comportement de la végétation pendant la saison de croissance dépend de plusieurs facteurs et l'augmentation de la respiration pourrait relâcher davantage de carbone que les gains par photosynthèse (Myers-Smith *et al.*, 2020 ; Lamarque *et al.*, 2023). On observe notamment des stocks de carbone nouvellement accessible pour la décomposition dû au dégel du pergélisol (Schuur *et al.*, 2015 ; Natali *et al.*, 2021 ; Miner *et al.*, 2022).

Les températures plus chaudes de l'air et du sol favorisent la production et la libération de dioxyde de carbone ( $CO_2$ ) par respiration des écosystèmes, comprenant la respiration hétérotrophe des microbes décomposant la matière organique du sol et la respiration autotrophe des composantes végétales (Bond-Lamberty et Thomson, 2010). Dans un climat en réchauffement, si l'augmentation de la respiration des écosystèmes dépasse l'augmentation de la capture de  $CO_2$  par photosynthèse, les régions arctiques et boréales pourraient passer de faible puits de  $CO_2$  net à sources nettes de  $CO_2$ , générant ainsi une rétroaction potentiellement importante sur le système climatique mondial (Hayes *et al.*, 2011 ; Gauthier *et al.*, 2015 ; Natali *et al.*, 2019 ; Bruhwiler *et al.*, 2021 ; Virkkala *et al.*, 2021 ; Braghieri *et al.*, 2023).

Les sols comprennent des micro-organismes produisant du méthane ( $CH_4$ ) lors de la décomposition de la matière organique et des micro-organismes oxydant le  $CH_4$  pour combler leur besoin en carbone et en énergie (Topp et Pattey, 1997). Une modification des régimes d'échange de  $CH_4$  pourrait générer une rétroaction potentiellement non négligeable sur le système climatique mondial dû à son potentiel de réchauffement global environ 25 fois supérieur au  $CO_2$  à masse égale (Natali *et al.*, 2021 ; Rößger *et al.*, 2022 ; Schuur *et al.*, 2022). La majorité des études portant sur les flux de  $CH_4$  dans les régions arctiques et boréales se concentre sur la saison de croissance (e.g., Ullah *et al.*, 2009 ; Zona *et al.*, 2009 ; Helbig *et al.*, 2016 ; Kuhn *et al.*, 2021). Néanmoins, les rares études portant sur les flux de  $CH_4$  en hiver en arctique ont montré que l'hiver peut contribuer jusqu'à 40 à 50 % des émissions annuelles nettes de  $CH_4$  (Zona *et al.*, 2016 ; Treat *et al.*, 2018 ; Rößger *et al.*, 2022 ; Ito *et al.*, 2023). La plupart des études sur le  $CH_4$  en hiver dans les régions arctiques et boréales se concentrent sur les zones humides et les tourbières où de fortes émissions sont attendues, avec peu d'attention portée aux zones mieux drainées qui agissent comme des puits de  $CH_4$  malgré qu'elles couvrent environ 80% des biomes

arctiques et boréals (Treat *et al.*, 2018 ; Raynolds *et al.*, 2019 ; Olefeldt *et al.*, 2021 ; Voigt *et al.*, 2023). Davantage d'études sur les flux de  $CH_4$  en hiver ont été réalisées en forêt boréale que dans l'Arctique. Dans les deux cas, elles demeurent rares par rapport aux études au cours de la saison de croissance (Viru *et al.*, 2020 ; Hiyama *et al.*, 2021 ; Lee *et al.*, 2023).

Une compréhension insuffisante des contrôles environnementaux sur les échanges de carbone en hiver constitue une importante source d'incertitude pour le budget de carbone des régions arctiques et boréales (McGuire *et al.*, 2012 ; Mastepanov *et al.*, 2013). Les fortes incertitudes dans les échanges de carbone hivernaux entre la surface du sol et l'atmosphère dans ces régions sont en partie dues à la disponibilité limitée des données en raison des difficultés d'accès à ces vastes régions éloignées et les conditions hivernales rigoureuses créant des défis techniques pour la mesure des flux de carbone (Natali *et al.*, 2019 ; Virkkala *et al.*, 2022).

### 1.3 Objectifs

L'objectif principal de la thèse est de mieux comprendre les échanges naturels de  $CO_2$  et de  $CH_4$  en hiver dans les régions arctiques et boréales en déterminant les principaux contrôles environnementaux et l'impact des flux hivernaux sur le bilan annuel de carbone. Cet objectif principal se décline en trois objectifs spécifiques (Fig. ??) :

1. Quantifier les flux hivernaux de  $CO_2$  et  $CH_4$  (Chap. 3 et 4).
2. Déterminer les contrôles environnementaux sur les flux hivernaux de  $CO_2$  et  $CH_4$  (Chap. 3 et 4).
3. Déterminer la contribution des flux hivernaux de  $CO_2$  et de  $CH_4$  aux bilans annuels des flux de carbone (Chap. 5).

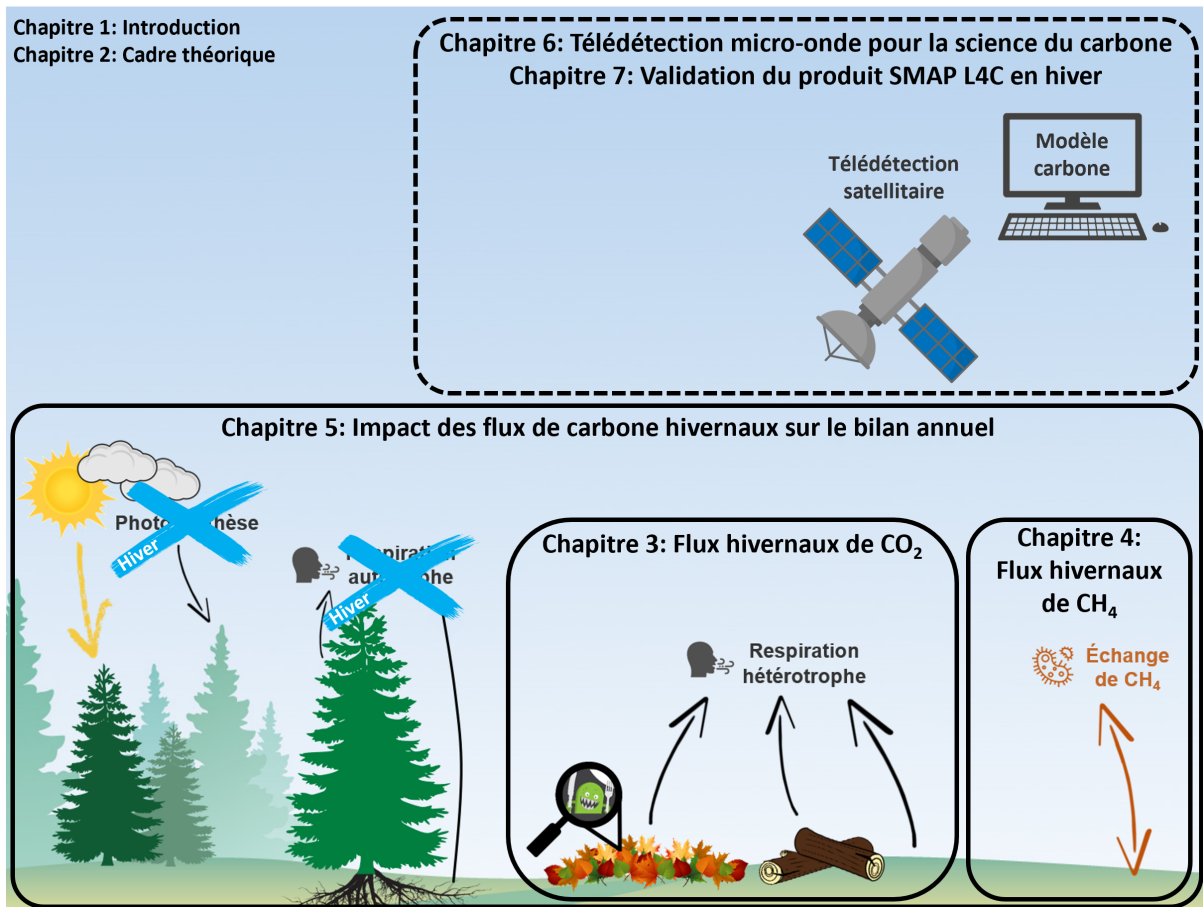


FIGURE 1.1 – Structure de la thèse.

Afin d'accomplir ces trois objectifs, une méthode de mesure robuste des flux de carbone hivernaux a été implémentée et déployée sur plusieurs sites d'études en régions arctiques et boréales. Cette méthode se base sur le gradient de diffusion du  $CO_2$  et du  $CH_4$  à travers le couvert neigeux (Sommerfield *et al.*, 1993). Le détail de cette méthode se trouve à la Sect. 3.3.2 ( $CO_2$ ) et 4.3.2 ( $CH_4$ ). Un protocole détaillé de la méthode se trouve à l'Annexe A.

## 1.4 Structure de la thèse

La thèse débute par le cadre théorique au chapitre 2 portant sur le cycle du carbone et le potentiel de la télédétection pour supporter la science du carbone en régions nordiques. Les résultats de la thèse sont divisés en trois chapitres principaux. Les chapitres 3 et 4 répondent aux deux premiers objectifs spécifiques. Le chapitre 5 répond au troisième objectif spécifique. Deux chapitres additionnels complémentent la thèse. Le chapitre 6 présente le potentiel de la télédétection micro-onde pour informer les modèles écosystémiques pour l'étude du cycle du carbone dans les régions arctiques et boréales. Le chapitre 7 présente une comparaison entre le produit d'un modèle écosystémique exploitant la télédétection micro-onde (SMAP L4C; Jones *et al.*, 2017) et des données *in*

*situ* de flux de  $CO_2$  hivernaux. Un dernier chapitre apporte une conclusion globale à la thèse et les perspectives futures de l'étude du cycle du carbone dans les régions arctiques et boréales (Chap. 8). Tous les articles publiés au cours de la thèse à titre de premier auteur (5) et de co-auteur (3) se trouvent à l'Annexe C.

# Chapitre 2 : Cadre théorique

## 2.1 Cycle du carbone

Le dioxyde de carbone ( $CO_2$ ) et le méthane ( $CH_4$ ) sont deux gaz générant un important effet de serre dont la dynamique d'échange naturelle entre la surface terrestre et l'atmosphère est très active. Le  $CO_2$  est absorbé par la végétation via les processus de photosynthèse et est libéré par la végétation et le sol par respiration (c'est-à-dire la respiration autotrophe,  $R_a$ , et la respiration hétérotrophe,  $R_h$ ) (Chapin III *et al.*, 2006). Le  $CH_4$  quant à lui est produit par les méthanogènes dans des conditions typiquement anaérobiques et consommé lors de son oxydation par les méthanotrophes dans des conditions typiquement aérobiques (Lai, 2009). Le transport du méthane se fait par diffusion et ébullition à travers la colonne de sol vers l'atmosphère, et par transport médié par les plantes (Lai, 2009). En ce qui concerne les processus régissant les échanges de  $CH_4$ , ils sont dus à l'activité microbienne dans le sol où les microorganismes assimilent ou produisent du  $CH_4$ , principalement en fonction de la disponibilité de l'oxygène, et de la quantité et qualité du carbone organique disponible (Voigt *et al.*, 2023).

### 2.1.1 Dioxyde de carbone

La végétation peut séquestrer le  $CO_2$  atmosphérique en générant de la biomasse (i.e., croissance de la végétation) grâce à la photosynthèse, souvent appelés production primaire brute (Gross Primary Production : GPP). Simultanément, la végétation émet du  $CO_2$  par le biais de la respiration autotrophe ( $R_a$ ). L'impact net de la végétation sur le bilan du carbone est appelé production primaire nette ( $NPP = GPP - R_a$ ). La décomposition de la matière organique dans le sol par l'activité microbienne génère également des émissions de  $CO_2$  appelées respiration hétérotrophe ( $R_h$ ). La respiration d'un écosystème est donc constituée d'une composante autotrophe et d'une autre hétérotrophe ( $R_{eco} = R_a + R_h$ ). Le bilan net de  $CO_2$  des régions arctiques et boréales doit tenir compte de tous ces processus de flux de  $CO_2$  à la fois pendant la période de croissance (saison estivale) et la période de dormance (saison hivernale). La somme de ces processus est appelée production nette de l'écosystème (Net Ecosystem Production : NEP ; unité) ou échange net de l'écosystème (Net Ecosystem Exchange : NEE = - NEP) (Fig. 6.4) (Chapin III *et al.*, 2006). Tous ces termes décrivant les échanges de  $CO_2$  d'un écosystème sont données en  $C\ m^{-2}\ an^{-1}$  ou l'une de ses nombreuses déclinaisons. Les processus de photosynthèse et de respiration répondent à des facteurs environnementaux distincts. Par conséquent, ils sont généralement abordés séparément, bien qu'ils ne soient pas entièrement indépendants. Certains micro-organismes sont également autotropes et peuvent absorber le  $CO_2$  atmosphérique pour combler leur besoin en carbone et en énergie (Wu *et al.*, 2024). Ces processus sont généralement considérés comme négligeables.

En plus des processus biotiques réguliers, des événements de perturbation non anthropiques tels que les incendies de forêt, les maladies et les épidémies d'insectes peuvent avoir des effets drastiques sur le bilan de carbone des écosystèmes (Seidl *et al.*, 2014 ; Helbig *et al.*, 2016). De tels événements sporadiques sont complexes à prendre en compte dans les modèles écosystémiques basés sur les processus, ainsi plusieurs modèles ne les incorporent pas pour l'instant dû à la nature stochastique de ces phénomènes (Arora et Boer, 2005). Ces perturbations peuvent tout de même être repérées et identifiées à l'aide de la télédétection visible, infrarouge et micro-onde (Senf *et al.*, 2017 ; McCarthy *et al.*, 2019 ; Xiao *et al.*, 2019). Bien que cruciaux pour la modélisation climatique, les perturbations ne sont pas adressées dans le cadre de cette thèse.

Dans la plupart des régions du globe, les effets anthropiques peuvent avoir un impact significatif sur les écosystèmes et le bilan de carbone. La déforestation et l'exploitation forestière peuvent avoir des effets aussi importants que les incendies de forêt (GOFC-GOLD, 2016), et la modification de l'utilisation des terres peut altérer de manière importante la capacité d'un écosystème à stocker ou à émettre du carbone (Arora et Boer, 2010 ; Bayer *et al.*, 2021). Cependant, l'activité humaine tend à être minimale dans les hautes latitudes par rapport à d'autres régions plus tempérées et n'a pas été examinée dans cette thèse (Gauthier *et al.*, 2015).

### 2.1.2 Méthane

Bien que les concentrations atmosphériques de  $CH_4$  soient plus faibles que celles de  $CO_2$  (valeur moyenne d'environ 1.9 ppm versus 420 ppm, respectivement), le  $CH_4$  possède un potentiel de réchauffement global environ 25 fois supérieure au  $CO_2$  à masse égale (Harvey, 1993 ; Boucher *et al.*, 2009). Les flux nets de  $CH_4$  provenant du sol sont le résultat de trois processus : la production, l'oxydation et le transport du  $CH_4$ . Le  $CH_4$  est produit dans le sol par les méthanogènes lors de la décomposition de la matière organique dans des conditions anaérobiques, généralement retrouvées dans les couches profondes du sol ou dans les sols saturés d'eau liquide dans les zones humides et des tourbières (Zhang *et al.*, 2017 ; Feng *et al.*, 2020 ; Bastviken *et al.*, 2023). À l'opposé, le  $CH_4$  est oxydé par les méthanolotrophes comme source d'énergie et de carbone dans des conditions aérobiques (Lai, 2009 ; Bastviken *et al.*, 2023). De telles conditions se retrouvent généralement dans les couches supérieures des sols minéraux qui sont bien drainées. Dans de tels sols, l'oxydation du  $CH_4$  dépasse généralement la production et, par conséquent, le sol agit comme un puits de  $CH_4$ , absorbant du  $CH_4$  de l'atmosphère (Topp et Pattey, 1997 ; Roslev *et al.*, 1997). Au cours du processus d'oxydation, le  $CH_4$  est transformé en  $CO_2$  et en eau ( $H_2O$ ). Le transport du  $CH_4$ , c'est-à-dire le déplacement du  $CH_4$  depuis son

lieu de production vers l'atmosphère, joue également un rôle important dans la régulation de l'oxydation du  $CH_4$  en limitant le temps pendant lequel les méthanotrophes peuvent consommer le  $CH_4$  (Bastviken *et al.*, 2023). Le transport du  $CH_4$  se fait par diffusion et ébullition à travers la colonne de sol vers l'atmosphère, et par transport médié par les plantes (Lai, 2009). La composition végétale de l'écosystème a un impact significatif sur les flux de  $CH_4$ , notamment en fournissant le substrat de matière organique pour la production de  $CH_4$ , en réduisant l'oxydation du  $CH_4$  par les voies de transport médiées par les plantes, en fournissant de grandes surfaces pour la production de  $CH_4$ , et par son impact indirect sur la profondeur de la nappe phréatique (Fig. 2.1 ; Bastviken *et al.*, 2023). Les plantes possédant des aérenchymes, des canaux favorisant les échanges gazeux, vont limiter le potentiel de méthanotrophie en fournissant un chemin préférentiel pour le  $CH_4$  nouvellement produit. À l'opposé, les surfaces végétales sont aussi des niches écologiques abritant des méthanotrophes, permettant alors d'augmenter la surface d'échange possible favorisant la consommation du  $CH_4$ . Les principaux facteurs influençant les flux de  $CH_4$  sont la température du sol, l'humidité du sol, la profondeur de la nappe phréatique, la profondeur de la couche active du pergélisol, ainsi que la quantité et la qualité de la matière décomposable (Torn and Chapin III, 1993 ; Christensen *et al.*, 2003 ; Gedney *et al.*, 2004).

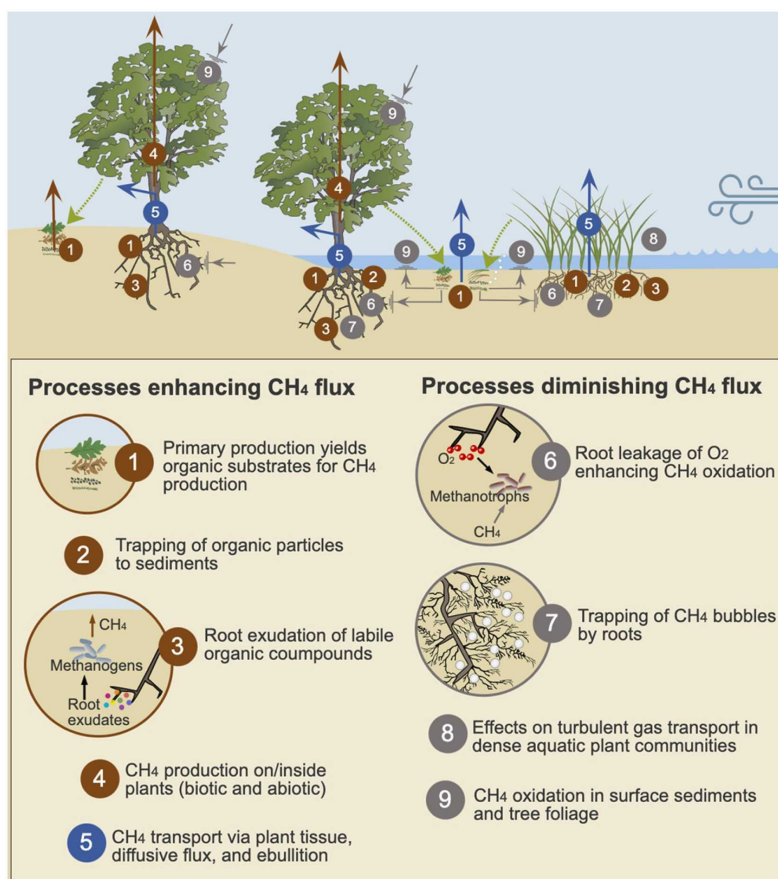


FIGURE 2.1 – Impact de la végétation sur les flux de  $CH_4$ . Source : Bastviken *et al.*, 2023.

## 2.2 Composantes des flux de carbone et modélisation écosystémique

Les modèles écosystémiques basés sur les processus des écosystèmes peuvent être utilisés pour estimer et prédire les échanges de  $CO_2$  et de  $CH_4$  entre la surface terrestre et l'atmosphère. Ces modèles prennent en compte les effets des interactions complexes entre le sol, la végétation et l'hydrologie sur les processus de production et de consommation  $CO_2$  et de  $CH_4$ . Les modèles écosystémiques tentent de reproduire les processus physiques du système climatique et leurs interactions avec les processus biogéochimiques, dont le cycle du carbone (Arora *et al.*, 2018). La modélisation est une approche permettant d'étendre les observations ponctuelles à des échelles régionales ou globales. À ce jour, plusieurs modèles basés sur les processus ont été développés, chacun possédant ses propres méthodes pour modéliser la complexité des écosystèmes (Ito *et al.*, 2023). Les sous-sections suivantes présentent quelques caractéristiques communes à la plupart des modèles du cycle du carbone.

### 2.2.1 Photosynthèse

Les modèles d'efficacité d'utilisation de la lumière (Light Use Efficiency : LUE) représentent le type de modèle le plus répandu pour estimer la séquestration du carbone par photosynthèse. Les modèles de LUE se basent sur l'hypothèse qu'il existe une relation linéaire entre la GPP et le rayonnement photosynthétiquement actif absorbé par la végétation (Absorbed Photosynthetically Active Radiation : APAR ; unité : W/m<sup>2</sup>) dans des conditions environnementales optimales (Monteith, 1972). Le APAR dépend du rayonnement photosynthétiquement actif total disponible (Photosynthetically Active Radiation : PAR ; unité : W/m<sup>2</sup>) qui représente la quantité de lumière disponible pour la photosynthèse ( $\sim 400$  à  $700$  nm). Le PAR dépend principalement de la couverture nuageuse et des effets d'ombrage (c'est-à-dire de l'ombre de la canopée). La fraction de lumière réellement absorbée par la végétation est représentée par le FPAR (sans unité, valeur de 0 à 1; APAR = FPAR · PAR). La FPAR est déterminée par des relations empiriques dérivées d'indices de végétation tels que le NDVI (Normalized Difference Vegetation Index), l'EVI (Enhanced Vegetation Index), le REP (Red Edge Position index) et le PRI (Photochemical Reflectance Index) (Lees *et al.*, 2018 ; Huemmrich *et al.*, 2010). La forme d'un modèle de LUE est la suivante :

$$GPP = fPAR \cdot PAR \cdot \eta \quad (1)$$

où  $\eta$  représente l'efficacité de conversion de la lumière en biomasse (C/J), une mesure de la capacité de la végétation à transformer le carbone en biomasse à partir de l'énergie.

gie solaire absorbée. Cette efficacité est généralement définie comme spécifique à chaque écosystème ou type de végétation, mais doit être ajustée en fonction de contraintes environnementales telles que la température de l'air, la disponibilité en eau et la disponibilité en nutriments. Par conséquent,  $\eta$  peut être exprimé comme suit :

$$\eta = \min(f(x_1), f(x_2), \dots, f(x_n)) \cdot \eta_{max} \quad (2)$$

où  $\eta_{max}$  représente l'efficacité de conversion de la lumière en biomasse dans des conditions optimales et les  $f(x_i)$  représentent les fonctions de stress environnemental dont les valeurs sont contraintes entre 0 et 1. Dans les régions arctiques et boréales, la disponibilité en eau et la température de l'air sont considérées comme des limitations environnementales importantes (Angert *et al.*, 2005; Jones *et al.*, 2017; Stocker *et al.*, 2018). Dans de tels environnements, l'humidité du sol est couramment utilisée pour évaluer la disponibilité en eau.

Une approche alternative pour estimer la NPP consiste à calculer les échanges moyens de carbone à partir de la dynamique de la biomasse au-dessus du sol (Above-Ground Biomass ; AGB). Les variations d'AGB sur une période de temps donné peuvent être interprétées comme un gain ou une perte de carbone par la végétation (Turner *et al.*, 2004; Gough, 2011). Une source importante d'incertitudes à prendre en compte lors de l'utilisation de cette technique est le stockage d'eau par la végétation, qui peut être facilement interprété à tort comme de la biomasse. Ce défi peut être mitigé en séparant les variations de courte durée (i.e., diurne) associées principalement à la variation des stocks d'eau de la végétation, aux variations de longue durée (i.e., saisonnière ou interannuelle) associées principalement aux variations de biomasse végétale (Konings *et al.*, 2019). La simplicité de la méthode AGB lui confère un avantage évident, bien qu'elle ne fournisse que des échanges de carbone moyens entre deux acquisitions de données et ne permet pas de comprendre les processus sous-jacents au cycle du carbone.

Pendant la saison de croissance, à la fois dans la toundra arctique et la forêt boréale, la GPP domine généralement la NEP faisant de ces environnements des puits de carbone (Ciais *et al.*, 2019). Cependant, en hiver, la photosynthèse cesse ( $GPP \approx 0$ ) puisque le sol gèle, la végétation au niveau du sol est recouverte de neige, la végétation entre dans un état de dormance déclenché par des températures sous zéro et l'illumination solaire qui diminue considérablement (Kimball *et al.*, 2004b). Néanmoins, la respiration au niveau du sol perdure tout au long de la saison hivernale bien qu'elle soit ralentie (Natali *et al.*, 2019; Mavrovic *et al.*, 2023b).

### **2.2.2 Respiration autotrophe**

La  $R_a$  de la végétation est étroitement liée à la photosynthèse. Par conséquent, la  $R_a$  est généralement estimée comme une fraction fixe de la GPP dans les modèles écosystémiques. Cette fraction fixe est spécifique à chaque biome ou type de végétation et est évaluée de manière empirique (Kimball *et al.*, 2009; Jones *et al.*, 2017). Par conséquent, les facteurs qui influencent la  $R_a$  sont les mêmes que ceux qui influencent la GPP.

### **2.2.3 Respiration hétérotrophe**

La majeure partie des stocks de carbone des régions arctiques et boréales se trouve sous forme de carbone organique du sol (Soil Organic Carbon : SOC). Le SOC représente au moins cinq fois plus de carbone que la biomasse au-dessus du sol dans la forêt boréale et une proportion encore plus grande dans la toundra arctique (Malhi *et al.*, 1999; Bradshaw and Warkentin, 2015). La catégorisation et la terminologie des différents types de SOC sont des sujets controversés et débattus par les experts (Derrien *et al.*, 2023). La catégorisation du modèle d'échange de carbone L4C de la NASA (Sect. 7.2) sera présentée ici afin de fournir une vie d'ensemble simplifiée des modèles de dégradation en cascade du SOC. Pour ce faire, trois types de SOC seront distingués : le carbone labile ou métabolique provenant principalement des ajouts récents de matière organique et ayant un taux de renouvellement rapide (feuilles, racines fines et branches), le carbone structurel composé de carbone à taux de renouvellement modéré (grosses racines et troncs) et le carbone récalcitrant ou stable composé de carbone à taux de renouvellement lent (carbone lié à l'argile, à des minéraux secondaires et au pergélisol, tanins et phénols). Les carbones labile et structurel ont généralement un taux de renouvellement de moins de cinq ans, tandis que le carbone récalcitrant peut avoir un taux de renouvellement de plusieurs centaines voire milliers d'années. L'accumulation du SOC provient de la litière qui contribue au carbone labile et structurel. La  $R_h$  représente les pertes de SOC provoquées par la respiration microbienne du sol. La  $R_h$  est typiquement estimé à partir d'un modèle de dégradation en cascade des différents types de SOC (Fig. 2.2). La chute de litière est typiquement estimée comme une fraction de la NPP en fonction du type de végétation. Par la suite, le carbone peut migrer vers un type de carbone à taux de renouvellement plus lent en fonction des conditions environnementales telles que la composition, la température et l'humidité du sol. Les principaux facteurs des taux de décomposition des différents types de SOC sont la température du sol, l'humidité du sol et la profondeur de la couche active du pergélisol (Sitch *et al.*, 2007; Kimball *et al.*, 2009; Jones *et al.*, 2017; Huntzinger *et al.*, 2020). Alors que la  $R_h$  a tendance à augmenter avec la température du sol, l'influence de l'humidité du sol décroît par rapport à un seuil optimal. L'impact de l'humidité du sol est particulièrement prévalent dans les tourbières puisque ce type d'environnement contient les plus grands stocks de carbone des latitudes nordiques. Dans

les tourbières, on retrouve généralement une  $R_h$  plus élevée à des niveaux d'humidité du sol inférieurs à la normale (Lees *et al.*, 2018).

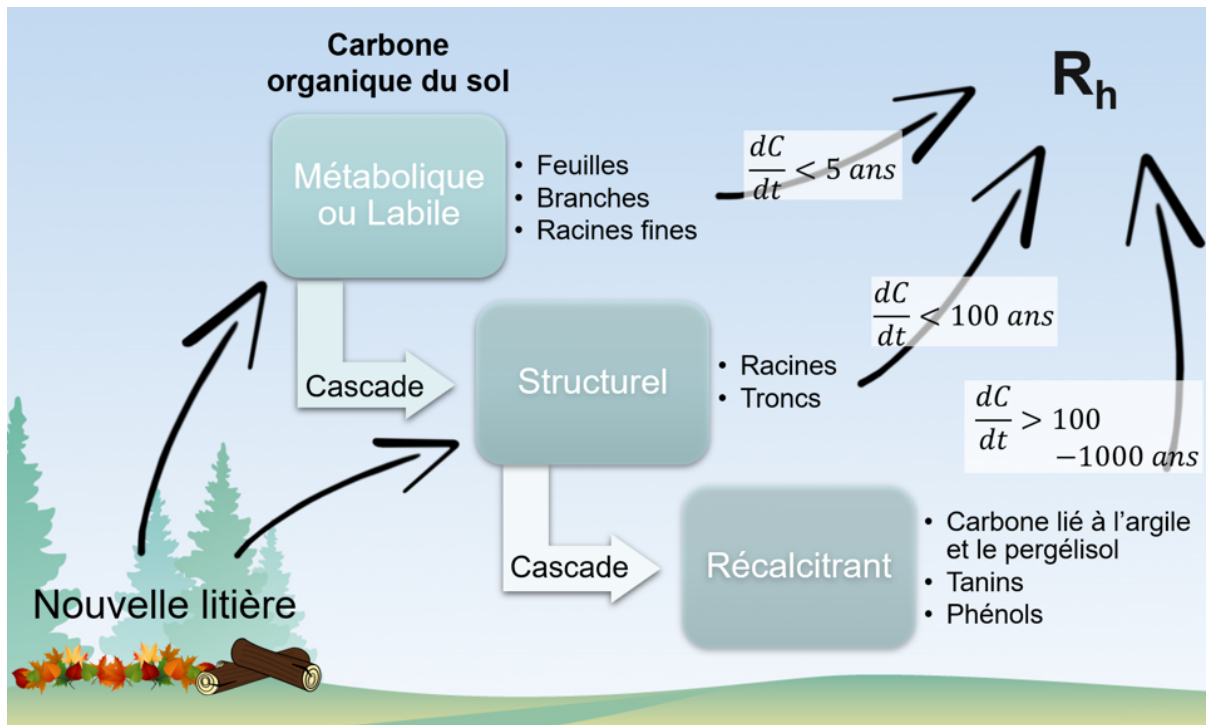


FIGURE 2.2 – Modèle de dégradation en cascade des différents types de carbone organique du sol pour estimer la respiration hétérotrophe. Ce modèle est similaire à celui du produit SMAP L4C (Jones *et al.*, 2017).

Contrairement à la photosynthèse, la  $R_{eco}$  se poursuit pendant les mois d'hiver dans les régions arctiques et boréales. Bien que les flux soient plus faibles que lors de la saison de croissance, la respiration hivernale a un impact significatif sur le bilan annuel, en particulier dans les régions où la saison de croissance ne dure que quelques mois (Elberling *et al.*, 2007 ; Webb *et al.*, 2016 ; Natali *et al.*, 2019). Les flux de  $CO_2$  en hiver ne sont pas aussi bien compris et étudiés que les flux de la saison de croissance en raison de la disponibilité limitée des données. Cependant, il a été démontré lors d'expériences en laboratoire et sur le terrain que les flux de  $CO_2$  ne sont pas négligeables en dessous du point de congélation et présentent une forte corrélation avec la température du sol (Fahnestock *et al.*, 1998 et 1999 ; Welker *et al.*, 2000 ; Mikan *et al.*, 2002 ; Panikov *et al.*, 2006 ; Natali *et al.*, 2019). Si la respiration microbienne est possible en hiver, c'est grâce aux propriétés isolantes de la neige qui permettent au sol de maintenir des températures suffisamment élevées pour la  $R_h$  malgré les températures glaciales de l'air ambiant (Brooks *et al.*, 1997 ; Brooks and Williams, 1999 ; Elberling *et al.*, 2007). Certaines études ont démontré une corrélation entre les flux de carbone et la profondeur de la neige (Welker *et al.*, 2000 ; Elberling *et al.*, 2007 ; Björkman *et al.*, 2010 ; Rogers *et al.*, 2010 ; Natali *et al.*, 2019).

#### 2.2.4 Méthane

Les bilans annuels et les processus régissant les échanges de  $CH_4$  ne sont pas aussi bien compris que ceux du  $CO_2$  (Saunois *et al.*, 2016; Arora *et al.*, 2018). Notamment, les émissions de méthane provenant des milieux humides et la séquestration du  $CH_4$  atmosphérique par sols bien drainés sont typiquement évaluées séparément puisque peu de modèles généralistes fiables semblent pas disponibles actuellement. Bien que les estimations des modèles se comparent favorablement aux mesures *in situ* dans certaines circonstances durant la saison de croissance, il reste beaucoup d'améliorations à apporter aux modèles pour en dire autant en hiver (Ito *et al.*, 2023).

La production de  $CH_4$  des milieux humides sont typiquement estimées à partir de relations empiriques basées sur ses principaux contrôles environnementaux. Les principaux contrôles sont : (1) la position de la nappe phréatique, en dessous de laquelle le  $CH_4$  est produit en raison de la décomposition anoxique de la matière organique disponible et au-dessus de laquelle le  $CH_4$  est oxydé, (2) la température du sol déterminant la vitesse de décomposition de la matière organique disponible, (3) la disponibilité et qualité de la matière organique disponible pour les processus de décomposition, et (4) les voies de transports par lesquelles le  $CH_4$  se déplace vers l'atmosphère (Walter et Heimann, 2000; Arora *et al.*, 2018; Kleinen *et al.*, 2020; Liu *et al.*, 2020). La  $R_h$  est fréquemment utilisée comme contrôle environnemental afin d'estimer les émissions de  $CH_4$  à partir de relations empiriques (Arora *et al.*, 2018).

La séquestration du  $CH_4$  par les sols bien drainés est typiquement estimé à partir de relations empiriques basées sur la diffusion et l'oxydation du  $CH_4$  (Curry, 2007; Arora *et al.*, 2018; Liu *et al.*, 2020; Shu *et al.*, 2020). La diffusion du  $CH_4$  dépend principalement de la porosité du sol et augmente à mesure que l'humidité du sol diminue. L'oxydation du  $CH_4$  par les micro-organismes dépend principalement de l'humidité et de la température du sol (Christensen *et al.*, 2003; Gedney *et al.*, 2004; Luo *et al.*, 2013). L'oxydation est maximisée lorsque les sols ne sont ni trop secs (lorsque l'activité microbienne est limitée par le faible taux d'humidité du sol) ni trop humides (lorsque les micro-organismes sont privés d'oxygène) tandis que l'oxydation du  $CH_4$  dans le sol augmente avec la température.

### 2.3 Télédétection et science du carbone

La vaste étendue et l'isolement des régions arctiques et boréales rendent les observations *in situ* difficiles et coûteuses. Afin d'étendre la modélisation du cycle du carbone à l'échelle régionale ou globale, il est souvent nécessaire d'exploiter les données de télédétection satellitaire (Fisher *et al.*, 2018; Lees *et al.*, 2018). Bien qu'il ne soit pas possible

d'obtenir des mesures directes de flux de  $CO_2$  et de  $CH_4$  par télédétection satellitaire, il est possible de collecter des données temporelles sur les variables clés impliquées dans les processus du cycle du carbone et, par conséquent, critiques pour les modèles écosystémiques (Du *et al.*, 2019).

Au cours de la dernière décennie, la télédétection visible et infrarouge a été largement utilisée pour soutenir la science du cycle du carbone dans les régions arctiques et boréales (Turner *et al.*, 2004 ; Mao *et al.*, 2016, Lees *et al.*, 2018 ; Xiao *et al.*, 2019). Ces observations ont été notamment utilisées pour évaluer les indices spectraux de végétation reliés à l'abondance et la productivité de la végétation (e.g., indice de végétation par différence normalisée [Normalized difference vegetation index : NDVI] ; Tucker, 1979 ; Lees *et al.*, 2018 ; Du *et al.*, 2019), les perturbations forestières (e.g., incendies, mortalité des arbres ; Kim *et al.*, 2012), le type d'occupation du sol (Kimball *et al.*, 2009), la structure de la végétation (e.g., détection et estimation de la distance par laser [Light Detection and Ranging : LiDAR] ; Xiao *et al.*, 2019), l'étendue de la couverture de neige (Hori *et al.*, 2017), la température de surface (Sitch *et al.*, 2007 ; Xiao *et al.*, 2019), l'albédo (Xiao *et al.*, 2019), la fluorescence de la chlorophylle induite par le soleil (Wohlfahrt *et al.*, 2018 ; Magney *et al.*, 2019) et la concentration en  $CO_2$  atmosphérique (Buchwitz *et al.*, 2007 ; Tu *et al.*, 2020 ; Lorente *et al.*, 2021).

La télédétection micro-onde n'a pas été autant exploité que le visible et l'infrarouge pour le cycle du carbone, mais présente plusieurs avantages tels que sa relative insensibilité à l'atténuation atmosphérique, à la couverture nuageuse et à l'illumination solaire, ce qui est essentiel pendant les mois d'hiver dans les régions connaissant la nuit polaire (Sitch *et al.*, 2007 ; Kim *et al.*, 2012 ; Du *et al.*, 2019). La télédétection par micro-onde peut également être utilisée en synergie avec les radiomètres visibles et infrarouges pour maximiser les avantages d'une plus large gamme de fréquences du spectre électromagnétique (Sitch *et al.*, 2007 ; Kimball *et al.*, 2009 ; Arslan *et al.*, 2011 ; Kim *et al.*, 2012 ; Xiao *et al.*, 2019). Contrairement à la télédétection dans le visible et l'infrarouge, qui se limite à une information de surface, les longueurs d'onde plus longues des micro-ondes permettent aux micro-ondes de pénétrer dans la végétation, le sol et la couverture nuageuse, produisant ainsi des mesures en profondeur (Ulaby *et al.*, 1986). Cependant, une pénétration plus profonde signifie que le signal reçu est une combinaison de différentes composantes de l'environnement, généralement la végétation, le sol, la neige et l'atmosphère (Kerr *et al.*, 2012, Roy *et al.*, 2012 et 2014), ce qui rend l'interprétation du signal plus complexe. La télédétection micro-onde permet notamment d'estimer certaines propriétés de la neige tel que la profondeur et l'humidité de la neige (e.g., Nagler and Rott, 2000 ; Takala *et al.*, 2011 ; Lievens *et al.*, 2019), la profondeur optique de la végétation (Vegetation Optical Depth : VOD) qui est reliée à la biomasse au-dessus du sol et à la

teneur en eau liquide de la végétation (Konings *et al.*, 2017 et 2019 ; Mialon *et al.*, 2020), l’humidité du sol (Kerr *et al.*, 2012 ; Colliander *et al.* 2017) et l’état de gel/dégel (Kim *et al.*, 2012 ; Roy *et al.*, 2015 ; Rautiainen *et al.*, 2016 ; Derksen *et al.*, 2017 ; Prince *et al.*, 2019).

La télédétection offre des opportunités sans précédent pour caractériser le moment, l’ampleur, les patrons et les tendances des changements environnementaux. La nature multi-échelle de la télédétection offre également un aperçu des propriétés spatiales et temporelles émergeantes des écosystèmes qui ne peuvent pas être observées ni comprises à l’échelle locale tout en fournissant des opportunités pour tester les modèles écosystémiques à grande échelle. Les observations à long terme provenant des capteurs satellitaires de télédétection ont produit des bases de données relativement précises documentant des changements significatifs dans les régions arctiques et boréales, mais leur amélioration nécessite des mesures *in situ* fiables, souvent spatialement et temporellement rares dans les régions arctiques et boréales (Sitch *et al.*, 2007 ; Lees *et al.*, 2018 ; Du *et al.*, 2019).

## Chapitre 3 : Flux hivernaux de $CO_2$

### 3.1 Présentation de l'article scientifique

L'article scientifique qui suit a été soumis à la revue scientifique *Biogeosciences* (European Geosciences Union : EGU) le 29 mai 2023, a été accepté pour publication le 2 novembre 2023 et a été publié le 20 décembre 2023. L'article y est présenté de façon intégrale tel que publié. La numérotation des lignes, sections, figures, tableaux et équations est indépendante du reste de la thèse. Les références citées dans cet article ne sont pas répétées à la bibliographie complémentaire de la thèse (Sect. 10). Le matériel supplémentaire accompagnant l'article se trouve à la suite de ce dernier (Sect. 3.3.6).

Cet article présente des mesures de flux de  $CO_2$  hivernaux sur différents sites en régions arctiques et boréales afin de déterminer les principaux contrôles environnementaux (Objectifs spécifiques # 1 et # 2). La méthode de mesure des flux de  $CO_2$  à partir de la méthode du gradient de diffusion à travers le couvert neigeux est une technique qui avait déjà été explorée à dans d'autres études (Sommerfeld *et al.*, 1993; Jones *et al.*, 1999; McDowell *et al.*, 2000; Seok *et al.*, 2009; Zhu *et al.*, 2014). Néanmoins, cette technique n'avait été utilisée que dans un contexte exploratoire de validation ou pour des études portant sur un très petit nombre de sites d'études. Dans le cadre de cette thèse, la méthode du gradient de diffusion à travers le couvert neigeux a été optimisée, testée et validée avant d'être déployée à une échelle inédite en termes de quantité de mesures, de sites d'études et de types d'environnements. Ceci a permis d'obtenir la plus grande base de données actuellement disponible sur la variabilité spatiale des flux de  $CO_2$  en hiver dans les régions arctiques et boréales. Pour la première fois, une analyse complète et détaillée de l'incertitude de cette méthode est présentée dans l'article qui suit.

Contribution en tant que premier auteur : Conception et planification de l'étude. Organisation des campagnes de terrains. Implémentation de la méthode de mesure. Collecte, traitement et analyse des données. Rédaction du manuscrit.

Référence complète de l'article :

**Mavrovic, A., Sonnentag, O., Lemmetyinen, J., Voigt, C., Rutter, N., Mann, P., Sylvain, J.-D., and Roy, A. (2023b)** Environmental controls of winter soil carbon dioxide fluxes in boreal and tundra environments. *Biogeosciences*, vol. 20, no<sup>o</sup> 24, p. 5087–5108, doi : [10.5194/bg-20-5087-2023](https://doi.org/10.5194/bg-20-5087-2023).

### 3.2 Résumé de l'article scientifique en français

Le cycle du carbone dans les régions arctiques et boréales (RAB) est une composante importante du bilan de carbone planétaire présentant des préoccupations croissantes concernant les conséquences du réchauffement climatique des RAB sur le système climatique global. L'hiver est la période de l'année où la plus grande incertitude dans les bilans annuels de dioxyde de carbone ( $CO_2$ ) demeure en raison des défis liés à la rareté et la couverture spatiale limitée des données disponibles. L'objectif de cette étude est de déterminer les principaux contrôles environnementaux des flux de  $CO_2$  en hiver dans les RAB sur un gradient latitudinal (de 45°N à 69°N) comprenant quatre types d'écosystèmes différents : forêt boréale de conifères à couronne fermée, forêt boréale de conifères à couronne ouverte, toundra à arbustes dressés et toundra à arbustes couchés. Les flux de  $CO_2$  calculés à l'aide de la méthode du gradient de diffusion à travers la couverture neigeuse ( $n = 560$ ) variaient de 0 à  $1,05 \text{ gC m}^2 \text{ jour}^{-1}$ . Afin de déterminer les principaux contrôles environnementaux sur les flux de  $CO_2$  en hiver, l'approche d'apprentissage automatique Random Forest a été utilisée. Nous avons ainsi déterminé que la température du sol était le principal contrôle des flux de  $CO_2$  en hiver, avec 68 % d'importance relative dans le modèle, sauf lorsque de l'eau liquide se trouvait dans le sol (c'est-à-dire  $T_{sol} \approx 0^\circ C$  et coexistence d'eau liquide avec de la glace dans les pores du sol). Dans ces conditions, la teneur en eau liquide est devenue le principal contrôle des flux de  $CO_2$ , avec 87 % d'importance relative dans le modèle. Nous avons observé des régressions exponentielles entre les flux de  $CO_2$  et la température du sol lorsque le sol était complètement gelé ( $RMSE = 0,024 \text{ gC m}^2 \text{ jour}^{-1}$ ; 70,3 % des  $F_{CO_2}$  moyens) et dans les sols près du point de congélation ( $RMSE = 0,286 \text{ gC m}^2 \text{ jour}^{-1}$ ; 112,4 % des  $F_{CO_2}$  moyens).  $F_{CO_2}$  augmente plus rapidement avec  $T_{sol}$  autour du point de congélation que lorsque  $T_{sol} < 5^\circ C$ . Dans des conditions près du point de congélation, la corrélation la plus forte a été trouvée avec la teneur en eau liquide dans le sol ( $RMSE = 0,137 \text{ gC m}^2 \text{ jour}^{-1}$ ; 49,1 % des  $F_{CO_2}$  moyens). Notre étude met en évidence le rôle de plusieurs variables environnementales dans la variabilité spatio-temporelle des flux de  $CO_2$  dans les RAB pendant l'hiver et souligne que les interactions complexes entre la végétation, la neige et le sol dans les environnements nordiques doivent être prises en compte afin d'évaluer la variabilité spatiale des émissions de  $CO_2$  du sol en hiver.



## Environmental controls of winter soil carbon dioxide fluxes in boreal and tundra environments

Alex Mavrovic<sup>1,2,3,4</sup>, Oliver Sonnentag<sup>2,4</sup>, Juha Lemmetyinen<sup>5</sup>, Carolina Voigt<sup>4,6,9</sup>, Nick Rutter<sup>7</sup>, Paul Mann<sup>7</sup>, Jean-Daniel Sylvain<sup>8</sup>, and Alexandre Roy<sup>1,2</sup>

<sup>1</sup>Département des sciences de l'environnement, Université du Québec à Trois-Rivières, Trois-Rivières, Quebec, G9A 5H7, Canada

<sup>2</sup>Centre d'Études Nordiques, Québec, Quebec, G1V 0A6, Canada

<sup>3</sup>Polar Knowledge Canada, Canadian High Arctic Research Station campus, Cambridge Bay, Nunavut, X0B 0C0, Canada

<sup>4</sup>Département de géographie, Université de Montréal, Montréal, Quebec, H3T 1J4, Canada

<sup>5</sup>Finnish Meteorological Institute, Helsinki, 00560, Finland

<sup>6</sup>Department of Environmental and Biological Sciences, University of Eastern Finland, Kuopio, 70211, Finland

<sup>7</sup>Geography and Environmental Sciences Department, Northumbria University, Newcastle upon Tyne, NE1 8ST, UK

<sup>8</sup>Ministère des Ressources naturelles et des Forêts, Québec, Quebec, G1H 6R1, Canada

<sup>9</sup>Institute of Soil Science, Universität Hamburg, Hamburg, 20146, Germany

**Correspondence:** Alex Mavrovic (alex.mavrovic@uqtr.ca)

Received: 29 May 2023 – Discussion started: 12 June 2023

Revised: 22 October 2023 – Accepted: 2 November 2023 – Published: 20 December 2023

**Abstract.** The carbon cycle in Arctic–boreal regions (ABRs) is an important component of the planetary carbon balance, with growing concerns about the consequences of ABR warming for the global climate system. The greatest uncertainty in annual carbon dioxide ( $\text{CO}_2$ ) budgets exists during winter, primarily due to challenges with data availability and limited spatial coverage in measurements. The goal of this study was to determine the main environmental controls of winter  $\text{CO}_2$  fluxes in ABRs over a latitudinal gradient (45° to 69° N) featuring four different ecosystem types: closed-crown coniferous boreal forest, open-crown coniferous boreal forest, erect-shrub tundra, and prostrate-shrub tundra.  $\text{CO}_2$  fluxes calculated using a snowpack diffusion gradient method ( $n = 560$ ) ranged from 0 to 1.05  $\text{g C m}^{-2} \text{ d}^{-1}$ . To assess the dominant environmental controls governing  $\text{CO}_2$  fluxes, a random forest machine learning approach was used. We identified soil temperature as the main control of winter  $\text{CO}_2$  fluxes with 68 % of relative model importance, except when soil liquid water occurred during 0 °C curtain conditions (i.e.,  $T_{\text{soil}} \approx 0^\circ\text{C}$  and liquid water coexist with ice in soil pores). Under zero-curtain conditions, liquid water content became the main control of  $\text{CO}_2$  fluxes with 87 % of relative model importance. We observed expo-

nential regressions between  $\text{CO}_2$  fluxes and soil temperature in fully frozen soils ( $\text{RMSE} = 0.024 \text{ g C m}^{-2} \text{ d}^{-1}$ ; 70.3 % of mean  $F_{\text{CO}_2}$ ) and soils around the freezing point ( $\text{RMSE} = 0.286 \text{ g C m}^{-2} \text{ d}^{-1}$ ; 112.4 % of mean  $F_{\text{CO}_2}$ ).  $F_{\text{CO}_2}$  increases more rapidly with  $T_{\text{soil}}$  around the freezing point than at  $T_{\text{soil}} < 5^\circ\text{C}$ . In zero-curtain conditions, the strongest regression was found with soil liquid water content ( $\text{RMSE} = 0.137 \text{ g C m}^{-2} \text{ d}^{-1}$ ; 49.1 % of mean  $F_{\text{CO}_2}$ ). This study shows the role of several variables in the spatio-temporal variability in  $\text{CO}_2$  fluxes in ABRs during winter and highlights that the complex vegetation–snow–soil interactions in northern environments must be considered when studying what drives the spatial variability in soil carbon emissions during winter.

### 1 Introduction

Carbon stocks and fluxes in the Arctic and boreal biomes (hereafter called Arctic–boreal regions; ABRs) constitute large components of the planetary carbon balance (Tarnocai et al., 2009; van Huissteden and Dolman, 2012; Carreiras et al., 2017). ABRs store substantial quantities of carbon due to inherently slow decomposition rates, largely attributable

to cold temperatures (Ravn et al., 2020). ABRs are warming up to 4 times faster than the rest of the planet with potential feedbacks to the global climate system (Derksen et al., 2019; Rantanen et al., 2022). Although ongoing warming of ABRs has the potential to lengthen growing seasons, enhance plant growth, and increase aboveground carbon storage (Sturm et al., 2005; McMahon et al., 2010), the growing-season vegetation response is variable and complex (Myers-Smith et al., 2020). Warmer air and soil temperatures enhance production and release of carbon dioxide ( $\text{CO}_2$ ) from ecosystem respiration, comprising heterotrophic respiration by microbes decomposing soil organic matter, and autotrophic respiration by above- and belowground plant components (Bond-Lamberty and Thomson, 2010). The release of previously frozen carbon stocks is particularly important in regions undergoing permafrost thaw (ground completely frozen for at least 2 consecutive years) (Schuur et al., 2015; Natali et al., 2021; Miner et al., 2022). If increases in ecosystem respiration exceed those of photosynthetic  $\text{CO}_2$  uptake from enhanced plant growth, ABRs may shift from a weak net  $\text{CO}_2$  sink to a net  $\text{CO}_2$  source, thereby generating a potentially non-negligible positive feedback to the global climate system (Hayes et al., 2011; Gauthier et al., 2015; Natali et al., 2019; Bruhwiler et al., 2021; Virkkala et al., 2021; Braghieri et al., 2023).

During winter months in ABRs, landscapes are generally snow-covered and photosynthesis is considered negligible, and therefore winter  $\text{CO}_2$  fluxes derive primarily from soil respiration (Christiansen et al., 2012; Webb et al., 2016). It is expected that complex soil–vegetation–snow interactions will lead to regional and local variability in soil respiration rates across ABRs because of relationships between vegetation types, snow cover, soil properties, soil moisture, and soil temperature (Gouttevin et al., 2012; Busseau et al., 2017; Lorranty et al., 2018; Grünberg et al., 2020; Royer et al., 2021). Higher soil temperatures promote microbial activity and increase  $\text{CO}_2$  production from soil organic matter decomposition during winter (Natali et al., 2019). A snowpack acts as an important thermal insulative layer for the soil during winter, keeping soils warmer than the ambient air (Domine et al., 2016b). Vegetation affects snow properties by increasing snow depth where wind trapping occurs (Callaghan et al., 2011a, b; Busseau et al., 2017), decreasing snow density and thermal conductivity around shrubs (Gouttevin et al., 2012; Domine et al., 2015, 2016a), decreasing albedo due to protruding branches (Ménard et al., 2012), and causing earlier spring snowmelt due to vegetation thermal conductivity (Wilcox et al., 2019; Kropp et al., 2022). However, Dominé et al. (2022) showed that shrub branches within the snowpack can contribute to mid-winter soil cooling by conducting temperature through the snowpack. Hence, the complex vegetation–snow–soil interactions in northern environments must be considered when studying what drives the spatial variability in soil carbon emissions during winter. Soil microbial activity can also be limited by lack or saturation of available water, meaning that higher amounts of available soil liq-

uid water content (LWC) should allow higher heterotrophic respiration rates by increasing soil microbial activity as long as the soil environment is not anaerobic (Linn and Doran, 1984; Knowles et al., 2015). Anaerobic soil conditions are usually found in fully water saturated soils.

High uncertainties in winter ABR  $\text{CO}_2$  exchange between the ground surface and atmosphere are in part due to limited data availability because of difficulties in accessing these vast, remote regions and the harsh winter conditions creating technical challenges for  $\text{CO}_2$  fluxes measurements (Natali et al., 2019; Virkkala et al., 2022). Methods currently available to measure wintertime  $\text{CO}_2$  fluxes include (1) the eddy covariance technique (Baldocchi, 2003), (2) chamber measurements under or above the snowpack (McDowell et al., 2000), and (3) snowpack gradient diffusion methods (Sommerfeld et al., 1993). Each of these has their advantages and limitations. The eddy covariance (EC) technique exploits the atmosphere's turbulent nature to estimate net  $\text{CO}_2$  fluxes at high temporal resolution without environmental disturbance (Baldocchi et al., 2001; Pastorello et al., 2020). Data gaps are common during the ABR winter since the EC equipment is energy-intensive and prone to failure in low temperatures. In addition, solar power supply systems are limited by low sunlight (Jentzsch et al., 2021; Pallandt et al., 2022). Furthermore, the EC equipment is stationary and covers a large footprint (250–3000 m). In contrast, plot-scale chamber techniques for measuring  $\text{CO}_2$  fluxes are portable methods with a small footprint (< 1 m) (Subke et al., 2021; Maier et al., 2022). Chambers can be used either above the snowpack or directly on the ground. Placing a chamber on the snowpack does not provide a direct measurement of soil  $\text{CO}_2$  fluxes due to  $\text{CO}_2$  retention and lateral diffusion within snowpacks, generally creating a negative bias and uncertainties linking the snow and/or atmosphere fluxes to soil fluxes (McDowell et al., 2000; Björkman et al., 2010; Webb et al., 2016). Chambers can also be placed directly on the ground by excavating the snow cover (Elberling, 2007), providing a direct measurement of soil  $\text{CO}_2$  fluxes that is, however, prone to a positive bias generated by a tunnel effect due to the snow excavation (McDowell et al., 2000; Björkman et al., 2010). Unavoidable snow cover disturbance also reduces the possibility of revisiting locations for temporal surveys because the soil thermal regime is altered by the snow disturbance. Alternatively, permanent chambers can be installed before the first snowfall, but this disturbs the state of the ground and snow cover around the chamber (Webb et al., 2016). The snowpack diffusion gradient method uses snow porosity and tortuosity to estimate  $\text{CO}_2$  fluxes from the gas concentration gradient along a vertical snow profile including ambient air above the snowpack (Sommerfeld et al., 1993; Pirk et al., 2016; Kim et al., 2019). In this study, the snowpack diffusion gradient method will be used to evaluate the spatial variability in  $\text{CO}_2$  fluxes in ABRs because of its portability and minimal environmental disturbance.

The goal of this study was to determine the main environmental controls of winter CO<sub>2</sub> fluxes in ABRs. A total of 560 snowpack diffusion gradient measurements were made over a latitudinal gradient of four different ecosystem types common in ABRs in Canada: closed-crown coniferous boreal forest, open-crown coniferous boreal forest, erect-shrub tundra, and prostrate-shrub tundra. Spatio-temporal measurements of snowpack CO<sub>2</sub> diffusion gradients were performed at several locations in the four sites during the 2020–2021 and 2021–2022 winters (December to May). Firstly, a random forest (RF) machine learning analysis was used to evaluate the relative importance of the following environmental variables known to exert control over winter CO<sub>2</sub> fluxes: soil temperature, soil LWC, vegetation type, snow water equivalent, snow depth, and several snow-density-related measurements. Secondly, the response of and uncertainty in winter CO<sub>2</sub> fluxes to the most impactful environment variables determined by the RF model were quantified through regression analysis.

## 2 Method

### 2.1 Study sites

To cover different vegetation types and a wide range of soil temperature ( $T_{\text{soil}}$ ) regimes and snow conditions found in ABRs, four study sites were selected across Canada (Fig. 1 and Table 1). Each site represents a specific ecosystem type (Royer et al., 2021), and vegetation types within each of those ecosystems were determined using vegetation maps specific to each site. Cambridge Bay (CB), situated on Victoria Island in the Canadian Arctic Archipelago was the northernmost site located in the Arctic tundra, dominated by lichen and prostrate-shrub tundra. Ponomarenko et al. (2019) generated a detailed ecotype map of the Arctic tundra biome present in the CB study area. Here, these ecotypes were grouped by water availability into three tundra vegetation types from which the sampling locations ( $S$ ) were selected: dry ( $S = 94$ ), sub-hydric ( $S = 24$ ), and hydric ( $S = 110$ ). Trail Valley Creek (TVC), Northwest Territories, situated just north of the treeline in the transitional zone between the boreal and Arctic biomes close to the Mackenzie Delta, is dominated by erect-shrub tundra with remaining tree patches (Martin et al., 2022). Grünberg et al. (2020) produced a vegetation map of the TVC study area using airborne orthophotos, vegetation height, and field observations from which seven vegetation types and landforms were identified: lichen ( $S = 68$ ), tussock ( $S = 21$ ), dwarf shrub ( $S = 19$ ), tall shrub ( $S = 26$ ), polygon ( $S = 21$ ), riparian shrub ( $S = 17$ ), and black spruce tree patch ( $S = 18$ ). Havikpak Creek (HPC) is located just south of the treeline, at about 50 km south of TVC in an open-crown black-spruce-dominated forest constituting the only type of vegetation present ( $S = 30$ ) (Krogh et al., 2017). Montmorency Forest (MM) is the southern-

most site located in a closed-crown balsam-fir-dominated boreal forest constituting the only type of vegetation present ( $S = 110$ ) (Barry et al., 1988). The CB, TVC, and HPC sites are underlain by continuous permafrost, while the MM site is permafrost-free.

### 2.2 Snowpack diffusion gradient method

#### 2.2.1 Theoretical framework for CO<sub>2</sub> flux calculation

During winter in ABRs, soil respiration produces CO<sub>2</sub> below the snowpack. Consequently, a vertical CO<sub>2</sub> diffusion gradient is maintained through the snowpack ( $d[\text{CO}_2]/dz$ ; g C m<sup>-4</sup>), with CO<sub>2</sub> concentration ([CO<sub>2</sub>]; g C m<sup>-3</sup>) decreasing with snow height from the soil surface ( $z$ ; m) (Jones et al., 1999). Hereafter, [CO<sub>2</sub>] is expressed in grams of carbon per cubic meter but units of concentration could also be expressed in relative units (i.e., parts per million – ppm) using the ideal gas law. The snowpack diffusion gradient method uses  $d[\text{CO}_2]/dz$  within the snowpack and Fick's first law for gas diffusion through porous media to estimate CO<sub>2</sub> fluxes ( $F_{\text{CO}_2}$ ; g C m<sup>-2</sup> d<sup>-1</sup>) (Sommerfeld et al., 1993; Zhu et al., 2014):

$$F_{\text{CO}_2} = -\varphi \tau D_a \frac{d[\text{CO}_2]}{dz}, \quad (1)$$

where  $\varphi$  represents the porosity of the snow medium,  $\tau$  its tortuosity, and  $D_a$  the air diffusion coefficient of the diffused gas in square meters per day. The porosity of snow can be assessed from its density (Kinar and Pomeroy, 2015):

$$\varphi = 1 - \frac{\rho_{\text{snow}}}{\rho_{\text{ice}}} + \theta \cdot \left( \frac{\rho_{\text{water}}}{\rho_{\text{ice}}} - 1 \right), \quad (2)$$

where  $\rho$  represents the density of snow, water, and pure ice ( $\rho_{\text{ice}} = -0.0001 \cdot T_{\text{ice}} + 0.9168$  with  $T_{\text{ice}}$  as ice temperature in °C and  $\rho_{\text{ice}}$  in g cm<sup>-3</sup>; Harvey et al., 2017) and  $\theta$  is the snow liquid water content. The tortuosity is strongly correlated with porosity. Du Plessis and Masliyah (1991) established the following relationship:

$$\tau = \frac{1 - (1 - \varphi)^{2/3}}{\varphi}. \quad (3)$$

Tortuosity can also be approximated as  $\tau \approx \varphi^{1/3}$  (Millington, 1959; Mast et al., 1998).  $d[\text{CO}_2]/dz$  is obtained by measuring the [CO<sub>2</sub>] vertical profile at various snow depths. Standard air diffusion coefficients of CO<sub>2</sub> (unit: m<sup>2</sup> d<sup>-1</sup>) are available in the literature but must be corrected for temperature and pressure (Marrero and Mason, 1972; Massman, 1998):

$$D_a = 0.2020 \cdot \left( \frac{T}{T_0} \right)^{1.590} \cdot e^{-\frac{0.3738}{T/T_0}}, \quad (4)$$

where  $T$  is the air temperature and  $T_0$  is the freezing point in kelvins. The diffusion gradient method assumes that gas

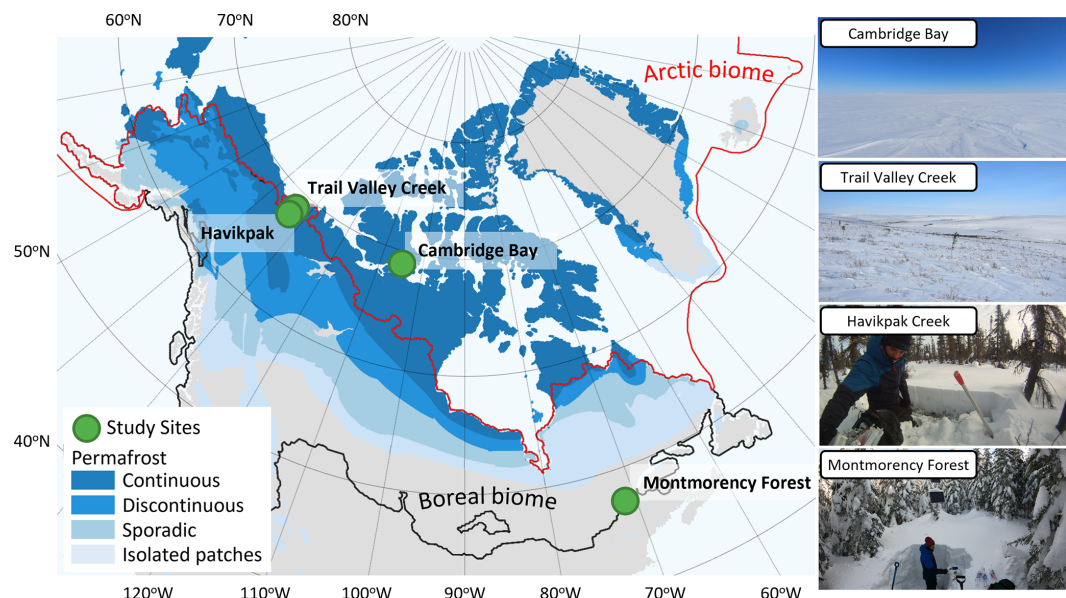


**Figure 1.** Study site locations in Canada. The Arctic biome is delimited following the Conservation of Arctic Flora and Fauna (CAFF) working group of the Arctic Council, and the boreal biome is delimited following Potapov et al. (2008). Permafrost extent (Brown et al., 2002) is estimated in percent area: continuous (> 90 %–100 %), discontinuous (> 50 %–90 %), sporadic (10 %–50 %), and isolated patches (< 10 %).

**Table 1.** Study sites with the number of sampling locations in Canada and the number of CO<sub>2</sub> flux measurements (*N*) for each site.

Site	Province/territory	Latitude, longitude	Ecosystem	Sampling locations	<i>N</i>	Measurement dates (YYYY-MM)	Site reference
Cambridge Bay	Nunavut	69°13' N, 104°54' W	Prostrate-shrub tundra	47	230	2021-04, 2021-15 2022-01 to 2022-05	Ponomarenko et al. (2019)
Trail Valley Creek	Northwest Territories	68°46' N, 133°28' W	Erect-shrub tundra	34	190	2021-03, 2021-04	Grünberg et al. (2020)
Havikpak Creek	Northwest Territories	68°19' N, 133°31' W	Open-crown coniferous boreal forest (black spruce)	5	30	2022-03	Krogh et al. (2017)
Montmorency Forest	Quebec	47°18' N, 71°10' W	Closed-crown coniferous boreal forest (balsam fir)	12	110	2021-01, 2021-02, 2021-12, 2022-01 to 2022-05	Barry et al. (1988)

fluxes are the result of simple, linear, gradient-induced diffusion in uniform porosity through snow cover (McDowell et al., 2000). A snowpack with strongly heterogeneous density (i.e., vertical stratification) can induce a bias when gas flow is altered by dense layers or ice crusts, typically leading to  $F_{\text{CO}_2}$  overestimation (Seok et al., 2009). Such layers were rarely found in our study sites. The diffusion gradient assumption also does not hold when strong wind events occur, decreasing snowpack CO<sub>2</sub> concentration through wind-pumping and inducing a negative bias in CO<sub>2</sub> fluxes (Seok et al., 2009). Consequently,  $d[\text{CO}_2]/dz$  was not measured in days following a strong wind event. Monitoring of  $F_{\text{CO}_2}$  at

a few sampling locations did not show any relationship between  $F_{\text{CO}_2}$  and wind speed or atmospheric pressure (e.g., Fig. A1).

### 2.2.2 Data collection

All data were collected during the 2020–2021 and 2021–2022 winters between December and May (Table 1). The CO<sub>2</sub> concentration gradient was measured by collecting gas samples at various depths in the snowpack. Each gradient profile consisted of five gas samples collected at (1) 5 cm above the snowpack (ambient air), (2) 5 cm depth below the

snowpack surface, (3) 1/3 of total snow depth, (4) 2/3 of total snow depth, and (5) the soil–snow interface. Gas present in snow pores was collected with a thin, hollow, stainless-steel rod (50–120 cm long, 4 mm outer diameter, and 2 mm inner diameter), starting with gas samples in the upper snowpack and then pushing the sampling rod downward to collect gas samples deeper in the snowpack to minimize snow disturbance (Fig. 2a). Gas was collected in a 60 mL syringe (Air-Tite Luer Lock, Virginia Beach, Virginia) connected to the rod via a three-way valve. Gases were transferred into 12 mL hermetic glass vials (Labco Exetainer®, Labco Ltd., Lampeter, UK), which were sent to the Université du Québec à Trois-Rivières laboratory to be measured with a gas analyzer to obtain CO<sub>2</sub> concentrations. At each site, several sampling locations were selected to cover the maximum range of vegetation types and snowpack characteristics, covering areas of 0.05–22.5 km<sup>2</sup>. At each sampling location, two to four replicate profiles were measured at 50 cm spacing to test the repeatability of the sampling. A minimal spacing of 57.5 cm was required between sampling positions, since it corresponds to the radius of the 60 mL sampling volume of each gas sample, based on a snow density range of 100–650 kg m<sup>-3</sup>.

For typical Arctic snowpacks, samples at 1/3 depth are usually in wind slabs, the dense and cohesive surface snow layer formed by strong Arctic winds. Samples at 2/3 depth are usually in depth hoar, the lower snow layer with low density and cohesion formed by a strong temperature gradient driving vertical vapor flux through the snowpack (Fig. 2b). Typically, boreal snowpacks are deeper than in Arctic tundra and display a more continuous vertical stratification with increasing snow density at the bottom of the snowpack. In HPC, snowpack depths were 40–80 cm in March, while snowpack depths at MM were 100–200 cm (Fig. A2). For comparison, by March, snowpacks at CB were 10–75 cm deep and 15–150 cm at TVC.

Once the gas samples were collected, a vertical profile of snow and soil properties was measured to calculate the CO<sub>2</sub> air diffusion coefficient from the snow temperature, as well as snow porosity and tortuosity from snow density. Snow properties were measured every 5 cm, including snow temperature (Snowmetrics digital thermometer; Fort Collins, Colorado; 1/10° resolution), snow density (Snowmetrics digital scale, 100 and 250 cm<sup>3</sup> snow cutters used to weigh snow samples;  $\sigma(\rho_{\text{snow}}) \approx 9\%$ ; Proksch et al., 2016), snow liquid water content (hand test from Fierz et al., 2009), and snow stratigraphy. Examples of snow vertical stratification along with CO<sub>2</sub> concentration measurements can be found in Appendix A (Fig. A3).  $T_{\text{soil}}$  was measured at 1 cm depth under the soil–snow interface as it was not possible to go deeper in frozen soil and no permanent sensors were installed (Snowmetrics digital thermometer; Fort Collins, Colorado; 1/10° resolution); three measurements of  $T_{\text{soil}}$  were averaged. Snow depth measurements were done with a ruler graduated every 1 cm ( $\sigma(d_{\text{snow}}) \approx 0.5$  cm).

The CO<sub>2</sub> concentration of 86 % of gas samples was measured using a LI-COR LI-7810 CH<sub>4</sub>/CO<sub>2</sub>/H<sub>2</sub>O Trace Gas Analyzer (LI-COR Biosciences, Lincoln, Nebraska;  $\sigma < 1\%$ ;  $N = 483$ ). The gas samples were passed through an open loop along a continuous flow of a 200 ppm CO<sub>2</sub> calibration gas (Linde Canada, Ottawa, Ontario, Canada). Based on a calibration curve using 0, 400, and 1000 ppm CO<sub>2</sub> calibration gases (Linde Canada), the CO<sub>2</sub> concentration of gas samples was calculated (detailed protocol: <https://www.licor.com/documents/xst0ld9jzfb78bmpdq9i7rmjjjmg>, last access: 9 December 2023).

Randomly distributed gas samples collected during the 2020–2021 winter were analyzed with a Picarro G2201-i CRDS gas analyzer (Picarro, Santa Clara, California;  $\sigma < 0.1\%$ ;  $N = 26$ ) to validate the method used with the LI-7810 to determine CO<sub>2</sub> concentration. CO<sub>2</sub> concentrations estimated from the LI-7810 and Picarro G2201-i gas analyzers were not significantly different in their concentration range and distribution (Fig. A4;  $R^2 = 0.92$ ). At TVC in March 2022, a portable LI-850 CO<sub>2</sub>/H<sub>2</sub>O Gas Analyzer was used ( $\sigma < 1.5\%$ ;  $N = 38$ ), allowing for CO<sub>2</sub> concentrations to be measured on the same day as sample collection (avoiding the need for bottling and transportation). CO<sub>2</sub> concentrations estimated from the LI-7810 and LI-850 gas analyzers were not significantly different in their concentration range and distribution (Fig. A4b;  $R^2 = 0.82$ ).

## 2.2.3 Evaluation of CO<sub>2</sub> flux uncertainties

An uncertainty assessment was conducted to evaluate CO<sub>2</sub> flux precision based on the snowpack diffusion gradient method. The uncertainty assessment focuses on random errors, as systematic errors are discussed at the end of Sect. 2.2.1. From sampling to flux estimation, several steps could add uncertainty to the results. Uncertainties can be subdivided into four sources: gas concentration estimates; gas transfer, transport, and storage; evaluation of the snowpack  $d[\text{CO}_2]/dz$ ; and snow pit measurements (i.e., snow density and temperature). Gas concentration uncertainties were evaluated from the gas analyzer precision as assessed by the manufacturer and tested using calibration gases. Six CO<sub>2</sub> reference gases of 400 ppm were bottled during two different field campaigns and were processed among the gas samples from the snowpack to ensure the transfer, transport, and storage protocol did not lead to sample contamination. The  $d[\text{CO}_2]/dz$  uncertainties were evaluated with the standard deviation from the coefficient of determination ( $\sigma = \sqrt{(1 - R^2)/(N - 1)}$ ; Bowley, 1928).  $F_{\text{CO}_2}$  uncertainty was estimated by propagation of the uncertainties in  $d[\text{CO}_2]/dz$  and snow density using Eq. (1) (Taylor, 1997). The uncertainty in  $\rho_{\text{snow}}$  was fixed at 9 % (Proksch et al., 2016), while the uncertainty in  $d[\text{CO}_2]/dz$  was estimated based on the root mean squared error of the linear regression for each snowpack concentration gradient measurement.

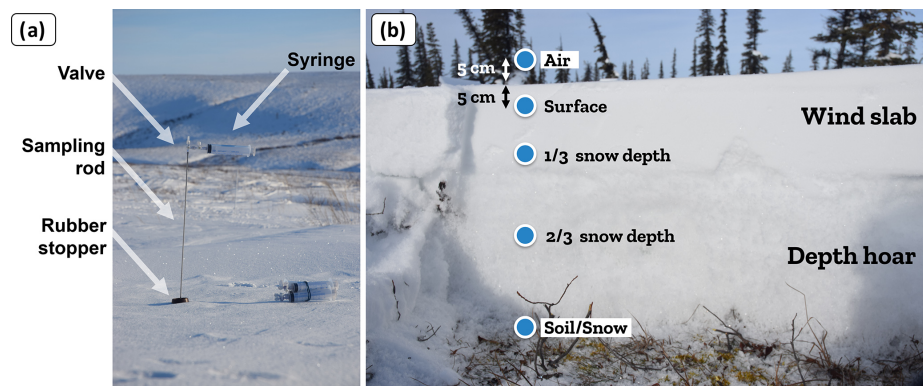


**Figure 2.** (a) Gas sampling equipment for the CO<sub>2</sub> concentration gradient measurement. (b) Typical snow depth profile of an Arctic snowpack (picture from Trail Valley Creek close to a tree patch).

### 2.3 Soil volumetric liquid water content at the Montmorency Forest site

Conditions of a 0 °C curtain exist when the soil temperature is around freezing point (0 °C) and a mix of ice and liquid water coexist in the soil pore space because the phase transition between water and ice is slowed due to latent heat (Outcalt et al., 1990). Hence, liquid water content (LWC; m<sup>3</sup> m<sup>-3</sup>) and ice fractions can be used as a freezing–thawing indicator during the zero-curtain period. The MM study sites were equipped with TEROS 12 soil moisture sensors (METER Group) at 5 cm depth. LWC was only monitored at the MM site since it was the only site where  $T_{\text{soil}}$  in upper layers remained around 0 °C for the whole winter, allowing the presence of liquid water in the soil throughout winter. The Zhang et al. (2010) empirical soil liquid water and ice mixing model was used to calculate soil liquid water content ( $m_{\text{uw}}$ ) (Eqs. 5 to 8). LWC was estimated to be negligible at the CB, TVC, and HPC sites since  $T_{\text{soil}}$  was between −5 and −25 °C. The model from Zhang et al. (2010) supports LWC, at  $T_{\text{soil}}$  colder than −5 °C, being negligible.

$$\text{LWC} = a \cdot \frac{\rho_b}{\rho_w} \cdot |T_{\text{soil}}|^{-b}, \quad (5)$$

$$\ln a = 0.5519 \cdot \ln \text{SSA} + 0.2618, \quad (6)$$

$$\ln b = -0.264 \cdot \ln \text{SSA} + 0.3711, \quad (6)$$

where  $\rho_w$  and  $\rho_b$  (g cm<sup>-3</sup>) represent liquid water and soil bulk density respectively,  $T_{\text{soil}}$  (°C) represents soil temperature, and SSA (m<sup>-1</sup>) represents soil particles' specific surface area described by Sepaskhah et al. (2010).

$$\text{SSA} = 3.89 \cdot d_g^{-0.905}, \quad (7)$$

$$\ln d_g = f_c \cdot \ln M_c + f_{si} \cdot \ln M_{si} + f_{sa} \cdot \ln M_{sa}, \quad (8)$$

where  $d_g$  represents the soil geometric mean particle-size diameter (mm) and  $f$  and  $M$  represent soil component fraction and mean particle-size diameter (mm). Soil components

are clay ( $M_c = 0.001$  mm), silt ( $M_{si} = 0.026$  mm), and sand ( $M_{sa} = 1.025$  mm). Soil bulk density and gravimetry was evaluated using a soil sampling protocol similar to the National Forest Inventory protocol (CFI, 2008). Undisturbed soil samples were collected in three homogenous horizons of a soil profile using 400 cm<sup>2</sup> cores. Volumetric soil samples were dried (103 °C) and weighed to determine bulk density. Gravimetric samples were used to determine sand (%), 50–2000 µm), silt (%), 2–50 µm), clay (%), < 2 µm), and organic content (g kg<sup>-1</sup>). The soil texture was determined by the hydrometer method (Bouyoucos, 1962), whereas the organic content was determined with a LECO organic analysis instrument (LECO Corporation, St. Joseph, Michigan).

### 2.4 Random forest algorithm

Random forest (RF) is an ensemble machine learning method based on a multitude of decision trees (Breiman, 2001). Each decision tree of our RF model (scikit-learn 1.2.1 library from Python 3.10.3) is trained on a random subset of environmental variables drawn from the dataset input:  $T_{\text{soil}}$ , LWC, vegetation type, snow water equivalent, snow depth, snow mean density, snow maximum density, snow porosity, snow tortuosity, wind slab thickness (if present), and wind slab fraction relative to total snow depth (if present). Each decision tree generates a  $F_{\text{CO}_2}$  prediction, and the overall RF prediction is the average of all prediction trees. A strength of the RF algorithm is that it performs well even when input variables are correlated with each other (Liaw and Wiener, 2002; Strobl et al., 2008; Kibria et al., 2020). Our RF model was composed of 500 fully decomposed decision trees. Our dataset was randomly divided into a training subset (75 %) and a testing subset (25 %), preserving the relative distribution between vegetation types. Our RF model performance was assessed using the coefficient of determination ( $R^2$ ), explained variance, and mean absolute error. We used our RF model to identify the relative importance of winter CO<sub>2</sub> flux predic-

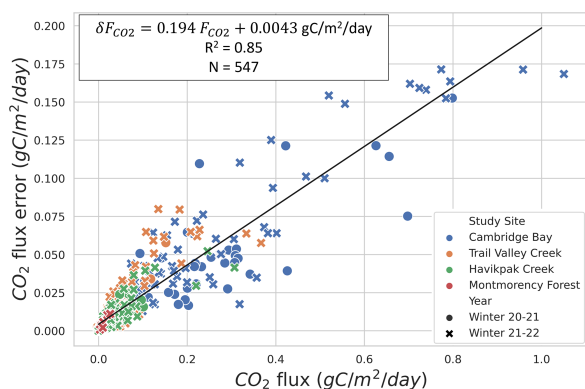


**Figure 3.**  $F_{\text{CO}_2}$  flux ( $F_{\text{CO}_2}$ ) uncertainty relationship to  $F_{\text{CO}_2}$  for four study sites and two winters: 2020–2021 and 2021–2022. Specifications of the linear fit can be found in the upper left. The data dot color indicates the study site, and its symbol (i.e., circle or x-shaped) indicates the winter during which it was collected.

tors. Relative importance of each environmental variable was computed with the permutation method, i.e., alternatively removing variables from the RF model and evaluating the performance decrease, which was measured via the coefficient of determination.

### 3 Results

#### 3.1 $\text{CO}_2$ flux uncertainties

Evaluation of  $F_{\text{CO}_2}$  precision showed that the two main sources of uncertainty are associated with snow density measurements, in agreement with Sommerfeld et al. (1996), and with  $d[\text{CO}_2]/dz$  linear regression (mean  $R^2 = 0.790$  ( $\sigma = 0.236$ ) for  $F_{\text{CO}_2} \geq 0.01 \text{ g C m}^{-2} \text{ d}^{-1}$ ;  $N = 398$ ) (Table A1). Snow density uncertainty ( $\sigma(\rho_{\text{snow}}) \approx 9\%$ ) impacted snow porosity and tortuosity in Eq. (1). From the linear fit of Fig. 3, the average  $F_{\text{CO}_2}$  uncertainty can be estimated at 19.4 %, which provides sufficient accuracy to observe the impact of environmental variables on winter  $F_{\text{CO}_2}$ .

The overall  $[\text{CO}_2]$  precision of around 1 % shows that the measurement technique is not a main source of uncertainty in  $F_{\text{CO}_2}$  estimates. Gas concentration estimations from the LI-7810 have a precision of 0.88 % at 400 ppm according to the manufacturer. The stability of the  $[\text{CO}_2]$  measurement was evaluated over 169 measurements, displaying a standard deviation of 0.09 %. The LI-7810 was further tested using a 400 ppm calibration gas with a 1 %  $[\text{CO}_2]$  precision (Linde Canada). A linear calibration fit equation was used to estimate  $[\text{CO}_2]$  of small gas samples, using three calibration gases (200, 400, 1000 ppm) plus the theoretical zero intercept. Average uncertainty in the linear regression was 0.76 % over six calibration runs with a standard deviation of 0.15 %.

The average accuracy of the reference  $[\text{CO}_2]$  bottled among the gas samples from the snowpack was 1.11 %.

#### 3.2 Spatio-temporal variability in winter $\text{CO}_2$ fluxes associated with abiotic controls

The RF model determined  $T_{\text{soil}}$  and LWC to be the two main predictors of winter  $F_{\text{CO}_2}$  fluxes. We found two temperature and LWC regimes of winter  $F_{\text{CO}_2}$  (Fig. 4). The first regime was when the soil was frozen with  $T_{\text{soil}} < 0^\circ\text{C}$  and  $\text{LWC} < 0.2 \text{ m}^3 \text{ m}^{-3}$ , leading to  $F_{\text{CO}_2}$  being mainly controlled by  $T_{\text{soil}}$ . The second regime was when  $\text{LWC} > 0.2$  and  $< 0.42 \text{ m}^3 \text{ m}^{-3}$  but with a fraction of its water in the form of ice (zero-curtain condition), causing LWC to be the main control of  $F_{\text{CO}_2}$  instead of  $T_{\text{soil}}$ . While the first regime mostly corresponds to Arctic study sites, the second regime only includes one study site (MM) located in the southern boreal forest. Therefore, conclusions from the second regime should be less generalized than those from the first regime. Subsequent evaluation focused on the response of winter  $\text{CO}_2$  fluxes to  $T_{\text{soil}}$  and LWC using exponential regressions in order to better understand the role of these two variables in winter  $\text{CO}_2$  fluxes.

##### 3.2.1 Variable importance determined by the random forest model

$T_{\text{soil}}$  was the  $F_{\text{CO}_2}$  predictor with the highest relative importance (68 %) when using the complete dataset (Fig. 4a), followed by LWC (17 %). Snowpack characteristics,  $\rho_{\text{snow}}$  (11 %) and snow water equivalent (SWE) (2 %), had a lower relative importance in the RF model. Contrary to what might be expected, the vegetation type had near-negligible relative importance (1 %) in  $F_{\text{CO}_2}$  prediction. The RF model was developed starting with all environmental variables available:  $T_{\text{soil}}$ , LWC, vegetation type, SWE, snow depth, mean  $\rho_{\text{snow}}$ , max  $\rho_{\text{snow}}$ ,  $\varphi$ ,  $\tau$ , wind slab fraction, and wind slab thickness. Although the correlation of several snow parameters did not decrease the RF model performance, snow parameters impacted the assessment of variable relative importance by splitting the relative importance between the correlated variables. Consequently, variables with lower importance and with no significant impacts on the RF performance were progressively removed. The two selected snow parameters that had significant impact were SWE and  $\rho_{\text{snow}}$ . MM was the only site where soil LWC was present, enabling the assessment of the relative importance of this variable. When using only data from MM in the RF model (Fig. 4b), the relative importance of  $T_{\text{soil}}$  (12 %) for  $F_{\text{CO}_2}$  was lower than with all combined datasets since  $T_{\text{soil}}$  was near  $0^\circ\text{C}$  for all measurements. At MM, LWC becomes the main predictor (87 %) of  $F_{\text{CO}_2}$ , while  $\rho_{\text{snow}}$  importance drops (2 %) and SWE importance remains similar (< 1 %).

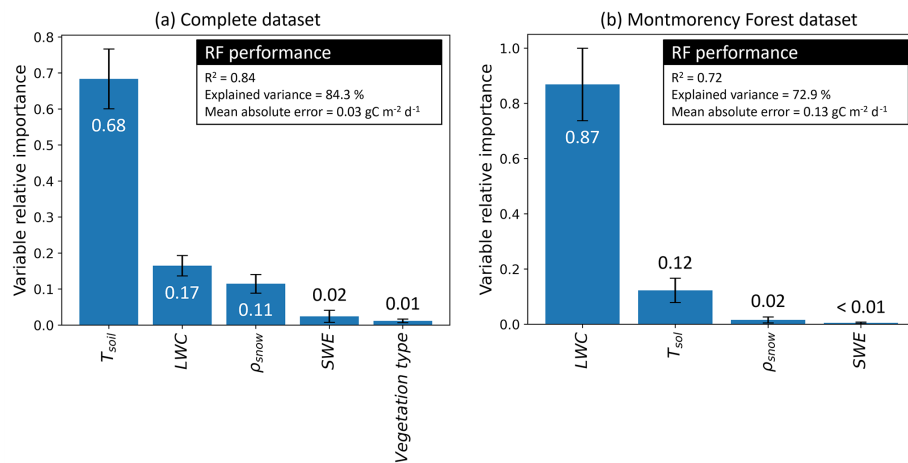


**Figure 4.** Random forest (RF) performance and variable relative importance. Variables used are soil temperature ( $T_{\text{soil}}$ ), soil liquid water content (LWC), snow density ( $\rho_{\text{snow}}$ ), snow water equivalent (SWE), and vegetation type. **(a)** The first iteration integrated the complete dataset, and **(b)** the second iteration only integrated the Montmorency Forest dataset with  $LWC > 0 \text{ m}^3 \text{ m}^{-3}$ . The values displayed by the bar plot are the mean variable relative importance over 100 permutations, while the error bars are the standard deviation.

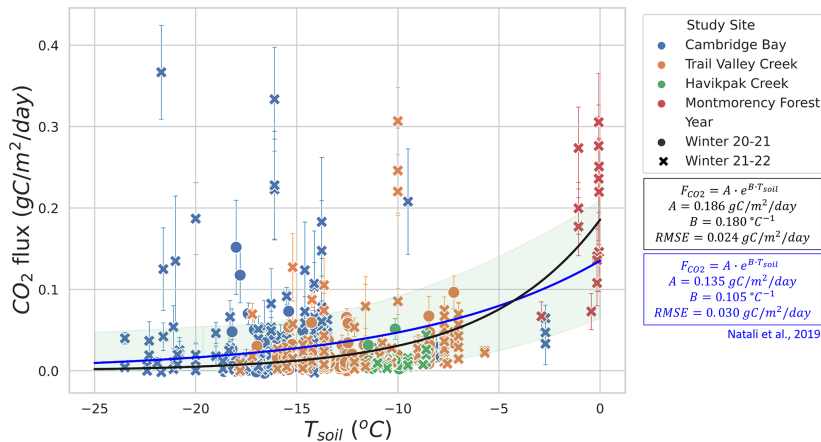


**Figure 5.**  $CO_2$  flux ( $F_{CO_2}$ ) as a function of surface soil temperature ( $T_{\text{soil}}$ ) for  $T_{\text{soil}} < 0^\circ\text{C}$ . An exponential regression was fitted with the data (black line) and compared to the exponential regression by Natali et al. (2019) from an external dataset (blue line).

### 3.2.2 Soil temperature

Figures 5 and 6 show the relationship between winter  $F_{CO_2}$  and  $T_{\text{soil}}$ . Figure 5 focuses on  $T_{\text{soil}} < 0^\circ\text{C}$  from CB, TVC, HPC, and MM. An exponential regression was used to evaluate the relationship between  $T_{\text{soil}}$  and  $F_{CO_2}$  estimates ( $RMSE = 0.024 \text{ g C m}^{-2} \text{ d}^{-1}$ ).  $F_{CO_2}$  values at MM when  $T_{\text{soil}} < 0^\circ\text{C}$  and  $LWC < 0.2 \text{ m}^3 \text{ m}^{-3}$  were included in this graph because they are more strongly correlated to  $T_{\text{soil}}$  than LWC (see Sect. 3.2.3). Note that the low number of  $F_{CO_2}$  measurements with  $T_{\text{soil}}$  between  $-6$  and  $-0.5^\circ\text{C}$  restrict the capacity to evaluate the regression within this range. Using the exponential regression of Natali et al. (2019), we ob-

tained an  $RMSE$  of  $0.030 \text{ g C m}^{-2} \text{ d}^{-1}$ . The regression of Natali et al. (2019) generally shows an overestimation of fluxes for  $T_{\text{soil}} < -5^\circ\text{C}$  but an underestimation for  $T_{\text{soil}} > 5^\circ\text{C}$  when compared to our exponential regression. The systematic bias between our dataset and the regression of Natali et al. (2019) is minimal (mean bias =  $-0.0025 \text{ g C d}^{-1} \text{ m}^{-2}$ ). We also observed the isolated occurrence of comparably large winter  $F_{CO_2}$  of up to  $0.36 \text{ g C m}^{-2} \text{ d}^{-1}$  at temperatures below  $-10^\circ\text{C}$  (Fig. 5). These measurements of high  $F_{CO_2}$  at low temperature seem to be genuine since the repeatability was verified over the three sampling profiles performed at each site. Nevertheless, we were not able to explain these strong  $F_{CO_2}$  fluxes and no environmental vari-

ables measured in our study could be linked to those occurrences. It has been suggested that gas bursts during autumn freeze-up in permafrost environments might be due to gas compression by ice formation and ground cracking (Pirk et al., 2015). This hypothesis can be considered to explain the high  $F_{CO_2}$  observed in this study, although the high  $F_{CO_2}$  observed occurred at a near-surface  $T_{soil}$  between  $-25$  and  $-10^{\circ}C$ , so the freeze-up would have to occur at lower depths in the soil. Figure 6 displays the higher winter  $F_{CO_2}$  from MM where  $T_{air}$  values are higher and the important snowpack insulation keeps the soil at temperatures of around  $0^{\circ}C$  through the entire winter.  $F_{CO_2}$  increases more rapidly with  $T_{soil}$  around freezing point than at  $T_{soil} < 5^{\circ}C$ , which is shown by the higher temperature-dependency parameter ( $B = 2.82^{\circ}C^{-1}$ ) of the MM site exponential regression ( $RMSE = 0.286 \text{ g C m}^{-2} \text{ d}^{-1}$ ) compared to the exponential regression of Fig. 5 ( $B = 0.18^{\circ}C^{-1}$ ). This discrepancy in temperature dependency creates a discontinuity between the measurements at  $T_{soil} < 5^{\circ}C$  and  $T_{soil} \approx 0^{\circ}C$  that did not allow for a continuous temperature-dependency regression across all the study sites. The lower RMSE of the exponential regression of Fig. 5 ( $RMSE = 0.024 \text{ g C m}^{-2} \text{ d}^{-1}$ ; 70.3 % of mean  $F_{CO_2}$ ) compared to the exponential regression of the MM site ( $RMSE = 0.286 \text{ g C m}^{-2} \text{ d}^{-1}$ ; 112.4 % of mean  $F_{CO_2}$ ) might be due to the impact of soil LWC at the MM site (see Sect. 3.2.3).

### 3.2.3 Soil liquid water content

The relationship between LWC and  $F_{CO_2}$  during winter at MM ( $RMSE = 0.137 \text{ g C m}^{-2} \text{ d}^{-1}$ ; 49.1 % of mean  $F_{CO_2}$ ) was stronger than between  $T_{soil}$  and  $F_{CO_2}$  ( $RMSE = 0.286 \text{ g C m}^{-2} \text{ d}^{-1}$ ; 112.4 % of mean  $F_{CO_2}$ ), when excluding the sampling location that contained a thick organic soil layer with very high soil moisture due to its location near the bottom of a microtopographic depression (Fig. 7). Other MM sampling locations with a thin organic layer shared a similar soil composition dominated by mineral soils. The strong correlation between LWC and  $F_{CO_2}$  was mostly observed at  $LWC > 0.2$  and  $< 0.42 \text{ m}^3 \text{ m}^{-3}$ . The plateau observed in Fig. 7 indicates that  $T_{soil}$  might be a better predictor than LWC at  $LWC < 0.2 \text{ m}^3 \text{ m}^{-3}$ .

### 3.2.4 Vegetation types

Figure 8 shows winter  $F_{CO_2}$  across the four study sites for different vegetation types. Since CB vegetation is mostly prostrate-shrub tundra, CB ecosystems were regrouped by water availability. On average, higher winter  $F_{CO_2}$  values at CB were observed in environments experiencing wetter conditions during the growing season. At TVC, several vegetation and land cover types are present.  $F_{CO_2}$  values from MM were higher than for the other sites. Higher  $F_{CO_2}$  can be explained by warmer mean annual average tempera-

ture, a deeper snowpack, and winter  $T_{soil}$  around  $0^{\circ}C$  (see Sect. 3.4).

Vegetation type was not identified as a strong predictor of  $F_{CO_2}$  by the RF model. Nonetheless, we observed differences in the mean and range of  $F_{CO_2}$  for the various vegetation types probed in this study. This might be due to the strong correlation between vegetation type and soil temperature (Fig. A5), as well as relationships between vegetation and soil type, including soil organic matter content and soil pore size. The RF algorithm showed vegetation type relative importance increased to 42 % when  $T_{soil}$  was removed from the environmental variables, although the removal of  $T_{soil}$  decreased RF performance substantially ( $R^2 = 0.40$ ). Therefore, vegetation could be used as a proxy variable for  $T_{soil}$  if the latter is not available to predict  $F_{CO_2}$ , but with poorer results.

## 4 Discussion

### 4.1 Controls of winter CO<sub>2</sub> fluxes

The RF model predictors' relative importance showed that during winter,  $T_{soil}$  emerged as the dominant predictor of  $F_{CO_2}$  when the soil was frozen. Nevertheless, in the closed-crown boreal forest site (i.e., MM) where zero-curtain conditions persisted throughout winter, soil LWC took precedence as the dominant predictor as there was minimal variation in  $T_{soil}$  under these conditions. Our results confirm the strong winter  $F_{CO_2}$  dependency on  $T_{soil}$  shown by Natali et al. (2019), although we observed fluxes lower than reported by Natali et al. (2019) at  $T_{soil} < -5^{\circ}C$  and mostly higher fluxes at  $T_{soil} > -5^{\circ}C$ . Considering the two regressions of the relationship between  $T_{soil}$  and  $F_{CO_2}$  have large uncertainties attached to them, the difference between them falls inside the uncertainty margin (Fig. 5). It should be noted that the Natali et al. (2019) regression was obtained using  $F_{CO_2}$  estimates from several methods including eddy covariance, chamber methods, and snowpack diffusion measurements, whereas our study exclusively uses the latter. Several studies have shown bias between the different measurement methods; eddy covariance and soil chamber methods displayed positive biases when compared to snowpack diffusion measurements (McDowell et al., 2000; Björkman et al., 2010; Webb et al., 2016), while the snow chamber displayed negative biases when compared to the snowpack diffusion measurements (McDowell et al., 2000). It should be remembered that the  $T_{soil}$  used in the latter study refers to near-surface temperature;  $T_{soil}$  at greater depths may vary and affect the correlation with  $F_{CO_2}$ .

### 4.2 Zero-curtain conditions

Soil LWC was observed only at the MM site, where  $T_{soil}$  was around  $0^{\circ}C$  throughout winter. In zero-curtain conditions, LWC was shown to become the dominant control of

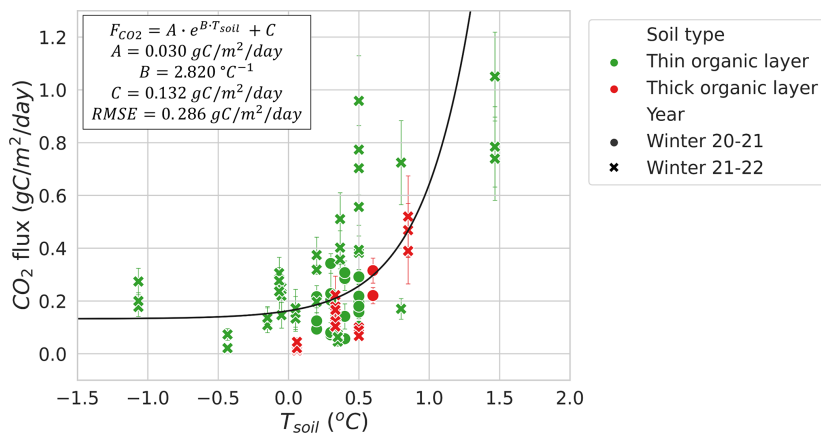


**Figure 6.**  $\text{CO}_2$  flux ( $F_{\text{CO}_2}$ ) as a function of soil temperature ( $T_{\text{soil}}$ ) at the Montmorency Forest study sites where soil liquid water content (LWC) was greater than  $0 \text{ m}^3 \text{ m}^{-3}$  throughout winter. An exponential regression was fitted to the data (black line).

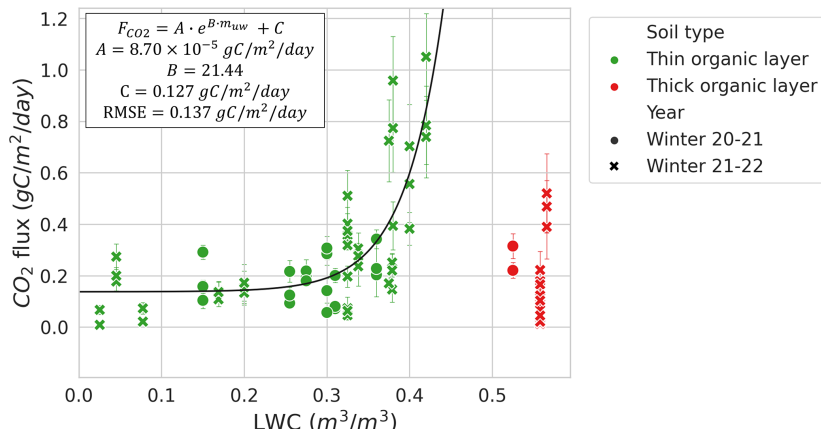


**Figure 7.**  $\text{CO}_2$  flux ( $F_{\text{CO}_2}$ ) as a function of soil volumetric liquid water content (LWC) at the Montmorency Forest study site. An exponential regression was fitted to the data (black line), excluding the thick-organic-layer site (red markers).

winter  $F_{\text{CO}_2}$ , while  $T_{\text{soil}}$  importance diminished. It should be noted that it would be ill-advised to generalize the relationship between soil LWC and  $F_{\text{CO}_2}$  as it is only based on data from one study site, and it cannot be ruled out that this relationship is site-specific depending on soil and vegetation composition. Nevertheless, our study highlighted the important impact of LWC on  $F_{\text{CO}_2}$  around the soil freezing point when there is a mixed state of ice and free water in soils. When the soil is under zero-curtain conditions, the latent heat governs the ice and liquid water ratio in the soil (Devoie et al., 2022). Hence, LWC and ice fractions can be used as a freezing–thawing indicator during the zero-curtain period and help better quantify the  $F_{\text{CO}_2}$  fluxes in boreal forest environments where zero-curtain conditions prevail (Prince et al., 2019). This result is particularly important in ABRs since the duration and frequency of zero-curtain periods are

expected to increase in a warming climate (Yi et al., 2015, 2019; Tao et al., 2021). Further research on winter  $F_{\text{CO}_2}$  in zero-curtain conditions should investigate different sites to assess if the relationship between  $F_{\text{CO}_2}$  and soil LWC is site-specific or dependent on soil properties. It should be noted that one of the measurement locations at MM displayed low  $F_{\text{CO}_2}$  despite its LWC being the highest of all sites. The soil composition of this site consisted of a thick ( $> 30 \text{ cm}$ ) soil organic top layer, whereas all other measurements were done at sites with thinner ( $3\text{--}10 \text{ cm}$ ) organic layers on top of mineral soil. It is well known that anaerobic conditions created by high soil moisture (at least  $> 50 \%$ ) constrain soil  $\text{CO}_2$  respiration rates during the growing season because many microorganisms require oxygen for organic matter decomposition, which they lack if soil pores are filled with water (Linn and Doran, 1984; Davidson and Janssens, 2006).

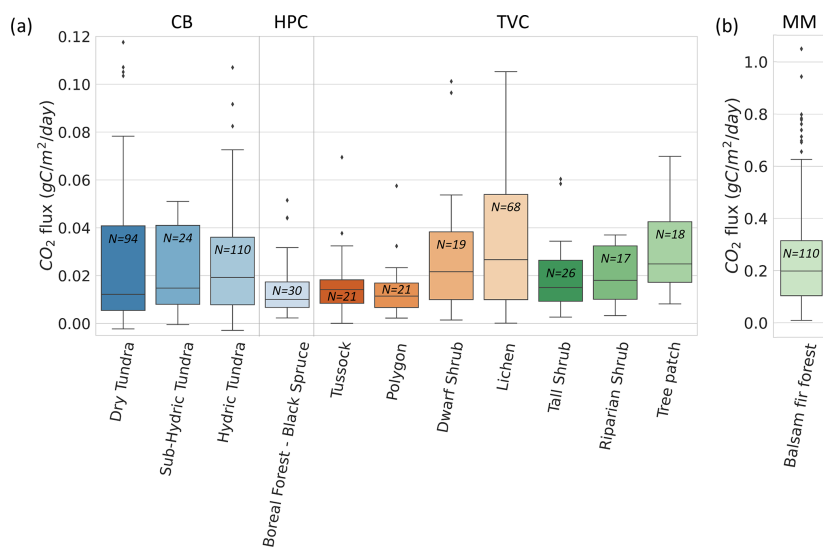


**Figure 8.** Boxplot of  $\text{CO}_2$  flux ( $F_{\text{CO}_2}$ ) across 12 vegetation types and 4 sites.  $F_{\text{CO}_2}$  values from Montmorency Forest (MM) are on a separate scale because they are much higher than the colder environments (b). Cambridge Bay (CB) sites are ordered by increasing water availability, and Trail Valley Creek (TVC) sites are ordered by increasing mean soil surface temperature in March 2021 and 2022 (a). Havikpak Creek (HPC) and MM were composed of a single vegetation type (a). Outliers were defined as  $F_{\text{CO}_2} > Q_3 + 1.5 \text{ IQR}$ , where  $Q_3$  is the third quartile and IQR the interquartile range. Outliers are out of the y-axis range for the dry tundra (four), sub-hydric tundra (four), hydric tundra (four) and lichen (three). The outliers can be found in Fig. 5.

#### 4.3 Snowpack importance

Our study shows that abiotic variables related to  $T_{\text{soil}}$ , LWC, and physical snowpack properties explain the majority of variance in winter  $\text{CO}_2$  fluxes. It should be noted that we did not incorporate variables related to temporal dynamics such as the previous days' soil temperature and LWC, which have been shown by Harel et al. (2023) to be of importance during the growing season. However, winter soil variables are not expected to be as dynamic as during the growing season because of the snowpack insulating properties. The RF model showed that SWE and mean snow density were the snow characteristics that provided the greatest improvement of the RF model, although to a lesser degree than  $T_{\text{soil}}$  and LWC. The importance of snow characteristics in  $F_{\text{CO}_2}$  is linked with the strong correlation to  $T_{\text{soil}}$  (Domine et al., 2016b; Pedron et al., 2023), although a snapshot of snow conditions provides limited abilities to infer  $T_{\text{soil}}$ , as shown in Slater et al. (2017). Snow properties' temporal information is required to predict the impact of snow insulation on  $T_{\text{soil}}$ , with the most important period being in the autumn freeze-up when air temperature decreases below the freezing point. Snow characteristics are closely linked to topography (Meloche et al., 2021) and thus soil wetness and soil carbon content (Gouttevin et al., 2012). Regarding the snowpack diffusion gradient method, the snowpack is used to estimate winter  $\text{CO}_2$  fluxes. An average snow density was used to estimate snow porosity and tortuosity used in  $\text{CO}_2$  flux cal-

culations (Eq. 1), which does not consider the vertical stratification of the snowpack. However, the diffusion gradient remained linear despite vertical stratification in snow density (e.g., Fig. A3 where the average ratio between the standard deviation and mean of  $D_{\text{air}} \cdot \varphi \cdot \tau$  is around 10 %), which points toward a minimal impact of this assumption on our results.

#### 4.4 Soil biogeochemistry

The unexplained variance (16 %) suggests that winter  $\text{CO}_2$  fluxes might have been controlled by other environmental variables such as soil physical–chemical properties regulating soil biogeochemistry and soil redox conditions, which were neither addressed nor measured in this study.  $\text{CO}_2$  production is governed by the availability and quality of labile C compounds regulating the decomposition of soil organic matter (Michaelson and Ping, 2005; Wang et al., 2011) and by the activity and composition of the soil microbial community (Monson et al., 2006). Soil type and structure, for example the thickness of the organic layer, soil pore size distribution, and soil pH, may be further strong controls on  $\text{CO}_2$  production (Steponavičienė et al., 2022; Yli-Halla et al., 2022). All these variables vary widely across the heterogeneous tundra terrain (Virtanen and Ek, 2014), where small-scale moisture, vegetation, and soil conditions occur among hummock and inter-hummock depressions (Wilcox et al., 2019). Further analysis is required to understand the role of physical–chemical soil properties in  $F_{\text{CO}_2}$  during winter.

#### 4.5 Relevance for terrestrial biosphere models

Large uncertainties remain in terrestrial biosphere models used to estimate CO<sub>2</sub> fluxes in ABRs (Fisher et al., 2014; Tei and Sugimoto, 2020; Birch et al., 2021; Virkkala et al., 2021), especially regarding the respiratory release of CO<sub>2</sub> via soil respiration (the sum of heterotrophic respiration and belowground autotrophic respiration) during winter (Natali et al., 2019). The limited number of observational data available has restricted model improvements, testing, and evaluation (Virkkala et al., 2022). Modeling the ABR carbon cycle is critical for climate projections since a warmer climate should lead to higher  $T_{\text{soil}}$ , thus increasing ABR winter  $F_{\text{CO}_2}$  (Mellander et al., 2007; Throop et al., 2012; Wieder et al., 2019). Several terrestrial biosphere models are currently in use (Fisher et al., 2022), such as CLM (Community Land Model; Lawrence et al., 2019) and CLASSIC (Canadian Land Surface Scheme Including Biogeochemical Cycles; Melton et al., 2020; Seiler et al., 2021). The  $F_{\text{CO}_2}$  relationships to  $T_{\text{soil}}$  and LWC observed in this study could be used to inform terrestrial biosphere models through the parametrization of winter soil respiration sensitivity to soil temperature (e.g., Q10 temperature coefficient) and LWC in zero-curtain conditions. Our study shows that permanent installation of the snow gradient method (Seok et al., 2009; Zhu et al., 2014; Graham and Risk, 2018) would be suitable for gathering the temporal non-growing-season CO<sub>2</sub> fluxes in ABRs required to fully test terrestrial biosphere models.

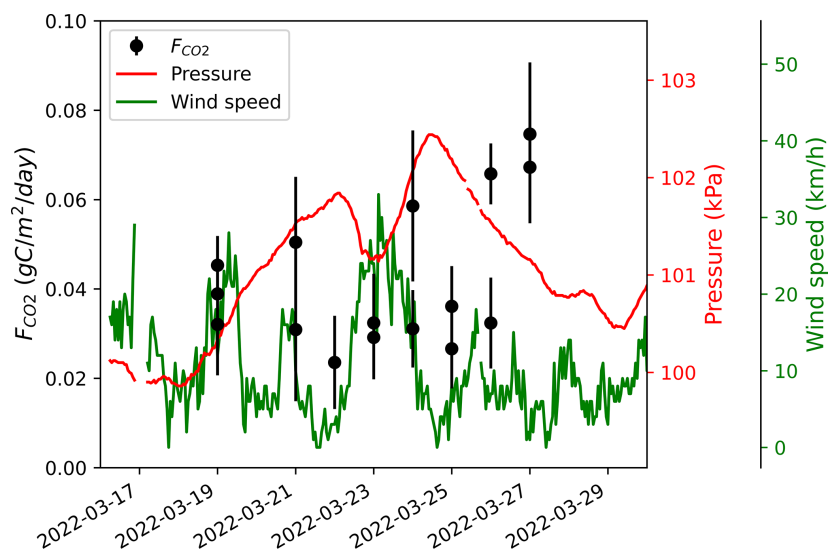
#### 5 Conclusion

Our study showed that  $T_{\text{soil}}$  is the main control of winter  $F_{\text{CO}_2}$  at  $T_{\text{soil}} < 0^{\circ}\text{C}$  in ABRs. The relative importance analysis of our RF model showed that  $T_{\text{soil}}$  was the main predictor of  $F_{\text{CO}_2}$ , followed by LWC. However, we found that at our site maintaining zero-curtain conditions throughout winter, LWC becomes the main control of winter  $F_{\text{CO}_2}$ . We observed non-negligible winter  $F_{\text{CO}_2}$  that may partially offset growing-season CO<sub>2</sub> uptake in ABRs. Consequently, winter  $F_{\text{CO}_2}$  must be properly estimated in terrestrial biosphere models and climate models. Additionally, future research should focus on linking the effects of abiotic variables on  $F_{\text{CO}_2}$  during winter, as we determined here, with soil biogeochemistry, microbial functioning, and vegetation.

## Appendix A

**Table A1.** Uncertainty sources in  $F_{CO_2}$  and their uncertainty. [CO<sub>2</sub>] precision was evaluated at a concentration of 400 ppm.

$F_{CO_2}$ uncertainty source	Uncertainty
[CO <sub>2</sub> ] estimate	
– LI-7810 precision	3.52 ppm (0.88 %)
– Measurement stability	3.6 ppm (0.09 %; $N = 169$ )
– Reference gas	4 ppm (1 %)
– Calibration fit	3.04 ppm (0.76 %; $N = 6$ ; $\sigma = 0.15$ )
– Transfer, transport, and storage test	4.44 ppm (1.11 %; $N = 6$ )
Snow density ( $kg\ m^{-3}$ )	9 %
$d[CO_2]/dz$ linear regression ( $g\ C\ m^{-4}$ )	19.4 %

**Figure A1.** CO<sub>2</sub> fluxes ( $F_{CO_2}$ ) at a sampling location in the Trail Valley Creek erect-shrub tundra (lichen) between 19 March and 27 March 2022. Atmospheric pressure and wind speed were obtained from Environment and Climate Change Canada's Meteorological Service of Canada meteorological station at Trail Valley Creek ([https://climate.weather.gc.ca/historical\\_data/search\\_historic\\_data\\_e.html](https://climate.weather.gc.ca/historical_data/search_historic_data_e.html), last access: 21 November 2023). The date format is YYYY-MM-DD.

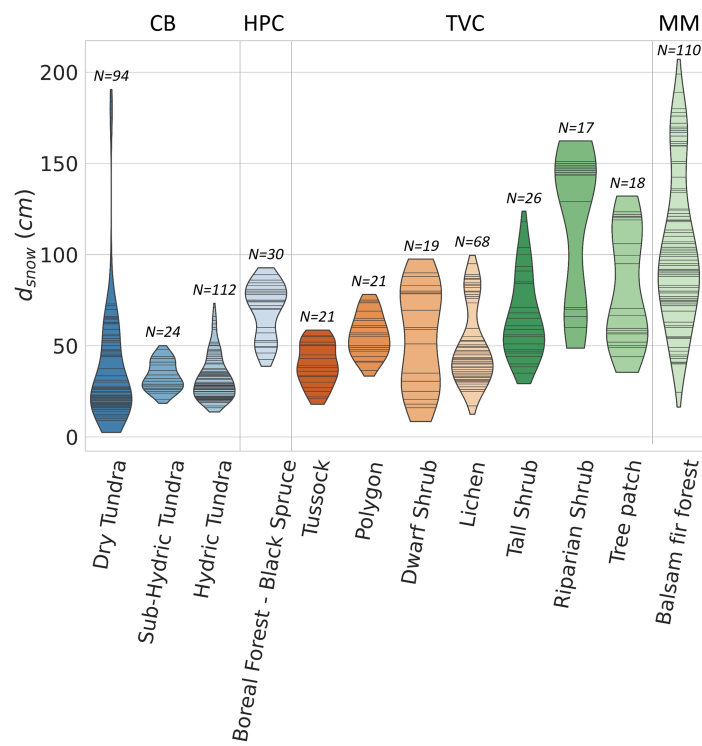


**Figure A2.** Violin plot of the snow depth range of sites where  $F_{\text{CO}_2}$  was estimated. The black stripes inside the violins represent data points. The study sites are Cambridge Bay (CB), Havikpak Creek (HPC), Trail Valley Creek (TVC), and Montmorency Forest (MM). CB sites are ordered by increasing hydricity, and TVC sites are ordered by increasing mean soil surface temperature in March 2021 and 2022.

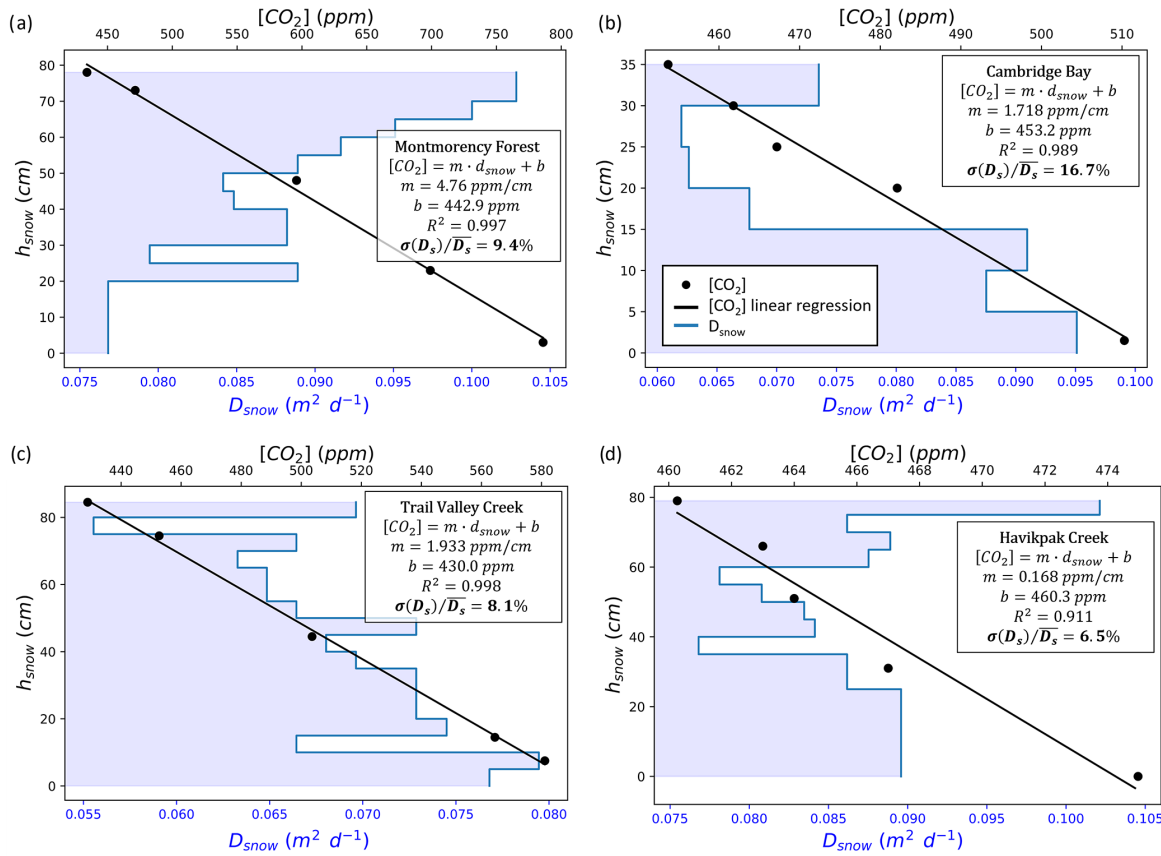


**Figure A3.** Examples of snow diffusion coefficient ( $D_{\text{snow}} = D_{\text{air}} \cdot \varphi \cdot \tau$ ) vertical stratification and CO<sub>2</sub> concentration ([CO<sub>2</sub>]) gradient measurements as a function of snow height ( $h_{\text{snow}}$ ) from the ground level. The coefficient of determination ( $R^2$ ), [CO<sub>2</sub>] gradient ( $m$ ), and y-axis intercept ( $b$ ) for the linear regressions on the [CO<sub>2</sub>] gradient measurements are provided. The ratio between  $D_{\text{snow}}$  standard deviation ( $\sigma(D_s)$ ) and average ( $\bar{D}_s$ ) is provided in percent. The data come from (a) Montmorency Forest balsam fir closed-crown coniferous boreal forest on 26 February 2021, (b) Cambridge Bay prostrate-shrub tundra (hydric tundra: hydric sedge fen) on 15 April 2022, (c) Trail Valley Creek erect-shrub tundra (lichen) on 26 March 2022, and (d) Havikpak Creek black spruce open-crown coniferous boreal forest on 16 March 2022.

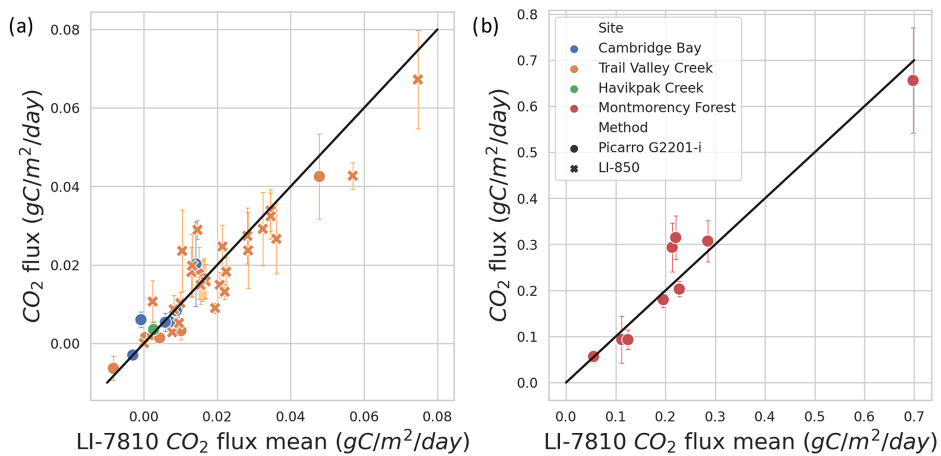


**Figure A4.** Comparison of winter CO<sub>2</sub> flux calculated from CO<sub>2</sub> concentration estimated with different gas analyzers. The LI-7810 gas analyzer was used as the reference and is compared to a Picarro G2201-i and LI-850. In the Arctic biome (a), the correlation coefficient is 0.924 for the Picarro instrument and 0.821 for the LI-850. In the boreal biome (b), the correlation coefficient is 0.929 for the Picarro instrument.

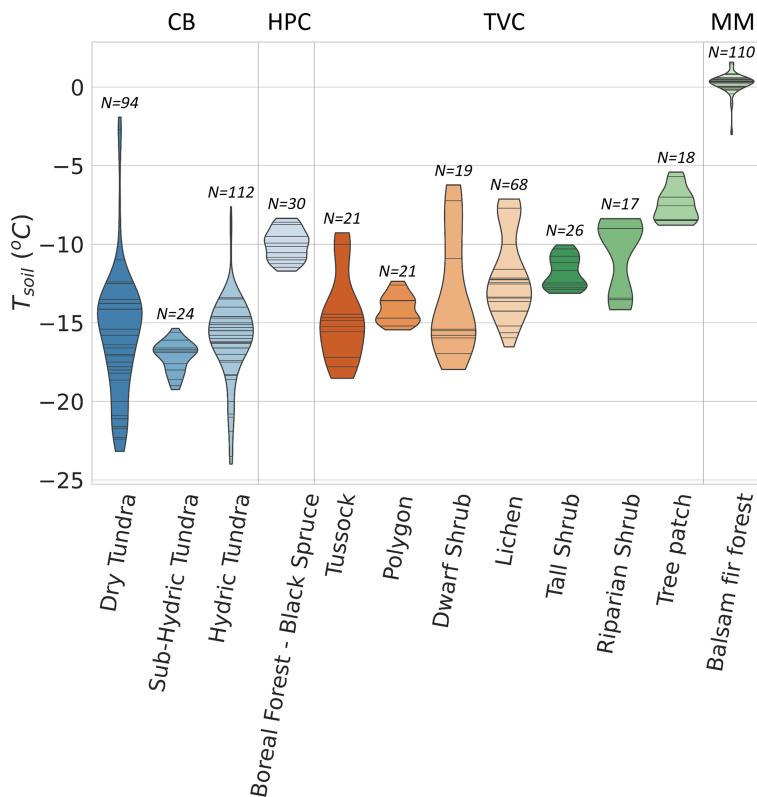


**Figure A5.** Violin plot of the soil temperature ( $T_{soil}$ ) range of sites where  $F_{CO_2}$  was estimated. The black stripes inside the violins represent data points. CB sites are ordered by increasing hydricity, and TVC sites are ordered by increasing soil surface temperature in March 2021 and 2022.

*Data availability.* Data are available via Mavrovic et al. (2023, <https://doi.org/10.5683/SP3/COWXAZ>).

*Author contributions.* AM, OS, JL, and AR conceived and planned the study. AM, NR, PM, JD, and AR carried out the experiments and sampling collection. AM performed the data processing and analysis. OS, JL, CV, JD, and AR contributed to dataset analysis. AM wrote the manuscript. All authors contributed to editing and reviewing the manuscript.

*Competing interests.* The contact author has declared that none of the authors has any competing interests.

*Disclaimer.* Publisher's note: Copernicus Publications remains neutral with regard to jurisdictional claims made in the text, published maps, institutional affiliations, or any other geographical representation in this paper. While Copernicus Publications makes every effort to include appropriate place names, the final responsibility lies with the authors.

*Acknowledgements.* This work was made possible thanks to the contributions of the Natural Sciences and Engineering Research Council of Canada (NSERC), the Fonds de recherche du Québec – Nature et technologies (FRQNT), and Polar Knowledge Canada (POLAR). A special thanks goes to everybody that contributed to data collection and gas analyzing: Elise Imbeau (Viventem), Gabriel Ferland (Viventem), Aili Pedersen (POLAR), Gabriel Hould Gosselin (Université de Montréal (UdeM) and Wilfrid Laurier University (WLU)), Emma Riley (WLU), Rosy Tutton (WLU), Victoria Dutch (Northumbria University (NU)), Georgina Woolley (NU), Élise Groulx (Université de Sherbrooke (UdeS)), Charlotte Crevier (UdeS), Érika Boisvert (UdeS), Alain Royer (UdeS), Patrick Ménard (UdeS), Vincent Sasseville (UdeS), Célia Trunz (UdeS), Daniel Kramer (UdeS), Estéban Hamel Jomphe (UQTR), Samuel Goulet (UQTR), Alex Gélinas (UQTR), David de Courville (UQTR), Juliette Ortet (UQTR), and Chris Derksen (Environment and Climate Change Canada). We would also like to thank Ian Hogg, Johann Wagner, and Scott Johnson from POLAR for their logistical support.

*Financial support.* This research has been supported by the Natural Sciences and Engineering Research Council of Canada, the Fonds de recherche du Québec – Nature et technologies, and Polar Knowledge Canada.

*Review statement.* This paper was edited by Andreas Ibrom and reviewed by two anonymous referees.

## References

- Baldocchi, D.: Assessing the eddy covariance technique for evaluating carbon dioxide exchange rates of ecosystems: past, present and future, *Global Change Biol.*, 9, 479–492, <https://doi.org/10.1046/j.1365-2486.2003.00629.x>, 2003.
- Baldocchi, D., Falge, E., Gu, L., Olson, R., Hollinger, D., Running, S., Anthoni, P., Bernhofer, C., Davis, K., Evans, R., Fuentes, J., Goldstein, A., Katul, G., Law, B., Lee, X., Malhi, Y., Meyers, T., Munger, W., Oechel, W., Paw U, K., Pilegaard, K., Schmid, H., Valentini, R., Verma, S., Vesala, T., Wilson, K., and Wofsy, S.: FLUXNET: A New Tool to Study the Temporal and Spatial Variability of Ecosystem-Scale Carbon Dioxide, Water Vapor, and Energy Flux Densities, *B. Am. Meteorol. Soc.*, 82, 2415–2434, [https://doi.org/10.1175/1520-0477\(2001\)082<2415:fants>2.3.co;2](https://doi.org/10.1175/1520-0477(2001)082<2415:fants>2.3.co;2), 2001.
- Barry, R., Plamondon, A. P., and Stein, J.: Hydrologic soil properties and application of a soil moisture model in a balsam fir forest, *Can. J. Forest Res.*, 18, 427–434, <https://doi.org/10.1139/x88-063>, 1988.
- Birch, L., Schwalm, C. R., Natali, S., Lombardozzi, D., Keppel-Aleks, G., Watts, J., Lin, X., Zona, D., Oechel, W., Sachs, T., Black, T. A., and Rogers, B. M.: Addressing biases in Arctic-boreal carbon cycling in the Community Land Model Version 5, *Geosci. Model Dev.*, 14, 3361–3382, <https://doi.org/10.5194/gmd-14-3361-2021>, 2021.
- Björkman, M., Morgner, E., Cooper, E., Elberling, B., Klemetsen, L., and Björk, R.: Winter carbon dioxide effluxes from Arctic ecosystems: An overview and comparison of methodologies, *Global Biogeochem. Cy.*, 24, GB3010, <https://doi.org/10.1029/2009GB003667>, 2010.
- Bond-Lamberty, B. and Thomson, A.: Temperature-associated increases in the global soil respiration record, *Nature*, 464, 579–582, <https://doi.org/10.1038/nature08930>, 2010.
- Bouyoucos, G. J.: Hydrometer Method Improved for Making Particle Size Analyses of Soils, *Agron. J.*, 54, 464–465, <https://doi.org/10.2134/agronj1962.00021962005400050028x>, 1962.
- Bowley, A.: The Standard Deviation of the Correlation Coefficient, *J. Am. Stat. Assoc.*, 23, 31–34, <https://doi.org/10.2307/2277400>, 1928.
- Braghiere, R., Fisher, J., Miner, K., Miller, C., Worden, J., Schimel, D., and Frankenberg, C.: Tipping point in North American Arctic-Boreal carbon sink persists in new generation Earth system models despite reduced uncertainty, *Environ. Res. Lett.*, 18, 025008, <https://doi.org/10.1088/1748-9326/acb226>, 2023.
- Breiman, L.: Random forests, *Mach. Learn.*, 45, 5–32, <https://doi.org/10.1023/A:1010933404324>, 2001.
- Brown, J., Ferrians, O., Heginbottom, J., and Melnikov, E.: Circum-Arctic Map of Permafrost and Ground-Ice Conditions, Version 2, Boulder, Colorado USA, NSIDC: National Snow and Ice Data Center, <https://doi.org/10.7265/skbg-kf16>, 2002.
- Bruhwiler, L., Parmentier, F.-J., Crill, P., Leonard, M., and Palmer, P.: The Arctic Carbon Cycle and Its Response to Changing Climate, *Curr. Clim. Change Rep.*, 7, 14–34, <https://doi.org/10.1007/s40641-020-00169-5>, 2021.
- Busseau, B.-C., Royer, A., Roy, A., Langlois, A., and Dominé, F.: Analysis of snow-vegetation interactions in the low Arctic-Subarctic transition zone (northeastern Canada), *Phys. Geogr.*,

- 38, 159–175, <https://doi.org/10.1080/02723646.2017.1283477>, 2017.
- Callaghan, T., Johansson, M., Brown, R., Groisman, P., Labba, N., Radionov, V., Bradley, R., Blangy, S., Bulygina, O., Christensen, T., Colman, J., Essery, R., Forbes, B., Forchhammer, M., Golubev, V., Honrath, R., Juday, G., Meshcherskaya, A., Phoenix, G., Pomeroy, J., Rautio, A., Robinson, D., Schmidt, N., Serreze, M., Shevchenko, V., Shiklomanov, A., Shmakin, A., Sköld, P., Sturm, M., Woo, M.-k., and Wood, E.: Multiple Effects of Changes in Arctic Snow Cover, *Ambio*, 40, 32–45, <https://doi.org/10.1007/s13280-011-0213-x>, 2011a.
- Callaghan, T., Tweedie, C., Akerman, J., Andrews, C., Bergstedt, J., Butler, M., Christensen, T., Cooley, D., Dahlberg, U., Danby, R., Daniëls, F., de Molenaar, J., Dick, J., Mortensen, C. E., Ebert-May, D., Emanuelsson, U., Eriksson, H., Hedenås, H., Henry, G., Hik, D., Hobbie, J., Jantze, E., Jaspers, C., Johansson, C., Johansson, M., Johnson, D., Johnstone, J., Jonasson, C., Kennedy, C., Kenney, A., Keuper, F., Koh, S., Krebs, C., Lantuit, H., Lara, M., Lin, D., Lougheed, V., Madsen, J., Matveyeva, N., McEwen, D., Myers-Smith, I., Narozhnyi, Y., Olsson, H., Pohjola, V., Price, L., Rigét, F., Rundqvist, S., Sandström, A., Tamstorf, M., Bogaert, R. V., Villarreal, S., Webber, P., and Zemtsov, V.: Multi-Decadal Changes in Tundra Environments and Ecosystems: Synthesis of the International Polar Year-Back to the Future Project (IPY-BTF), *Ambio*, 40, 705–716, <https://doi.org/10.1007/s13280-011-0179-8>, 2011b.
- Canadian Forest Inventory Committee (CFI): Canada's National Forest Inventory ground sampling guidelines: specifications for ongoing measurement, Pacific Forestry Centre, Victoria, British Columbia, Canada, Catalog ID 29402, ISBN 978-1-100-11329-6, 271 pp., 2008.
- Carreiras, J., Quegan, S., Le Toan, T., Ho Tong Minh, D., Saatchi, S., Carvalhais, N., Reichstein, M., and Scipal, K.: Coverage of high biomass forests by the ESA BIOMASS mission under defense restrictions, *Remote Sens. Environ.*, 196, 154–162, <https://doi.org/10.1016/j.rse.2017.05.003>, 2017.
- Christiansen, C., Schmidt, N., and Michelsen, A.: High Arctic dry heath CO<sub>2</sub> exchange during the early cold season, *Ecosystems*, 15, 1083–1092, <https://doi.org/10.1007/s10021-012-9569-4>, 2012.
- Davidson, E. and Janssens, I.: Temperature sensitivity of soil carbon decomposition and feedbacks to climate change, *Nature*, 440, 165–173, <https://doi.org/10.1038/nature04514>, 2006.
- Derkzen, C., Burgess, D., Duguay, C., Howell, S., Mudryk, L., Smith, S., Thackeray, C., and Kirchmeier-Young, M.: Changes in snow, ice, and permafrost across Canada, Canada's Changing Climate Report, Chap. 5, Government of Canada, Ottawa, Ontario, Canada, 194–260, <https://changingclimate.ca/CCCR2019/> (last access: 18 December 2023), 2019.
- Devoie, É. G., Gruber, S., and McKenzie, J. M.: A repository of measured soil freezing characteristic curves: 1921 to 2021, *Earth Syst. Sci. Data*, 14, 3365–3377, <https://doi.org/10.5194/essd-14-3365-2022>, 2022.
- Domine, F., Barrere, M., Sarrazin, D., Morin, S., and Arnaud, L.: Automatic monitoring of the effective thermal conductivity of snow in a low-Arctic shrub tundra, *The Cryosphere*, 9, 1265–1276, <https://doi.org/10.5194/tc-9-1265-2015>, 2015.
- Domine, F., Barrere, M., and Morin, S.: The growth of shrubs on high Arctic tundra at Bylot Island: impact on snow physical properties and permafrost thermal regime, *Biogeosciences*, 13, 6471–6486, <https://doi.org/10.5194/bg-13-6471-2016>, 2016a.
- Domine, F., Barrere, M., and Sarrazin, D.: Seasonal evolution of the effective thermal conductivity of the snow and the soil in high Arctic herb tundra at Bylot Island, Canada, *The Cryosphere*, 10, 2573–2588, <https://doi.org/10.5194/tc-10-2573-2016>, 2016b.
- Dominé, F., Fourteau, K., Picard, G., Lackner, G., Sarrazin, D., and Poirier, M.: Permafrost cooled in winter by thermal bridging through snow-covered shrub branches, *Nat. Geosci.*, 15, 554–560, <https://doi.org/10.1038/s41561-022-00979-2>, 2022.
- Du Plessis, P. and Masliyah, J.: Flow through isotropic granular porous media, *Transport Porous Med.*, 6, 207–221, <https://doi.org/10.1007/BF00208950>, 1991.
- Elberling, B.: Annual soil CO<sub>2</sub> effluxes in the High Arctic: The role of snow thickness and vegetation type, *Soil Biol. Biochem.*, 39, 646–654, <https://doi.org/10.1016/j.soilbio.2006.09.017>, 2007.
- Fierz, C., Armstrong, R. L., Durand, Y., Etchevers, P., Green, E., McClung, D., Nishimura, K., Satyawali, P., and Sokratov, S.: The International Classification for Seasonal Snow on the Ground, IHP-VII Technical Documents in Hydrology N83, IACS Contribution N1, UNESCO-IHP, Paris, <https://www.dora.lib4ri.ch/wsl/islandora/object/wsl:10162> (last access: 18 December 2023), 2009.
- Fisher, J., Sikka, M., Block, G., Schwalm, C., Parazoo, N., Kulus, H., Sok, M., Wang, A., Gagne-Landmann, A., Lawal, S., Guillaume, A., Poletti, A., Schaefer, K., El Masri, B., Levy, P., Wei, Y., Dietze, M., and Huntzinger, D.: The Terrestrial Biosphere Model Farm, *J. Adv. Model. Earth Sy.*, 14, e2021MS002676, <https://doi.org/10.1029/2021MS002676>, 2022.
- Fisher, J. B., Sikka, M., Oechel, W. C., Huntzinger, D. N., Melton, J. R., Koven, C. D., Ahlström, A., Arain, M. A., Baker, I., Chen, J. M., Ciais, P., Davidson, C., Dietze, M., El-Masri, B., Hayes, D., Huntingford, C., Jain, A. K., Levy, P. E., Lomas, M. R., Poultier, B., Price, D., Sahoo, A. K., Schaefer, K., Tian, H., Tomelleri, E., Verbeeck, H., Viovy, N., Wania, R., Zeng, N., and Miller, C. E.: Carbon cycle uncertainty in the Alaskan Arctic, *Biogeosciences*, 11, 4271–4288, <https://doi.org/10.5194/bg-11-4271-2014>, 2014.
- Gauthier, S., Bernier, P., Kuuluvainen, T., Shvidenko, A., and Schepaschenko, D.: Boreal forest health and global change, *Science*, 349, 819–822, <https://doi.org/10.1126/science.aaa9092>, 2015.
- Gouttevin, I., Menegoz, M., Dominé, F., Krinner, G., Koven, C., Ciais, P., Tarnocai, C., and Boike, J.: How the insulating properties of snow affect soil carbon distribution in the continental pan-Arctic area, *J. Geophys. Res.-Biogeo.*, 117, G02020, <https://doi.org/10.1029/2011JG001916>, 2012.
- Graham, L. and Risk, D.: Explaining CO<sub>2</sub> fluctuations observed in snowpacks, *Biogeosciences*, 15, 847–859, <https://doi.org/10.5194/bg-15-847-2018>, 2018.
- Grünberg, I., Wilcox, E. J., Zwieback, S., Marsh, P., and Boike, J.: Linking tundra vegetation, snow, soil temperature, and permafrost, *Biogeosciences*, 17, 4261–4279, <https://doi.org/10.5194/bg-17-4261-2020>, 2020.
- Harel, A., Sylvain, J., Drolet, G., Thiffault, E., Thiffault, N., and Tremblay, S.: Fine scale assessment of seasonal, intra-seasonal and spatial dynamics of soil CO<sub>2</sub> effluxes over a balsam fir-dominated perhumid boreal landscape, *Agr. Forest Meteorol.*, 335, 109469, <https://doi.org/10.1016/j.agrformet.2023.109469>, 2023.

- Harvey, A., In Haynes, W., Lide, D., and Bruno, T.: CRC Handbook of Chemistry and Physics, 97th edn.: Properties of Ice and Super-cooled Water, CRC Press, Boca Raton, Florida, United States, 2666 pp., ISBN 978-1-4987-5429-3, 2017.
- Hayes, J., McGuire, A., Kicklighter, D., Gurney, K., Burnside, T., and Melillo, J.: Is the northern high-latitude land-based CO<sub>2</sub> sink weakening?, *Global Biogeochem. Cy.*, 25, GB3018, <https://doi.org/10.1029/2010GB003813>, 2011.
- Jentzsch, K., Boike, J., and Foken, T.: Importance of the Webb, Pearman, and Leuning (WPL) correction for the measurement of small CO<sub>2</sub> fluxes, *Atmos. Meas. Tech.*, 14, 7291–7296, <https://doi.org/10.5194/amt-14-7291-2021>, 2021.
- Jones, H., Pomeroy, J., Davies, T., Tranter, M., and Marsh, P.: CO<sub>2</sub> in Arctic snow cover: landscape form, in-pack gas concentration gradients, and the implications for the estimation of gaseous fluxes, *Hydrol. Process.*, 13–18, 2977–2989, [https://doi.org/10.1002/\(SICI\)1099-1085\(19991230\)13:18<2977::AID-HYP12>3.0.CO;2-%23](https://doi.org/10.1002/(SICI)1099-1085(19991230)13:18<2977::AID-HYP12>3.0.CO;2-%23), 1999.
- Kibria, H., Abdullah, S., and Bustamam, A.: Comparison of random forest and support vector machine for prediction of cognitive impairment in Parkinson's disease, *AIP Conf. Proc.*, 2296, 020093, <https://doi.org/10.1063/5.0030332>, 2020.
- Kim, Y., Tsunogai, S., and Tanaka, N.: Winter CO<sub>2</sub> emission and its production rate in cold temperate soils of northern Japan: 222Rn as a proxy for the validation of CO<sub>2</sub> diffusivity, *Polar Sci.*, 22, 100480, <https://doi.org/10.1016/j.polar.2019.09.002>, 2019.
- Kinar, N. and Pomeroy, J.: Measurement of the physical properties of the snowpack, *Rev. Geophys.*, 53, 481–544, <https://doi.org/10.1002/2015RG000481>, 2015.
- Knowles, J., Blanken, P., and Williams, M.: Soil respiration variability across a soil moisture and vegetation community gradient within a snow-scoured alpine meadow, *Biogeochemistry*, 125, 185–202, <https://doi.org/10.1007/s10533-015-0122-3>, 2015.
- Krogh, S., Pomeroy, J., and Marsh, P.: Diagnosis of the hydrology of a small Arctic basin at the tundra-taiga transition using a physically based hydrological model, *J. Hydrol.*, 550, 685–703, <https://doi.org/10.1016/j.jhydrol.2017.05.042>, 2017.
- Kropp, H., Loranty, M., Rutter, N., Fletcher, C., Derksen, C., Mudryk, L., and Todt, M.: Are vegetation influences on Arctic-boreal snow melt rates detectable across the Northern Hemisphere?, *Environ. Res. Lett.*, 17, 104010, <https://doi.org/10.1088/1748-9326/ac8fa7>, 2022.
- Lawrence, D., Fisher, R., Koven, C., Oleson, K., Swenson, S., Bonan, G., Collier, N., Ghimire, B., Kampenhout, L., Kennedy, D., Kluzek, E., Lawrence, P., Li, F., Li, H., Lombardozzi, D., Riley, W., Sacks, W., Shi, M., Vertenstein, M., Wieder, W., Xu, C., Ali, A., Badger, A., Bisht, G., Broeke, M., Brunke, M., Burns, S., Buzan, J., Clark, M., Craig, A., Dahlin, K., Drewniak, B., Fisher, J., Flanner, M., Fox, A., Gentine, P., Hoffman, F., Keppel-Aleks, G., Knox, R., Kumar, S., Lenaerts, J., Leung, L. R., Lipscomb, W., Lu, Y., Pandey, A., Pelletier, J., Perket, J., Randerston, J., Ricciuti, D., Sanderson, B., Slater, A., Subin, Z., Tang, J., Thomas, R. Q., Val Martin, M., and Zeng, X.: The Community Land Model version 5: Description of new features, benchmarking, and impact of forcing uncertainty, *J. Adv. Model. Earth Sy.*, 11, 4245–4287, <https://doi.org/10.1029/2018MS001583>, 2019.
- Liaw, A. and Wiener, M.: Classification and Regression by Randomforest, *R News*, 2, 18–22, 2002.
- Linn, D. and Doran, J.: Effect of Water Filled Pore Space on Carbon Dioxide and Nitrous Oxide Production in Tilled and Non-Tilled Soils, *Soil Sci. Soc. Am. J.*, 48, 1267–1272, <https://doi.org/10.2136/sssaj1984.03615995004800060013x>, 1984.
- Loranty, M. M., Abbott, B. W., Blok, D., Douglas, T. A., Epstein, H. E., Forbes, B. C., Jones, B. M., Kholodov, A. L., Kropp, H., Malhotra, A., Mamet, S. D., Myers-Smith, I. H., Natali, S. M., O'Donnell, J. A., Phoenix, G. K., Rocha, A. V., Sonnentag, O., Tape, K. D., and Walker, D. A.: Reviews and syntheses: Changing ecosystem influences on soil thermal regimes in northern high-latitude permafrost regions, *Biogeosciences*, 15, 5287–5313, <https://doi.org/10.5194/bg-15-5287-2018>, 2018.
- Maier, M., Weber, T., Fiedler, J., Fuß, R., Glatzel, S., Huth, V., Jordan, S., Jurasiński, G., Kutzbach, L., Schäfer, K., Weymann, D., and Hagemann, U.: Introduction of a guideline for measurements of greenhouse gas fluxes from soils using non-steady-state chambers, *J. Soil Sci. Plant Nut.*, 185, 447–461, <https://doi.org/10.1002/jpln.202200199>, 2022.
- Marrero, T. and Mason E.: Gaseous diffusion coefficients, *J. Phys. Chem. Ref. Data*, 1, 3–117, <https://doi.org/10.1063/1.3253094>, 1972.
- Martin, M., Kumar, P., Sonnentag, O., and Marsh, P.: Thermodynamic basis for the demarcation of Arctic and alpine treelines, *Sci. Rep.-UK*, 12, 12565, <https://doi.org/10.1038/s41598-022-16462-2>, 2022.
- Massman, W.: A review of the molecular diffusivities of H<sub>2</sub>O, CO<sub>2</sub>, CH<sub>4</sub>, CO, O<sub>3</sub>, SO<sub>2</sub>, NH<sub>3</sub>, N<sub>2</sub>O, NO, and NO<sub>2</sub> in air, O<sub>2</sub> and N<sub>2</sub> near STP, *Atmos. Environ.*, 32, 1111–1127, [https://doi.org/10.1016/S1352-2310\(97\)00391-9](https://doi.org/10.1016/S1352-2310(97)00391-9), 1998.
- Mast, M. A., Wickland, K., Striegl, R., and Clow, D.: Winter fluxes of CO<sub>2</sub> and CH<sub>4</sub> from subalpine soils in Rocky Mountain National Park, Colorado, *Global Biogeochem. Cy.*, 12, 607–620, <https://doi.org/10.1029/98GB02313>, 1998.
- Mavrovic, A., Sonnentag, O., Voigt, C., and Roy, A.: Winter CO<sub>2</sub> fluxes over arctic and boreal environments, *Borealis*, [data set], <https://doi.org/10.5683/SP3/COWXAZ>, 2023.
- McDowell, N., Marshall, J., Hooker, T., and Musselman, R.: Estimating CO<sub>2</sub> flux from snowpacks at three sites in the Rocky Mountains, *Tree Physiol.*, 20, 745–753, <https://doi.org/10.1093/treephys/20.11.745>, 2000.
- McMahon, S., Parker, G., and Miller, D.: Evidence for a recent increase in forest growth, *P. Natl. Acad. Sci. USA*, 107, 3611–3615, <https://doi.org/10.1073/pnas.0912376107>, 2010.
- Mellander, P., Löfvenius, M., and Laudon, H.: Climate change impact on snow and soil temperature in boreal Scots pine stands, *Climatic Change*, 85, 179–193, <https://doi.org/10.1007/s10584-007-9254-3>, 2007.
- Meloche, J., Langlois, A., Rutter, N., McLennan, D., Royer, A., Billecocq, P., and Ponomarenko, S.: High-resolution snow depth prediction using Random Forest algorithm with topographic parameters: A case study in the Greiner watershed, Nunavut, *Hydrol. Process.*, 36, e14546, <https://doi.org/10.1002/hyp.14546>, 2021.
- Melton, J. R., Arora, V. K., Wisernig-Cojo, E., Seiler, C., Fortier, M., Chan, E., and Teckentrup, L.: CLASSIC v1.0: the open-source community successor to the Canadian Land Surface Scheme (CLASS) and the Canadian Terrestrial Ecosystem Model (CTEM) – Part 1: Model framework and site-

- level performance, *Geosci. Model Dev.*, 13, 2825–2850, <https://doi.org/10.5194/gmd-13-2825-2020>, 2020.
- Ménard, C., Essery, R., Pomeroy, J., Marsh, P., and Clark, D.: A shrub bending model to calculate the albedo of shrub-tundra, *Hydro. Process.*, 28, 341–351, <https://doi.org/10.1002/hyp.9582>, 2012.
- Michaelson, G. J. and Ping, C. L.: Soil organic carbon and CO<sub>2</sub> respiration at subzero temperature in soils of Arctic Alaska, *J. Geophys. Res.-Atmos.* 108, 8164, <https://doi.org/10.1029/2001JD000920>, 2005.
- Millington, R. J.: Gas Diffusion in Porous Media, *Science*, 130, 100–102, <https://doi.org/10.1126/science.130.3367.100.b>, 1959.
- Miner, K., Turetsky, M., Malina, E., Bartsch, A., Tamminen, J., McGuire, A. D., Fix, A., Sweeney, C., Elder, C., and Miller, C.: Permafrost carbon emissions in a changing Arctic, *Nat. Rev. Earth Environ.*, 3, 55–67, <https://doi.org/10.1038/s43017-021-00230-3>, 2022.
- Monson, R., Lipson, D., Burns, S., Turnipseed, A., Delany, A., Williams, M., and Schmidt, S.: Winter forest soil respiration controlled by climate and microbial community composition, *Nature*, 439, 711–714, <https://doi.org/10.1038/nature04555>, 2006.
- Myers-Smith, I. H., Kerby, J., Phoenix, G., Bjerke, J., Epstein, H., Assmann, J., John, C., Andreu-Hayles, L., Angers-Blondin, S., Beck, P., Berner, L., Bhatt, U., Björkman, A., Blok, C., Bryn, A., Christiansen, C., Cornelissen, J. H. C., Cunliffe, A., Elmedorf, S., Forbes, B., Goetz, S., Hollister, R., de Jong, R., Loranty, M., Macias-Fauria, M., Maseyk, K., Normand, S., Olofsson, J., Parker, T., Parmentier, F.-J., Post, E., Schaepman-Strub, G., Stordal, F., Sullivan, P., Thomas, H., Tømmervik, H., Treharne, R., Tweedie, C., Walker, D., Wilming, M., and Wipf, S.: Complexity revealed in the greening of the Arctic, *Nat. Clim. Change*, 10, 106–117, <https://doi.org/10.1038/s41558-019-0688-1>, 2020.
- Natali, S., Watts, J., Rogers, B., Potter, S., Ludwig, S., Selbmann, A.-K., Sullivan, P., Abbott, B., Arndt, K., Birch, L., Björkman, M., Bloom, A., Celis, G., Christensen, T., Christiansen, C., Commane, R., Cooper, E., Crill, P., Czimczik, C., Davydov, S., Du, J., Egan, J., Elberling, B., Euskirchen, E., Friborg, T., Genet, H., Göckede, M., Goodrich, J., Grogan, P., Helbig, M., Jafarov, E., Jastrow, J., Kalhorai, A., Kim, Y., Kimball, J., Kutzbach, L., Lara, M., Larsen, K., Lee, B.-Y., Liu, Z., Loranty, M., Lund, M., Lupascu, M., Madani, N., Malhotra, A., Matamala, R., McFarland, J., McGuire, A., Michelsen, A., Minions, C., Oechel, W., Olefeldt, D., Parmentier, F.-J., Pirk, N., Poulter, B., Quinton, W., Rezanezhad, F., Risk, D., Sachs, T., Schaefer, K., Schmidt, N., Schuur, E., Semenchuk, P., Shaver, G., Sonnentag, O., Starr, G., Treat, C., Waldrop, M., Wang, Y., Welker, J., Wille, C., Xu, X., Zhang, Z., Zhuang, Q., and Zona, D.: Large loss of CO<sub>2</sub> in winter observed across the northern permafrost region, *Nat. Clim. Change*, 9, 852–857, <https://doi.org/10.1038/s41558-019-0592-8>, 2019.
- Natali, S., Holdren, J., Rogers, B., Treharne, R., Duffy, P., Pomerance, R., and MacDonald, E.: Permafrost carbon feedbacks threaten global climate goals, *P. Natl. Acad. Sci. USA*, 118, e2100163118, <https://doi.org/10.1073/pnas.2100163118>, 2021.
- Outcalt, S., Nelson, F., and Hinkel, K.: The zero-curtain effect: Heat and mass transfer across an isothermal region in freezing soil, *Water Resour. Res.*, 26, 1509–1516, <https://doi.org/10.1029/WR026i007p01509>, 1990.
- Pallandt, M. M. T. A., Kumar, J., Mauritz, M., Schuur, E. A. G., Virkkala, A.-M., Celis, G., Hoffman, F. M., and Göckede, M.: Representativeness assessment of the pan-Arctic eddy covariance site network and optimized future enhancements, *Biogeosciences*, 19, 559–583, <https://doi.org/10.5194/bg-19-559-2022>, 2022.
- Pastorello, G., Trotta, C., Canfora, E., et al.: The FLUXNET2015 dataset and the ONEFlux processing pipeline for eddy covariance data, *Sci. Data*, 7, 225, <https://doi.org/10.1038/s41597-020-0534-3>, 2020.
- Pedron, S., Jespersen, R., Xu, X., Khazindar, Y., Welker, J., and Czimczik, C.: More Snow Accelerates Legacy Carbon Emissions From Arctic Permafrost, *AGU Adv.*, 4, e2023AV000942, <https://doi.org/10.1029/2023AV000942>, 2023.
- Pirk, N., Santos, T., Gustafson, C., Johansson, A., Tufveson, F., Tamstorf, Parmentier, F.-J., Mastepanov, M., and Christensen, T.: Methane emission bursts from permafrost environments during autumn freeze-in: New insights from ground-penetrating radar, *Geophys. Res. Lett.*, 42, 6732–6738, <https://doi.org/10.1002/2015GL065034>, 2015.
- Pirk, N., Tamstorf, M., Lund, M., Mastepanov, M., Pedersen, S., Myllus, M., Parmentier, F.-J., Christiansen, H., and Christensen, T.: Snowpack fluxes of methane and carbon dioxide from high Arctic tundra, *Biogeosciences*, 121, 2886–2900, <https://doi.org/10.1002/2016JG003486>, 2016.
- Ponomarenko, S., McLennan, D., Pouliot, D., and Wagner, J.: High Resolution Mapping of Tundra Ecosystems on Victoria Island, Nunavut – Application of a Standardized Terrestrial Ecosystem Classification, *Can. J. Remote Sens.*, 45, 551–571, <https://doi.org/10.1080/07038992.2019.1682980>, 2019.
- Potapov, P., Hansen, M., Stehman, S., Loveland, T., and Pittman, K.: Combining MODIS and Landsat imagery to estimate and map boreal forest cover loss, *Remote Sens. Environ.*, 112, 3708–3719, <https://doi.org/10.1016/j.rse.2008.05.006>, 2008.
- Prince, M., Roy, A., Royer, A., and Langlois, A.: Timing and spatial variability of fall soil freezing in boreal forest and its effect on SMAP L-band radiometer measurements, *Remote Sens. Environ.*, 231, 111230, <https://doi.org/10.1016/j.rse.2019.111230>, 2019.
- Proksch, M., Rutter, N., Fierz, C., and Schneebeli, M.: Intercomparison of snow density measurements: bias, precision, and vertical resolution, *The Cryosphere*, 10, 371–384, <https://doi.org/10.5194/tc-10-371-2016>, 2016.
- Rantanen, M., Karpechko, A. Y., Lipponen, A., Nordling, K., Hyvärinen, O., Ruosteenoja, K., Vihma, T., and Laaksonen, A.: The Arctic has warmed nearly four times faster than the globe since 1979, *Commun. Earth Environ.*, 3, 1–10, <https://doi.org/10.1038/s43247-022-00498-3>, 2022.
- Ravn, N., Elberling, B., and Michelsen, A.: Arctic soil carbon turnover controlled by experimental snow addition, summer warming and shrub removal, *Soil Biol. Biochem.*, 142, 107698, <https://doi.org/10.1016/j.soilbio.2019.107698>, 2020.
- Royer, A., Dominé, F., Roy, A., Langlois, A., Marchand, N., and Davesne, G.: New northern snowpack classification linked to vegetation cover on a latitudinal megatract across northeastern Canada, *Écoscience*, 28, 225–242, <https://doi.org/10.1080/11956860.2021.1898775>, 2021.
- Schuur, E., McGuire, A., Schädel, C., Grosse, G., Harden, J., Hayes, D., Hugelius, G., Koven, C., Kuhry, P., Lawrence,

- D., Natali, S., Olefeldt, D., Romanovsky, V., Schaefer, K., Turetsky, M., Treat, C., and Vonk, J.: Climate change and the permafrost carbon feedback, *Nature*, 520, 171–179, <https://doi.org/10.1038/nature14338>, 2015.
- Seiler, C., Melton, J. R., Arora, V. K., and Wang, L.: CLASSIC v1.0: the open-source community successor to the Canadian Land Surface Scheme (CLASS) and the Canadian Terrestrial Ecosystem Model (CTEM) – Part 2: Global benchmarking, *Geosci. Model Dev.*, 14, 2371–2417, <https://doi.org/10.5194/gmd-14-2371-2021>, 2021.
- Seok, B., Helmig, D., Williams, M., Liptzin, D., Chowanski, K., and Hueber, J.: An automated system for continuous measurements of trace gas fluxes through snow: an evaluation of the gas diffusion method at a subalpine forest site, Niwot Ridge, Colorado, *Biogeochemistry*, 95, 95–113, <https://doi.org/10.1007/s10533-009-9302-3>, 2009.
- Sepaskhah, A., Tabarzad, A., and Fooladmand, H.: Physical and empirical models for estimation of specific surface area of soils, *Arch. Agron. Soil Sci.*, 56, 325–335, <https://doi.org/10.1080/03650340903099676>, 2010.
- Slater, A. G., Lawrence, D. M., and Koven, C. D.: Process-level model evaluation: a snow and heat transfer metric, *The Cryosphere*, 11, 989–996, <https://doi.org/10.5194/tc-11-989-2017>, 2017.
- Sommerfeld, R., Mosier, A., and Musselman, R.: CO<sub>2</sub>, CH<sub>4</sub> and N<sub>2</sub>O flux through a Wyoming snowpack and implications for global budgets, *Nature*, 361, 140–142, <https://doi.org/10.1038/361140a0>, 1993.
- Sommerfeld, R., Massman, W., Musselman, R., and Mosier, A.: Diffusional flux of CO<sub>2</sub> through snow: spatial and temporal variability among alpine–subalpine sites, *Global Biogeochem. Cy.*, 10, 473–482, <https://doi.org/10.1029/96GB01610>, 1996.
- Steponavičienė, V., Bogužas, V., Sinkevičienė, A., Skinulienė, L., Vaisvalavičius, R., and Sinkevičius, A.: Soil Water Capacity, Pore Size Distribution, and CO<sub>2</sub> Emission in Different Soil Tillage Systems and Straw Retention, *Plants*, 11, 614, <https://doi.org/10.3390/plants11050614>, 2022.
- Strobl, C., Boulesteix, A.-L., Kneib, T., Augustin, T., and Zeileis, A.: Conditional variable importance for random forests, *BMC Bioinformatics*, 9, 307, <https://doi.org/10.1186/1471-2105-9-307>, 2008.
- Sturm, M., Schimel, J., Michaelson, G., Welker, J., Oberbauer, S., Liston, G., Fahnestock, J., and Romanovsky, V.: Winter biological processes could help convert arctic tundra to shrubland, *Bioscience*, 55, 17–26, [https://doi.org/10.1641/0006-3568\(2005\)055\[0017:WBPCHC\]2.0.CO;2](https://doi.org/10.1641/0006-3568(2005)055[0017:WBPCHC]2.0.CO;2), 2005.
- Subke, J., Kutzbach, L., and Risk, D.: Soil Chamber Measurements, in: Springer Handbook of Atmospheric Measurements, Springer Nature Switzerland AG, Cham, Switzerland, 1806 pp., [https://doi.org/10.1007/978-3-030-52171-4\\_60](https://doi.org/10.1007/978-3-030-52171-4_60), 2021.
- Tao, J., Zhu, Q., Riley, W. J., and Neumann, R. B.: Improved ELMv1-ECA simulations of zero-curtain periods and cold-season CH<sub>4</sub> and CO<sub>2</sub> emissions at Alaskan Arctic tundra sites, *The Cryosphere*, 15, 5281–5307, <https://doi.org/10.5194/tc-15-5281-2021>, 2021.
- Tarnocai, C., Canadell, J., Schuur, E., Kuhry, P., Mazhitova, G., and Zimov, S.: Soil organic carbon pools in the northern circumpolar permafrost region, *Global Biogeochem. Cy.*, 23, GB2023, <https://doi.org/10.1029/2008GB003327>, 2009.
- Taylor, J. R.: An Introduction to Error Analysis: The Study of Uncertainties in Physical Measurements, 2nd edn., University Science Books, Sausalito, United States, 343 pp., ISBN-10 093570275X, 1997.
- Tei, S. and Sugimoto, A.: Excessive positive response of model-simulated land net primary production to climate changes over circumboreal forests, *Plant-Environment Interactions*, 1, 102–121, <https://doi.org/10.1002/peis.10025>, 2020.
- Throop, J., Lewkowicz, A., and Smith, S.: Climate and ground temperature relations at sites across the continuous and discontinuous permafrost zones, northern Canada, *Can. J. Earth Sci.*, 49, 865–876, <https://doi.org/10.1139/e11-075>, 2012.
- van Huissteden, J. and Dolman, A.: Soil carbon in the Arctic and the permafrost carbon feedback, *Curr. Opin. Env. Sust.*, 4, 545–551, <https://doi.org/10.1016/j.cosust.2012.09.008>, 2012.
- Virkkala, A.-M., Aalto, J., Rogers, B., Tagesson, T., Treat, C., Natali, S., Watts, J., Potter, S., Lehtonen, A., Mauritz, M., Schuur, E., Kochendorfer, J., Zona, D., Oechel, W., Kobayashi, H., Humphreys, E., Goekcede, M., Iwata, H., Lafleur, P., Euskirchen, E., Bokhorst, S., Marushchak, M., Martikainen, P., Elberling, B., Voigt, C., Biasi, C., Sonnentag, O., Parmentier, F.-J., Ueyama, M., Celis, G., St.Louis, V., Emmerton, C., Peichl, M., Chi, J., Järveoja, J., Nilsson, M., Oberbauer, S., Torn, M., Park, S.-J., Dolman, H., Mammarella, I., Chae, N., Poyatos, R., López-Blanco, E., Christensen, T., Kwon, M., Sachs, T., Holl, D., and Luoto, M.: Statistical upscaling of ecosystem CO<sub>2</sub> fluxes across the terrestrial tundra and boreal domain: Regional patterns and uncertainties, *Global Change Biol.*, 27, 4040–4059, <https://doi.org/10.1111/gcb.15659>, 2021.
- Virkkala, A.-M., Natali, S. M., Rogers, B. M., Watts, J. D., Savage, K., Connon, S. J., Mauritz, M., Schuur, E. A. G., Peter, D., Minions, C., Nojeim, J., Commane, R., Emmerton, C. A., Goeckede, M., Helbig, M., Holl, D., Iwata, H., Kobayashi, H., Kolar, P., López-Blanco, E., Marushchak, M. E., Mastepanov, M., Merbold, L., Parmentier, F.-J. W., Peichl, M., Sachs, T., Sonnentag, O., Ueyama, M., Voigt, C., Aurela, M., Boike, J., Celis, G., Chae, N., Christensen, T. R., Bret-Harte, M. S., Dengel, S., Dolman, H., Edgar, C. W., Elberling, B., Euskirchen, E., Grellé, A., Hatakia, J., Humphreys, E., Järveoja, J., Kotani, A., Kutzbach, L., Laurila, T., Lohila, A., Mammarella, I., Matsuura, Y., Meyer, G., Nilsson, M. B., Oberbauer, S. F., Park, S.-J., Petrov, R., Prokushkin, A. S., Schulze, C., St. Louis, V. L., Tuittila, E.-S., Tuovinen, J.-P., Quinton, W., Varlagin, A., Zona, D., and Zyryanov, V. I.: The ABCflux database: Arctic–boreal CO<sub>2</sub> flux observations and ancillary information aggregated to monthly time steps across terrestrial ecosystems, *Earth Syst. Sci. Data*, 14, 179–208, <https://doi.org/10.5194/essd-14-179-2022>, 2022.
- Virtanen, T. and Ek, M.: The fragmented nature of tundra landscape, *Int. J. Appl. Earth Obs.*, 27, 4–12, <https://doi.org/10.1016/j.jag.2013.05.010>, 2014.
- Wang, T., Ciais, P., Piao, S. L., Ottlé, C., Breden, P., Maigann, F., Arain, A., Cescatti, A., Gianelle, D., Gough, C., Gu, L., Lafleur, P., Laurila, T., Marcolla, B., Margolis, H., Montagnani, L., Moors, E., Saigusa, N., Vesala, T., Wohlfahrt, G., Koven, C., Black, A., Dellwik, E., Don, A., Hollinger, D., Knoll, A., Monson, R., Munger, J., Suyker, A., Varlagin, A., and Verma, S.: Controls on winter ecosystem respiration in temperate and boreal ecosystems, *Biogeosciences*, 8, 2009–2025, <https://doi.org/10.5194/bg-8-2009-2011>, 2011.

- Wieder, W., Sulman, B., Hartman, M., Koven, C., and Bardford, M.: Arctic Soil Governs Whether Climate Change Drives Global Losses or Gains in Soil Carbon, *Geophys. Res. Lett.*, 46, 14486–14495, <https://doi.org/10.1029/2019GL085543>, 2019.
- Wilcox, E. J., Keim, D., de Jong, T., Walker, B., Sonnentag, O., Sniderhan, A. E., Mann, P., and Marsh, P.: Tundra shrub expansion may amplify permafrost thaw by advancing snowmelt timing, *Arct. Sci.*, 5, 202–217, <https://doi.org/10.1139/as-2018-0028>, 2019.
- Webb, E., Schuur, E., Natali, S., Oken, K., Bracho, R., Krapek, J., Risk, D., and Nickerson, N.: Increased wintertime CO<sub>2</sub> loss as a result of sustained tundra warming, *J. Geophys. Res.-Biogeo.*, 121, 249–265, <https://doi.org/10.1002/2014JG002795>, 2016.
- Yi, Y., Kimball, J. S., Rawlins, M. A., Moghaddam, M., and Euskirchen, E. S.: The role of snow cover affecting boreal-arctic soil freeze-thaw and carbon dynamics, *Biogeosciences*, 12, 5811–5829, <https://doi.org/10.5194/bg-12-5811-2015>, 2015.
- Yi, Y., Kimball, J. S., Chen, R. H., Moghaddam, M., and Miller, C. E.: Sensitivity of active-layer freezing process to snow cover in Arctic Alaska, *The Cryosphere*, 13, 197–218, <https://doi.org/10.5194/tc-13-197-2019>, 2019.
- Yli-Halla, M., Lötjönen, T., Kekkonen, J., Virtanen, S., Marttila, H., Liimatainen, M., Saari, M., Mikkola, J., Suomela, R., and Joki-Tokola, E.: Thickness of peat influences the leaching of substances and greenhouse gas emissions from a cultivated organic soil, *Sci. Total Environ.*, 806, 150499, <https://doi.org/10.1016/j.scitotenv.2021.150499>, 2022.
- Zhang, L., Zhao, T., Jiang, L., and Zhao, K.: Estimate of Phase Transition Water Content in Freeze–Thaw Process Using Microwave Radiometer, *IEEE T. Geosci. Remote*, 48, 4248–4255, <https://doi.org/10.1109/TGRS.2010.2051158>, 2010.
- Zhu, C., Nakayama, M., and Inouye, H. Y.: Continuous measurement of CO<sub>2</sub> flux through the snowpack in a dwarf bamboo ecosystem on Rishiri Island, Hokkaido, Japan, *Polar Sci.*, 8, 218–231, <https://doi.org/10.1016/j.polar.2014.04.003>, 2014.

# Chapitre 4 : Flux hivernaux de $CH_4$

## 4.1 Présentation de l'article scientifique

Le manuscrit scientifique qui suit a été soumis à la revue scientifique *Geophysical Research Letters* (American Geophysical Union : AGU) le 21 décembre 2023. Le manuscrit y est présenté de façon intégrale tel que soumis. La numérotation des lignes, sections, figures, tableaux et équations est indépendante du reste de la thèse. Les références citées dans ce manuscrit ne sont pas répétées à la bibliographie complémentaire de la thèse (Sect. 10). Le matériel supplémentaire accompagnant l'article se trouve à la suite de ce dernier (Sect. 4.3.5).

Ce manuscrit présente des mesures de flux de  $CH_4$  hivernaux afin de déterminer les principaux contrôles environnementaux et de contraster les flux provenant de différents types d'écosystèmes arctiques et boréaux (Objectifs spécifiques # 1 et # 2). Les mesures de flux de  $CH_4$  proviennent principalement des mêmes campagnes de terrains que l'article précédent (Chap. 3) puisque la méthode du gradient de diffusion à travers le couvert nival permet de mesurer les flux de  $CO_2$  et de  $CH_4$  de façon concomitante. Les mesures de flux de  $CH_4$  portent donc sur les mêmes sites et périodes d'études que l'article portant sur les flux de  $CO_2$  (Chap. 3) en y ajoutant un nouveau site finlandais.

Contribution en tant que premier auteur : Conception et planification de l'étude. Organisation des campagnes de terrains. Implémentation de la méthode de mesure. Collecte, traitement et analyse des données. Rédaction du manuscrit.

Référence complète du manuscrit :

**Mavrovic, A., Sonnentag, O., Lemmetyinen, J., Voigt, C., Aurela, M., and Roy, A. (in review)** *Contrasting winter methane fluxes over boreal and Arctic environments. Geophysical Research Letters.*

## 4.2 Résumé de l'article scientifique en français

Le réchauffement du climat des régions arctiques et boréales (RAB) a des conséquences encore mal comprises sur les processus du cycle du carbone. Notamment, les incertitudes sur les bilans annuels de méthane ( $CH_4$ ) découlent en partie du fait que les données sur la contribution hivernale sont limitées. Dans cette étude, des mesures de flux de  $CH_4$  en hiver ont été réalisées à l'aide de la méthode du gradient de diffusion à travers la couverture neigeuse sur cinq types d'écosystèmes des RAB : forêt boréale de conifères à couronne fermée et à couronne ouverte, tourbière boréale, toundra à arbustes dressés et toundra à arbustes couchés. Les sites en forêt boréale ont agi comme des puits de  $CH_4$  en hiver, tandis que ceux de la tourbière boréale ont agi comme des sources de  $CH_4$  en hiver. De plus, nous avons identifié plusieurs points chauds d'émission de  $CH_4$  aux sites en toundra arctique et une grande variabilité spatiale des émissions de  $CH_4$  dans la tourbière boréale. Aux sites en forêt boréale, la teneur en eau liquide du sol a été identifiée comme un contrôle environnemental important des flux de  $CH_4$  en hiver.

## 1 Winter methane fluxes over boreal and Arctic environments

2

3 **Alex Mavrović<sup>1-2-3-4</sup>, Oliver Sonnentag<sup>2-4</sup>, Juha Lemmetyinen<sup>5</sup>, Carolina Voigt<sup>4-6</sup>, Mika**  
4 **Aurela<sup>5</sup>, Alexandre Roy<sup>1-2</sup>**

5

6 <sup>1</sup>Université du Québec à Trois-Rivières, Département des sciences de l'environnement, Trois–  
7 Rivières, Québec, G9A 5H7, Canada

8 <sup>2</sup>Centre d'Études Nordiques, Québec, Québec, G1V 0A6, Canada

9 <sup>3</sup>Polar Knowledge Canada, Canadian High Arctic Research Station campus, Cambridge Bay,  
10 Nunavut, X0B 0C0, Canada

11 <sup>4</sup>Université de Montréal, Département de géographie, Montréal, Québec, H3T 1J4, Canada

12 <sup>5</sup>Finnish Meteorological Institute, Helsinki, FI-00560, Finland

13 <sup>6</sup>Universität Hamburg, 20146 Hamburg, Germany

14

15 Corresponding author: Alex Mavrović (alex.mavrović@uqtr.ca)

16

### 17 **Key Points:**

- 18
- Boreal forest upland soils acted as net methane sink during winter.
  - Boreal wetland soils acted as net winter methane source, while tundra wetlands emissions  
20 were generally low except for a few hotspots.
  - In boreal forests, the soil liquid water content was one of the main environmental controls  
22 on winter methane fluxes.
- 23

### 24 **Keywords:**

25 Methane flux, Methane exchange, Arctic–boreal regions, Carbon cycle, Winter, Non-growing  
26 season.

27

28

29

30

31

32

33 **Abstract**

34 Unprecedented warming of Arctic–boreal regions (ABR) has poorly understood  
35 consequences on carbon cycle processes. Uncertainties in annual methane ( $\text{CH}_4$ ) budgets partly  
36 arise because of limited data availability during winter. In this study, winter  $\text{CH}_4$  flux  
37 measurements were conducted using the snowpack diffusion gradient method over five ABR  
38 ecosystem types in Canada and Finland: closed–crown and open–crown coniferous boreal forest,  
39 boreal wetland, and erect–shrub and prostrate–shrub tundra. Boreal forest uplands acted as net  $\text{CH}_4$   
40 sinks, while the boreal wetland acted as net  $\text{CH}_4$  source during winter. We identified several  
41 wetland tundra  $\text{CH}_4$  emission hotspots and large spatial variability in boreal wetland  $\text{CH}_4$   
42 emissions. In the boreal forest uplands, soil liquid water content was identified as an important  
43 environmental control of winter  $\text{CH}_4$  fluxes. Our results indicate non–negligible winter  $\text{CH}_4$  flux,  
44 which must be accounted for in annual carbon balance and terrestrial biosphere models over ABR.

45 **Plain Language Summary**

46 The climate of our planet is closely linked to the atmospheric concentrations of greenhouse  
47 gases such as carbon dioxide and methane that partially retain the energy coming from the Sun.  
48 The Arctic and boreal regions are some of the environments that have been the least studied, mostly  
49 because of their remoteness. In those environments, winter is the least studied period of the year  
50 because of technical challenges posed by harsh winter conditions. Our study focused on winter  
51 methane exchange between the snow–covered ground surface and the atmosphere in Arctic–boreal  
52 regions. Methane is found in smaller quantities in the atmosphere compared to carbon dioxide but  
53 with a much stronger warming potential. We observed that the boreal forests acted as a sink of  
54 methane, removing methane from the atmosphere during winter. In contrast, boreal wetlands  
55 emitted significant amounts of methane into the atmosphere. We observed low methane emissions  
56 in the Arctic tundra except for a few hotspots with high methane emissions. All those observations  
57 show the variability of methane exchanges in different environments and highlight the importance  
58 of understanding those exchanges to improve our ability to predict the role of Arctic–boreal  
59 regions on the climate system.

60 **1 Introduction**

61 Methane ( $\text{CH}_4$ ) exchange between the ground surface and the atmosphere in Arctic and boreal  
62 biomes (hereafter called Arctic–boreal regions; ABR) play an important role in the global climate  
63 with potentially important responses to a warming climate (Bekryaev et al., 2010; Kirschke et al.,  
64 2013; Yvon–Durocher et al., 2014; Schuur et al., 2015; Dean et al., 2018; Rößger et al., 2022).  
65 The response of ABR  $\text{CH}_4$  fluxes to temperature is especially relevant since the ABR are warming  
66 up to four times faster than the rest of the planet (Derksen et al., 2019; Rantanen et al., 2022). The  
67 soils of ABR store a vast amount of labile organic matter due to inherently slow decomposition  
68 rates, largely attributable to cold temperatures (Tarnocai et al., 2009; Deluca and Boisvenue, 2012;  
69 Ravn et al., 2020). Therefore, altered  $\text{CH}_4$  exchange rates due to ABR warming up could generate  
70 potentially non–negligible, positive feedback to the global climate system (Natali et al., 2021;  
71 Rößger et al., 2022; Schuur et al., 2022). Poor understanding of environmental controls on  $\text{CH}_4$   
72 exchange during winter constitutes a large source of uncertainty in the ABR  $\text{CH}_4$  budget (McGuire  
73 et al., 2012; Mastepanov et al., 2013; Treat et al., 2018).

74

The net soil CH<sub>4</sub> flux is a result of three groups of processes: production, oxidation, and transport of CH<sub>4</sub>. CH<sub>4</sub> in soils is produced by methanogens during organic matter decomposition under mostly anoxic conditions, which typically occur in deeper soil layers or in water-saturated environments (Zhang et al., 2017; Feng et al., 2020; Bastviken et al., 2023). In contrast, under predominantly aerobic conditions, CH<sub>4</sub> is oxidized by methanotrophs as a source of energy and carbon (Lai, 2009; Bastviken et al., 2023). Such aerobic conditions are often found in drier upper soil layers in mineral upland soils. In well-drained soils, CH<sub>4</sub> oxidation typically exceeds production resulting in a net soil CH<sub>4</sub> sink that removes CH<sub>4</sub> from the atmosphere (Lai, 2009; Lee et al., 2023). In contrast, CH<sub>4</sub> oxidation in wetlands is lower than production resulting in net CH<sub>4</sub> emissions (Topp and Pattey, 1997; Roslev et al., 1997). Still, CH<sub>4</sub> oxidation in wetlands is an important process that removes a large percentage of CH<sub>4</sub> produced in saturated soil layers before it can reach the atmosphere (Oertel et al., 2016). During the oxidation process, CH<sub>4</sub> is oxidized to carbon dioxide (CO<sub>2</sub>) and water (H<sub>2</sub>O). Methane transport, i.e., the movement of CH<sub>4</sub> from its zone of production to the atmosphere by diffusion, ebullition, and plant-mediated transport also plays an important role in mitigating CH<sub>4</sub> oxidation by limiting the time during which methanotrophs can consume CH<sub>4</sub> (Bastviken et al., 2023). The vegetation composition of the ecosystem has been shown to impact CH<sub>4</sub> fluxes by providing the organic matter substrate for CH<sub>4</sub> production, bypassing zones of CH<sub>4</sub> oxidation by plant-mediated transport, and by its indirect impact on water table and thaw depth (King et al., 1998; Andresen et al., 2017; Bastviken et al., 2023).

The majority of prior CH<sub>4</sub> studies in the ABR has focused on snow-free growing season fluxes (e.g., Ullah et al., 2009; Zona et al., 2009; Helbig et al., 2016; Kuhn et al., 2021). The largest CH<sub>4</sub> flux measurement network, FLUXNET-CH<sub>4</sub>, provides limited winter data from ABR due to the failure of equipment in cold harsh conditions (Knox et al., 2019; Delwiche et al., 2021). The few studies on winter CH<sub>4</sub> fluxes in the Arctic biome that exist showed that winter can contribute up to 40 to 50% of the annual net CH<sub>4</sub> emissions (Zona et al., 2016; Treat et al., 2018; Rößger et al., 2022; Ito et al., 2023). The length of winter typically increases with latitude and can span the period from September to June. Most of the winter ABR CH<sub>4</sub> studies focus on wetlands and peatlands where higher emissions are expected, with little attention to CH<sub>4</sub> sinks (Treat et al., 2018). More studies of winter CH<sub>4</sub> fluxes have been carried out in the boreal biome than in the Arctic biome, but even in the boreal biome, winter CH<sub>4</sub> flux measurements remain scarce compared to growing season studies (Viru et al., 2020; Hiyama et al., 2021; Lee et al., 2023). Overall, the limited data available on ABR CH<sub>4</sub> fluxes translates into limited knowledge of environmental controls of winter CH<sub>4</sub> fluxes. This lack of knowledge is challenging terrestrial biosphere models, often using CH<sub>4</sub> emission schemes developed for the growing season or lower latitudes and more temperate environments which can be inaccurate when extrapolated to the ABR carbon cycle (Fisher et al., 2014; Ito et al., 2023).

The goal of this study is to quantify winter CH<sub>4</sub> fluxes in different ABR ecosystems and identify environmental controls on fluxes. Our study is based on 660 snowpack diffusion gradient and supporting measurements (snowpack properties, soil temperature and liquid water content) at five different ecosystems in Arctic and boreal biomes in Finland and Canada: a boreal wetland, a closed-crown coniferous boreal forest stand, two open-crown coniferous boreal forest stands, an erect-shrub tundra, and a prostrate-shrub tundra site. Spatially distributed measurements of snowpack CH<sub>4</sub> diffusion gradients were performed during the 2020–2021, 2021–2022 and 2022–

121 2023 winters (December to May). All CH<sub>4</sub> flux data were collected concurrently with CO<sub>2</sub> flux  
 122 data presented and analyzed in Marovic et al., 2024.

123 **2 Materials and Methods**

124 **2.1 Measurements sites**

125 Five study sites characteristic of five ABR ecosystems were selected (Fig. S1; Table S1  
 126 and S2). Cambridge Bay (CB; Nunavut, Canada) was the northernmost site located in the Arctic  
 127 biome dominated by lichen and prostrate shrub tundra. The CB site is constituted of mesic areas  
 128 (CB-mes) and wetland areas (CB-wet) (Ponomarenko et al., 2019), Trail Valley Creek (TVC;  
 129 Northwest Territories, Canada) is situated in the forest-tundra ecotone, the transitional zone  
 130 between the boreal and Arctic biomes. TVC is dominated by erect shrub tundra with remaining  
 131 tree patches (Martin et al., 2022; Voigt et al., 2023). Havikpak Creek (HPC; Northwest Territories,  
 132 Canada) is located about 50 km south of TVC in an open-crown black spruce dominated forest  
 133 stand, just south of the treeline (Krogh et al., 2017). Sodankylä (SOD, Lapland, Finland) is in the  
 134 northern boreal biome. The SOD study site comprises two study zones: a closed-crown Scots  
 135 pine-dominated forest stand (SOD-for) and adjacent open wetlands (*aapa mire*; SOD-wet)  
 136 (Ikonen et al., 2016). Montmorency Forest (MM; Québec, Canada) is the southernmost site located  
 137 in a closed-crown balsam fir dominated boreal forest (Barry et al., 1988). The CB, TVC and HPC  
 138 sites are underlain by continuous permafrost, while the MM and SOD sites are permafrost-free.  
 139

140 **2.2 CH<sub>4</sub> flux calculation**

141 In snow-covered regions, a vertical CH<sub>4</sub> diffusion gradient ( $d[\text{CH}_4]/dz$ ; g C m<sup>-4</sup>) is  
 142 maintained through the snowpack as a result of CH<sub>4</sub> production, oxidation and transport in soils.  
 143 Fick's first law for gas diffusion in porous media can be used to estimate CH<sub>4</sub> fluxes ( $F_{\text{CH}_4}$ ; mg C  
 144 m<sup>-2</sup> day<sup>-1</sup>) from  $d[\text{CH}_4]/dz$  (Sommerfeld et al., 1993; Zhu et al., 2014), with a positive  $F_{\text{CH}_4}$   
 145 representing CH<sub>4</sub> emission from the soil to the atmosphere and a negative  $F_{\text{CH}_4}$  representing CH<sub>4</sub>  
 146 uptake from the atmosphere to the soil:

$$147 \quad F_{\text{CH}_4} = -\varphi \cdot \tau \cdot D \cdot \frac{d[\text{CH}_4]}{dz} \quad (1)$$

150 where  $\varphi$  represents the snow porosity (unitless),  $\tau$  the snow tortuosity (unitless) and  $D$  the  
 151 diffusion coefficient of CH<sub>4</sub> through the air in m<sup>2</sup> day<sup>-1</sup>.  $\varphi$  and  $\tau$  can be estimated from snow  
 152 density ( $\rho_{\text{snow}}$ ) and snow liquid water content ( $\theta$ ) (Du Plessis and Masliyah 1991; Kinar and  
 153 Pomeroy, 2015; Madore et al., 2022):

$$154 \quad \varphi = 1 - \frac{\rho_{\text{snow}}}{\rho_{\text{ice}}} + \theta \cdot \left( \frac{\rho_{\text{water}}}{\rho_{\text{ice}}} - 1 \right) \quad (2)$$

$$157 \quad \tau = \frac{1 - (1 - \varphi)^{2/3}}{\varphi} \approx \varphi^{1/3} \quad (3)$$

159 where  $\rho$  represents the density of snow, pure ice and water in g cm<sup>-3</sup> ( $\rho_{\text{water}} = 0.99984$  g  
 160 cm<sup>-3</sup> at T = 0 °C; Harvey et al., 2017). Ice density ( $\rho_{\text{ice}}$ ) must be adjusted for ice temperature ( $T_{\text{ice}}$ )  
 161 (Harvey et al., 2017):

$$\rho_{ice} = -0.0001 \cdot T_{ice} + 0.9168 \quad (4)$$

Standard diffusion coefficients of CH<sub>4</sub> are available in literature but must be corrected for temperature and pressure (Marrero and Mason, 1972; Massman, 1988):

$$D = 0.1859 \cdot \left( \frac{T}{T_o} \right)^{1.747} \quad (5)$$

where  $T$  is the air temperature and  $T_o$  is the freezing point (273.15 K). The diffusion gradient method assumes that gas fluxes are the result of simple, linear, gradient-induced diffusion through snowpack porosities (McDowell et al., 2000). If the gas flow is altered by ice crusts or dense snow layers, it could lead to a positive bias (i.e.,  $F_{CH_4}$  overestimation; Seok et al., 2009). Such layers were rarely found in our study sites and did not cause the  $d[CH_4]/dz$  to diverge from its linear relationship. In contrast, the diffusion gradient assumption also does not hold when strong wind events occur, decreasing snowpack  $CH_4$  concentration through wind pumping and inducing a negative bias on  $CH_4$  fluxes (Seok et al., 2009). Consequently,  $d[CH_4]/dz$  was not measured in days following a strong wind event. Monitoring of  $F_{CH_4}$  at a few sampling locations did not show any relationship between  $F_{CH_4}$  and wind speed or atmospheric pressure (Mavrovic et al., 2023). At most sites, the vegetation or understory was fully snow-covered (Fig. S1). In the presence of standing shrubs higher than the snow cover (i.e., only the tall and riparian shrub sites at TVC), it is possible that the diffusion gradient method could underestimate  $F_{CH_4}$  because of the preferential channel created by the vegetation that would reduce the diffusion gradient inside the snow porosity.

### 2.3 Data collection

The  $d[\text{CH}_4]/dz$  was estimated by collecting gas samples along a vertical profile in the snowpack. Five gas samples were collected for each vertical profile: I) at 5 cm above the snowpack (ambient air), II) at 5 cm depth from the snowpack surface, III) at 1/3 of total snow depth, IV) at 2/3 of total snow depth and V) at the soil–snow interface. Snow pore gas was collected with a thin hollow stainless–steel rod (50–120 cm long, 4 mm outer diameter and 2 mm inner diameter). Gas was collected in a 60 mL syringe (Air–Tite Luer Lock, Virginia Beach, Virginia) connected to the rod via a three–way valve before being transferred into 12 mL hermetic glass vials (Labco Exetainer®, Labco Ltd., Lampeter, UK).  $\text{CH}_4$  concentration was measured with a Licor LI–7810  $\text{CH}_4/\text{CO}_2/\text{H}_2\text{O}$  Trace Gas Analyzer ( $\sigma < 0.03\%$  at 2 ppm; LI–COR Biosciences, Lincoln, Nebraska, US) using an open–loop method with a continuous flow of a 1.1 ppm  $\text{CH}_4$  calibration gas (Linde Canada, Ottawa, Ontario). The  $\text{CH}_4$  concentration of gas samples was calculated based on a calibration curve of gas standards ranging from 0 to 10 ppm of  $\text{CH}_4$ . At each site, several sampling locations were selected to cover the full range of vegetation types and snowpack characteristics, covering defined areas of 0.25–4 km<sup>2</sup>. At each sampling location, 2 to 4 replicate profiles were measured within 2–3 m to ensure sampling repeatability.

After gas sampling, a vertical profile of snow and soil properties was measured to calculate snow porosity, tortuosity and the CH<sub>4</sub> diffusion coefficient. Snow properties were measured at every 5 cm including snow temperature (Snowmetrics digital thermometer; a tenth of a degree resolution), snow density (Snowmetrics digital scale, 100 and 250 cm<sup>3</sup> snow cutters;  $\sigma(\rho_{\text{snow}}) \approx 9\%$ ; Proksch et al., 2016), snow liquid water content (hand test from Fierz et al., 2009) and snow

stratigraphy. Near-surface soil temperature ( $T_{\text{soil}}$ ) was measured at 1 cm depth below the soil–snow interface, and three measurements within a surface of 1 m<sup>2</sup> of  $T_{\text{soil}}$  were averaged. An uncertainty assessment was conducted to evaluate CH<sub>4</sub> flux precision based on the snowpack diffusion gradient method; the detailed method can be found in the supporting information (Table S3 and Fig. S2). Soil volumetric liquid water content (LWC) was estimated from dielectric sensors. MM was equipped with permanent TEROS 12 Soil Moisture Sensors (METER Group) at 5 cm depth. At SOD—for, instantaneous soil LWC measurements were conducted along with the snow and soil properties using a ML3 ThetaProbe Soil Moisture Sensor (Delta-T Devices). LWC was estimated to be negligible at the CB, TVC and HPC sites since  $T_{\text{soil}}$  was in-between -5°C and -25°C.

218

### 219 3 Results

220

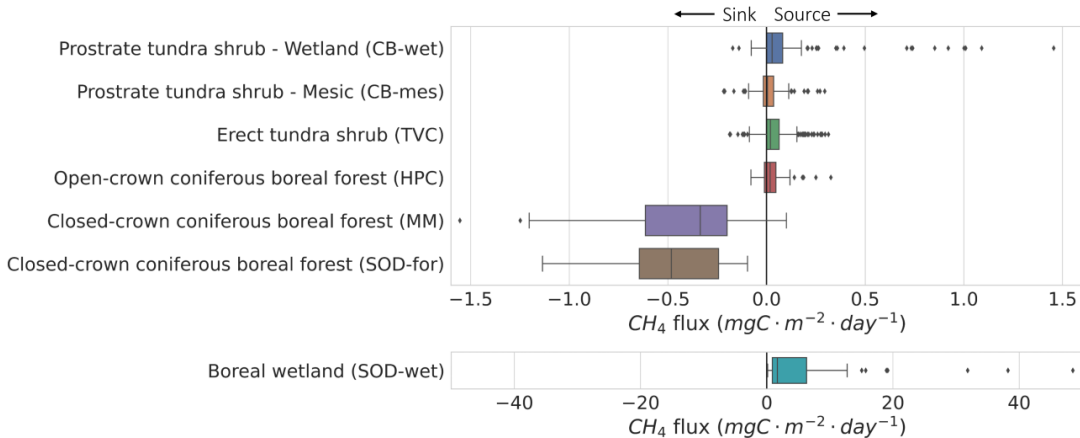
#### 221 3.1 Winter methane fluxes across ABR sites

222 Our results showed mostly low to negligible CH<sub>4</sub> emissions in tundra sites (CB and TVC) and  
223 open-crown boreal forest (HCP). At those sites, fluxes ranged from -0.21 mg C m<sup>-2</sup> day<sup>-1</sup> (CH<sub>4</sub>  
224 uptake) to 0.33 mg C m<sup>-2</sup> day<sup>-1</sup> (CH<sub>4</sub> emission) with a mean rate of  $0.03 \pm 0.08$  mg C m<sup>-2</sup> day<sup>-1</sup>  
225 (mean  $\pm$  standard deviation), except for a few hotspots at CB that emitted CH<sub>4</sub> up to 1.46 mg C m<sup>-2</sup>  
226 day<sup>-1</sup> with a mean rate of  $0.78 \pm 0.31$  mg C m<sup>-2</sup> day<sup>-1</sup> (Fig. 1). The winter CH<sub>4</sub> hotspot locations  
227 were revisited 10 times over a period of 8 weeks and consistently displayed high CH<sub>4</sub> emissions  
228 in time.

229

230 Several vegetation types were found in the Arctic tundra sites of CB and TVC. The main  
231 differences between CH<sub>4</sub> fluxes among vegetation types at CB followed soil water regimes as  
232 divided into mesic and wetland areas (Fig. 1). We observed some differences in the ranges and  
233 means of CH<sub>4</sub> fluxes among TVC vegetation types, although those differences were small  
234 compared to the variability between study sites (Fig. S3). The TVC vegetation types surveyed, by  
235 ascending mean CH<sub>4</sub> fluxes, are as follows: dwarf shrub, black spruce patch, riparian shrub, lichen,  
236 tussock, polygon, and tall shrub. The closed-crown coniferous boreal forest sites showed mean  
237 CH<sub>4</sub> uptake rates throughout winter of  $-0.43 \pm 0.34$  mg C m<sup>-2</sup> day<sup>-1</sup> (MM) and  $-0.47 \pm 0.26$  mg C  
238 m<sup>-2</sup> day<sup>-1</sup> (SOF—for). The SOD-wet boreal wetland displayed high CH<sub>4</sub> emissions throughout  
239 winter, with rates up to 48.51 mg C m<sup>-2</sup> day<sup>-1</sup> and an average of  $4.57 \pm 7.34$  mg C m<sup>-2</sup> day<sup>-1</sup>. The  
240 boreal wetland F<sub>CH4</sub> at SOD—for were at least one order of magnitude higher than any other site in  
241 this study. The boreal wetland sampling locations displayed an important spatial variability of F<sub>CH4</sub>  
242 with some sampling locations emitting CH<sub>4</sub> at average rates up to 50 times higher than the lowest  
243 ones (Fig. S4).

244



245

**Figure 1.** CH<sub>4</sub> flux across the study sites: Cambridge Bay (CB), Trail Valley Creek (TVC), Havikpak Creek (HPC), Montmorency Forest (MM), and Sodankylä (SOD–for). Outliers were defined as  $F_{CH_4} > Q3 + 1.5 \text{ IQR}$  where Q3 is the third quartile and IQR the interquartile range. The F<sub>CH<sub>4</sub></sub> from the boreal wetland is shown on a separate axis since the range of F<sub>CH<sub>4</sub></sub> is of a different order of magnitude.

251

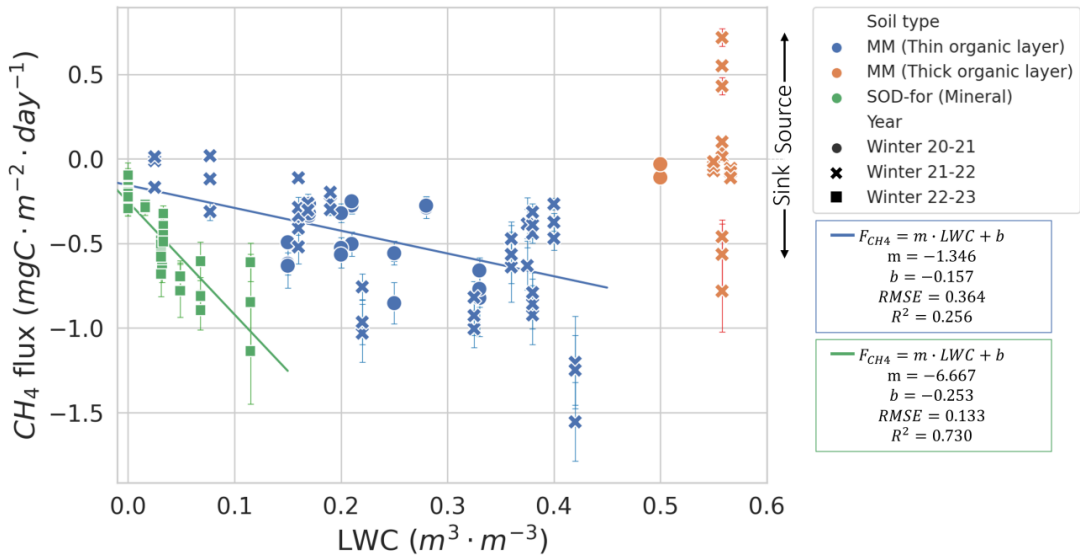
### 252 3.2 Environmental controls of winter methane fluxes

253 Statistical analyses were performed to identify the environmental variables (i.e., T<sub>soil</sub>, soil  
254 LWC, vegetation type and snow variables) controlling CH<sub>4</sub> fluxes at both the site-level and over  
255 the entire dataset in the different northern ecosystems. The statistical analysis approach included  
256 correlation, regression and machine learning (i.e., Random Forest). For tundra sites (i.e., CB and  
257 TVC), as the CH<sub>4</sub> fluxes were relatively small, none of these variables proved statistically  
258 significant (e.g., Fig. 3 for T<sub>soil</sub>). The correlation between F<sub>CH<sub>4</sub></sub> and snow variables was low at all  
259 study sites ( $R^2 < 0.13$  for total snow height, SWE and mean snow density; Fig. S5). However, at  
260 the closed-crown coniferous boreal forest sites of MM and SOD–for, our results show a site-  
261 specific linear relationship between winter F<sub>CH<sub>4</sub></sub> and soil LWC (Fig. 2). The correlation between  
262 F<sub>CH<sub>4</sub></sub> and T<sub>soil</sub> at 1 cm depth was low since T<sub>soil</sub> had a narrow range during the measurement  
263 campaigns at MM and SOD–for, being around freezing point for all measurements ( $R^2 = 0.035$ ;  
264 Fig. 3). MM and SOD–for boreal forest uplands were the only two sites with near-surface T<sub>soil</sub>  
265 close enough to 0°C to allow the coexistence of ice and liquid water in the soil. Water-saturated  
266 organic layers also occurred at the boreal wetland of SOD–wet, but the liquid water was trapped  
267 under a top-layer made mostly of solid ice with a thickness of several centimeters.

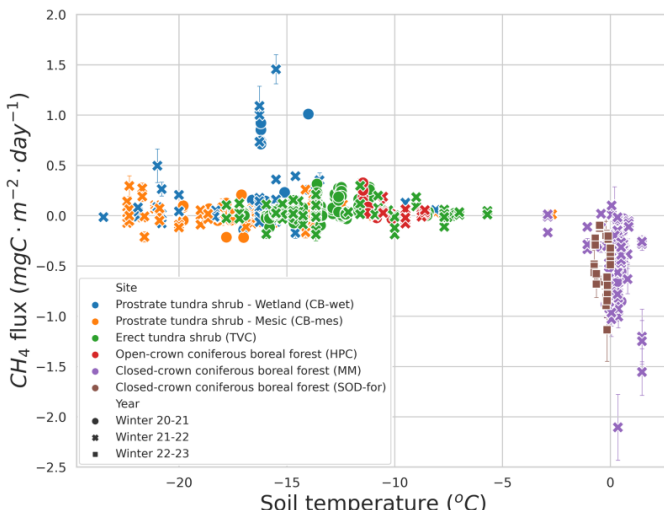
268

269 One sampling location at MM displayed different soil properties than the other sampling  
270 locations because of its thick organic soil layer and high soil moisture regime due to its location  
271 near the bottom of a microtopographic depression (Fig. 2). Other MM sampling locations with a  
272 thin organic layer shared a similar soil composition dominated by sandy loam mineral soils. The  
273 MM thick organic layer sampling location alternates between a CH<sub>4</sub> source or sink throughout the  
274 snow-covered season.

275



276  
277 **Figure 2.**  $\text{CH}_4$  flux as a function of soil volumetric liquid water content (LWC) at the  
278 Montmorency Forest (MM) and Sodankylä (SOD-for) boreal forest uplands study sites, the only  
279 sites where liquid water was present during our winter campaigns. A linear regression was fitted  
280 for the SOD-for boreal forest uplands data and MM data, excluding the thick organic layer site.  
281 All parameters of the linear regressions are in  $\text{mg C m}^{-2} \text{ day}^{-1}$ . There is only one sampling location  
282 for the MM thick organic layer, whereas there are 9 sampling locations for the MM thin organic  
283 layer and 9 for the SOD-for. The data with no apparent error bar have an error bar smaller than  
284 the size of the dot.



285  
286 **Figure 3.**  $\text{CH}_4$  flux as a function of soil temperature at 1 cm depth at the study sites of Cambridge  
287 Bay (CB), Trail Valley Creek (TVC), Havikpak Creek (HPC), Montmorency Forest (MM) during  
288 winter 2020–2021 and 2021–2022, and at Sodankylä (SOD-for). The data with no apparent error  
289 bar have an error bar smaller than the size of the dot.

290 **4 Discussion**

291

292 CH<sub>4</sub> flux regimes were previously observed mostly during the growing season, whereas  
 293 our study focused on winter CH<sub>4</sub> fluxes. Our findings support the prevailing notion of boreal forest  
 294 upland soils generally acting as CH<sub>4</sub> sinks (Lai, 2009; Lee et al., 2023) and wetlands acting as CH<sub>4</sub>  
 295 sources (Oertel et al., 2016), and that these patterns hold true for the winter period. The winter CH<sub>4</sub>  
 296 fluxes at the upland tundra sites were too low to classify these sites as either net sources or net  
 297 sinks. The study sites with milder climates, MM and SOD, displayed the highest CH<sub>4</sub> fluxes,  
 298 whether as CH<sub>4</sub> sink or source (Fig. 1). These sites have higher mean annual air temperatures (1.6  
 299 to 2.0 °C compared to -12.5 to -6.6 °C at CB, TVC, and HPC), no permafrost, longer growing  
 300 seasons (168 to 171 days compared to 94 to 113 days at CB, TVC, and HPC), and higher annual  
 301 precipitation (507 to 1293 mm compared to 152 to 198 mm at CB, TVC, and HPC). We also  
 302 identified a few CH<sub>4</sub> emission hotspots in Arctic tundra wetlands during winter that emitted on  
 303 average about 26 times more CH<sub>4</sub> than the average of other sampling locations (0.78 vs. 0.03 mg  
 304 C m<sup>-2</sup> day<sup>-1</sup>). All those CH<sub>4</sub> emission hotspots were found in wetland environments with high soil  
 305 nutrient content (soil nutrient content determined from Ponomarenko et al., 2019). However, it is  
 306 important to note that not all sampling locations in wetlands with high soil nutrient content  
 307 exhibited CH<sub>4</sub> emission hotspots ( $F_{CH_4} \geq 0.35 \text{ mg C m}^{-2} \text{ day}^{-1}$ ); only 37.5% of wetland sampling  
 308 locations exhibited high CH<sub>4</sub> emissions. Although we did not determine spatially integrated flux  
 309 estimates for our sites, these hotspots may dominate the winter CH<sub>4</sub> flux budget.

310

311 Our results do not show a strong correlation between winter CH<sub>4</sub> fluxes and T<sub>soil</sub> or snow  
 312 parameters, unlike some previous studies that have found a correlation between CH<sub>4</sub> flux and sub-  
 313 zero T<sub>soil</sub> (Rößger et al., 2022). However, Howard et al. (2020) also observed an unclear  
 314 relationship between T<sub>soil</sub> at 10 cm and F<sub>CH<sub>4</sub></sub> during winter in Arctic tundra ecosystems. It is also  
 315 possible that other factors are masking the temperature dependency of winter CH<sub>4</sub> fluxes, such as  
 316 soil LWC, soil organic carbon content, or a strong inter-site variability of fluxes between the  
 317 measurement locations at different land cover and vegetation types. Voigt et al. (2023) showed  
 318 that soil LWC was often the main control of F<sub>CH<sub>4</sub></sub> and was masking the weaker temperature  
 319 dependency. According to Lee et al. (2023), soil organic carbon content is an important control on  
 320 CH<sub>4</sub> sinks of forested regions which might explain why we observed a site-specific rate of CH<sub>4</sub>  
 321 uptake in regard to soil LWC (Fig. 2). We observed a correlation between F<sub>CH<sub>4</sub></sub> and F<sub>CO<sub>2</sub></sub> fluxes  
 322 (measured in our previous study; Mavrovic et al., 2023) at the boreal forest upland sites (Fig. S6),  
 323 which might be an indication of increased CH<sub>4</sub> uptake with higher soil carbon substrate availability  
 324 or soil microbial activity as discovered recently for growing season CH<sub>4</sub> uptake (Voigt et al. 2023).  
 325 It is possible that surface T<sub>soil</sub> at 1 cm depth in our study did not correlate with CH<sub>4</sub> fluxes, but that  
 326 deeper T<sub>soil</sub> could have a stronger correlation since most CH<sub>4</sub> production occurs in deeper soil  
 327 layers (Henneron et al., 2022; Li et al., 2023). If further investigations show that deeper T<sub>soil</sub> still  
 328 does not correlate strongly with winter CH<sub>4</sub> fluxes in ABR, several terrestrial biosphere models  
 329 would have to reassess how CH<sub>4</sub> fluxes are estimated as most use T<sub>soil</sub> or T<sub>air</sub> as a main control of  
 330 CH<sub>4</sub> flux computation. The slower diffusion of CH<sub>4</sub> to the atmosphere in winter due to the fraction  
 331 of soil pores filled with ice in frozen soils might also be contributing to masking the temperature  
 332 dependency of winter CH<sub>4</sub> fluxes assuming again that an important fraction of CH<sub>4</sub> emissions  
 333 occurs deeper than the measured soil temperature. Despite that the snow characteristics were  
 334 expected to have a strong impact on soil temperature and LWC because of the insulation properties  
 335 of the snowpack (Dominé et al., 2016; Pedron et al., 2023), we found an absence of a correlation

336 between CH<sub>4</sub> fluxes and snow conditions. However, a snapshot of snow conditions, as measured  
 337 in our study, provides limited information to infer soil conditions. Temporal information about  
 338 snow conditions is required to evaluate the impact of snow insulation, with the fall freeze-up being  
 339 the most critical period to determine the soil winter thermal regime (Slater et al., 2017).

340       The boreal forest upland sites (MM and SOD—for) displayed a relatively strong correlation  
 341 between F<sub>CH<sub>4</sub></sub> and soil LWC ( $R^2 = 0.21$  and 0.73, respectively), although the rate of CH<sub>4</sub> uptake  
 342 increases with soil LWC seemed to be site-specific. Despite differences in vegetation, soil,  
 343 latitude, and precipitation, both sites displayed a similar range of net CH<sub>4</sub> uptake from the  
 344 atmosphere. The main common characteristics between MM and SOD are the length of the  
 345 growing season and the mean average air temperature (Table S2). MM and SOD are also the only  
 346 study sites where the soil remained mostly unfrozen throughout winter. Unfrozen, well-drained  
 347 soils have more pore space than frozen ones because of ice volume expansion. Larger pore space  
 348 benefits CH<sub>4</sub> oxidation through increased diffusion rates (Ball et al., 1997; Smith et al., 2000). The  
 349 MM and SOD—for sites also displayed a similar range of CO<sub>2</sub> emissions during winter, stressing  
 350 that MM and SOD—for sites have comparable carbon flux regimes (Fig. S7; Mavrovic et al., 2023).

351       The SOD-wet boreal wetland CH<sub>4</sub> emissions were high but seemed to be limited by  
 352 transport through the thick solid ice that formed in the wetland's upper layer. In April, during  
 353 snowmelt, CH<sub>4</sub> concentrations under the 10–30 cm ice layer on top of the soil reached up to 1000  
 354 ppm at some sampling locations. The non-negligible F<sub>CH<sub>4</sub></sub> observed at the wetland indicates that  
 355 the thick ice layer is porous but the underlying CH<sub>4</sub> production is higher than what is released into  
 356 the atmosphere, at least for this part of winter. The trapped CH<sub>4</sub> is probably released during ice  
 357 melt, which is coherent with previous studies that showed bursts of CH<sub>4</sub> emissions during spring  
 358 melt (Song et al., 2012; Raz-Yaseef et al., 2016). Further investigation would be required to  
 359 determine if the strong spatial variability observed in the boreal wetland is mainly due to variability  
 360 in the upper ice layer porosity or variability in the underlying CH<sub>4</sub> production.

361       The shoulder seasons (i.e., autumn freeze and spring thaw) are important periods of change  
 362 in CH<sub>4</sub> exchange regimes with a significant contribution to the annual CH<sub>4</sub> budget (Arndt et al.,  
 363 2020; Bao et al., 2021). Whereas this study presents results from the sites of MM, CB, and SOD—  
 364 wet covering most of the winter with monthly flux measurements, the flux measurements of the  
 365 study sites of TVC, HPC, and SOD—for covered only short winter campaigns (Table S2).  
 366 Furthermore, the snowpack diffusive gradient method is limited to measurements within the snow—  
 367 covered period. Further investigation of shoulder seasons CH<sub>4</sub> fluxes should be conducted to  
 368 provide a better understanding of the inter-annual variability of the carbon cycle in ABR. Soil  
 369 biogeochemical properties such as the quantity and quality of available carbon compounds were  
 370 not addressed in this study but were shown to be important environmental controls of CH<sub>4</sub> fluxes  
 371 (Aronson et al., 2013; Kharitonov et al., 2021; Lee et al., 2023; Voigt et al., 2023). Soil  
 372 biogeochemical properties are generally strongly correlated with plant community composition  
 373 and thus CH<sub>4</sub> flux (Bastviken et al., 2023). Biogeochemical analyses, as well as studies on  
 374 microbial community composition and functioning during winter might help to explain the site—  
 375 specific linear relationship between CH<sub>4</sub> flux and soil LWC, and, importantly, the lack of  
 376 temperature dependence we observed in our study. Additionally, our study points towards the  
 377 relevance of ice conditions in wetlands for understanding winter CH<sub>4</sub> fluxes and highlights the  
 378 importance of an integrative view of CH<sub>4</sub> fluxes and soil properties.

383 **5 Conclusions**

384 We measured *in situ* winter CH<sub>4</sub> flux over five Arctic and boreal sites in Canada and  
385 Finland with diverse ecosystem types. Our findings indicate non-negligible winter F<sub>CH<sub>4</sub></sub>, which  
386 must be accounted for in annual carbon balance and terrestrial biosphere models over ABR.  
387 Although F<sub>CH<sub>4</sub></sub> of most Arctic sites was low, emission hotspots were observed in tundra and boreal  
388 wetlands. In the boreal forest uplands, soil liquid water content was identified as an important  
389 environmental control on net CH<sub>4</sub> uptake from the atmosphere, but the rate of CH<sub>4</sub> uptake increase  
390 with soil LWC dependency was different for the two boreal forest uplands study sites. It will be  
391 important to investigate if this site-specific LWC dependency could be related to other  
392 environmental controls such as soil physical-chemical properties and vegetation composition. The  
393 boreal wetland site displayed high CH<sub>4</sub> emissions throughout winter with high spatial variability,  
394 stressing the importance of further investigating the magnitude of these emissions from other sites  
395 and wetland ecotypes. Contrary to some other studies, we found a lack of temperature dependence  
396 on winter CH<sub>4</sub> flux across the different ABR ecosystems investigated, this is a significant finding  
397 that should be investigated further since several terrestrial biosphere models use soil temperature  
398 as a main control of winter CH<sub>4</sub> fluxes. Our study stresses the importance of considering ABR  
399 winter CH<sub>4</sub> flux to accurately calculate the carbon budget in these sensitive environments.

400 **Acknowledgment**

401       The authors would like to warmly thank the Indigenous communities who have welcomed  
402 us and shared their territory with us in Iqaluktuutiaq and Inuvik.  
403

404       This work was made possible thanks to the contributions of the Natural Sciences and  
405 Engineering Research Council of Canada (NSERC), the Fonds de recherche du Québec – Nature  
406 et technologies (FRQNT) and Polar Knowledge Canada (POLAR). Carolina Voigt was supported  
407 by the BMBF project MOMENT (no. 03F0931A). A special thanks to people that contributed to  
408 data collection and gas analyzing: Milja Männikkö (Finnish Meteorological Institute [FMI]),  
409 Jaakko Nissilä (FMI), Anna Kontu (FMI), Marika Honkanen (FMI), Aleksi Rimali (FMI), Elmeri  
410 Viuho Hanne Suokanerva (FMI), Elise Imbeau (Viventem), Gabriel Ferland (Viventem), Aili  
411 Pedersen (POLAR), Gabriel Hould Gosselin (Université de Montréal [UdeM] and Wilfrid Laurier  
412 University [WLU]), Rosy Tutton (WLU), Emma Riley (UdeM), Nick Rutter (Northumbria  
413 University [NU]), Paul Mann (NU), Victoria Dutch (NU), Georgina Woolley (NU), Élise Groulx  
414 (Université de Sherbrooke [UdeS]), Charlotte Crevier (UdeS), Érika Boisvert (UdeS), Alain Royer  
415 (UdeS), Patrick Ménard (UdeS), Vincent Sasseville (UdeS), Célia Trunz (UdeS), Daniel Kramer  
416 (UdeS), Estéban Hamel Jomphe (UQTR), Samuel Goulet (UQTR), Alex Gélinas (UQTR), David  
417 de Courville (UQTR), Juliette Ortet (UQTR) and Chris Derksen (Environment and Climate  
418 Change Canada). We would also like to thank Ian Hogg, Johann Wagner, and Scott Johnson from  
419 POLAR as well as Branden Walker and Philip Marsh from WLU for their logistical support.  
420

421 **Open Research**

422 All data presented in this article can be found in the following repository:  
423

424 Mavrovic, A., Sonnentag, O., Voigt, C., Roy, A. (2023). Winter CH<sub>4</sub> fluxes over arctic and  
425 boreal environments. <https://doi.org/10.5683/SP3/COWXAZ>, Borealis.

426 **References**

- 427 Andresen, C., Lara, M., Tweedie, C., & Lougheed, V. (2017), Rising plant-mediated methane  
428 emissions from arctic wetlands. *Global Change Biology*, 23(3), 1128–1139, doi:  
429 10.1111/gcb.13469
- 430 Arndt, K., Lipson, D., Hashemi, J., Oechel, W., & Zona, D. (2020), Snow melt stimulates  
431 ecosystem respiration in Arctic ecosystems. *Global Change Biology*, 26(9), 5042–5051, doi:  
432 10.1111/gcb.15193
- 433 Aronson, E., Allison, S., & Helliker, B. (2013), Environmental impacts on the diversity of  
434 methane-cycling microbes and their resultant function. *Frontiers in Microbiology*, 4, 225, doi:  
435 10.3389/fmicb.2013.00225
- 436 Ball, B., Smith, K., Klemedtsson, L., Brumme, R., Sitaula, B., Hansen, S., Priemé, A., MacDonald,  
437 J., & Horgan, G. (1997), The influence of soil gas transport properties on methane oxidation in a  
438 selection of northern European soils. *Journal of Geophysical Research: Atmospheres*, 102(D19),  
439 23309–23317, doi: 10.1029/97JD01663
- 440 Bao, T., Xu, X., Jia, G., Billesbach, D., & Sullivan, R. (2020), Much stronger tundra methane  
441 emissions during autumn-freeze than spring-thaw. *Global Change Biology*, 27(2), 376–387, doi:  
442 10.1111/gcb.15421
- 443 Barry R, Plamondon, AP, & Stein, J. (1988), Hydrologic soil properties and application of a soil  
444 moisture model in a balsam fir forest. *Canadian Journal of Forest Research*, 18(4), 427–434, doi:  
445 10.1139/x88-063
- 446 Bastviken, D., Treat, C., Pangala, S. R., Gauci, V., Enrich-Prast, A., Karlson, M., Gålfalk, M.,  
447 Romano, B., Sawakuchi, H. O. (2023), The importance of plants for methane emission at the  
448 ecosystem scale. *Aquatic Botany*, 184, 103596, doi: 10.1016/j.aquabot.2022.103596
- 449 Bekryaev, R. V., Polyakov, I. V., & Alexeev, V. A. (2010), Role of polar amplification in long-  
450 term surface air temperature variations and modern arctic warming. *Journal of Climate*, 23(14),  
451 3888–3906, doi:10.1175/2010jcli3297.1
- 452 Bowley, A. (1928), The standard deviation of the correlation coefficient. *Journal of the American  
453 Statistical Association*, 23(161), 31–34, doi:10.2307/2277400
- 454 Brown, J., Ferrians, O., Heginbottom, J., & Melnikov, E (2002), Circum-Arctic map of permafrost  
455 and ground-ice conditions, Version 2. Boulder, Colorado, USA, NSIDC: National Snow and Ice  
456 Data Center, doi: 10.7265/skbg-kf16
- 457 Dean, J., Middelburg, J., Röckmann, T., Aerts, R., Blauw, L. G., Egger, M., Jetten, M., de Jong,  
458 A., Meisel, O., Rasigraf, O., Slomp, C., in't Zandt, M., & Dolman, A. (2018), Methane feedbacks  
459 to the global climate system in a warmer world. *Reviews of Geophysics*, 56(1), 207–250.  
460 doi:10.1002/2017rg000559
- 461
- 462
- 463
- 464
- 465
- 466
- 467
- 468
- 469
- 470
- 471

- 472 Deluca, T., & Boisvenue, C. (2012), Boreal forest soil carbon: distribution, function and  
473 modelling. *Forestry*, 85(2), 161–184, doi: 10.1093/forestry/cps003
- 474
- 475 Delwiche, K., Knox, S., Malhotra, A., Fluet-Chouinard, E., McNicol, G., Feron, S., Ouyang, Z.,  
476 Papale, D., Trotta, C., Canfora, E., Cheah, Y.-W., Christianson, D., Alberto, M. C., Alekseychik,  
477 P., Aurela, M., Baldocchi, D., Bansal, S., Billesbach, D., Bohrer, G., Bracho, R., Buchmann, N.,  
478 Campbell, D., Celis, G., Chen, J., Chen, W., Chu, H., Dalmagro, H., Dengel, S., Desai, A., Detto,  
479 M., Dolman, H., Eichelmann, E., Euskirchen, E., Famulari, D., Fuchs, K., Goeckede, M., Gogo,  
480 S., Gondwe, M., Goodrich, J., Gottschalk, P., Graham, S., Heimann, M., Helbig, M., Helfter, C.,  
481 Hemes, K., Hirano, T., Hollinger, D., Hörtigl, L., Iwata, H., Jacotot, A., Jurasiczki, G., Kang,  
482 M., Kasak, K., King, J., Klatt, J., Koebisch, F., Krauss, K., Lai, D., Lohila, A., Mammarella, I.,  
483 Marchesini, L. B., Manca, G., Matthes, J. H., Maximov, T., Merbold, L., Mitra, B., Morin, T.,  
484 Nemitz, E., Nilsson, M., Niu, S., Oechel, W., Oikawa, P., Ono, K., Peichl, M., Peltola, O., Reba,  
485 M., Richardson, A., Riley, W., Runkle, B., Ryu, Y., Sachs, T., Sakabe, A., Sanchez, C., Schuur,  
486 E., Schäfer, K., Sonnentag, O., Sparks, J., Stuart-Haëntjens, E., Sturtevant, C., Sullivan, R., Szutu,  
487 D., Thom, J., Torn, M., Tuittila, E.-S., Turner, J., Ueyama, M., Valach, A., Vargas, R., Varlagin,  
488 A., Vazquez-Lule, A., Verfaillie, J., Vesala, T., Vourlitis, G., Ward, E., Wille, C., Wohlfahrt, G.,  
489 Wong, G., Zhang, Z., Zona, D., Windham-Myers, L., Poulter, B., & Jackson, R. (2021),  
490 FLUXNET-CH4: a global, multi-ecosystem dataset and analysis of methane seasonality from  
491 freshwater wetlands. *Earth System Science Data*, 13(7), 3607–3689, doi: 10.5194/essd-13-3607-  
492 2021
- 493
- 494 Derksen, C., Burgess, D., Duguay, C., Howell, S., Mudryk, L., Smith, S., Thackeray, C., &  
495 Kirchmeier-Young, M. (2019), Changes in snow, ice, and permafrost across Canada. Canada's  
496 Changing Climate Report – Chapter 5, Government of Canada, Ottawa, Ontario, Canada, 194–  
497 260.
- 498
- 499 Dominé, F., Barrère, M., & Morin, S. (2016), The growth of shrubs on high Arctic tundra at Bylot  
500 Island: Impact on snow physical properties and permafrost thermal regime. *Biogeosciences*,  
501 13(23), 6471–6486, doi: 10.5194/bg-13-6471-2016
- 502
- 503 Du Plessis, J. P., & Masliyah, J. H. (1991), Flow through isotropic granular porous media.  
504 *Transport in Porous Media*, 6, 207–221, doi: 10.1007/BF00208950
- 505
- 506 Fierz, C., A., Durand, Y., Etchevers, P., Green, E., McClung, D., Nishimura, K., Satyawali, P., &  
507 Sokratov, S. (2009), The international classification for seasonal snow on the ground, IHP-VII  
508 Technical Documents in Hydrology N83, IACS Contribution N1, UNESCO-IHP, Paris.
- 509
- 510 Fisher, J., Sikka, M., Oechel, W., Huntzinger, D., Melton, J., Koven, C., Ahlström, A., Arain, M.,  
511 Baker, I., Chen, J., Ciais, P., Davidson, C., Dietze, M., El-Masri, B., Hayes, D., Huntingford, C.,  
512 Jain, A., Levy, P., Lomas, R., Poulter, B., Price, D., Sahoo, A., Schaefer, K., Tian, H., Tomelleri,  
513 E., Verbeeck, H., Viovy, N., Wania, R., Zeng, N., & Miller, C. (2014), Carbon cycle uncertainty  
514 in the Alaskan Arctic. *Biogeosciences*, 11(15), 4271–4288, doi: 10.5194/bg-11-4271-2014
- 515

- 516 Fooladmand, H. R. (2011), Estimating soil specific surface area using the summation of the  
517 number of spherical particles and geometric mean particle-size diameter. *African Journal of*  
518 *Agricultural Research*, 6(7), 1758–1762, doi: 10.5897/AJAR11.19
- 519
- 520 Grünberg, I., Wilcox, E., Zwieback, S., Marsh, P., & Boike, J. (2020), Linking tundra vegetation,  
521 snow, soil temperature, and permafrost. *Biogeosciences*, 17(16), 4261–4279. doi: 10.5194/bg-17–  
522 4261–2020
- 523
- 524 Harvey, A., In Haynes, W., Lide, D., & Bruno, T. (2017), CRC Handbook of Chemistry and  
525 Physics (97th ed.): Properties of Ice and Supercooled Water. CRC Press, Boca Raton, Florida,  
526 United States, 2666 pages (6–12). ISBN 978-1-4987-5429-3
- 527
- 528 Helbig, M., Chasmer, L. E., Kljun, N., Quinton, W. L., Treat, C. C., & Sonnentag, O. (2016), The  
529 positive net radiative greenhouse gas forcing of increasing methane emissions from a thawing  
530 boreal forest–wetland landscape. *Global Change Biology*, 23(6), 2413–2427,  
531 doi:10.1111/gcb.13520
- 532
- 533 Henneron, L., Balesdent, J., Alvarez, G., Barré, P., Baudin, F., Basile–Doelsch, I., Cécillon, L.,  
534 Fernandez–Martinez, A., Hatté, C., & Fontaine, S. (2022), Bioenergetic control of soil carbon  
535 dynamics across depth. *Nature Communications*, 13, 7676, doi: 10.1038/s41467–022–34951–w
- 536
- 537 Hiyama, T., Ueyama, M., Kotani, A., Iwata, H., Nakai, T., Okamura, M., Ohta, T., Harazono, Y.,  
538 Petrov, R.E., & Maximov, T.C. (2020), Lessons learned from more than a decade of greenhouse  
539 gas flux measurements at boreal forests in eastern Siberia and interior Alaska, *Polar Science*, 27,  
540 100607, doi: 10.1016/j.polar.2020.100607
- 541
- 542 Howard, D., Agnan, Y., Helmig, D., Yang, Y., & Obrist, (2020), Environmental controls on  
543 ecosystem-scale cold-season methane and carbon dioxide fluxes in an Arctic tundra ecosystem.  
544 *Biogeosciences*, 17(15), 4025–4042, doi: 10.5194/bg-17-4025-2020
- 545
- 546 Ikonen, J., Vehviläinen, J., Rautiainen, K., Smolander, T., Lemmetyinen, J., Bircher, S., &  
547 Pulliainen, J. (2016), The Sodankylä in situ soil moisture observation network: an example  
548 application of ESA CCI soil moisture product evaluation. *Geoscientific Instrumentation, Methods  
549 and Data Systems*, 5, 95–108, doi:10.5194/gi–5–95–2016
- 550
- 551 Ito, A., Li, T., Qin, Z., Melton, J., Tian, H., Kleinen, T., Zhang, W., Zhang, Z., Joos, F., Ciais, P.,  
552 Hopcroft, P., Beerling, D., Liu, X., Zhuang, Q., Zhu, Q., Peng, C., Chang, K.–Y., Fluet–Chouinard,  
553 E., McNicol, G., Patra, P., Poulter, B., Sitch, S., Riley, W., & Zhu, Q. (2023), Cold–season  
554 Methane fluxes simulated by GCP–CH4 models. *Geophysical Research Letters*, 50(14),  
555 e2023GL103037, doi: 10.1029/2023GL103037
- 556
- 557 Kharitonov, S., Semenov, M., Sabrekov, A., Kotsyurbenko, O., Zhelezova, A., & Schegolkova, N.  
558 (2021), Microbial communities in methane cycle: modern molecular methods gain insights into  
559 their global ecology. *Environments*, 8(2), 16, doi: 10.3390/environments8020016
- 560

- 561 Kibria, H., Abdullah, S., & Bustamam, A. (2020), Comparison of random forest and support vector  
562 machine for prediction of cognitive impairment in Parkinson's disease. *AIP Conference  
563 Proceedings*, 2296(1), 020093. doi: 10.1063/5.0030332
- 564
- 565 Kim, Y., Ueyama, M., Nakagawa, F., Tsunogai, U., Harazono, Y., & Tanaka, N. (2007),  
566 Assessment of winter fluxes of CO<sub>2</sub> and CH<sub>4</sub> in boreal forest soils of central Alaska estimated by  
567 the profile method and the chamber method: a diagnosis of methane emission and implications for  
568 the regional carbon budget. *Tellus B: Chemical and Physical Meteorology*, 59(2), 223–233, doi:  
569 10.1111/j.1600-0889.2006.00233.x
- 570
- 571 Kim, Y., Tsunogai, S., & Tanaka, N. (2019), Winter CO<sub>2</sub> emission and its production rate in cold  
572 temperate soils of northern Japan: 222Rn as a proxy for the validation of CO<sub>2</sub> diffusivity. *Polar  
573 Science*, 22, 100480, doi: 10.1016/j.polar.2019.09.002
- 574
- 575 Kinar, N., & Pomeroy, J. (2015), Measurement of the physical properties of the snowpack. *Reviews  
576 of Geophysics*, 53(2), 481–544, doi: 10.1002/2015RG000481
- 577
- 578 King, J., Reeburgh, W., & Regli, S. K. (1998), Methane emission and transport by arctic sedges in  
579 Alaska: Results of a vegetation removal experiment. *Journal of Geophysical Research: Atmospheres*,  
580 103(D22), 29083–29092, doi:10.1029/98jd00052
- 581
- 582 Kirschke, S., Bousquet, P., Ciais, P., Saunois, M., Canadell, J., Dlugokencky, E., Bergamaschi, P.,  
583 Bergmann, D., Blake, D., Bruhwiler, L., Cameron-Smith, P., Castaldi, S., Chevallier, F., Feng, L.,  
584 Fraser, A., Heimann, M., Hodson, E., Houweling, S., Josse, B., Fraser, P., Krummel, P., Lamarque,  
585 J.-F., Langenfelds, R., Le Quéré, C., Naik, V., O'Doherty, S., Palmer, P., Pison, I., Plummer, D.,  
586 Poulter, B., Prinn, R., Rigby, M., Ringeval, B., Santini, M., Schmidt, M., Shindell, D., Simpson,  
587 I., Spahni, R., Steele, L. P., Strode, S., Sudo, K., Szopa, S., van der Werf, G., Voulgarakis, A., van  
588 Weele, M., Weiss, R., Williams, J., & Zeng, G. (2013), Three decades of global methane sources  
589 and sinks. *Nature Geoscience*, 6(10), 813–823, doi:10.1038/ngeo1955
- 590
- 591 Knox, S., Jackson, R., Poulter, B., McNicol, G., Fluet-Chouinard, E., Zhang, Z., Hugelius, G.,  
592 Bousquet, P., Canadell, J., Saunois, M., Papale, D., Chu, H., Keenan, T., Baldocchi, D., Torn, M.,  
593 Mammarella, I., Trotta, C., Aurela, M., Bohrer, G., Campbell, D., Cescatti, A., Chamberlain, S.,  
594 Chen, J., Chen, W., Dengel, S., Desai, A., Euskirchen, E., Friberg, T., Gasbarra, D., Goded, I.,  
595 Goeckede, M., Heimann, M., Helbig, M., Hirano, T., Hollinger, D., Iwata, H., Kang, M., Klatt, J.,  
596 Krauss, K., Kutzbach, L., Lohila, A., Mitra, B., Morin, T., Nilsson, M., Niu, S., Noormets, A.,  
597 Oechel, W., Peichl, M., Peltola, O., Reba, M., Richardson, A., Runkle, B., Ryu, Y., Sachs, T.,  
598 Schäfer, K., Schmid, H. P., Shurpali, N., Sonnentag, O., Tang, A., Ueyama, M., Vargas, R., Vesala,  
599 T., Ward, E., Windham-Myers, L., Wohlfahrt, G., & Zona, D. (2019), FLUXNET-CH<sub>4</sub> synthesis  
600 activity: objectives, observations, and future directions. *Bulletin of the American Meteorological  
601 Society*, 100(12), 2607–2632, doi:10.1175/bams-d-18-0268.1
- 602
- 603 Krogh, S., Pomeroy, J., & Marsh, P. (2017), Diagnosis of the hydrology of a small Arctic basin at  
604 the tundra–taiga transition using a physically based hydrological model. *Journal of Hydrology*,  
605 550, 685–703, doi: 10.1016/j.jhydrol.2017.05.042
- 606

- 607 Kuhn, M. A., Varner, R. K., Bastviken, D., Crill, P., MacIntyre, S., Turetsky, M., Walter Anthony,  
608 K., McGuire, A. D., & Olefeldt, D. (2021), BAWLD–CH<sub>4</sub>: a comprehensive dataset of methane  
609 fluxes from boreal and arctic ecosystems. *Earth System Science Data*, 13, 5151–5189, doi:  
610 10.5194/essd-13-5151-2021
- 611
- 612 Lai, D. (2009), Methane dynamics in northern peatlands: A Review. *Pedosphere*, 19(4), 409–421,  
613 doi: 10.1016/S1002-0160(09)00003-4
- 614
- 615 Lee, J., Oh, Y., Lee, S. T., Seo, Y. O., Yun, J., Yang, Y., Kim, J., Zhuang, Q., & Kang, H. (2023),  
616 Soil organic carbon is a key determinant of CH<sub>4</sub> sink in global forest soils. *Nature  
Communications*, 14, 3110, doi: 10.1038/s41467-023-38905-8
- 617
- 618 Li, K., Wang, Z., Xiang, Q., Zhao, X., Ji, L., Xin, Y., Sun, J., Liu, C., Shen, X., Xu, X., & Chen,  
619 Q. (2023), Coupling of soil methane emissions at different depths under typical coastal wetland  
620 vegetation types. *Chemosphere*, 338, 139505, doi: 10.1016/j.chemosphere.2023.139505
- 621
- 622 Liaw, A., & Wiener, M. (2002), Classification and regression by RandomForest. *R News*, 2(3),  
623 18–22.
- 624
- 625 Madore, J.–B., Fierz, C., & Langlois, A. (2022), Investigation into percolation and liquid water  
626 content in a multi–layered snow model for wet snow instabilities in Glacier National Park, Canada.  
627 *Frontiers in Earth Science*, 10, 898980, doi: 10.3389/feart.2022.898980
- 628
- 629 Marrero, T., & Mason E. (1972), Gaseous diffusion coefficients. *Journal of Physics and Chemistry  
Reference Data*, 1(1), 3–117, doi: 10.1063/1.3253094
- 630
- 631 Martin, M., Kumar, P., Sonnentag, O., & Marsh, P. (2022), Thermodynamic basis for the  
632 demarcation of Arctic and alpine treelines. *Scientific Reports*, 12, 12565, doi: 10.1038/s41598–  
633 022–16462–2
- 634
- 635 Massman, W. (1998), A review of the molecular diffusivities of H<sub>2</sub>O, CO<sub>2</sub>, CH<sub>4</sub>, CO, O<sub>3</sub>, SO<sub>2</sub>,  
636 NH<sub>3</sub>, N<sub>2</sub>O, NO, and NO<sub>2</sub> in air, O<sub>2</sub> and N<sub>2</sub> near STP. *Atmospheric Environment*, 32(6), 1111–1127,  
637 doi: 10.1016/S1352-2310(97)00391-9
- 638
- 639 Mastepanov M, Sigsgaard, C., Tagesson, T., Ström, L., Tamstorf, M., Lund, M., & Christensen,  
640 T. (2013), Revisiting factors controlling methane emissions from high–Arctic tundra.  
641 *Biogeosciences*, 10(7), 5139–5158, doi: 10.5194/bg–10–5139–2013
- 642
- 643 Mavrovic, A., Sonnentag, O., Lemmetynen, J., Voigt, C., Rutter, N., Mann, P., Sylvain, J.–D.,  
644 Roy, A. (2023), Environmental controls of winter soil carbon dioxide fluxes in boreal and tundra  
645 environments. *Biogeosciences*, 20(24), 5087–5108, doi: 10.5194/bg-20-5087-2023
- 646
- 647 McDowell, N., Marshall, J., Hooker, T., & Musselman, R. (1999), Estimating CO<sub>2</sub> flux from  
648 snowpacks at three sites in the Rocky Mountains. *Tree physiology*, 20, 745–753, doi:  
649 10.1093/treephys/20.11.745
- 650
- 651
- 652

- 653 McGuire, A., Christensen, T., Hayes, D., Heroult, A., Euskirchen, E., Kimball, J., Koven, C.,  
654 Lafleur, P., Miller, P., Oechel, W., Peylin, P., Williams, M., & Yi, Y. (2012), An assessment of  
655 the carbon balance of Arctic tundra: Comparisons among observations, process models, and  
656 atmospheric inversions. *Biogeosciences*, 9(8), 3185–3204, doi: 10.5194/bg-9-3185-2012  
657
- 658 Natali S., Holdren, J., Rogers, B., Treharne, R., Duffy, P., Pomerance, R., & MacDonald, E.  
659 (2021), Permafrost carbon feedbacks threaten global climate goals. *Proceedings of the National  
660 Academy of Sciences*, 118(21), e2100163118, doi: 10.1073/pnas.2100163118  
661
- 662 Oertel, C., Matschullat, J., Zurba, K., Zimmermann, F., & Erasmi, S. (2016), Greenhouse gas  
663 emissions from soils – A review. *Geochemistry*, 76(3), 327–352, doi:  
664 10.1016/j.chemer.2016.04.002  
665
- 666 Pedron, S., Jespersen, R., Xu, X., Khazindar, Y., Welker, J., & Czimczik, C., (2023), More Snow  
667 Accelerates Legacy Carbon Emissions From Arctic Permafrost. *AGU Advances*, 4(4),  
668 e2023AV000942, doi: 10.1029/2023AV000942  
669
- 670 Pirk, N., Tamstorf, M., Lund, M., Masteponov, M., Pedersen, S., Myllus, M., Parmentier, F.-J.,  
671 Christiansen, H., & Christensen, T. (2016), Snowpack fluxes of methane and carbon dioxide from  
672 high Arctic tundra. *Biogeosciences*, 121(11), 2886–2900, doi: 10.1002/2016JG003486  
673
- 674 Ponomarenko, S., McLennan, D., Pouliot, D., & Wagner, J. (2019), High Resolution Mapping of  
675 Tundra Ecosystems on Victoria Island, Nunavut – Application of a Standardized Terrestrial  
676 Ecosystem Classification. *Canadian Journal of Remote Sensing*, 45, 551–571, doi:  
677 10.1080/07038992.2019.1682980  
678
- 679 Potapov, P., Hansen, M., Stehman, S., Loveland, T., & Pittman, K. (2008), Combining MODIS  
680 and Landsat imagery to estimate and map boreal forest cover loss. *Remote Sensing of Environment*,  
681 112(9), 3708–3719, doi: 10.1016/j.rse.2008.05.006  
682
- 683 Proksch, M., Rutter, N., Fierz, C., & Schneebeli, M. (2016), Intercomparison of snow density  
684 measurements: bias, precision, and vertical resolution. *The Cryosphere*, 10(1), 371–384, doi:  
685 10.5194/tc-10-371-2016.  
686
- 687 Rantanen, M., Karpechko, A.Y., Lipponen, A., Nordling, K., Hyvärinen, O., Ruosteenoja, K.,  
688 Vihma, T. & Laaksonen, A. (2022), The Arctic has warmed nearly four times faster than the globe  
689 since 1979. *Communications Earth & Environment*, 3(1), 1–10, doi: 10.1038/s43247-022-00498–  
690 3.  
691
- 692 Ravn, N., Elberling, B., & Michelsen, A. (2020), Arctic soil carbon turnover controlled by  
693 experimental snow addition, summer warming and shrub removal. *Soil Biology and Biochemistry*,  
694 142, 107698, doi: 10.1016/j.soilbio.2019.107698  
695
- 696 Raz-Yaseef, N., Torn, M., Wu, Y., Billesbach, D., Liljedahl, A., Kneafsey, T., Romanovsky, V.,  
697 Cook, D., & Wullschleger, S. (2016), Large CO<sub>2</sub> and CH<sub>4</sub> emissions from polygonal tundra during

- 698 spring thaw in northern Alaska. *Geophysical Research Letters*, 44(1), 504–513, doi:  
699 10.1002/2016GL071220  
700
- 701 Roslev, P., Iversen, N., & Henriksen, K. (1997), Oxidation and assimilation of atmospheric  
702 methane by soil methane oxidizers. *Applied and Environmental Microbiology*, 63(3), 874–880,  
703 doi: 10.1128/aem.63.3.874–880.1997  
704
- 705 Rößger, N., Sachs, T., Wille, C., Boike, J., & Kutzbach, L. (2022), Seasonal increase of methane  
706 emissions linked to warming in Siberian tundra. *Nature Climate Change*, 12(11), 1031–1036, doi:  
707 10.1038/s41558–022–01512–4  
708
- 709 Schuur, E., McGuire, A., Schädel, C., Grosse, G., Harden, J., Hayes, D., Hugelius, G., Koven, C.,  
710 Kuhry, P., Lawrence, D., Natali, S., Olefeldt, D., Romanovsky, V., Schaefer, K., Turetsky, M.,  
711 Treat, C., & Vonk, J. (2015), Climate change and the permafrost carbon feedback. *Nature*, 520,  
712 171–179, doi: 10.1038/nature14338  
713
- 714 Schuur, E., Abbott, B., Commane, R., Ernakovich, J., Euskirchen, E., Hugelius, G., Grosse, G.,  
715 Jones, M., Koven, C., Leshyk, V., Lawrence, D., Loranty, M., Mauritz, M., Olefeldt, D., Natali,  
716 S., Rodenhizer, H., Salmon, V., Schädel, C., Strauss, J., Treat, C., & Turetsky, M. (2022),  
717 Permafrost and climate change: carbon cycle feedbacks from the warming Arctic. *Annual Review  
718 of Environment and Resources*, 47(1), 343–371, doi: 10.1146/annurev-environ–012220–011847  
719
- 720 Seok, B., Helmig, D., Williams, M., Liptzin, D., Chowanski, K., & Hueber, J. (2009), An  
721 automated system for continuous measurements of trace gas fluxes through snow: an evaluation  
722 of the gas diffusion method at a subalpine forest site, Niwot Ridge, Colorado. *Biogeochemistry*,  
723 95, 95–113, doi: 10.1007/s10533–009–9302–3  
724
- 725 Slater, A., Lawrence, D., & Koven, C., (2017), Process-level model evaluation: a snow and heat  
726 transfer metric. *Cryosphere*, 11(2), 989–996, doi: 10.5194/tc-11-989-2017  
727
- 728 Smith, K., Dobbie, K., Ball, B., Bakken, L., Sitaula, B., Hansen, S., Brumme, R., Borken, W.,  
729 Christensen, S., Priemé, A., Fowler, D., Macdonald, J., Skiba, U., Klemedtsson, L., Kasimir–  
730 Klemedtsson, A., Degórska, A., & Orlanski, P. (2000), Oxidation of atmospheric methane in  
731 Northern European soils, comparison with other ecosystems, and uncertainties in the global  
732 terrestrial sink. *Global Change Biology*, 6(7), 791–803, doi: 10.1046/j.1365–2486.2000.00356.x  
733
- 734 Sommerfeld, R., Mosier, A., & Musselman, R. (1993), CO<sub>2</sub>, CH<sub>4</sub> and N<sub>2</sub>O flux through a  
735 Wyoming snowpack and implications for global budgets. *Nature*, 361, 140–142, doi:  
736 10.1038/361140a0  
737
- 738 Song, C., Xu, X., Sun, X., Tian, H., Sun, L., Miao, Y., Wang, X., & Guo, Y. (2012), Large methane  
739 emission upon spring thaw from natural wetlands in the northern permafrost region. *Environmental  
740 Research Letters*, 7(3), 034009, doi: 10.1088/1748–9326/7/3/034009  
741
- 742 Tanja, S., Berninger, F., Vesala, T., Markkanen, T., Hari, P., Mäkelä, A., Ilvesniemi, H., Hänninen,  
743 H., Nikinmaa, E., Huttula, T., Laurila, T., Aurela, M., Grelle, A., Lindroth, A., Arneth, A.,

- 744 Shibistova, O., & Lloyd, J. (2003), Air temperature triggers the recovery of evergreen boreal forest  
745 photosynthesis in spring. *Global Change Biology*, 9(10), 1410–1426, doi: 10.1046/j.1365–  
746 2486.2003.00597.x
- 747 Tarnocai, C., Canadell, J., Schuur, E., Kuhry, P., Mazhitova, G., & Zimov, S. (2009), Soil organic  
748 carbon pools in the northern circumpolar permafrost region. *Global Biogeochemical Cycles*, 23(2),  
749 GB2023, doi: 10.1029/2008GB003327
- 750 Topp, E., & Pattey, E. (1997), Soils as sources and sinks for atmospheric methane. *Canadian  
751 Journal of Soil Science*, 77(2), 167–177, doi: 10.4141/S96–107
- 752 Treat, C. C., Bloom, A. A., & Marushchak, M. E. (2018), Nongrowing season methane fluxes – a  
753 significant component of annual fluxes across northern ecosystems. *Global Change Biology*, 24,  
754 3331–3343, doi: 10.1111/gcb.14137
- 755 Ullah, S., Frasier, R., Pelletier, L., & Moore, T., (2009), Greenhouse gas fluxes from boreal forest  
756 soils during the snow-free period in Quebec, Canada. *Canadian Journal of Forest Research*, 39(3),  
757 666–680, doi: 10.1139/X08–209
- 758 Virtanen, T., & Ek, M. (2014), The fragmented nature of tundra landscape. *International Journal  
759 of Applied Earth Observation*, 27(A), 4–12, doi: 10.1016/j.jag.2013.05.010
- 760 Viru, B., Veber, G., Jaagus, J., Kull, A., Maddison, M., Muñoz, M., Espenberg, M., Teemusk, A.,  
761 & Mander, Ü. (2020), Wintertime greenhouse gas fluxes in hemiboreal drained peatlands.  
762 *Atmosphere*, 11, 731, doi: 10.3390/atmos11070731
- 763 Voigt, C., Lamprecht, R., Marushchak, M., Lind, S., Novakovskiy, A., Aurela, M., Martikainen,  
764 P., & Biasi, C. (2017), Warming of subarctic tundra increases emissions of all three important  
765 greenhouse gases – carbon dioxide, methane, and nitrous oxide. *Global Change Biology*, 23(8),  
766 3121–3138, doi: 10.1111/gcb.13563
- 767 Voigt, C., Virkkala, A.–M., Hould Gosselin, G., Bennett, K., Black, T. A., Dett, M., Chevrier–  
768 Dion, C., Guggenberger, G., Hashmi, W., Kohl, L., Kou, D., Marquis, C., Marsh, P., Marushchak,  
769 M., Nesic, Z., Nykänen, H., Saarela, T., Sauheitl, L., Walker, B., Weiss, N., Wilcox, E., &  
770 Sonnentag, O. (2023) Arctic soil methane sink increases with drier conditions and higher  
771 ecosystem respiration. *Nature Climate Change*, 13, 1095–1104, doi: 10.1038/s41558–023–01785–  
772 3
- 773 Yvon–Durocher, G., Allen, A., Bastviken, D., Conrad, R., Gudasz, C., St–Pierre, A., Thanh–Duc,  
774 N., & del Giorgio, P. A. (2014), Methane fluxes show consistent temperature dependence across  
775 microbial to ecosystem scales. *Nature*, 507(7493), 488–491, doi:10.1038/nature13164
- 776 Zhang, Z., Zimmermann, N., Stenke, A., Li, X., Hodson, E., Zhu, G., Huang, C., & Poulter, B.  
777 (2017), Emerging role of wetland methane emissions in driving 21st century climate change.  
778 *Proceedings of the National Academy of Sciences*, 114(36), 9647–9652,  
779 doi:10.1073/pnas.1618765114

- 790  
791 Zhu, C., Nakayama, M., & Inouey, H. Y. (2014), Continuous measurement of CO<sub>2</sub> flux through  
792 the snowpack in a dwarf bamboo ecosystem on Rishiri Island, Hokkaido, Japan. *Polar Science*,  
793 8(3), 218–231, doi: 10.1016/j.polar.2014.04.003  
794  
795 Zona, D., Oechel, W., Kochendorfer, J., Paw U, K., Salyuk, A., Olivas, P., Oberbauer, S., &  
796 Lipson, D. (2009), Methane fluxes during the initiation of a large-scale water table manipulation  
797 experiment in the Alaskan Arctic tundra. *Global Biogeochemical Cycles*, 23(2), GB2013,  
798 doi:10.1029/2009GB003487  
799  
800 Zona, D., Giolo, B., Commane, R., Lindaas, J., Wofsy, S., Miller, C., Dinardo, S., Dengel, S.,  
801 Sweeney, C., Karion, A., Chang, R., Henderson, J., Murphy, P., Goodrich, J., Moreaux, V.,  
802 Liljedahl, A., Watts, J., Kimball, J., Lipson, D., & Oechel, W. (2015), Cold season emissions  
803 dominate the Arctic tundra methane budget. *Proceedings of the National Academy of Sciences*,  
804 113(1), 40–45, doi: 10.1073/pnas.1516017113  
805  
806  
807  
808  
809  
810  
811

812 **Supporting Information**

813 **Study sites**



814  
815 **Figure S1.** Study site locations. The Arctic biome is delimited following the Conservation of  
816 Arctic Flora and Fauna (CAFF) working group of the Arctic Council (Arctic SDI Catalogue,  
817 Identifier: 2ad7a7cb-2ad7-4517-a26e-7878ef134239, 2017) and the boreal biome is delimited  
818 following Potapov et al. (2008). Permafrost extent (Brown et al., 2002) is estimated in percent  
819 area: continuous (>90–100%), discontinuous (>50–90%), sporadic (>10–50%) and isolated  
820 patches (<10%). Figure modified from Mavrovic et al. (2023).

821  
822  
823  
824  
825  
826  
827  
828  
829  
830  
831  
832  
833  
834  
835  
836

837      **Table S1.** Study sites with the number of sampling locations and CH<sub>4</sub> flux measurement (N) for  
 838      each site. Some study sites have more sampling locations than others because there were more  
 839      vegetation types and a larger area to cover. Overall, every type of vegetation had 5–10 sampling  
 840      locations. Table modified from Mavrovic et al. (2023).

Site	Acronym	Location	Latitude/ longitude	Sampling locations	N	Measurement months	Site reference
Cambridge Bay	CB	Nunavut, Canada	69°13'N 104°54'W	47	230	2021: 04, 12 2022: 01-05	Ponomarenko et al., 2019
Trail Valley Creek	TVC	Northwest Territories, Canada	68°46'N 133°28'W	34	152	2021: 03, 12 2022: 03	Grünberg et al., 2020
Havikpak Creek	HPC	Northwest Territories, Canada	68°19'N 133°31'W	5	30	2021: 03, 04 2022: 03	Krogh et al., 2017
Montmorency Forest	MM	Quebec, Canada	47°18'N 71°10'W	12	110	2021: 01, 02, 12 2022: 01-05	Barry et al., 1988
Sodankylä	SOD	Lapland, Finland	67°22'N 26°38'E	30	138	2022: 02-04 2022-2023: 12-05	Ikonen et al., 2016

841

842

843

844

845

846

847

Table S2. Vegetation, soil, and climate properties of the study sites. Mean annual air temperature, annual precipitation, and growing season length were evaluated for the years with CH<sub>4</sub> flux measurements (2021–2022 for CB, TVC, HPC and MM; 2022 for SOD). Growing season length was estimated from the last to the first day of frost using a 5-day running-average daily mean air temperature (Tanja et al., 2003).

Site	Ecosystem	Dominant species	Acronym	Soil layers	Mean Annual T <sub>air</sub>	Annual Precipitation	Growing Season Length	Permafrost
Cambridge Bay	Prostrate tundra shrubs	Lichen and moss	CB-mes	Mesic: 0-5 cm organic over dry mineral	-12.5 °C	152 mm	94 days	Continuous
	Open wetland	Sedge fen	CB-wet	Wetland: 10-20 cm organic over wet mineral (clay)				
Trail Valley Creek	Erect tundra shrubs	Schurb, lichen, moss and tussock	TVC	30-60 cm organic (peat) over mineral	-7.8 °C	175 mm	111 days	Continuous
Havikpak Creek	Open-crown coniferous boreal forest	Black spruce	HPC	5-50 cm organic (peat) over mineral (silty clay)	-6.6 °C	198 mm	113 days	Continuous
Montmorency Forest	Closed-crown coniferous boreal forest	Balsam fir	MM	4-7 cm litter over 7-13 cm organic over wet mineral (sandy loam)	2.0 °C	1293 mm	171 days	Absent
Sodankylä	Closed-crown coniferous boreal forest	Scots pine	SOD-for	0-5 cm organic over dry mineral (sand)	1.6 °C	507 mm	168 days	Absent
	Open wetland	Fen and bog	SOD-wet	> 120 cm organic (peatland)				

848

849

850

851

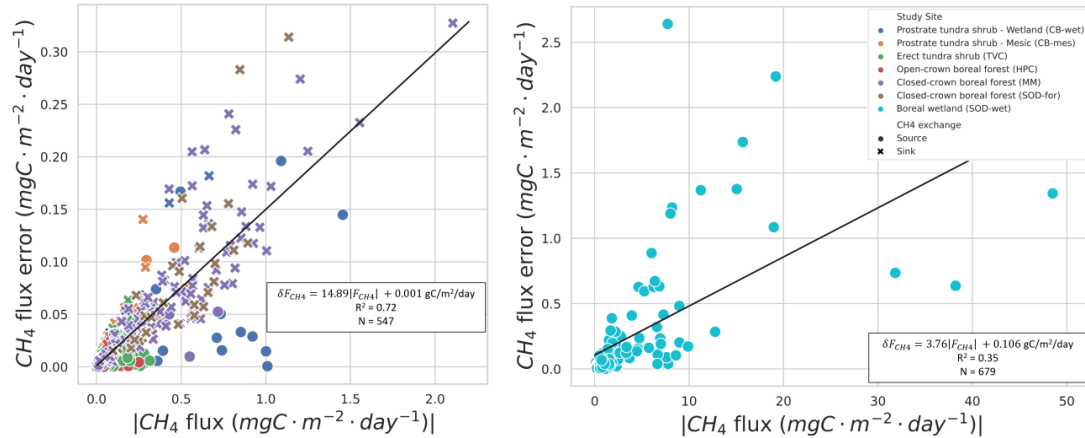
852 **CH<sub>4</sub> flux uncertainty assessment**

853 Sources of uncertainties for F<sub>CH<sub>4</sub></sub> can be subdivided into four categories: gas concentration  
 854 estimates, gas transfer/transport/storage, snow properties estimates and d[CH<sub>4</sub>]/dz estimates. The  
 855 uncertainty on [CH<sub>4</sub>] was evaluated from the gas analyzer precision as assessed by the  
 856 manufacturer. [CH<sub>4</sub>] uncertainty was further tested using calibration gases. The gas transfer,  
 857 transport and storage protocols were tested using calibration gases. The d[CH<sub>4</sub>]/dz linear  
 858 regression uncertainties were evaluated using the standard deviation from the Pearson correlation  
 859 coefficient ( $\sigma = \sqrt{(1 - R^2)/(N - 1)}$ ; Bowley, 1928). F<sub>CH<sub>4</sub></sub> uncertainty was calculated by  
 860 uncertainty propagation from d[CH<sub>4</sub>]/dz and snow density uncertainties.  
 861

862 The F<sub>CH<sub>4</sub></sub> uncertainty assessment showed that the two main sources of uncertainty are  
 863 associated with snow density measurements ( $\sigma(\rho_{\text{snow}}) \approx 9\%$ ); Proksch et al., 2016) and with  
 864 d[CH<sub>4</sub>]/dz (mean  $R^2 = 0.901$  ( $\sigma = 0.135$ ) for  $F_{\text{CH}_4} \geq 0.05 \text{ mg C m}^{-2} \text{ day}^{-1}$ ; N = 339) (Table S1).  
 865 The mean F<sub>CH<sub>4</sub></sub> uncertainty can be estimated at 16.89% for data from CB, TVC, MM and SOD—  
 866 for boreal forest, and 3.76% for data from SOD—wet boreal wetland (Fig. S1).

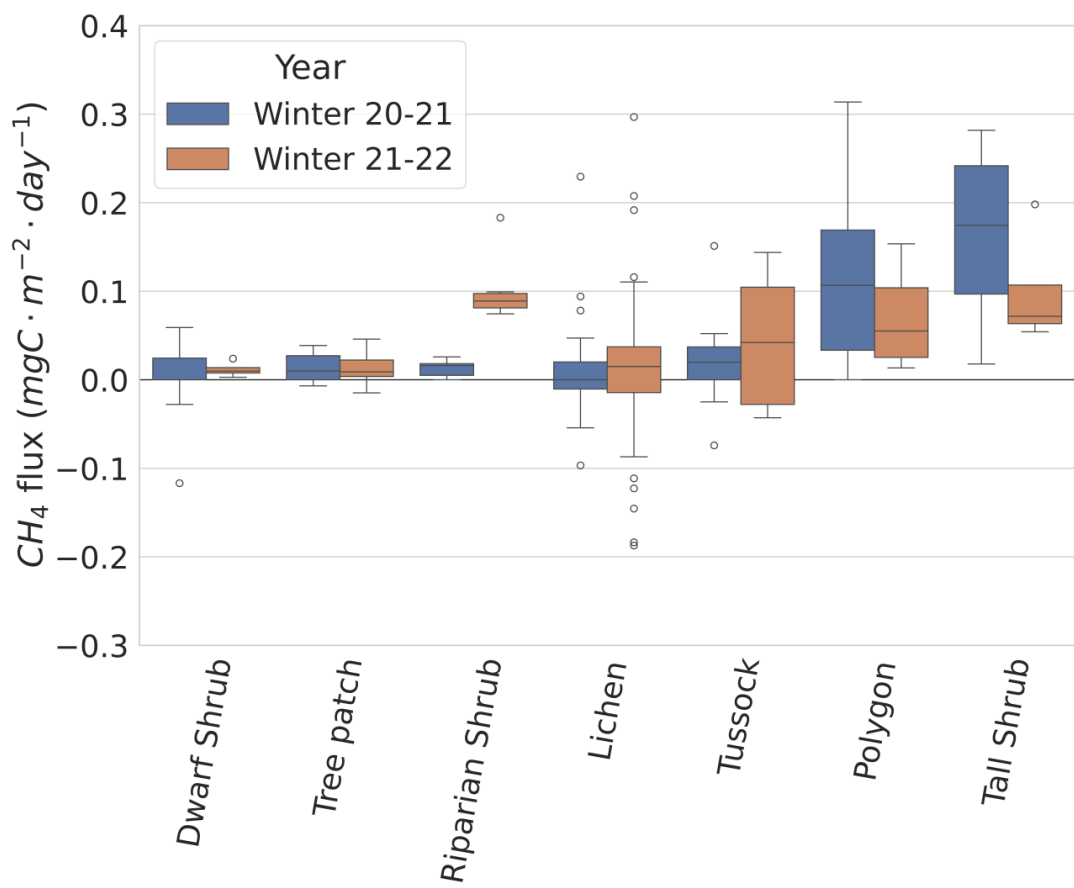
867 **Table S3.** F<sub>CH<sub>4</sub></sub> uncertainty sources. [CH<sub>4</sub>] precision was evaluated at a concentration of 2 ppm.

F <sub>CH<sub>4</sub></sub> uncertainty source	Uncertainty
[CH <sub>4</sub> ] estimate	
· LI-7810 precision	0.6 ppm (0.03%)
· Measurement stability	0.001 ppm (0.05%; N=169)
· Reference gas	0.018 ppm (1%)
· Calibration fit	0.005 ppm (0.25%; N=8; $\sigma = 0.067\%$ )
· Transfer, transport and storage test	0.012 ppm (0.63%; N=5)
Snow density (kg·m <sup>-3</sup> )	9%
d[CH <sub>4</sub> ]/dz linear regression (gC·m <sup>-4</sup> )	17.66% (N=339; $\sigma = 17.14\%$ )

869  
870

871 **Figure S2.** F<sub>CH<sub>4</sub></sub> uncertainty relationship to |F<sub>CH<sub>4</sub></sub>| for the five study sites: Montmorency Forest  
 872 (MM), Cambridge Bay (CB), Trail Valley Creek (TVC), Havikpakk Creek (HPC) and Sodankylä  
 873 (SOD).  
 874

875

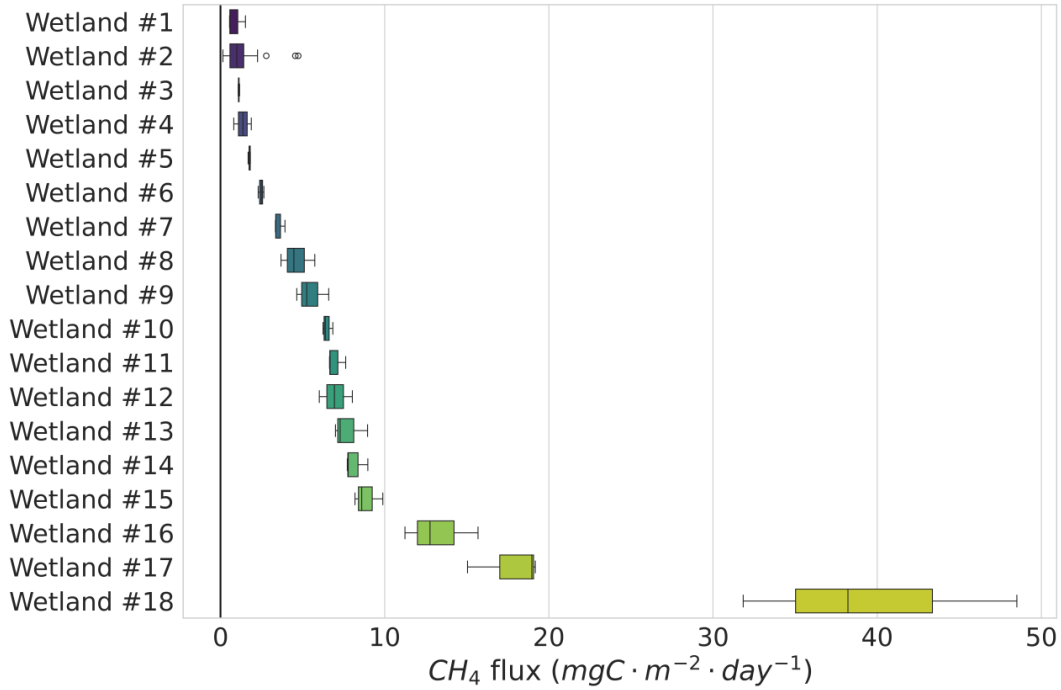
876 **CH<sub>4</sub> flux across vegetation types at Trail Valley Creek**

877

878

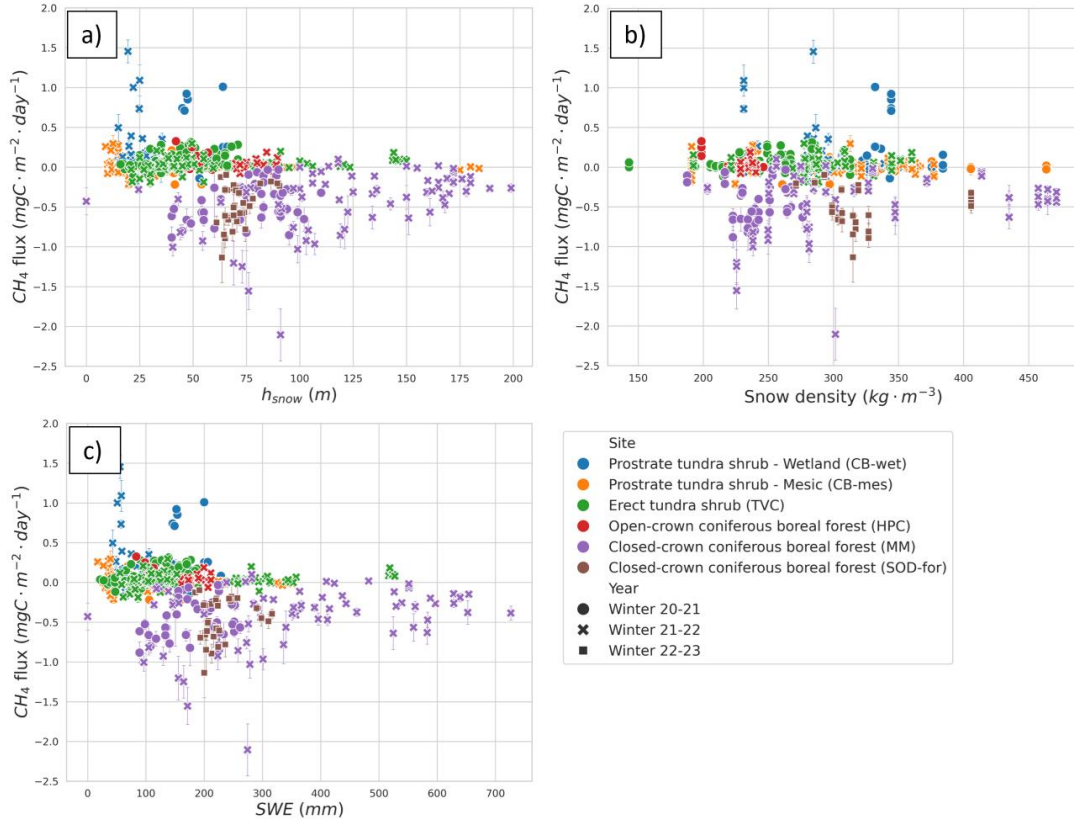
879 **Figure S3.** CH<sub>4</sub> flux across vegetation types at Trail Valley Creek. Vegetation types were not  
880 distinguished by soil moisture classes (like at the Cambridge Bay study site) since the information was not available at the scale of the sampling locations.

881 **Spatial variability of boreal wetland CH<sub>4</sub> fluxes**



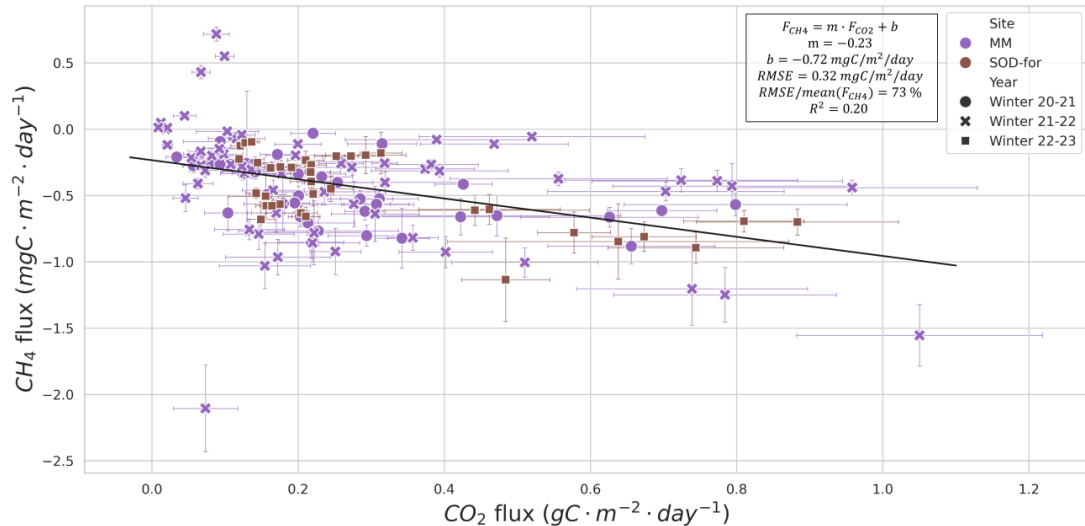
882  
883 **Figure S4.** CH<sub>4</sub> flux spatial variability in the boreal wetland at the Sodankylä study site (SOD–  
884 wet).

885  
886  
887  
888

889 **CH<sub>4</sub> fluxes relationship to snow conditions**

890

891 **Figure S5.** CH<sub>4</sub> flux as a function of a) snow height ( $h_{\text{snow}}$ ), b) snow density, and c) snow water  
 892 equivalent (SWE). The data with no apparent error bar have an error bar smaller than the size of  
 893 the dot.

894    **CH<sub>4</sub> fluxes relationship to CO<sub>2</sub> fluxes**

**Figure S6.** CH<sub>4</sub> flux as a function of CO<sub>2</sub> flux at the Montmorency Forest (MM) and Sodankylä (SOD-for) boreal forest uplands study sites. CO<sub>2</sub> flux data were estimated using the snowpack diffusive gradient method, the same method that was used to obtain the CH<sub>4</sub> flux data in this study. Details about CO<sub>2</sub> flux calculation can be found in Mavrovic et al. (2023).

900  
901    **Boreal forest CO<sub>2</sub> fluxes**

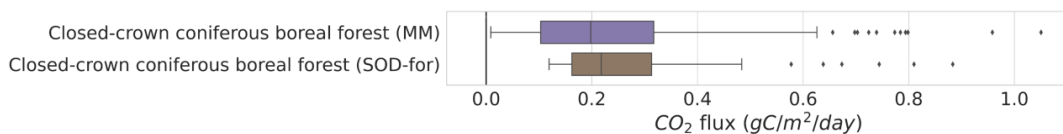


**Figure S7.** CO<sub>2</sub> flux at Montmorency Forest (MM) during winter 2020–2021 and 2021–2022, and at Sodankylä (SOD-for) during winters 2021–2022 and 2023. CO<sub>2</sub> flux data were estimated using the snowpack diffusive gradient method, the same method that was used to obtain the CH<sub>4</sub> flux data in this study. Details about CO<sub>2</sub> flux calculation can be found in Mavrovic et al. (2023). Outliers were defined as F<sub>CO2</sub> > Q3 + 1.5 IQR where Q3 is the third quartile and IQR the interquartile range.

# Chapitre 5 : Impact des flux de carbone hivernaux sur le bilan annuel

## 5.1 Présentation de l'article scientifique

Le chapitre qui suit a été écrit sous forme de manuscrit scientifique (format *Biogeosciences*, EGU). Du travail antérieur au dépôt de la thèse sera requis avant la soumission de ce manuscrit, dont l'intégration de données provenant d'un site d'étude additionnel (Sodankylä, Finlande) qui nous seront partagées dans les prochains mois. La numérotation des lignes, sections, figures, tableaux et équations du manuscrit en développement est indépendante du reste de la thèse. Les références citées dans ce manuscrit ne sont pas répétées à la bibliographie complémentaire de la thèse (Sect. 10). Le matériel supplémentaire accompagnant le manuscrit se trouve à la suite de ce dernier (Sect. 5.3.4).

Ce manuscrit présente des mesures de flux de carbone en hiver et durant la saison de croissance afin de déterminer la contribution des flux hivernaux de  $CO_2$  et de  $CH_4$  aux bilans annuels de flux de carbone de différents types d'écosystème arctiques et boréaux (Objectif spécifique # 3). Les mesures de flux hivernaux proviennent des articles portant sur les flux de  $CO_2$  (Chap. 3) et  $CH_4$  (Chap. 4), ainsi que les contrôles environnementaux identifiés dans ces articles. Les mesures de flux de carbone durant la saison de croissance de la végétation ont été acquises par covariance des turbulences. La majorité des mesures de covariance des turbulences exploitées nous ont été partagées par des collaborateurs, à l'exception du site de Cambridge Bay où une tour EC a été déployée et maintenue en fonction par l'auteur de l'étude.

Contribution en tant que premier auteur : Conception et planification de l'étude. Organisation des campagnes de terrains. Implémentation de la méthode de mesure. Collecte, traitement et analyse des données. Rédaction du manuscrit.

## **5.2 Résumé de l'article scientifique en français**

Les régions arctiques et boréales (RAB) renferment des quantités substantielles de carbone. Il y a une appréhension croissante concernant les impacts potentiels du réchauffement des RAB sur leur cycle du carbone et l'impact à long terme sur le système climatique mondial. La plupart des études se sont concentrées sur la saison de croissance, où l'on s'attend à des taux plus élevés d'échanges de carbone, bien que la saison de croissance soit souvent beaucoup plus courte que l'hiver. Cela a conduit à une disponibilité limitée des données hivernales et à une lacune de connaissances quant à la contribution de l'hiver au bilan annuel de carbone. L'objectif de cette étude est de déterminer la contribution du flux hivernal de dioxyde de carbone et de méthane sur le bilan annuel du carbone dans quatre écosystèmes typiques des RAB : forêt boréale de conifères à couronne fermée, forêt boréale de conifères à couronne ouverte, toundra à arbustes dressés et toundra à arbustes couchés. Nous avons estimé l'échange net des écosystèmes (Net Ecosystem Exchange : NEE) à partir de mesures de covariance de turbulences pendant la saison de croissance et à partir de la méthode du gradient de diffusion à travers le couvert neigeux pendant l'hiver. Nous avons estimé que la contribution hivernale au budget annuel variait de 5 % à 42 % pour les flux de dioxyde de carbone, et de 1 % à 6 % pour les flux de méthane, selon l'écosystème. Ces contributions se situent du côté des valeurs minimales que d'autres études ont estimées dans les RAB, mais nos résultats représentent des sols bien drainés qui sont davantage répandus dans les RAB, tandis que la plupart des autres études se sont concentrées sur les zones humides où des échanges de carbone plus importants sont attendus. Notre étude met en évidence que les flux de carbone hivernaux des sols bien drainés des RAB ne peuvent être négligés afin d'estimer avec précision le budget carbone de ces environnements sensibles et doivent être correctement estimés dans les modèles écosystémiques et les modèles climatiques.

# Winter carbon fluxes contribution to the annual budget in arctic and boreal environments

**Abstract.** Arctic and boreal regions (ABR) contain substantial amounts of carbon. There is a growing apprehension regarding the potential impacts of ABR warming on its carbon cycle and the extended effect on the global climate system. Most studies have focused on the growing season where higher rates of carbon exchanges are expected although the growing season is often much shorter than winter. This led to limited winter data availability and a knowledge gap in the contribution of winter to the annual carbon budget. The goal of this study was to determine the contribution of carbon dioxide and methane winter flux to the annual carbon budget in four different ABR ecosystems: closed-crown coniferous boreal forest, open-crown coniferous boreal forest, erect-shrub tundra, and prostrate-shrub tundra. We derived the net ecosystem exchange (NEE) from eddy covariance measurements during the growing season and from the interpolation of snowpack diffusion gradient measurements during winter. We calculated that the winter contribution to the annual budget for carbon dioxide flux ranged from 5 % to 42 % depending on the ecosystem, and the methane flux ranged from 1 % to 6 %. Those contributions are on the lower side of what other studies have found in ABR, but our results represent the more widespread well-drained soils of ABR whereas most other studies focused on wetlands. Our study stresses that ABR winter carbon flux in well-drained soils cannot be neglected to accurately estimate the carbon budget in these sensitive environments and that it must be properly estimated in terrestrial biosphere models and climate models.

20

**Keywords:** Arctic-boreal regions, Carbon budget, Carbon dioxide flux, Methane flux, Non-growing season, Winter.

## 1 Introduction

The climate of our planet is closely linked to the atmospheric concentrations of greenhouse gases such as carbon dioxide ( $\text{CO}_2$ ) and methane ( $\text{CH}_4$ ). The exchange of  $\text{CO}_2$  and  $\text{CH}_4$  between the land surface and atmosphere are critical components of the carbon cycle. Arctic and boreal regions (ABR) contain substantial amounts of carbon due to their inherently slow decomposition rates, largely attributable to their cold temperatures (Tarnocai et al., 2009; van Huissteden and Dolman, 2012; Carreiras et al., 2017; Ravn et al., 2020). Most of the ABR carbon is stored belowground, accounting for 30 to 40% of the planetary terrestrial carbon (Pan et al., 2011; Tarnocai et al., 2009). However, the ABR are warming up to four times faster than the rest of the planet, which could lead to significant feedback effects on the global climate system (Derksen et al., 2019; Rantanen et al., 2022). Terrestrial biosphere models and climate models used to predict the evolution of the climate system require a comprehensive understanding of ecosystems to determine if they act as carbon sinks (sequestration) or sources (emission). ABR are among the least understood areas due to their challenging accessibility. In these environments, winter is the most neglected season because of the technical challenges posed by harsh winter conditions. Studies have shown that the winter carbon flux

contribution to the annual budget is significant, accounting for 3 to 50% of annual CH<sub>4</sub> emissions (Panikov and Dedysh, 2000; Grogan and Jonasson, 2005; Zona et al., 2016; Rößger et al., 2022) and offsetting 2 to 230% of the growing season CO<sub>2</sub> sequestration by the vegetation (Euskirchen et al., 2012; Oechel et al., 2014; Arndt et al., 2020) (Table 1). However, studies on the winter carbon fluxes in ABR remain scarce and often focus on study sites where higher emissions or uptakes are expected, such as wetlands (Kuhn et al., 2021; Rößger et al., 2022; Voigt et al., 2023). Eddy covariance (EC) is the most widely used method for carbon fluxes measurement due to its high temporal resolution. However, data interruptions are common during winter in ABR because EC equipment is energy-intensive, prone to malfunction at low temperatures, unreliable when icing up, and solar power systems are limited by the low winter sunlight (Kittler et al., 2017; Jentzsch et al., 2021; Pallandt et al., 2022). The limited availability of carbon exchange data during winter is a hindrance to terrestrial biosphere model parametrization and validation (Pallandt et al., 2022). Despite improvement in modeling ABR carbon exchange during the growing season, estimating winter carbon exchange remains challenging (Virkkala et al., 2021; Ito et al., 2023; Hugelius et al., submitted).

50

The goal of this study is to determine the winter CO<sub>2</sub> and CH<sub>4</sub> flux contribution to the annual budget in ABR. We achieved this goal by using complementary measurements from the snowpack diffusion gradient method during winter (Mavrovic et al., 2023 and submitted), EC measurements during the growing season, and empirical modelling to gap fill the dataset. Our study covers four different ecosystem types common in ABR in Canada: closed-crown coniferous boreal forest, open-crown coniferous boreal forest, erect-shrub tundra, and prostrate-shrub tundra. Our results are compared to an exhaustive list of studies that estimated the winter CO<sub>2</sub> and CH<sub>4</sub> flux contribution to the annual budget in ABR.

## 2 Method

### 2.1 Study sites

60 Four study sites characteristic of four ABR ecosystems were selected. The Cambridge Bay study site (CB; Nunavut, Canada) is located in the Arctic biome and is dominated by lichen and prostrate shrub tundra. CB site is constituted of mesic and wetland areas (Ponomarenko et al., 2019). The Trail Valley Creek study site (TVC; Northwest Territories, Canada) is situated in the forest-tundra ecotone, the transitional zone between the boreal and Arctic biomes. TVC consists of a mineral upland tundra dominated by erect shrub tundra with (Martin et al., 2022; Voigt et al., 2023). The Havikpak Creek study site (HPC; Northwest Territories, Canada) is located about 50 km south of TVC in an open-crown black spruce dominated forest stand, just south of the treeline (Krogh et al., 2017). The Montmorency Forest study site (MM; Québec, Canada) is the southernmost site located in a closed-crown balsam fir dominated boreal forest (Barry et al., 1988). The CB, TVC and HPC sites are underlain by continuous permafrost, while the MM site is permafrost-free.

## **2.2 Growing season measurements: Eddy covariance measurements**

The growing season CO<sub>2</sub> and CH<sub>4</sub> flux were estimated from EC measurements. Eddy covariance relies on the principle of turbulent exchange (Baldocchi et al., 1988). By analyzing the covariance between the vertical wind speed fluctuations and the gas concentration fluctuations, the flux of gases between the surface and the atmosphere can be calculated. The EC systems at TVC and HPC comprised identical three-dimensional sonic anemometers (CSAT3A; Campbell Scientific Inc., Logan, UT), CO<sub>2</sub>/H<sub>2</sub>O open-path gas analyzers (EC150; Campbell Scientific Inc.), and CH<sub>4</sub> open-path gas analyzers (LI-7700; LI-COR Biosciences Inc., Lincoln, NE). The EC systems at CB comprised a three-dimensional sonic anemometer (CSAT3B; Campbell Scientific Inc., Logan, UT), enclosed-path CO<sub>2</sub>/H<sub>2</sub>O gas analyzer (LI-7200RS; LI-COR Biosciences Inc., Lincoln, NE) and CH<sub>4</sub> open-path gas analyzers (LI-7700; LI-COR Biosciences Inc., Lincoln, NE). The EC systems at MM comprised an IRGASON system (Campbell Scientific Inc., Logan, UT) which integrates a three-dimensional sonic anemometer (CSAT3A; Campbell Scientific Inc., Logan, UT) and open-path CO<sub>2</sub>/H<sub>2</sub>O gas analyzer (EC150; Campbell Scientific Inc.) in one instrument. All the EC systems measured high-frequency fluctuations (10 Hz) in 3D wind velocity, CO<sub>2</sub>, CH<sub>4</sub> (only TVC and HPC), and water vapor density. At TVC, HPC and CB, half-hourly EC fluxes were processed using the EddyPro software package (version 7.0.6; LI-COR Biosciences Inc) and only high-quality data were retained (Papale et al., 2006; Mauder & Foken, 2011). At MM, half-hourly EC fluxes were processed using the REddyProc (Wutzler et al., 2018). At all sites, EC fluxes were gap-filled using the Marginal Distribution Sampling algorithm (Reichstein et al., 2005). Half-hourly EC fluxes were aggregated to daily fluxes. Further details on the data processing are provided in Helbig et al. (2016 and 2017) and Graveline (submitted).

## **2.3 Winter measurements: Snowpack diffusion gradient method**

The winter CO<sub>2</sub> and CH<sub>4</sub> flux measurements used in this study are presented extensively in Mavrovic et al. (2023) and Mavrovic et al. (submitted) respectively. The snowpack diffusion gradient method was used to estimate winter carbon flux within the EC tower footprint at 6 sampling locations at CB and TVC, at 5 sampling locations at HPC, and at 12 sampling locations at MM. This method used Fick's first law for gas diffusion in porous media to estimate gas fluxes from the vertical gas diffusion gradient maintained through the snowpack and the snow microstructure (Sommerfeld et al., 1993; Zhu et al., 2014). In Mavrovic et al. (2023), two winter soil CO<sub>2</sub> flux regimes were identified. The first regime was when the soil was frozen leading to CO<sub>2</sub> fluxes being mainly controlled by soil temperature (T<sub>soil</sub>). The second regime was when a mix of liquid water and ice was present in the soil (zero-curtain conditions; Outcalt et al., 1990) causing soil liquid water content (LWC) to be the main control of CO<sub>2</sub> fluxes instead of T<sub>soil</sub>. The relationship between CO<sub>2</sub> fluxes (F<sub>CO2</sub>) and T<sub>soil</sub> is used in this study to estimate winter CO<sub>2</sub> fluxes when soil LWC is negligible:

$$F_{CO2} = A \cdot e^{B \cdot T_{soil}} \quad (1)$$

105

where the parameter A is  $0.186 \text{ gC m}^{-2} \text{ day}^{-1}$  and B is  $0.180 \text{ }^{\circ}\text{C}^{-1}$ . When soil LWC is present (unfrozen water), the relationship between  $F_{\text{CO}_2}$  and soil LWC is used in this study to estimate winter  $\text{CO}_2$  fluxes:

110      
$$F_{\text{CO}_2} = A \cdot e^{B \cdot \text{LWC}} + C \quad (2)$$

where the parameter A is  $8.70 \times 10^{-5} \text{ gC m}^{-2} \text{ day}^{-1}$ , B is 21.44 and C is  $0.127 \text{ gC m}^{-2} \text{ day}^{-1}$ . At the CB study site, soil temperature was monitored using i-Buttons (Maxim Integrated, San Jose, California, USA) compact, self-contained temperature sensors and data loggers. The average  $T_{\text{soil}}$  at 5 cm from 4 iButtons distributed across the EC tower footprint was used to estimate winter  $\text{CO}_2$  fluxes. No soil LWC data were available at the CB study site and not enough continuous LWC data were available at the TVC study site, therefore only Eq. (1) was used to estimate winter  $\text{CO}_2$  fluxes. Soil temperature and LWC at MM were measured using TEROS 12 sensors (METER Group, Pullman, Washington, USA) at 10 locations located within a 1 km radius of the EC tower. At MM, monthly winter  $\text{CO}_2$  flux measurements were acquired which allows for estimating the winter seasonal trend using a second-degree polynomial fit on snowpack diffusion gradient measurements as a function of the day of the year (DOY) with a minimum in February (Sect. A1, Fig. A2).

In Mavrovic et al. (submitted), no environmental control on winter  $\text{CH}_4$  fluxes was identified in Arctic tundra environments since the  $\text{CH}_4$  fluxes were low. Therefore, an average of winter  $\text{CH}_4$  fluxes is used in this study to estimate the winter contribution to the annual budget.

### 2.3 Seasonality

There are a multitude of approaches to define the growing season (e.g., Table B1 and B2). In this study, the growing season is delineated from the vegetation photosynthetic recovery in spring and cessation in fall. To evaluate the start and end of the growing season, we use the vegetation daily gross primary productivity (GPP) time series derived from the net ecosystem  $\text{CO}_2$  exchange (NEE) measurements obtained by EC systems (Baldocchi and Meyers, 1998). A double-logistic function is fitted to daily GPP and the day of the year of the curve inflection is highlighted using the first maximum (spring recovery) and last minimum (autumn cessation) of the third derivative of the double logistic function (Gonsamo et al., 2013; El-Amine et al., 2022).

### 135    2.4 Annual budget carbon estimation

The annual carbon budget is estimated 1) using EC data during the growing season as defined in section 2.3 and 2) using empirical relationships derived from snowpack diffusion gradient data in winter. The budget is computed using the trapezoidal rule for numerical integration (NumPy 1.24.2 library from Python 3.10.6). There is a gap of 5 days without EC data at the end of the growing season at the CB study site. Those days

140 were filled by interpolating the data from the last available data during the growing season and the first data in the winter season.

### 3 Results

#### 3.1 Annual carbon budget

At the CB mesic tundra study site, the growing season net CO<sub>2</sub> budget adds up to -43.4 gC m<sup>-2</sup> in 145 2022(CO<sub>2</sub> uptake from the atmosphere), while the winter net CO<sub>2</sub> budget adds up to 14.8 gC m<sup>-2</sup> from soil respiration (CO<sub>2</sub> emission to the atmosphere) (Fig. 1b). The net annual CO<sub>2</sub> budget is -28.6 gC m<sup>-2</sup> with winter soil respiration offsetting 34 % of the growing season CO<sub>2</sub> uptake. The start and end of the growing season are derived from the GPP estimates (Fig. 1a). No growing season F<sub>CH<sub>4</sub></sub> measurements are available at CB because of the CH<sub>4</sub> gas analyzer failure.

150

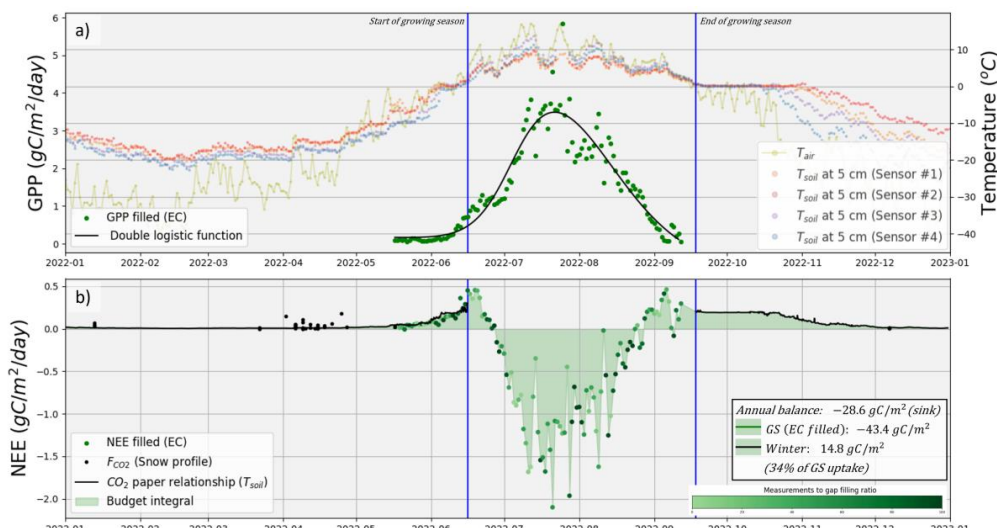
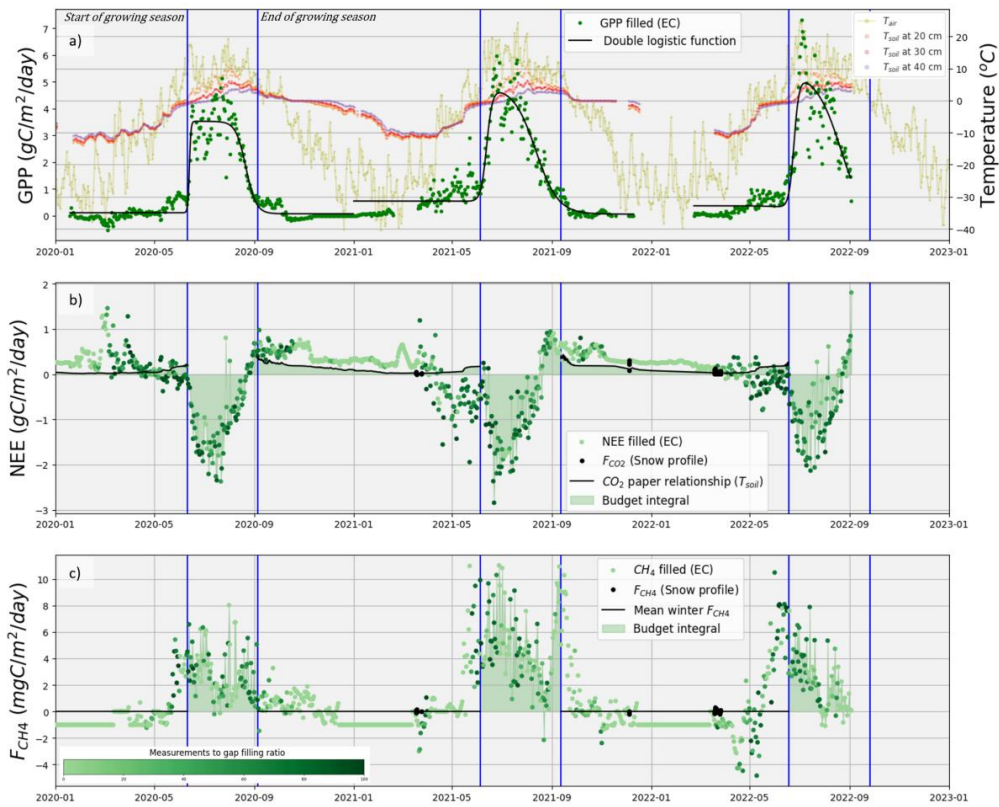


**Figure 1:** Yearly CO<sub>2</sub> exchanges at a mesic tundra site in Cambridge Bay in 2022. (a) The gross primary production (GPP) and (b) net ecosystem exchange (NEE) are presented. Growing season (GS) measurements were acquired from an eddy covariance system (EC) and have been gap-filled. The vertical blue line delineated the start and end of the growing season. Soil temperature ( $T_{\text{soil}}$ ) sensors were distributed across the EC tower footprint and air temperature ( $T_{\text{air}}$ ) was obtained from Environment and Climate Change Canada's Meteorological Service of Canada meteorological station at Cambridge Bay and soil temperature ( $T_{\text{soil}}$ ) was obtained from i-Buttons sensors distributed across the EC tower footprint.

155

At the TVC tundra erect shrub study site, the growing season net CO<sub>2</sub> budget adds up to -77.2 gC m<sup>-2</sup> in 160 2020 and -66.5 gC m<sup>-2</sup> in 2021, while the winter net CO<sub>2</sub> budget adds up to 29.6 gC m<sup>-2</sup> in 2020 and 28.1 gC m<sup>-2</sup> in 2021 from soil respiration (Fig. 2b). The net annual CO<sub>2</sub> budget is -47.6 gC m<sup>-2</sup> in 2020 and -38.4 gC m<sup>-2</sup> in 2021 with winter soil respiration offsetting 38 % in 2020 and 42 % in 2021 of the growing season CO<sub>2</sub> uptake. The growing season net CH<sub>4</sub> budget adds up to 244 mgC m<sup>-2</sup> in 2020 and 478 mgC m<sup>-2</sup> in 2021, while the winter net CH<sub>4</sub> budget adds up to 3.8 mgC m<sup>-2</sup> in 2020 and 3.6 mgC m<sup>-2</sup> in 2021 from soil respiration

165 (Fig. 2c). The net annual CH<sub>4</sub> budget is 248 gC m<sup>-2</sup> in 2020 and 481 gC m<sup>-2</sup> in 2021 accounting for 1.5 % and 0.8 % of the net annual budget for 2020 and 2021, respectively. The CH<sub>4</sub> seasonal trend seems to display an increase in CH<sub>4</sub> emissions around a month prior to the start of the growing season as defined by GPP (Fig. 2c). Since the biochemical processes generating CH<sub>4</sub> emissions are distinct from vegetation photosynthetic processes, the shift in seasonal trends between CO<sub>2</sub> and CH<sub>4</sub> flux is not surprising. Nevertheless, the transition  
170 of T<sub>soil</sub> between frozen to thaw occurs around the same date as the start of the growing season as defined by GPP. In contrast, the spring transition of T<sub>soil</sub> between thaw to frozen lasts longer because of an extended zero-curtain period. The end of the growing season as defined by GPP seems to correspond to the beginning of the zero-curtain period, although the decrease in solar illumination might be a more critical factor for the vegetation photosynthetic activities cessation than zero-curtain conditions (El-Amine et al., 2022). The  
175 relationship of T<sub>soil</sub> trends to the start and end of the growing season is very similar across all of our study sites (Fig. 1a, 2a and 3a). It can be noticed from the shades of green in Fig 2a that the winter NEE estimates from the EC method are gap-filled for extensive periods, darker green represents daily NEE estimated mostly from flux measurements and lighter green represents daily NEE estimated mostly from gap-filled data. Those EC winter NEE estimations are mostly deemed unreliable because they are extrapolated in conditions where  
180 no EC measurements of sufficient quality were obtained (e.g., instrument icing up, power shortage, malfunction; Fig. 2a, b and 3 a, b), and thus the use of empirical relationships between T<sub>soil</sub>, soil LWC, and F<sub>CO2</sub> measurements is essential to calculate the impact of winter respiration on the annual budget.



185 **Figure 2:** Yearly CO<sub>2</sub> and CH<sub>4</sub> exchanges at an erect shrub site in Trail Valley Creek from 2020 to 2022. (a) The gross primary production (GPP), (b) net ecosystem exchange (NEE), and (c) methane fluxes (F<sub>CH<sub>4</sub></sub>) are presented. Growing season (GS) measurements were acquired from an eddy covariance system (EC) and have been gap-filled. The vertical blue line delineated the start and end of the growing season. Air temperature (T<sub>air</sub>) was obtained from Environment and Climate Change Canada's Meteorological Service of Canada meteorological station at Trail Valley Creek.

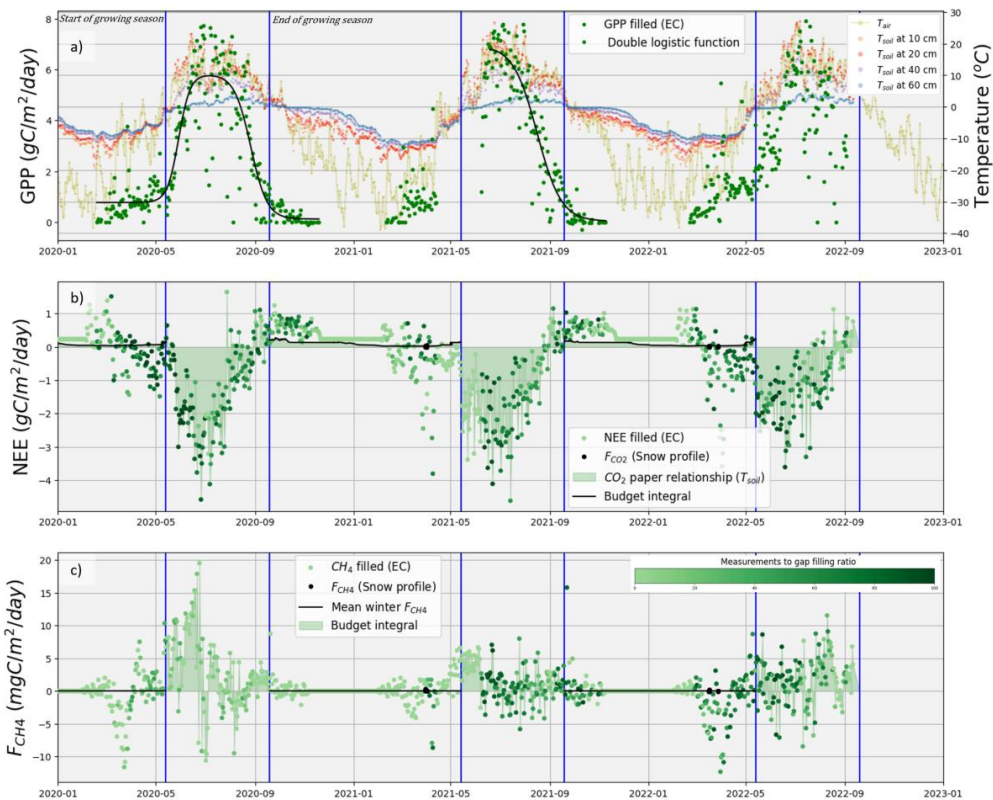
190

At the HPC black spruce boreal forest study site, the growing season net CO<sub>2</sub> budget adds up to -156.9 gC m<sup>-2</sup> in 2020 and -175.5 gC m<sup>-2</sup> in 2021, while the winter net CO<sub>2</sub> budget adds up to 24.9 gC m<sup>-2</sup> in 2020 and 21.6 gC m<sup>-2</sup> in 2021 from soil respiration (Fig. 3b). The net annual CO<sub>2</sub> budget is -132 gC m<sup>-2</sup> in 2020 and -153.9 gC m<sup>-2</sup> in 2021 with winter soil respiration offsetting 16 % in 2020 and 12 % in 2021 of the

195 growing season CO<sub>2</sub> uptake. The growing season net CH<sub>4</sub> budget adds up to 369 mgC m<sup>-2</sup> in 2020 and 172 mgC m<sup>-2</sup> in 2021, while the winter net CH<sub>4</sub> budget adds up to 9.2 mgC m<sup>-2</sup> in 2020 and 10 mgC m<sup>-2</sup> in 2021 from soil respiration (Fig. 3c). The net annual CH<sub>4</sub> budget is 378 gC m<sup>-2</sup> in 2020 and 182 gC m<sup>-2</sup> in 2021 accounting for 2.4 % and 5.6 % of the net annual budget for 2020 and 2021, respectively. The impact of using soil LWC when unfrozen water is present was small compared to the approach using exclusively T<sub>soil</sub>

200 (Eq. 1), reducing the net winter CO<sub>2</sub> budget by 6.5 % in 2020 and 8.7 % in 2021. In April and May 2021, instrument failure led to an important data gap that was filled for NEE but did not provide reliable GPP estimates. Consequently, it was not possible to determine the start of the 2021 growing season using the GPP method. The 2022 GPP partitioning did not follow a double-logistic function as expected (Fig. 3a), thus it

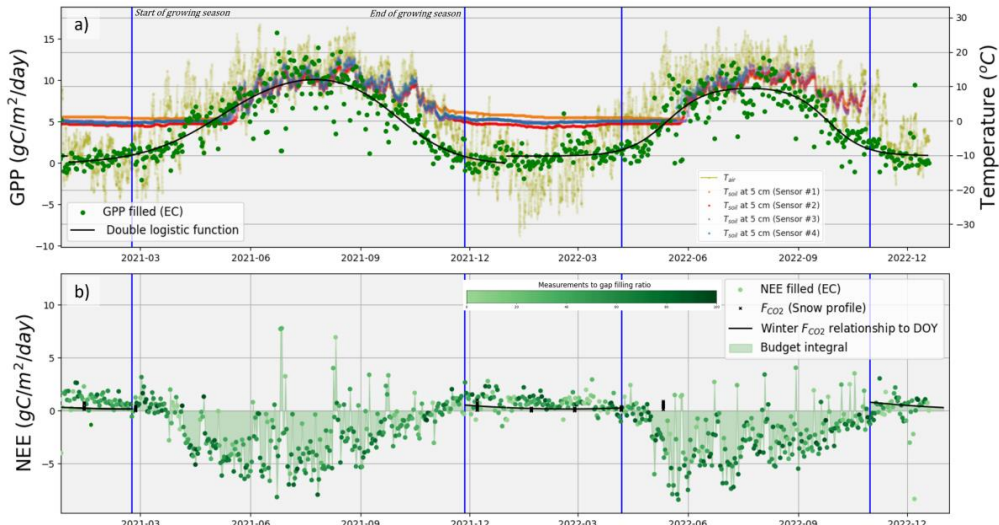
was not possible to determine the start and end of the 2022 growing season using the GPP method. All 205 growing season boundaries that were not determined using the GPP method were estimated from the average growing season boundaries from other years.



210 **Figure 3:** Yearly CO<sub>2</sub> and CH<sub>4</sub> exchanges at a black spruce boreal forest site in Havikpak Creek from 2020 to 2022. (a) The gross primary production (GPP), (b) net ecosystem exchange (NEE), and (c) methane fluxes (F<sub>CH<sub>4</sub></sub>) are presented. Growing season (GS) measurements were acquired from an eddy covariance system (EC) and have been gap-filled. The vertical blue line delineated the start and end of the growing season. Air temperature (T<sub>air</sub>) was obtained from Environment and Climate Change Canada's Meteorological Service of Canada meteorological station at Inuvik.

215 At the MM balsam fir boreal forest study site, the growing season net CO<sub>2</sub> budget adds up to -515 gC m<sup>-2</sup> in 2021, and -486.8 gC m<sup>-2</sup> in 2022, while the winter net CO<sub>2</sub> budget adds up to 23.5 gC m<sup>-2</sup> in 2021, and 49.9 gC m<sup>-2</sup> in 2022 from soil respiration (Fig. 4b). The net annual CO<sub>2</sub> budget is -491.5 gC m<sup>-2</sup> in 2021, and -436.9 gC m<sup>-2</sup> in 2022 with winter soil respiration offsetting the growing season CO<sub>2</sub> uptake by 5 % in 2021, and 10 % in 2022.

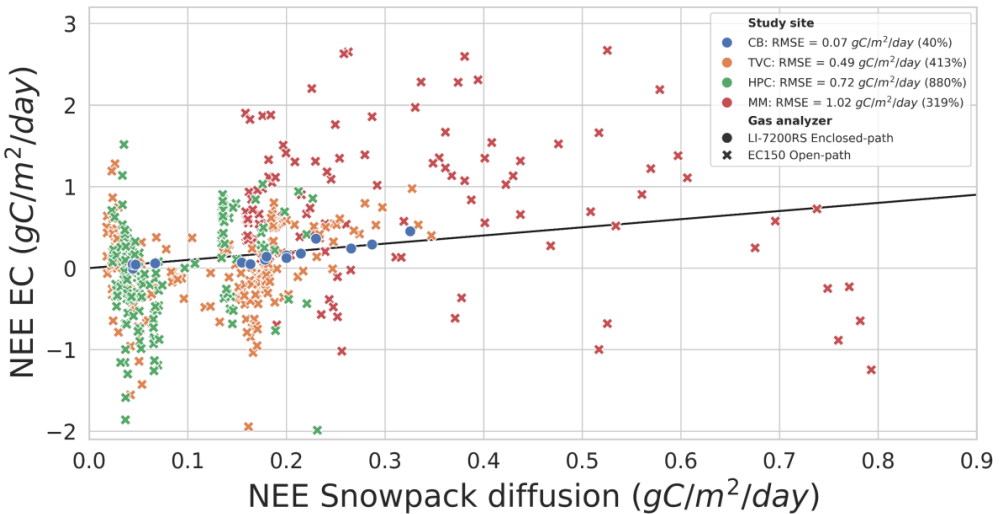
220



225 **Figure 4:** Yearly CO<sub>2</sub> exchanges at a balsam fir boreal forest site in Montmorency Forest from 2021 to 2022. (a) The  
growing season (GS) measurements were acquired from an eddy covariance system (EC) and have been gap-filled. The vertical blue line  
delineated the start and end of the growing season. Soil temperature (T<sub>soil</sub>) sensors were distributed among the winter  
CO<sub>2</sub> flux measurement sites and air temperature (T<sub>air</sub>) was obtained from the EC tower.

### 3.2 Comparison of snowpack diffusion gradient and the EC measurements

There are important discrepancies between the winter NEE derived from EC measurements compared to  
230 winter NEE derived from snowpack diffusion gradient measurements taken as the reference since the  
reliability of EC data in winter conditions remains uncertain (Fig. 5). Only days where fewer than 50%  
missing half-hourly measurements were selected for this analysis, which were mostly found in the month  
before and after the growing season which we can call the shoulder seasons. The CB study site stands out as  
displaying NEE derived from EC measurement much closer to NEE derived from snowpack diffusion  
235 gradient measurements compared to TVC, HPC and MM: CB RMSE = 0.07 gC m<sup>-2</sup> day<sup>-1</sup> (40 % of mean  
NEE) compared to TVC RMSE = 0.49 gC m<sup>-2</sup> day<sup>-1</sup> (413 % of mean NEE), HPC RMSE = 0.72 gC m<sup>-2</sup> day<sup>-1</sup>  
(880 % of mean NEE) and MM RMSE = 1.02 gC m<sup>-2</sup> day<sup>-1</sup> (319 % of mean NEE). For all the sites, the  
EC method underestimates in average the NEE compared to the snowpack diffusion method: CB bias = -0.02  
gC m<sup>-2</sup> day<sup>-1</sup> (-12 % of mean NEE), TVC bias = -0.13 gC m<sup>-2</sup> day<sup>-1</sup> (-114 % of mean NEE), HPC bias = -  
240 0.16 gC m<sup>-2</sup> day<sup>-1</sup> (-198 % of mean NEE), and MM bias = -0.48 gC m<sup>-2</sup> day<sup>-1</sup> (+151 % of mean NEE).



245 **Figure 5:** Comparison of net ecosystem exchange (NEE) derived from eddy covariance (EC) and snowpack diffusion gradient measurements. Data comes from four study sites: Cambridge Bay (CB; N = 15), Trail Valley Creek (TVC; N = 206), Havikpak Creek (HPC; N = 154), and Montmorency Forest (MM; N = 114).

#### 4 Discussion

Our results show the overall non-negligible winter contribution of ABR to the net annual carbon budget (Fig. 6 and 7). Our estimates of the winter contribution of Arctic tundra sites to the net annual carbon budget are on the lower side when compared to other studies. Many studies selected sites in wetlands where high 250 CO<sub>2</sub> and CH<sub>4</sub> emissions were expected (Voigt et al., 2023), while our study sites are more representative of the common well-drained soils found in ABR.

The Arctic tundra site of TVC displayed low to negligible CH<sub>4</sub> winter emissions. We provide one of the rare estimates of the winter CH<sub>4</sub> fluxes contribution of a black spruce boreal forest site since most studies in 255 boreal regions focused on wetlands where it was shown in Mavrovic et al. (submitted) that there is strong winter CH<sub>4</sub> emissions, while in well-drained boreal forest soils, there is winter CH<sub>4</sub> uptake. Our assessment of the winter CH<sub>4</sub> fluxes contribution to the annual budget of the Arctic sites of TVC and HPC was limited to measurements in the middle of winter close to the minimum CO<sub>2</sub> fluxes related to low T<sub>soil</sub>. The average CH<sub>4</sub> flux used to estimate the winter net budget should be considered as minimum estimates since it is 260 expected that the CH<sub>4</sub> fluxes should be higher toward the shoulder seasons. It can be noticed that the definition of winter varies between studies presented in Fig. 6 and 7 with definitions based on GPP, solar radiation, T<sub>soil</sub>, and fixed dates (Tables A1 and A2). The various winter definitions make the budgets not fully comparable, although it provides a relevant overview.

265

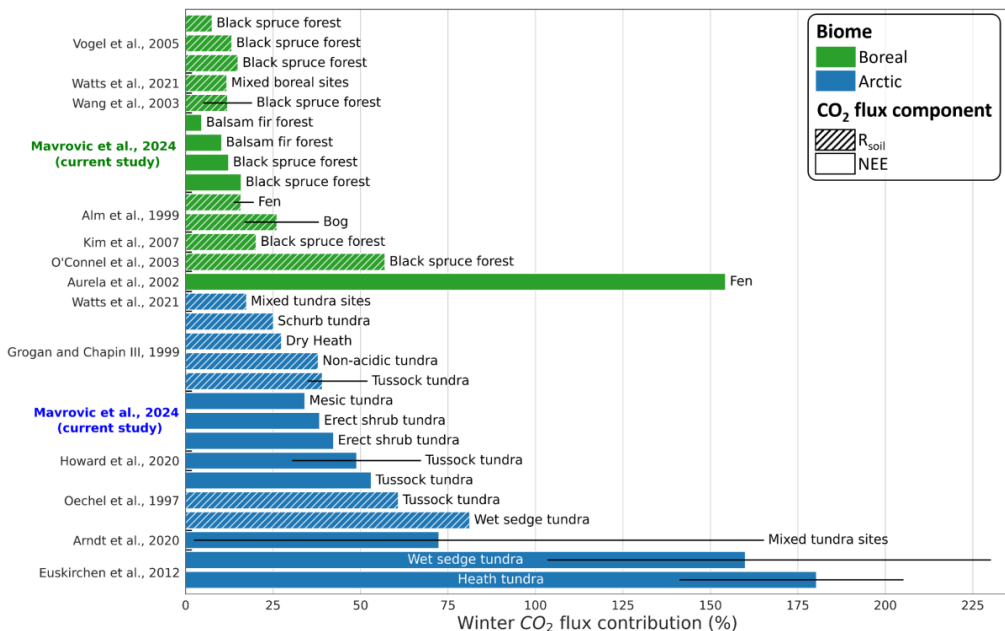


**Figure 6:** Winter CO<sub>2</sub> flux contribution to the annual CO<sub>2</sub> budget in Arctic and boreal environments. Depending on the study, the net ecosystem exchange (NEE) or the soil respiration (R<sub>soil</sub>) is presented. The main color bars represent the mean value and the black horizontal lines represent the range of values found in a given study. Further details on each study are presented in Table A1.

270

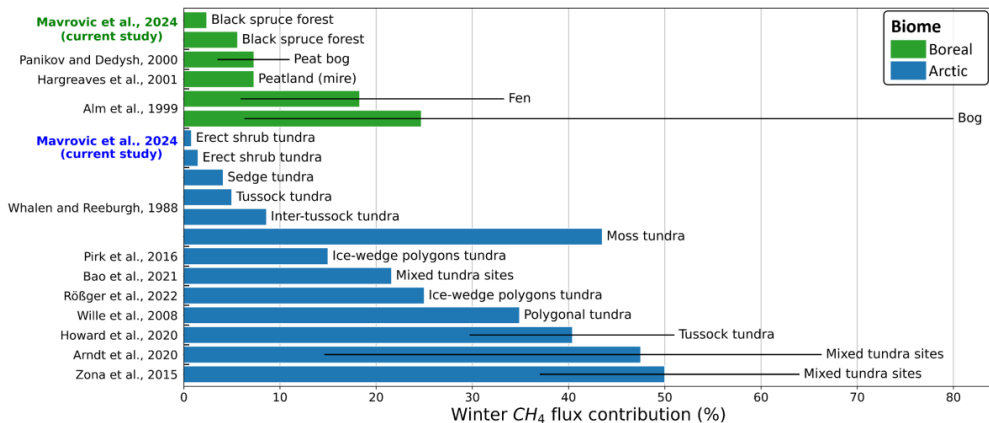


**Figure 7:** Winter CH<sub>4</sub> flux contribution to the annual budget CH<sub>4</sub> in Arctic and boreal environments. The main color bars represent the mean value and the black horizontal lines represent the range of values found in a given study. Further details on each study are presented in Table A2.

275

In this study, we are comparing the winter CO<sub>2</sub> flux contribution as estimated from soil respiration measurement (i.e., snowpack diffusion gradient method) to growing season NEE measurements (i.e., EC method). For winter soil respiration to be equal to winter NEE, we assumed that GPP is negligible because standing vegetation is dormant during winter. This should hold true at sites like CB where the prostrate shrub

280 vegetation is fully covered by snow during winter and sites like TVC where the erect shrub vegetation is mostly covered by snow during winter. In forested areas such as the HPC and MM sites, it is more uncertain that the GPP is negligible during winter. The low negative air temperature in the middle of winter makes it unlikely that the vegetation is active, but the shoulder seasons might be more complex as we observed at MM where the growing season and the snow-covered period overlap in the spring (Larsen et al., 2007). In Pierrat 285 et al. (2021), it was shown that black spruce photosynthetic activity can start as soon as liquid water is available in the soil even if snow is present on the ground. If photosynthesis occurs during the shoulder season, it will reduce the winter CO<sub>2</sub> flux contribution.

In the shoulder season, we have an overlapping period with estimates derived from the snowpack 290 diffusion gradient method and the EC measurements. It is known that open-path gas analyzers have issues with icing during winter (Kittler et al., 2017), which is corroborated by the poor comparison of NEE derived from EC measurements compared to NEE derived from the snowpack gradient method (Fig. 4) for the three sites with open-path CO<sub>2</sub> gas analyzers (i.e., TVC, HPC and MM). The enclosed-path CO<sub>2</sub> gas analyzer installed at CB fared much better with a relatively small spread and bias between the NEE derived from EC 295 measurements and from the snowpack gradient method (Fig. 4). However, the number of days with EC measurements during the shoulder season is much lower for CB than for TVC, HPC and MM. Further studies should investigate other sites to validate the use of enclosed-path CO<sub>2</sub> gas analyzers in winter conditions.

## 5 Conclusion

Our study shows that the winter contribution of carbon flux in Arctic and boreal regions is not negligible 300 when accounting for the annual carbon balance of such environments. We estimated that the winter contribution to the annual budget for carbon dioxide flux ranged from 34 % to 42 % in arctic biomes and from 5 % to 16 % in boreal biomes. We estimated that the winter contribution of methane flux to the annual budget ranged from 1 % to 2 % in arctic biomes and from 2 to 6 % in boreal biomes. Although our estimates of the winter carbon flux contributions are on the lower side of other studies for Arctic and boreal regions, 305 we focused on well-drained soils contrary to most other studies that have focused on wetlands. Well-drained soil winter carbon flux might be typically lower than in wetlands, but those environments represent larger areas in Arctic and boreal regions.

## 6 Acknowledgements

The authors would like to warmly thank the Indigenous communities who have welcomed us and 310 shared their territory with us in Iqaluktuutiaq and Inuvik.

This work was made possible thanks to the contributions of the Natural Sciences and Engineering Research Council of Canada (NSERC), the Fonds de recherche du Québec – Nature et technologies (FRQNT)

and Polar Knowledge Canada (POLAR). Carolina Voigt was supported by the BMBF project MOMENT  
315 (no. 03F0931A). A special thanks to people that contributed to data collection and processing: Elise Imbeau  
(Viventem), Gabriel Ferland (Viventem), Aili Pedersen (POLAR), Gabriel Hould Gosselin (Université de  
Montréal [UdeM] and Wilfrid Laurier University [WLU]), Rosy Tutton (WLU) , Emma Riley (UdeM), Nick  
Rutter (Northumbria University [NU]), Paul Mann (NU), Victoria Dutch (NU), Georgina Woolley (NU),  
Élise Groulx (Université de Sherbrooke [UdeS]), Charlotte Crevier (UdeS), Érika Boisvert (UdeS), Alain  
320 Royer (UdeS), Patrick Ménard (UdeS), Vincent Sasseville (UdeS), Célia Trunz (UdeS), Daniel Kramer  
(UdeS), Estéban Hamel Jomphe (UQTR), Samuel Goulet (UQTR), Alex Gélinas (UQTR), David de  
Courville (UQTR), Juliette Ortet (UQTR) and Chris Derksen (Environment and Climate Change Canada).  
We would also like to thank Ian Hogg, Johann Wagner, and Scott Johnson from POLAR as well as Branden  
Walker and Philip Marsh from WLU for their logistical support.

### 325 **7 Competing interests**

The authors declare that they have no conflict of interest.

### **8 Data availability**

Winter CO<sub>2</sub> flux data from the snowpack diffusion gradient method presented in this article can be found in  
the following repository:

330 Mavrovic, A., Sonnentag, O., Voigt, C., Roy, A. (2023). Winter CO<sub>2</sub> fluxes over arctic and boreal  
environments. Borealis, V1, doi: 10.5683/SP3/R3KZEQ.

Winter CH<sub>4</sub> flux data from the snowpack diffusion gradient method presented in this article can be found in  
335 the following repository:

Mavrovic, A., Sonnentag, O., Voigt, C., Roy, A. (2023). Winter CH<sub>4</sub> fluxes over arctic and boreal  
environments. Borealis, V1, doi: 10.5683/SP3/COWXAZ.

340

345

350

## References

- Alm, J., Saarnio, S., Nykänen, H., Silvola, J., and Martikainen, P.: Winter CO<sub>2</sub>, CH<sub>4</sub> and N<sub>2</sub>O fluxes on some natural and  
355 drained boreal peatlands. *Biogeochemistry*, 44, 163–186, doi: 10.1007/BF00992977, 1999.
- Arndt, K., Lipson, D., Hashemi, J., Oechel, W., and Zona, D.: Snow melt stimulates ecosystem respiration in Arctic  
ecosystems. *Glob. Change Biol.*, 26(9), 5042-5051, doi:10.1111/gcb.15193, 2020.
- 360 Aurela, M., Laurila, T., and Tuovinen, J.-P.: Annual CO<sub>2</sub> balance of a subarctic fen in northern Europe: Importance of  
the wintertime efflux. *J. Geophys. Res. Atmos.*, 107(D21), 4607, doi: 10.1029/2002JD002055, 2002.
- Baldocchi, D., and Meyers, T.: On using eco-physiological, micrometeorological and biogeochemical theory to evaluate  
carbon dioxide, water vapor and trace gas fluxes over vegetation: a perspective. *Agric. For. Meteorol.*, 90(1-  
365 2), 1-25, doi: 10.1016/S0168-1923(97)00072-5, 1998.
- Bao, T., Xu, X., Jia, G., Billesbach, D., and Sullivan, R.: Much stronger tundra methane emissions during autumn-freeze  
than spring-thaw. *Glob. Change Biol.*, 27(2), 376-387, doi: 10.1111/gcb.15421, 2020.
- 370 Barry R, Plamondon, AP, and Stein, J.: Hydrologic soil properties and application of a soil moisture model in a balsam  
fir forest. *Can. J. For. Res.*, 18(4), 427– 434, doi: 10.1139/x88-063, 1988.
- Carreiras, J., Quegan, S., Le Toan, T., Ho Tong Minh, D., Saatchi, S., Carvalhais, N., Reichstein, M., and Scipal, K.:  
Coverage of high biomass forests by the ESA BIOMASS mission under defense restrictions. *Remote Sens.  
375 Environ.*, 196, 154-162, doi: 10.1016/j.rse.2017.05.003, 2017.
- Derkzen, C., Burgess, D., Duguay, C., Howell, S., Mudryk, L., Smith, S., Thackeray, C., and Kirchmeier-Young, M.:  
Changes in snow, ice, and permafrost across Canada. Canada's Changing Climate Report – Chapter 5,  
Government of Canada, Ottawa, Ontario, Canada, 194–260, 2019.
- 380 Dierking, W., Linow, S., and Rack, W.: Toward a robust retrieval of snow accumulation over the Antarctic ice sheet  
using satellite radar. *J. Geophys. Res. Atmos.*, 117(D9), D09110. doi: 10.1029/2011jd017227, 2012.
- El-Amine, M., Roy, A., Koebisch, F., Baltzer, J., Barr, A. Black, A., Ikawa, H., Iwata, H., Kobayashi, H., Ueyama, M.,  
385 and Sonnentag, O.: What explains the year-to-year variation in growing season timing of boreal black spruce  
forests?. *Agric. For. Meteorol.*, 324, 109113, doi: 10.1016/j.agrformet.2022.109113, 2022.
- Euskirchen, E., Bret-Harte, M., Scott, G., Edgar, C., and Shaver, G.: Seasonal patterns of carbon dioxide and water fluxes  
in three representative tundra ecosystems in northern Alaska. *Ecosphere*, 3(1), 1-19, doi: 10.1890/es11-  
390 00202.1, 2012.
- Gonsamo, A., Chen, J. M., and D'Odorico, P.: Deriving land surface phenology indicators from CO<sub>2</sub> eddy covariance  
measurements. *Ecol. Indic.*, 29:203–207, doi: 10.1016/j.ecolind.2012.12.026, 2013.

- 395 Graveline, V., Helbig, M., Hould Gosselin, G., Alcock, H., Dett, M., Marsh, P., and Sonentag, O.: Surface-atmosphere  
energy exchanges and their effects on surface climate and atmospheric boundary layer characteristics in the  
forest-tundra ecotone in northwestern Canada. *Agric. For. Meteorol.*, submitted.
- 400 Grogan, P., and Chapin III, F. S.: Arctic soil respiration: Effects of climate and vegetation depend on Season. *Ecosyst.*,  
2(5), 451-459, 1999.
- Grogan, P., and Jonasson, S.: Temperature and substrate controls on intra-annual variation in ecosystem respiration in  
two subarctic vegetation types. *Glob. Chang. Biol.*, 11, 465-475, doi: 10.1111/j.1365-2486.2005.00912.x,  
2005.
- 405 Harel, A., Sylvain, J.-D., Drolet, G., Thiffault, E., Thiffault, N., and Tremblay, S.: Fine scale assessment of seasonal,  
intra-seasonal and spatial dynamics of soil CO<sub>2</sub> effluxes over a balsam fir-dominated perhumid boreal  
landscape. *Agric. For. Meteorol.*, 335, 109469, doi: 10.1016/j.agrformet.2023.109469, 2023.
- 410 Hargreaves, K., Fowler, D., Pitcairn, C., and Aurela, M.: Annual methane emission from Finnish mires estimated from  
eddy covariance campaign measurements. *Theor. Appl. Climatol.*, 70, 203–213, doi: 10.1007/s007040170015,  
2001.
- 415 Helbig, M., Wischnewski, K., Gosselin, G. H., Biraud, S., Bogoev, I., Chan, W., Euskirchen, E., Glenn, A., Marsh, P.,  
Quinton, W., and Sonnentag, O.: Addressing a systematic bias in carbon dioxide flux measurements with the  
EC150 and the IRGASON open-path gas analyzers. *Agric. For. Meteorol.*, 228-229, 349-359. doi:  
10.1016/j.agrformet.2016.07.018, 2016.
- 420 Helbig, M., Chasmer, L., Desai, A., Kljun, N., Quinton, W. L., and Sonnentag, O.: Direct and indirect climate change  
effects on carbon dioxide fluxes in a thawing boreal forest-wetland landscape. *Glob. Chang. Biol.*, 23(8), 3231-  
3248. doi: 10.1111/gcb.13638, 2017.
- Howard, D., Agnan, Y., Helmig, D., Yang, Y., and Obrecht, D.: Environmental controls on ecosystem-scale cold-season  
methane and carbon dioxide fluxes in an Arctic tundra ecosystem. *Biogeosciences*, 17(15), 4025–4042, doi:  
10.5194/bg-17-4025-2020, 2020.
- 425 van Huissteden, J., and Dolman, A.: Soil carbon in the Arctic and the permafrost carbon feedback. *Current Opinion in  
Environmental Sustainability*, 4(5), 545-551, doi: 10.1016/j.cosust.2012.09.008, 2012.
- 430 Hugelius, G., Ramage, J., Burke, E., Chatterjee, A., Smallman, T., Aalto, T., Bastos, A., Biasi, C., Canadell, J., Chandra,  
N., Chevallier, F., Ciais, P., Chang, J., Feng, L., Jones, M., Kleinen, T., Kuhn, M., Lauerwald, R., Liu, J.,  
López-Blanco, E., Luijkx, I., Marushchak, M., Natali, S., Niwa, Y., Olefeldt, D., Palmer, P., Patra, P., Peters,  
W., Potter, S., Poulter, B., Rogers, B., Riley, W., Saunois, M., Schuur, T., Thompson, R., Treat, C., Tsuruta,  
A., Turetsky, M., Virkkala, A.-M., Voigt, C., Watts, J., Zhu, Q., and Zheng, B.: Two decades of permafrost

- 435 region CO<sub>2</sub>, CH<sub>4</sub>, and N<sub>2</sub>O budgets suggest a small net greenhouse gas source to the atmosphere. ESS Open  
Archive, doi: 10.22541/essoar.169444320.01914726/v1, submitted.
- 440 Ito, A., Li, T., Qin, Z., Melton, J., Tian, H., Kleinen, T., Zhang, W., Zhang, Z., Joos, F., Ciais, P., Hopcroft, P., Beerling,  
D., Liu, X., Zhuang, Q., Zhu, Q., Peng, C., Chang, K.-Y., Fluet-Chouinard, E., McNicol, G., Patra, P., Poulter,  
B., Sitch, S., Riley, W., and Zhu, Q.: Cold-season Methane fluxes simulated by GCP-CH<sub>4</sub> models. *Geophys.*  
*Res. Lett.*, 50(14), e2023GL103037, doi: 10.1029/2023GL103037, 2023.
- 445 Jentzsch, K., Boike, J., and Foken, T.: Importance of the Webb, Pearman, and Leuning (WPL) correction for the  
measurement of small CO<sub>2</sub> fluxes. *Atmos. Meas. Tech.*, 14(11), 7291-7296, doi: 10.5194/amt-14-7291-2021,  
2021.
- 450 Kim, Y., Ueyama, M., Nakagawa, F., Tsunogai, U., Harazono, Y., and Tanaka, N.: Assessment of winter fluxes of CO<sub>2</sub>  
and CH<sub>4</sub> in boreal forest soils of central Alaska estimated by the profile method and the chamber method: a  
diagnosis of methane emission and implications for the regional carbon budget. *Tellus B: Chem. Phys.*  
*Meteorol.*, 59(2), 223-233, doi: 10.1111/j.1600-0889.2006.00233.x, 2007.
- Kittler, F., Eugster, W., Foken, T., Heimann, M., Kolle, O., and Göckede, M.: High-quality eddy-covariance CO<sub>2</sub> budgets  
under cold climate conditions. *Biogeosciences*, 122(8), 2064-2084, doi: 10.1002/2017JG003830, 2017.
- 455 Krogh, S., Pomeroy, J., and Marsh, P.: Diagnosis of the hydrology of a small Arctic basin at the tundra-taiga transition  
using a physically based hydrological model. *J. Hydrol.*, 550, 685-703, doi: 10.1016/j.jhydrol.2017.05.042,  
2017.
- 460 Kuhn, M., Varner, R., Bastviken, D., Crill, P., MacIntyre, S., Turetsky, M., Walter Anthony, K., McGuire, A., and  
Olefeldt, D.: BAWLD-CH<sub>4</sub>: a comprehensive dataset of methane fluxes from boreal and arctic ecosystems.  
*Earth Syst. Sci. Data*, 13, 5151–5189, doi: 10.5194/essd-13-5151-2021, 2021.
- Larsen, K. S., Ibrom, A., Jonasson, S., Michelsen, A., and Beier, C.: Significance of cold-season respiration and  
photosynthesis in a subarctic heath ecosystem in Northern Sweden. *Glob. Chang. Biol.*, 13, 1498-1508, doi:  
465 10.1111/j.1365-2486.2007.01370.x, 2007.
- Martin, M., Kumar, P., Sonnentag, O., and Marsh, P.: Thermodynamic basis for the demarcation of Arctic and alpine  
treelines. *Sci. Rep.*, 12, 12565, doi: 10.1038/s41598-022-16462-2, 2022.
- 470 Mauder M., and Foken T.: Documentation and Instruction Manual of the Eddy-Covariance Software Package TK3, pp.  
1– 60. Univ. Bayreuth, Abt. Mikrometeorologie, Bayreuth, Germany, 2011.
- 475 Mavrovic, A., Sonnentag, O., Lemmetyinen, J., Voigt, C., Rutter, N., Mann, P., Sylvain, J.-D., and Roy, A.:  
Environmental controls of winter soil carbon dioxide fluxes in boreal and tundra environments.  
*Biogeosciences*, 20(24), 5087–5108, doi: 10.5194/bg-20-5087-2023, 2023.

- Mavrovic, A., Sonnentag, O., Lemmetyinen, J., Voigt, C., Aurela, M., and Roy, A.: Winter methane fluxes over boreal and Arctic environments. *Geophys. Res. Lett.*, submitted.
- 480 O'Connell, K., Gower, S., and Norman, J.: Net Ecosystem Production of Two Contrasting Boreal Black Spruce Forest Communities. *Ecosyst.*, 6(3), 248–260, doi: 10.1007/s10021-002-0202-9, 2003.
- Oechel, W., Vourlitis, G., and Hastings, S.: Cold season CO<sub>2</sub> emission from Arctic soils. *Glob. Biogeochem. Cycles*, 11(2), 163–172. doi: 10.1029/96gb03035, 1997.
- 485 Oechel, W., Laskowski, C., Burba, G., Gioli, B., and Kalhorri, A.: Annual patterns and budget of CO<sub>2</sub> flux in an Arctic tussock tundra ecosystem. *J. Geophys. Res. Biogeosci.*, 119(3), 323–339. doi: 10.1002/2013jg002431, 2014.
- Outcalt, S., Nelson, F., and Hinkel, K.: The zero-curtain effect: Heat and mass transfer across an isothermal region in freezing soil. *Water Resour. Res.*, 26(7), 1509–1516, doi: 10.1029/WR026i007p01509, 1990.
- 490 Pallandt, M., Kumar, J., Mauritz, M., Schuur, E., Virkkala, A.-M., Celis, G., Hoffman, F., and Göckede, M.: Representativeness assessment of the pan-Arctic eddy-covariance site network, and optimized future enhancements. *Biogeosciences*, 19(3), 559–583, doi: 10.5194/bg-19-559-2022, 2022.
- Pan, Y., Birdsey, R., Fang, J., Houghton, R., Kauppi, P., Kurz, W., Phillips, O., Shvidenko, A., Lewis, S., Canadell, J., Ciais, P., Jackson, R., Pacala, S., McGuire, A., Piao, S., Rautiainen, A., Sitch, S., and Hayes, D.: A large and persistent carbon sink in the world's forests. *Science*, 333, 988–993, doi: 10.1126/science.1201609, 2011.
- 500 Panikov, N., and Dedysh, S.: Cold season CH<sub>4</sub> and CO<sub>2</sub> emission from boreal peat bogs (West Siberia): Winter fluxes and thaw activation dynamics. *Glob. Biogeochem. Cycles*, 14(4), 1071–1080. doi:10.1029/1999gb900097, 2000.
- Papale, D., Reichstein, M., Aubinet, M., Canfora, E., Bernhofer, C., Kutsch, W., Longdoz, B., Rambal, S., Valentini, R., Vesala, T., and Yakir, D.: Towards a standardized processing of Net Ecosystem Exchange measured with eddy covariance technique: algorithms and uncertainty estimation. *Biogeosciences*, 3(4), 571–583. doi: 10.5194/bg-3-571-2006, 2006.
- 505 Pierrat, Z., Nehemy, M. F., Roy, A., Magney, T., Parazoo, N., Laroque, C., Pappas, C., Sonnentag, O., Grossman, K., Bowling, D. R., Seibt, U., Ramirez, A., Johnson, B., Helgason, W., Barr, A., and Stutz, J.: Tower-based remote sensing reveals mechanisms behind a two-phased spring transition in a mixed species boreal forest. *Biogeosciences*, doi: 10.1029/2020JG006191, 2021.
- Pirk, N., Tamstorf, M., Lund, M., Mastepanov, M., Pedersen, S., Myllus, M., Parmentier, F.-J., Christiansen, H., and Christensen, T.: Snowpack fluxes of methane and carbon dioxide from high Arctic tundra. *Biogeosciences*, 121(11), 2886–2900, doi: 10.1002/2016JG003486, 2016.

- Ponomarenko, S., McLennan, D., Pouliot, D., and Wagner, J.: High Resolution Mapping of Tundra Ecosystems on Victoria Island, Nunavut – Application of a Standardized Terrestrial Ecosystem Classification. *Can. J. Remote.*, 45(5), 551-571, doi: 10.1080/07038992.2019.1682980, 2019.
- Rantanen, M., Karpechko, A.Y., Lipponen, A., Nordling, K., Hyvärinen, O., Ruosteenoja, K., Vihma, T. and Laaksonen, A.: The Arctic has warmed nearly four times faster than the globe since 1979. *Commun. Earth Environ.*, 3(1), 1-10, doi: 10.1038/s43247-022-00498-3, 2022.
- Ravn, N., Elberling, B., and Michelsen, A.: Arctic soil carbon turnover controlled by experimental snow addition, summer warming and shrub removal. *Soil Biol. Biochem.*, 142, 107698, doi: 10.1016/j.soilbio.2019.107698, 2020.
- Reichstein, M., Falge, E., Baldocchi, D., Papale, D., Aubinet, M., Berbigier, P., Bernhofer, C., Buchmann, N., Gilmanov, T., Granier, A., Grünwald, T., Havráneková, K., Ilvesniemi, H., Janous, D., Knöhl, A., Laurila, T., Lohila, A., Loustau, D., Matteucci, G., Meyers, T., Miglietta, F., Ourcival, J.-M., Pumpanen, J., Rambal, S., Rotenberg, E., Sanz, M., Tenhunen, J., Seufert, G., Vaccari, F., Vesala, T., Yakir, D., and Valentini, R.: On the separation of net ecosystem exchange into assimilation and ecosystem respiration: review and improved algorithm. *Glob. Chang. Biol.*, 11(9), 1424-1439, doi: 10.1111/j.1365-2486.2005.001002.x, 2005.
- Roy, A., Royer, A., St-Jean-Rondeau, O., Montpetit, B., Picard, G., Mavrovic, A., Marchand, N., and Langlois, A.: Microwave snow emission modeling uncertainties in boreal and subarctic environments. *Cryosphere*, 10(2), 623–638, doi: 10.5194/tc-10-623-2016, 2016.
- Rößger, N., Sachs, T., Wille, C., Boike, J., and Kutzbach, L.: Seasonal increase of methane emissions linked to warming in Siberian tundra. *Nat. Clim. Change*, 12(11), 1031–1036, doi: 10.1038/s41558-022-01512-4, 2022.
- Sommerfeld, R., Mosier, A., and Musselman, R.: CO<sub>2</sub>, CH<sub>4</sub> and N<sub>2</sub>O flux through a Wyoming snowpack and implications for global budgets. *Nature*, 361, 140-142, doi: 10.1038/361140a0, 1993.
- Tarnocai, C., Canadell, J., Schuur, E., Kuhry, P., Mazhitova, G., and Zimov, S.: Soil organic carbon pools in the northern circumpolar permafrost region. *Glob. Biogeochem. Cycles*, 23(2), GB2023, doi: 10.1029/2008GB003327, 2009.
- Virkkala, A.-M., Aalto, J., Rogers, B., Tagesson, T., Treat, C., Natali, S., Watts, J., Potter, S., Lehtonen, A., Mauritz, M., Schuur, E., Kochendorfer, J., Zona, D., Oechel, W., Kobayashi, H., Humphreys, E., Goeckede, M., Iwata, H., Lafleur, P., Euskirchen, E., Bokhorst, S., Marushchak, M., Martikainen, P., Elberling, B., Voigt, C., Biasi, C., Sonnentag, O., Parmentier, F.-J., Ueyama, M., Celis, G., St.Louis, V., Emmerton, C., Peichl, M., Chi, J., Järveoja, J., Nilsson, M., Oberbauer, S., Torn, M., Park, S.-J., Dolman, H., Mammarella, I., Chae, N., Poyatos, R., López-Blanco, E., Christensen, T. R., Kwon, M. J., Sachs, T., Holl, D., and Luotonen M.: Statistical upscaling of ecosystem CO<sub>2</sub> fluxes across the terrestrial tundra and boreal domain: Regional patterns and uncertainties. *Glob. Chang. Biol.*, 27(17), 4040-4059, doi: 10.1111/gcb.15659, 2021.

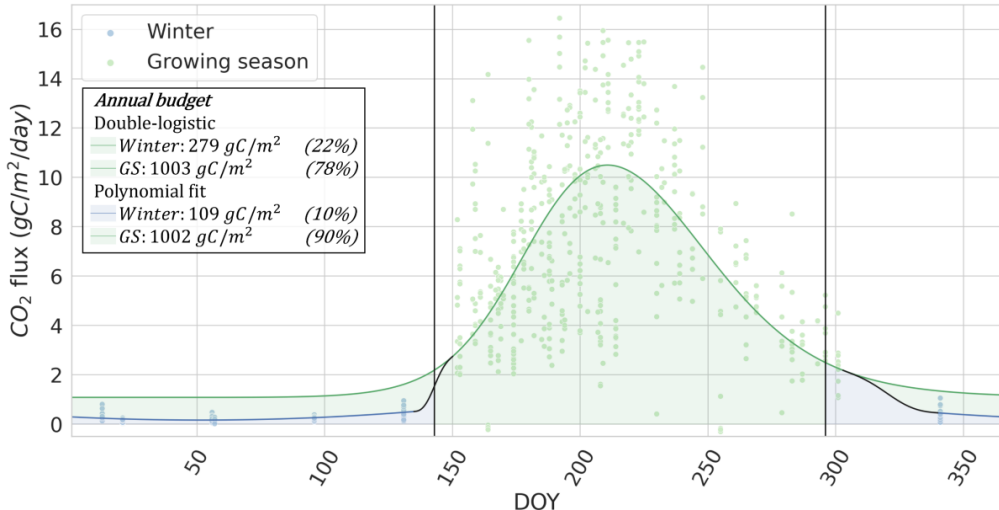
- 560 Vogel, J., Valentine, D., and Ruess, R.: Soil and root respiration in mature Alaskan black spruce forests that vary in soil organic matter decomposition rates. *Can. J. For. Res.*, 35(1), 161–174. doi: 10.1139/x04-159, 2005.
- 565 Voigt, C., Virkkala, A.-M., Hould Gosselin, G., Bennett, K., Black, T. A., Detto, M., Chevrier-Dion, C., Guggenberger, G., Hashmi, W., Kohl, L., Kou, D., Marquis, C., Marsh, P., Marushchak, M., Nesic, Z., Nykänen, H., Saarela, T., Sauheitl, L., Walker, B., Weiss, N., Wilcox, E., and Sonnentag, O.: Arctic soil methane sink increases with drier conditions and higher ecosystem respiration. *Nat. Clim. Change*, 13, 1095–1104, doi: 10.1038/s41558-023-01785-3, 2023.
- 570 Wang, C., Bond-Lamberty, B., and Gower, S.: Soil surface CO<sub>2</sub> flux in a boreal black spruce fire chronosequence. *J. Geophys. Res. Atmos.*, 108(D3), WFX 5-1-WFX 5-8, doi: 10.1029/2001jd000861, 2002.
- 575 Watts, J., Natali, S., Minions, C., Risk, D., Arndt, K., Zona, D., Euskirchen, E., Rocha, A., Sonnentag, O., and Helbig, M.: Soil respiration strongly offsets carbon uptake in Alaska and Northwest Canada. *Environ. Res. Lett.*, 16(8), 084051, doi: 10.1088/1748-9326/ac1222, 2021.
- 580 Whalen, S., and Reeburgh, W.: A methane flux time series for tundra environments. *Glob. Biogeochem. Cycles*, 2(4), 399-409, doi: 10.1029/GB002i004p00399, 1988.
- 585 Wille, C., Hutzbach, L., Sachs, T., Wagner, D., and Pfeiffer, E.-M.: Methane emission from Siberian arctic polygonal tundra: eddy covariance measurements and modeling. *Glob. Change Biol.*, 14(6), 1395–1408. doi: 10.1111/j.1365-2486.2008.01586.x, 2008.
- Wutzler, T., Lucas-Moffat, A., Migliavacca, M., Knauer, J., Sickel, K., Sigut, L., Menzer, O., and Reichstein, M.: Basic and extensible post-processing of eddy covariance flux data with REddyProc. *Biogeosciences*, 15(16), 5015–5030, doi: 10.5194/bg-15-5015-2018, 2018.
- 590 Zhu, C., Nakayama, M., and Inouey, H. Y.: Continuous measurement of CO<sub>2</sub> flux through the snowpack in a dwarf bamboo ecosystem on Rishiri Island, Hokkaido, Japan. *Polar Sci.*, 8(3), 218-231, doi: 10.1016/j.polar.2014.04.003, 2014.
- Zona, D., Giolo, B., Commane, R., Lindaas, J., Wofsy, S., Miller, C., Dinardo, S., Dengel, S., Sweeney, C., Karion, A., Chang, R., Henderson, J., Murphy, P., Goodrich, J., Moreaux, V., Liljedahl, A., Watts, J., Kimball, J., Lipson, D., and Oechel, W.: Cold season emissions dominate the Arctic tundra methane budget. *Proc. Natl. Acad. Sci. U.S.A.*, 113(1), 40-45, doi: 10.1073/pnas.1516017113, 2015.
- 595

## Appendix A

### A.1 Montmorency Forest soil respiration

Figure A1 shows the combined time series of winter and growing season CO<sub>2</sub> fluxes estimates from a boreal forest site dominated by balsam fir in Montmorency Forest (Québec, Canada). The winter CO<sub>2</sub> fluxes were estimated from the snowpack diffusion gradient method, measurements were conducted during the 2020-2021 and 2021-2022 winters. The growing season CO<sub>2</sub> fluxes were acquired by Harel et al. (2023) and were estimated using two LI-8100 portable infrared gas analyzers (IRGA) and two survey chambers (8100–102 10 cm) (LI-COR inc., Lincoln, Nebraska, USA). The growing season CO<sub>2</sub> flux measurements from Harel et al. (2023) presented in Fig. A1 only correspond to growing season sampling locations where winter measurements were conducted as well. The growing season chamber and winter snowpack diffusion gradient CO<sub>2</sub> fluxes correspond to soil respiration ( $R_{soil}$ ). Harel et al. (2023) estimated the seasonal trend of  $R_{soil}$  using a double-logistic function based on the day of the year (DOY) in 2020 (Fig. B1). Harel et al. (2023) also proposed a Random Forest model for in-depth analysis of intra-seasonal and spatial dynamics of  $R_{soil}$ . The Random Forest model can be more broadly generalized than the DOY double-logistic trend, but the double-logistic approach was used in our study since we are only looking at the large seasonal trend and it was evaluated in the same year as our winter measurements. A second-degree polynomial fit on snowpack diffusion gradient measurements was used to estimate the seasonal trend of winter  $R_{soil}$  as a function of DOY with a minimum in February (Fig. A2). There is a gap in measurement during the shoulder season, i.e. the season when there is too much snow for the chamber method and too little snow for the snowpack diffusion gradient method. This gap was filled using an empirical extrapolation spline fitted in both validity ranges of the growing season double-logistic and winter polynomial functions (Dierking et al., 2012; Roy et al., 2016) (black curve in Fig. A1). The start and end of the growing season were determined from the  $R_{soil}$  double-logistic trend as it was done with GPP in Sect. 2.3: using the curve inflection determined from the first maximum and last minimum of the third derivative of the double logistic function (Gonsamo et al., 2013; El-Amine et al., 2022).  $R_{soil}$  is not linked to vegetation photosynthetic recovery in spring and cessation in fall as strongly as GPP but a change in  $R_{soil}$  regime (i.e., the curve inflection) remains an indicator of frost and seasonality.

Since Harel et al. (2023) did not acquire winter data because it did not focus on winter, the minimal winter  $R_{soil}$  value (1.08 gC m<sup>-2</sup> day<sup>-1</sup>) predicted by the growing season double-logistic function is significantly higher than the winter snowpack diffusion gradient measurements. Consequently, the growing season double-logistic function overestimates the  $R_{soil}$  winter contribution (279 gC m<sup>-2</sup>; 22% of net annual  $R_{soil}$ ) compared to the winter second-degree polynomial fit  $R_{soil}$  winter contribution (109 gC m<sup>-2</sup>; 10% of net annual  $R_{soil}$ ). The Montmorency Forest winter net  $R_{soil}$  budget and its contribution to the net annual  $R_{soil}$  budget, as evaluated using the polynomial fit, is on the lower side of values found among other studies on boreal forests (Table A1), although no estimation on balsam fir stands was found in the scientific literature since most studies focused on black spruce stands.



635 **Figure A1:** Yearly soil respiration CO<sub>2</sub> exchanges at a balsam fir boreal forest site in Montmorency Forest in 2020-2022. The gross primary production (GPP) and net ecosystem exchange (NEE) are presented. The growing season (GS) and winter measurements were acquired from a chamber system and the snowpack diffusion method, respectively. The double-logistic function (green curve) is from Harel et al. (2023). A second-degree polynomial fit is presented along the winter measurements (blue curve). The black curve is a splined fitted empirical extrapolation of the GS double-logistic and winter polynomial functions. The vertical black line delineated the start and end of the growing season.

640

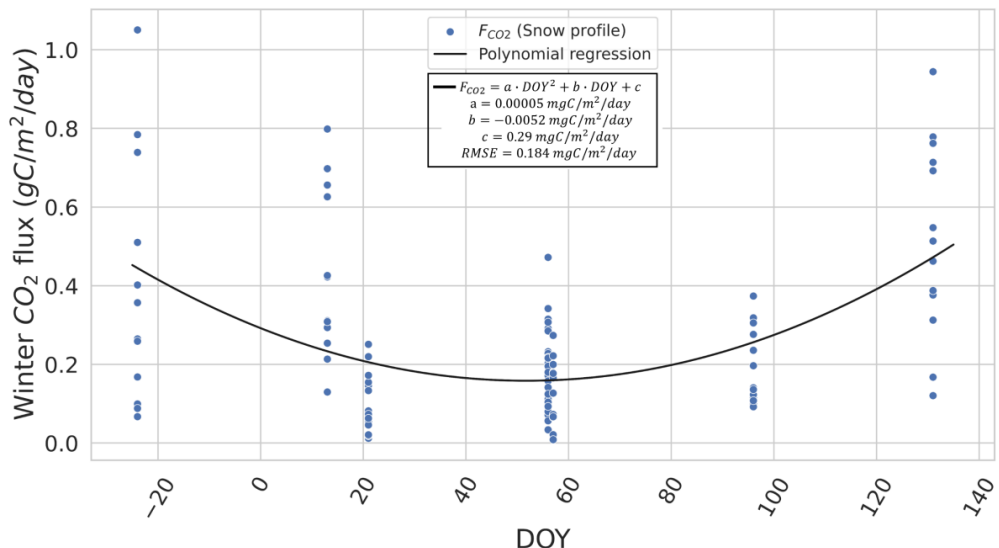


**Figure A2:** Winter soil respiration CO<sub>2</sub> exchanges as a function of the day of the year (DOY) at a balsam fir boreal forest site in Montmorency Forest in 2020-2022 using the snowpack diffusion method. A second-degree polynomial fit of the CO<sub>2</sub> flux ( $F_{CO_2}$ ) is presented (black line) along the winter measurements (blue dots).

645

## A.2 Winter carbon flux contribution to the annual budget

**Table A1:** Winter CO<sub>2</sub> flux contribution to the annual budget in Arctic and boreal environments. SS represents the shoulder season and GS represents the growing season. Depending on the study, the net ecosystem exchange (NEE) or the soil respiration ( $R_{soil}$ ) is presented. Studies are ordered by ascending mean winter contribution in percentage.

Reference	Winter	SS	GS	Annual budget	GS offset by winter %	Winter annual contribution %	CO <sub>2</sub> flux component	Winter definition	Winter duration	Method	Biome	Ecosystem	Location	Permafrost
	gC m <sup>-2</sup>	gC m <sup>-2</sup>	gC m <sup>-2</sup>	gC m <sup>-2</sup>										
Vogel et al., 2005	36	436	472			7.6 %	$R_{soil}$	Oct-April	210 days	EC and Chamber	Boreal	Black spruce forest	Alaska	Mixed sites
	54	354	408			13.2 %						Black spruce forest		
	54	307	361			15.0 %						Black spruce forest		
Wang et al., 2003	[15:64]		[146:413]		[5:19]	%	$R_{soil}$	Nov-April	181 days	Chamber	Boreal	Black spruce forest	Canada	Discontinuous
Watts et al., 2021	36.2	98.8	172	307	11.8 %	17.4 %	$R_{soil}$	Nov-Mar SS: Sept-Oct-April-May	151 days SS: 122 days	EC and Chamber	Boreal	Mixed Boreal sites	Alaska and Canada	Mixed sites
	27.2	42.7	86.5	156.4								Mixed tundra sites		
Kim et al., 2007	36	142	178		20.2 %		$R_{soil}$		212 days	Snow profile and Chamber	Boreal	Black spruce forest	Alaska	Discontinuous
Aim et al., 1999	53.4 [30:86]	193.3 [110:238]	208 [151:286]		26.1 % [16.8:38.1]		$R_{soil}$	Nov15-May15	180 days	Chamber and Snow/Soil profile	Boreal	Bogs	Finland	No
	77.8 [30:143]	391 [188:592]	468.8 [218:735]		15.8 % [13.8:19.5]							Fens		
Grogan and Chapin III, 1999 <sup>i</sup>	50	149	199		25.1 %		$R_{soil}$	Daily mean $T_{soil} \leq 0^\circ\text{C}$ at 5 cm depth		Soda lime and Chamber	Arctic	Shrub tundra	Alaska	Yes
	43	115	158		27.4 %							Dry Heath		
	42	59	111		27.9 %							Non-acidic tundra		
	38	59	91		39.1 %							Tussock tundra		
	[30:52]	[4:66]	[91:102]		[32:52]									
Mavrovic et al., 2024	14.8 29.6 28.1 24.9 21.5 57.3 23.5 49.9	-43.4 -77.2 -47.6 -66.5 -38.4 -156.9 -179.5 -390.6 -491.5 -486.8	-28.6 38.3 % 42.3 % 15.9 % 12.3 % 12.7 % 4.6 % 10.3 %		34.1 %		NEE	GPP regime	271 days	Snow profile and EC	Arctic	Mesic tundra	Canada	Yes
									279 days			Erect shrub tundra		Yes
									266 days			Erect shrub tundra		Yes
									236 days			Black spruce forest		Yes
									260 days			Balsam fir forest		Yes
									199 days			Balsam fir forest		No
									276 days			Balsam fir forest		No
									207 days			Balsam fir forest		No
Oechel et al., 2014	12.9	25.0	-24.3	13.6	53.1 %		NEE	Solar radiation threshold	205 days	EC	Arctic	Tussock tundra	Alaska	Yes
O'Connell et al., 2003	321	242	563		57 %		$R_{soil}$	Sept22-May22	241 days	Chamber	Boreal	Black spruce forest	Canada	No
Oechel et al., 1997	68.5 19	44.1 4.4	112.5 23.4		60.8 % 81.2 %		$R_{soil}$	Oct14-May15	230 days	Chamber	Arctic	Tussock tundra	Alaska	Yes
Arndt et al., 2020	44.5 [1:5:106.2]	2.24 [-19.3: 17.1]	-63.95 [-111.3:-30.3]	-17.2 [-75.6:47.7]	72.4 % [2.4: 165.3]		NEE	NEE > 0 SS: Snowmelt to $T_{soil} > 2^\circ\text{C}$		EC	Arctic	Mixed tundra sites	Alaska	Yes
Howard et al., 2020	148 142	327 152	14 -211	485 89	67.3 %	30.5 % 159.6 %	NEE	$T_{soil} < 0^\circ\text{C}$ SS: zero-curtain	155 days SS: 92 days	EC and Soil profile	Arctic	Tussock tundra	Alaska	Yes
									155 days SS: 92 days			Tussock tundra		
Aurela et al., 2002	28.7	27.4	-74.7	-18.6	154.3 %		NEE	Solar radiation	186 days SS: 108 days	EC	Boreal	Fen	Finland	No
Euskirchen et al., 2012	72 105 119 61 139 145	-51 -54 -58 -59 -95 -63	21 51 61 2 44 82	141.2 % 194.4 % 205.2 % 103.4 % 146.3 % 230.2 %			NEE	Oct-May	181 days	EC	Arctic	Heath tundra	Alaska	Yes
												Heath tundra		
												Arctic		
												Heath tundra		
												Arctic		
												Wet sedge tundra		
												Arctic		
												Wet sedge tundra		
												Arctic		
												Wet sedge tundra		

<sup>i</sup>Units converted from mmol m<sup>-2</sup> using molar mass.

<sup>j</sup>Units converted from gCH<sub>4</sub> m<sup>-2</sup> using molar mass.

<sup>k</sup>Units converted from mgC m<sup>-2</sup>.

**Table A2:** Winter CH<sub>4</sub> flux contribution to the annual budget in arctic and boreal environments. SS represents the shoulder season and GS represents the growing season. Studies are ordered by ascending mean winter contribution in percentage.

Reference	Winter	SS	GS	Annual budget	Winter annual contribution %	Winter definition	Winter duration	Method	Biome	Ecosystem	Location	Permafrost
	gC m <sup>-2</sup>	gC m <sup>-2</sup>	gC m <sup>-2</sup>	gC m <sup>-2</sup>								
Mavrovic et al., 2024	0.0038 0.0036 0.0092 0.001	0.244 0.478 0.369 0.172	0.248 0.481 0.378 0.182	1.5 % 0.8 % 2.4 % 5.6 %	GPP regime	279 days 266 days 236 days 260 days	Snow profile and EC	Arctic Arctic Boreal Boreal	Erect shrub tundra Erect shrub tundra Black spruce forest Black spruce forest	Canada	Yes	
Whalen and Reeburgh, 1988 <sup>j</sup>	0.15 0.3 0.2	3.5 5.7 0.32	3.65 6.03 0.35	4.1 % 5.0 % 8.6 %	Soil fully frozen	215 days	Chamber	Arctic Arctic Arctic	Sedge tundra Tussock tundra Inter-tussock tundra	Alaska	Yes	
Panikov and Dedysh, 2000	1.7 [1.7:2.4]	24.2 [11.5:41.9]	25.9 [13.9:43.4]	7.3 % [3.5:11]	Frost days	275 days	Chamber and Snow profile	Boreal	Peat bog	Siberia	No	
Hargreaves et al., 2001	0.4	0.6	4.5	5.5	7.3 %	Nov1-May10 SS: May11-June9	191 days SS: 30 days	EC	Boreal	Peatland (mire)	Finland	No
Pirk et al., 2016	1.1	1.0	5.0	7.1	15 %	Nov-May SS: Sept-Oct	180 days SS: 61 days	Snowpack gradient	Arctic	Ice-wedge polygons	Svalbard	Yes
Alm et al., 1999	0.7 [0.2:1.7]	3.0 [1.0:4.8]	3.7 [1.2:5.1]	18.3 % [5.9:33.3]	Nov15-May15	180 days	Chamber and Snow/Soil profile	Boreal	Bogs	Finland	No	
	2.0 [0.02:6]	13.8 [-0.16:31]	15.1 [-0.18:35.8]	24.7 % [6.3:80]								
Bao et al., 2021 <sup>k</sup>	1.26	1.49	3.08	5.83 [1.79:8.48]	21.6 %	$T_{soil} < 0^\circ\text{C}$ SS: zero-curtain	177 days SS: 97 days	EC	Arctic	Mixed tundra sites	Alaska	Yes
Rößger et al., 2022 <sup>j</sup>	0.69	0.39	1.68	2.75	25 %	Soil fully frozen $T_{soil} < T_{soil, ref}$	180 days SS: 56 days	EC	Arctic	Ice-wedge polygons	Siberia	Yes
Howard et al., 2020	1.1 2.5	0.9 1.5	1.7 0.9	3.7 4.9	29.7 % 51 %	EC and Soil profile	Arctic Arctic	Tussock tundra	Alaska	Yes		
Wille et al., 2008 <sup>j</sup>	0.82		1.54	2.36	34.9 %	Oct-May	243 days	EC	Arctic	Polygonal tundra	Siberia	Yes
Arndt et al., 2020	1.5 [0.4:4.4]	0.16 [0.01:0.6]	1.4 [0.5-2.3]	3.1 [1.6:6.7]	47.5 % [14.6:66.3]	NEE > 0 gC m <sup>-2</sup> h <sup>-1</sup> SS: Solar radiation for snowmelt and $T_{soil, lim} > 2^\circ\text{C}$	EC	Arctic	Mixed tundra sites	Alaska	Yes	
Zona et al., 2015	1.7 [0.3:2.4]	1.7	3.4	50 % [37:64]	$T_{soil} < 0.75^\circ\text{C}$ SS: zero-curtain $\pm 0.75^\circ\text{C}$	261 days SS: 76 days	EC	Arctic	Mixed tundra sites	Alaska	Yes	

<sup>i</sup>Units converted from mmol m<sup>-2</sup> using molar mass.

<sup>j</sup>Units converted from gCH<sub>4</sub> m<sup>-2</sup> using molar mass.

<sup>k</sup>Units converted from mgC m<sup>-2</sup>.

# Chapitre 6 : Télédétection micro-onde pour la science du carbone

## 6.1 Présentation de l'article scientifique

L'article scientifique qui suit a été soumis à la revue scientifique *Biogeosciences* (EGU) le 31 janvier 2023, a été accepté pour publication le 19 juin 2023 et a été publié le 21 juillet 2023. L'article y est présenté de façon intégrale tel que publié. La numérotation des lignes, sections, figures, tableaux et équations est indépendante du reste de la thèse. Les références citées dans cet article ne sont pas répétées à la bibliographie complémentaire de la thèse (Sect. 10).

Cet article de synthèse se veut un plaidoyer pour une intégration plus rapide des données de télédétection satellitaire micro-onde en appui à la science du cycle du carbone dans les régions arctiques et boréales. Cet article explore l'utilisation essentielle de la modélisation et des données de télédétection afin de passer de l'échelle locale (i.e., données ponctuelles *in situ*) à l'échelle régionale et globale. Ce changement d'échelle est nécessaire afin d'estimer les bilans de carbones globaux des régions arctiques et boréales. Cet article synthèse ne présente pas de résultats originaux, seulement quelques exemples du produit d'un modèle écosystémique intégrant des données de télédétection satellitaire micro-onde (SMAP L4C). Cet article met en évidence l'importance des modèles écosystémiques pour la science du carbone dans les régions arctiques et boréales et la rareté des données *in situ* disponibles pour paramétriser et valider ces modèles. La base de données de flux de carbone hivernaux en régions arctiques et boréales produites dans cette thèse offre une excellente opportunité de comparaison avec les modèles écosystémiques et les produits dérivés de la télédétection.

Contribution en tant que premier auteur : Conception et planification de l'étude.  
Rédaction du manuscrit.

Référence complète de l'article :

**Mavrovic, A., Sonnentag, O., Lemmetyinen, J., Baltzer, J., Kinnard, C., and Roy, A. (2023a) Reviews and syntheses : Recent advances in microwave remote sensing in support of arctic-boreal carbon cycle science. Biogeosciences, vol. 20, no° 14, p. 2941–2970, doi : [10.5194/bg-20-2941-2023](https://doi.org/10.5194/bg-20-2941-2023).**

## 6.2 Résumé de l'article scientifique en français

La télédétection micro-onde satellitaire (300 MHz - 100 GHz) offre plusieurs opportunités pour caractériser les changements environnementaux, en particulier dans les régions arctiques et boréales où les observations terrestres sont spatialement et temporellement limitées. Bien qu'ils ne soient pas aptes à mesurer directement les flux de carbone, les radiomètres et radars micro-ondes satellitaires sont capables de mesurer diverses variables environnementales de surface affectant les processus du cycle du carbone terrestre, tel que les flux de dioxyde de carbone ( $CO_2$ ) d'origine respiratoire ; la capture de  $CO_2$  par la photosynthèse ; et les processus liés aux échanges nets de méthane ( $CH_4$ ), y compris la production, le transport et la consommation de  $CH_4$ . Des exemples de ces variables environnementales comprennent l'humidité et la température du sol, les cycles de gel-dégel de surface, le stockage d'eau dans la végétation, les propriétés du manteau neigeux et l'occupation des sols. La télédétection micro-onde permet également d'estimer la biomasse au-dessus du sol de manière indépendante, permettant ainsi d'estimer les stocks de carbone au-dessus du sol. Les données micro-onde couvrent plusieurs décennies, remontant aux années 1970, avec une couverture globale fréquente (quotidienne à hebdomadaire), indépendamment des conditions atmosphériques et de l'illumination solaire. Ensemble, ces avantages offrent un grand potentiel inexploité pour suivre et mieux comprendre les processus du cycle du carbone dans les régions arctiques et boréales. Considérant le réchauffement rapide du climat des régions nordiques et les rétroactions potentielles du cycle du carbone sur le système climatique planétaire, cette étude plaide en faveur de l'intégration rapide des données micro-onde dans la science du cycle du carbone terrestre des régions arctiques et boréales.



## Reviews and syntheses: Recent advances in microwave remote sensing in support of terrestrial carbon cycle science in Arctic–boreal regions

Alex Mavrovic<sup>1,2,3,4</sup>, Oliver Sonnentag<sup>2,4</sup>, Juha Lemmetyinen<sup>5</sup>, Jennifer L. Baltzer<sup>6</sup>, Christophe Kinnard<sup>1,2</sup>, and Alexandre Roy<sup>1,2</sup>

<sup>1</sup>Département des sciences de l'environnement, Université du Québec à Trois-Rivières, Trois-Rivières, Quebec, Canada

<sup>2</sup>Centre d'Études Nordiques, Université Laval, Québec, Quebec, Canada

<sup>3</sup>Canadian High Arctic Research Station Campus, Polar Knowledge Canada, Cambridge Bay, Nunavut, Canada

<sup>4</sup>Département de géographie, Université de Montréal, Montréal, Quebec, Canada

<sup>5</sup>Finnish Meteorological Institute, Helsinki, Finland

<sup>6</sup>Biology Department, Wilfrid Laurier University, Waterloo, Ontario, Canada

**Correspondence:** Alex Mavrovic (alex.mavrovic@uqtr.ca)

Received: 31 January 2023 – Discussion started: 2 March 2023

Revised: 2 June 2023 – Accepted: 19 June 2023 – Published: 21 July 2023

**Abstract.** Spaceborne microwave remote sensing (300 MHz–100 GHz) provides a valuable method for characterizing environmental changes, especially in Arctic–boreal regions (ABRs) where ground observations are generally spatially and temporally scarce. Although direct measurements of carbon fluxes are not feasible, spaceborne microwave radiometers and radar can monitor various important surface and near-surface variables that affect terrestrial carbon cycle processes such as respiratory carbon dioxide (CO<sub>2</sub>) fluxes; photosynthetic CO<sub>2</sub> uptake; and processes related to net methane (CH<sub>4</sub>) exchange including CH<sub>4</sub> production, transport and consumption. Examples of such controls include soil moisture and temperature, surface freeze–thaw cycles, vegetation water storage, snowpack properties and land cover. Microwave remote sensing also provides a means for independent aboveground biomass estimates that can be used to estimate aboveground carbon stocks. The microwave data record spans multiple decades going back to the 1970s with frequent (daily to weekly) global coverage independent of atmospheric conditions and solar illumination. Collectively, these advantages hold substantial untapped potential to monitor and better understand carbon cycle processes across ABRs. Given rapid climate warming across ABRs and the associated carbon cycle feedbacks to the global climate system, this review

argues for the importance of rapid integration of microwave information into ABR terrestrial carbon cycle science.

### 1 Introduction

Northern regions host two important terrestrial biomes, the boreal and the Arctic (hereafter called Arctic–boreal regions, ABRs). Belowground carbon (C) stocks in ABRs comprise 30 %–40 % of the planetary terrestrial carbon and, as such, understanding changes in carbon cycle processes in this vast region has global importance (Pan et al., 2011; Tarnocai et al., 2009). Arctic–boreal regions store substantial quantities of belowground C due to their inherently slow decomposition rates, largely attributable to cold temperatures (Ravn et al., 2020). A large portion of ABRs is underlain by permafrost (perennially frozen ground), which contains approximately half of the world's belowground C stocks (1672 Pg C in the top 3 m of soil; Tarnocai et al., 2009; van Huissteden and Dolman, 2012). In contrast, C stocks in aboveground biomass in ABRs are relatively trivial. For example, although the boreal biome constitutes the second-largest terrestrial biome with a third of the world's forested area, it contains only approximately 15 % of the global forest aboveground biomass (FAO, 2001; Pan et al., 2011, 2013; Carreiras

et al., 2017) but 32 % of the global forest carbon stocks (Pan et al., 2011).

Above- and belowground C pools in ABRs are vulnerable to climate change (Grosse et al., 2011). Arctic–boreal regions are warming at a disproportional rate compared to the rest of the planet with potential feedbacks to the global climate system (Box et al., 2019; Derksen et al., 2019; IPCC, 2019; Rantanen et al., 2022). In conjunction with warming temperatures, ABRs are experiencing altered precipitation regimes (Callaghan et al., 2011; Bokhorst et al., 2016; Dolant et al., 2018); permafrost thawing and deepening of the hydrologically and biogeochemically active layer (Liljedahl et al., 2016; Miner et al., 2022); spatially variable vegetation responses associated with “greening” and “browning” (i.e., increasing and decreasing productivity, respectively; Sulla-Menashe et al., 2018; Myers-Smith et al., 2020); earlier spring thaw; later freeze-up and lengthening of the growing season (Kimball et al., 2004a; Euskirchen et al., 2006; Kim et al., 2012); modifications of land cover (Wang et al., 2020); and intensifying disturbance regimes such as fire, drought, pervasive insect infestation and disease (Peng et al., 2011; Yi et al., 2013; Foster et al., 2022). Although ongoing warming has the potential to enhance photosynthesis and plant growth across ABRs, which would also increase above-ground C storage (Sturm et al., 2005; McMahon et al., 2010; Myers-Smith et al., 2020), the vegetation response to climate change is variable and complex. Furthermore, warmer air and soil temperatures enhance soil organic matter decomposition and the subsequent release of carbon dioxide ( $\text{CO}_2$ ) via respiration (Schädel et al., 2016). Large uncertainties remain in terrestrial biosphere models used to estimate  $\text{CO}_2$  and  $\text{CH}_4$  fluxes in ABRs (Tei and Sugimoto, 2020; Fisher et al., 2018), including the amount of  $\text{CO}_2$  and  $\text{CH}_4$  released during winter (Natali et al., 2019; Zona et al., 2015). If increases in ecosystem respiration exceed those of photosynthetic  $\text{CO}_2$  uptake from enhanced plant growth, ABRs may shift from a weak net  $\text{CO}_2$  sink to a net  $\text{CO}_2$  source, thereby generating a potentially non-negligible, positive feedback to the global climate system. This potential change underlines the importance of understanding changes in ABR C pools and fluxes (Hayes et al., 2011; Schuur et al., 2015; Gauthier et al., 2015; Virkkala et al., 2021).

The vastness and remoteness of ABRs make in situ observations challenging and costly. For example, although FLUXNET, the global initiative of tower-based eddy covariance flux observations (Baldocchi et al., 2001; Pastorello et al., 2020), is the most broadly used reference for C-flux measurements at the ecosystem scale, ABRs are notoriously underrepresented in this network (Fig. 1; Baldocchi et al., 2001; Pastorello et al., 2020; Pallandt et al., 2022). Satellite remote sensing and terrestrial biosphere models show promise for monitoring land surface–atmosphere interactions across ABRs (Fisher et al., 2018; Lees et al., 2018). Although direct measurement of C fluxes is not yet possible through remote sensing, it is possible to use spaceborne sensors to monitor

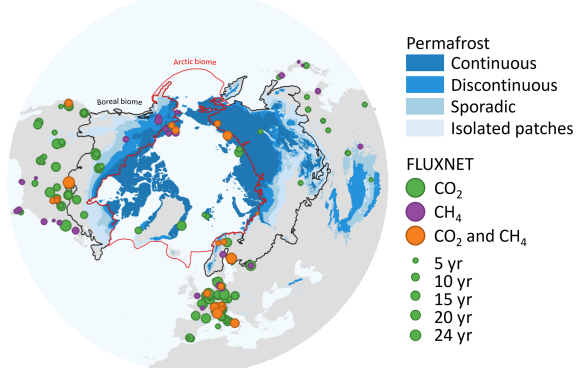


**Figure 1.** Permafrost extent (Brown et al., 2002) and distribution of eddy covariance sites where ecosystem fluxes are monitored continuously (Baldocchi et al., 2001; Pallandt et al., 2022; dot size represents the number of years of available data). The Arctic biome is delineated following the Conservation of Arctic Flora and Fauna working group of the Arctic Council, and the boreal biome is delineated following Potapov et al. (2008). Permafrost extent is estimated in percent areal coverage: continuous (> 90 %–100 % areal extent), discontinuous (> 50 %–90 %), sporadic (10 %–50 %) and isolated patches (< 10 %).

variables and ecosystem structural parameters that exert control over various ecosystem processes (J. Du et al., 2019). In the last decade, radiometers sensitive to wavelengths in the visible and infrared portions of the electromagnetic spectrum have been widely used to support C-cycle science in ABRs (Turner et al., 2004; Mao et al., 2016; Lees et al., 2018; Xiao et al., 2019). Visible and infrared remote sensing observations have been used in C-cycle science to map spectral vegetation indices as proxies for vegetation abundance and productivity (e.g., normalized difference vegetation index, NDVI; Tucker, 1979; Lees et al., 2018; S. Du et al., 2019), forest disturbance (e.g., fire, tree mortality; Kim et al., 2012), land cover (Kimball et al., 2009), vegetation structure (e.g., light detection and ranging, lidar; Xiao et al., 2019), snow cover extent (Hori et al., 2017), land surface temperature (Sitch et al., 2007; Xiao et al., 2019), albedo (Xiao et al., 2019), solar-induced chlorophyll fluorescence (Wohlfahrt et al., 2018; Magney et al., 2019), and atmospheric  $\text{CO}_2$  concentration (Buchwitz et al., 2007; Tu et al., 2020; Lorente et al., 2021). However, spaceborne visible and infrared radiometers are affected by signal degradation from atmospheric effects, have minimal signal penetration depth in vegetation and depend on solar illumination meaning they are restricted to daytime, clear-sky observations (Kim et al., 2012).

Spaceborne microwave remote sensing can be used in synergy with visible and infrared radiometers to maximize the benefits of a wider frequency span in the electromagnetic spectrum (Sitch et al., 2007; Kimball et al., 2009; Arslan et

al., 2011; Kim et al., 2012; Xiao et al., 2019). Microwaves encompass electromagnetic radiation within the frequency range of 0.3–300 GHz, which corresponds to wavelengths from 1 mm to 1 m. Microwave remote sensing provides several advantages such as its relative insensitivity to atmospheric attenuation, cloud cover and solar illumination at frequencies below 100 GHz, which is essential during winter months in regions undergoing polar night (Sitch et al., 2007; J. Du et al., 2019). The spatial resolution of microwave imagery ranges from coarse (several-kilometer scale) to fine (meter scale) with varying temporal resolutions that can reach more than one observation per day. Microwave remote sensing is particularly suitable for ABRs since the signal penetration depth range allows for the retrieval of (1) volumetric information such as certain snow properties including density and microstructure (e.g., Nagler and Rott, 2000; Takala et al., 2011; Lievens et al., 2019) and vegetation optical depth (VOD), which relates to aboveground biomass and vegetation liquid water content (Konings et al., 2017, 2019; Mialon et al., 2020), and (2) near-surface information on variables such as soil moisture (Kerr et al., 2012; Colliander et al., 2017) and the freeze–thaw state (Kim et al., 2012; Roy et al., 2015; Rautiainen et al., 2016; Derksen et al., 2017; Prince et al., 2019) because of its sensitivity to liquid water.

This paper aims to introduce to the C-cycle science community the potential of spaceborne microwave remote sensing to help overcome some of the challenges specifically posed by ABRs for terrestrial C-cycle science and monitoring. We focus on the main vertical C fluxes between the land surface and the atmosphere, specifically, respiratory CO<sub>2</sub> fluxes; photosynthetic CO<sub>2</sub> uptake; and processes related to net methane (CH<sub>4</sub>) fluxes governed by CH<sub>4</sub> production, transport and consumption. After summarizing the principles of microwave remote sensing (Sect. 2), we review how spaceborne microwave remote sensing can be exploited to help monitor key variables important for CO<sub>2</sub> and CH<sub>4</sub> fluxes in ABRs. These include soil moisture (Sect. 3.1) and temperature (Sect. 3.2), the surface freeze–thaw status (Sect. 3.3), aboveground biomass (Sect. 3.4), the vegetation water status (Sect. 3.5), land cover (Sect. 3.6), and snow cover (Sect. 3.7). For each variable, we will first explain how the variable at least partially governs C exchanges, outline the potential of microwave remote sensing to monitor the key variable and then introduce presently available microwave remote sensing products related to each variable.

## 2 Principles of microwave remote sensing

Microwave remote sensing can be used passively, by measuring the natural microwave emission from the planetary surface (using radiometers; receiving only), or actively, by measuring the backscattering of a previously emitted signal (using radar instruments; emitting and receiving).

Radiometers measure the natural microwave emission coming from the planetary surface. This emission is quantified as the brightness temperature ( $T_B$ ; Fig. 2b), which corresponds to the temperature of a blackbody delivering the same luminance as the studied surface. Brightness temperature is related to the physical temperature of a surface ( $T_B = e \cdot T$ ) through emissivity ( $e$ ; unitless). Emissivity is an inherent material property ranging from 0, for a perfectly non-emitting material, to 1, for a purely emitting material (blackbody). The microwave electric field generally displays a preferred orientation, called the microwave polarization, and is often related to the geometric structure of the source or target (Ulaby et al., 1982, 1983). The spatial resolution of passive microwave radiometers is generally coarser than many visible and infrared radiometers owing to the longer wavelengths and practical restrictions of the receiving antenna dimensions on spacecraft (Jenson, 2006). Spaceborne passive microwave radiometers typically have spatial resolutions in the 10–100 km range. Although passive microwave spatial resolutions are often too coarse to capture small-scale landscape heterogeneity (meter to kilometer scale), it is not an obstacle for regional or global applications of terrestrial biosphere models commonly run at spatial resolutions of several kilometers. The temporal resolution of most microwave instruments is generally less than 2–3 d, and in polar regions several overpasses a day may be achieved. The fine temporal resolution might be more critical for terrestrial biosphere models than good spatial resolution since computational power limits the spatial resolution of such models (Washington et al., 2009; Schär et al., 2020).

Radar emit electromagnetic waves to calculate the backscattering coefficient ( $\sigma$ ; Fig. 2b) of a target area from the power ratio between the emitted and returned pulse (Ulaby et al., 1982, 1986). The return signal of a radar carries three main pieces of information: the magnitude of  $\sigma$ ; the phase of the electromagnetic wave returning; and a delay between the emitted and received signal, which is related to the distance between the radar and the target area. Scatterometers focus particularly on the magnitude of the backscattered signal by a medium to extract backscattering coefficient (Figa-Saldafia et al., 2002). Synthetic-aperture radar (SAR) measures backscattering coefficients using a radar technique that can achieve spatial resolutions at a meter scale by combining scenes of the target area from multiple points of view (Tomiyasu, 1978; Bamler, 2000). Synthetic-aperture radars achieve comparable resolutions to visible and infrared radiometers (i.e., below 10 m of spatial resolution). However, radar transmitters are much more energy-consuming than radiometers because of the power requirement for emitting microwaves. Because of high energy demands, most SAR transmitters operate during a small fraction (1 %–30 %; Grasso et al., 2021; Leanza et al., 2019; Dubock et al., 2001) of their orbit around Earth. The lower the transmission time, the greater the duration between measurements at a given point, often several days (Marghany, 2019). This is currently being over-

come via deployment of several satellites equipped with SAR instruments flying in tandem (Sentinel-1; RADARSAT Constellation Mission).

Unlike visible and infrared remote sensing that are limited to information from the surface of any target, the longer wavelengths of microwaves allow for microwaves to penetrate vegetation, ground and snowpack, allowing for subsurface measurements (Ulaby et al., 1986); the longer the microwave, the deeper the penetration depth. However, deeper penetration means that the received signal is a combination of different contributing components, i.e., usually vegetation, soil, snow and atmosphere (Kerr et al., 2012; Roy et al., 2012, 2014), challenging the interpretation of the signal. Consequently, microwave remote sensing is often used together with radiative transfer models to decouple and extract the information on terrestrial surface conditions from microwave observations. These models generally calculate the scattering, reflection and attenuation of the electromagnetic waves of the different components of the surface (Fig. 2) (Mo et al., 1982; El-Rayes and Ulaby, 1987; Huang et al., 2017; Picard et al., 2018). By considering the contribution of each component of the surface (i.e., soil, vegetation and/or snow), radiative transfer models allow for disentangling microwave signals to retrieve key surface state variables of interest (Wigneron et al., 2007).

Multiple microwave radiometers have been launched in recent decades covering most of the microwave portion of the electromagnetic spectrum: L-band (1–2 GHz), C-band (4–8 GHz), X-band (8–12 GHz), K-band (18–26.5 GHz), K<sub>a</sub>-band (26.5–40 GHz) and W-band (75–110 GHz) (Table A1 in Appendix A). There is a nearly continuous publicly available radiometric dataset from 1978 to the present covering the microwave bands from the C-band to the W-band (Fig. 3a). Additionally, in the last decade, L-band data have become accessible through the launch of the Soil Moisture Ocean Salinity mission (SMOS; Kerr et al., 2010), the Aquarius mission (Brucker et al., 2004) and the NASA (National Aeronautics and Space Administration) Soil Moisture Active Passive mission (SMAP; Entekhabi et al., 2010). An exhaustive list of radars would be too long to present here; instead we focus on a selection of recent radar missions (Fig. 3b). These spaceborne radars were selected for the purpose of the review to represent a range of frequencies and available temporal coverage.

### 3 Microwave remote sensing for retrieval of surface variables

Although direct measurements of vertical C fluxes are not feasible through microwave remote sensing, it is possible to use spaceborne radiometers and radar to monitor key variables important for different C-cycle processes (Fig. 4). Carbon dioxide and CH<sub>4</sub> fluxes, two of the most potent greenhouse gases, are continuously exchanged between Earth's

surface and the atmosphere. Carbon dioxide is absorbed through photosynthesis by vegetation and is released by plants and soil through respiration (i.e., autotrophic respiration,  $R_a$ , and heterotrophic respiration,  $R_h$ , respectively) (Chapin et al., 2006). In ecosystems, CH<sub>4</sub> is produced by methanogens under anaerobic conditions and consumed during oxidation by methanotrophs under aerobic conditions (Lai, 2009). Methane transport through the soil column and to the atmosphere occurs through diffusion, ebullition and plant-mediated transport (Lai, 2009).

#### 3.1 Soil moisture

In ABRs, water availability and air and soil temperatures are considered important environmental constraints on photosynthesis and thus C sequestration (Lieffers and Rothwell, 1987; Angert et al., 2005; Jones et al., 2017). For example, both heat stress and drought can limit tree growth across latitudes in boreal forest stands (Walker and Johnstone, 2014; Sniderhan et al., 2021). Near-surface soil moisture also affects methanogenesis and methanotrophy, which depends strongly on oxygen availability (Lai, 2009). Environmental controls on soil respiration, i.e., the sum of belowground  $R_a$  and  $R_h$ , include soil moisture and temperature, which in ABRs are both influenced by permafrost and active (seasonally thawed) layer dynamics (Huntzinger et al., 2020). Hence, in a changing climate where soils across ABRs are generally expected to be drying (e.g., Gauthier et al., 2015; Andresen et al., 2020), reliably quantifying soil moisture dynamics and thus water availability will become essential for a predictive understanding of C-cycle dynamics.

The sensitivity of the microwave signal to soil moisture content has been widely demonstrated previously, but several challenges remain including accounting for vegetation attenuation and scattering related to the surface roughness (Das and Paul, 2015; Colliander et al., 2022), as well as organic soil model parametrization (Mironov and Savin, 2015; Bircher et al., 2016). The sensitivity to soil moisture generally increases with lower microwave frequencies, making the L-band the most sensitive to soil moisture content. The depth over which soil moisture content can be estimated from microwave remote sensing is limited at best to the top 5 cm of the soil profile (roots are most dense in the top 20 cm). Measurement depth depends on the frequency used (longer wavelengths realize greater depths; Adams et al., 2015), the soil moisture content, and the vegetation type and density (Wigneron et al., 2007). These measurement depths do not capture the water availability in the full rooting zone, which will be most relevant to predicting the photosynthetic CO<sub>2</sub> update. However, it remains possible to estimate root zone soil moisture content from near-surface soil moisture content using pedotransfer equations, meaning these surface measurements can be quite useful (Stefan et al., 2021; Dimitrov et al., 2022).

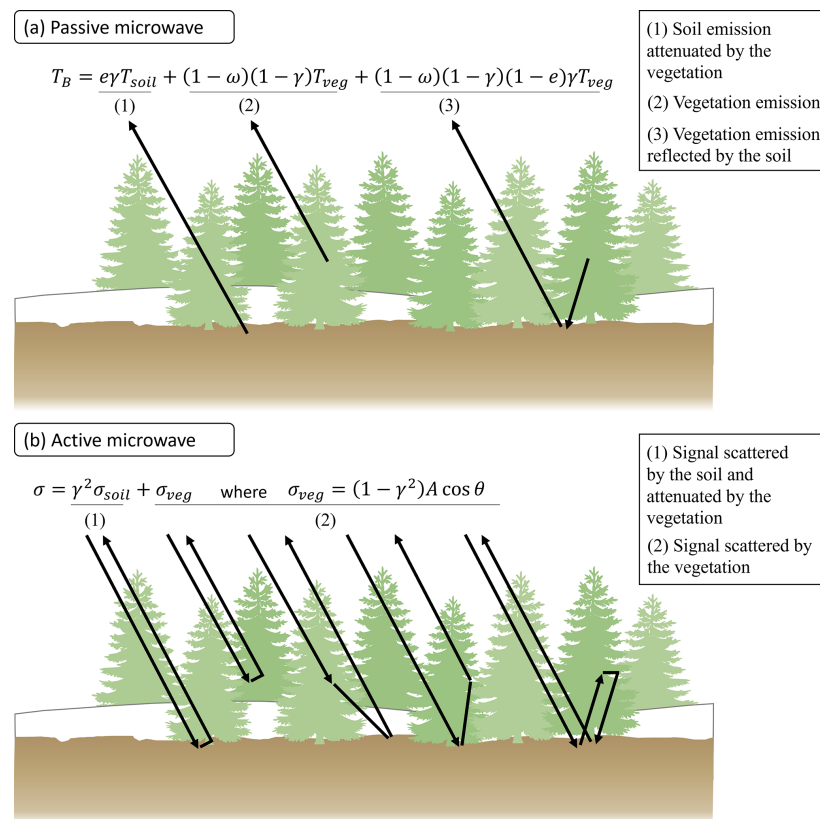


**Figure 2.** Microwave-signal decoupling through electromagnetic wave interaction with matter. **(a)** Mo et al. (1982) model for passive microwaves with  $T_B$  representing the brightness temperature,  $e$  being the soil emissivity,  $\gamma$  being the vegetation attenuation,  $\omega$  being the vegetation single-scattering albedo, and  $T$  being the thermodynamic temperature of soil and vegetation (Mo et al., 1982). **(b)** Water cloud model for active microwaves with  $\sigma$  representing the backscattering coefficient,  $\gamma$  being vegetation attenuation,  $A$  being a vegetation empirical parameter and  $\theta$  being the radar incident angle (Attema and Ulaby, 1978). The  $\sigma_{veg}$  term is an approximation for the first-order vegetation scattering processes. Snow increases the complexity of the interaction between the microwave and the ground level because it is acting as an additional semi-opaque layer comparable to the vegetation layer. Snow and atmosphere are not accounted for in the equations presented.

Extensive methodological research to develop soil moisture retrievals from microwave remote sensing has been motivated for agricultural applications (Engman, 1991; Wigneron et al., 2007; Lakhankar et al., 2009). Soil moisture retrieval was the main motivation behind several passive L-band satellite missions, including SMAP and SMOS. The resulting expertise and soil moisture products present a promising data stream to inform terrestrial biosphere models (see Sect. 4). Table 1 presents several available soil moisture products. The European Space Agency (ESA) Climate Change Initiative (CCI) project produces a soil moisture product merging active and passive microwave sensors, exploiting the microwave instruments temporal coverage since 1978 (Gruber et al., 2019).

### 3.2 Soil temperature

Rates of photosynthesis and ecosystem respiration ( $R_{eco}$ ; Fig. 4) are generally strongly controlled by soil temperature (Angert et al., 2005; Jones et al., 2017; Stocker et al., 2018). Similarly, laboratory and field observations have shown that  $R_h$ -related  $CO_2$  fluxes are non-negligible below the freezing point and increase with warming soil temperatures (Fahnestock et al., 1998, 1999; Welker et al., 2000; Mikan et al., 2002; Panikov et al., 2006; Natali et al., 2019). Despite lower fluxes, winter  $CO_2$  emissions from soil respiration may constitute an important contribution to annual net ecosystem productivity (NEP), especially in ABRs with very short growing seasons (Elberling et al., 2007; Webb et al., 2016; Natali et al., 2019).

Microwave  $T_B$  depends on thermodynamic temperature ( $T_B = e \cdot T$ ); thus it is possible to retrieve land surface tem-

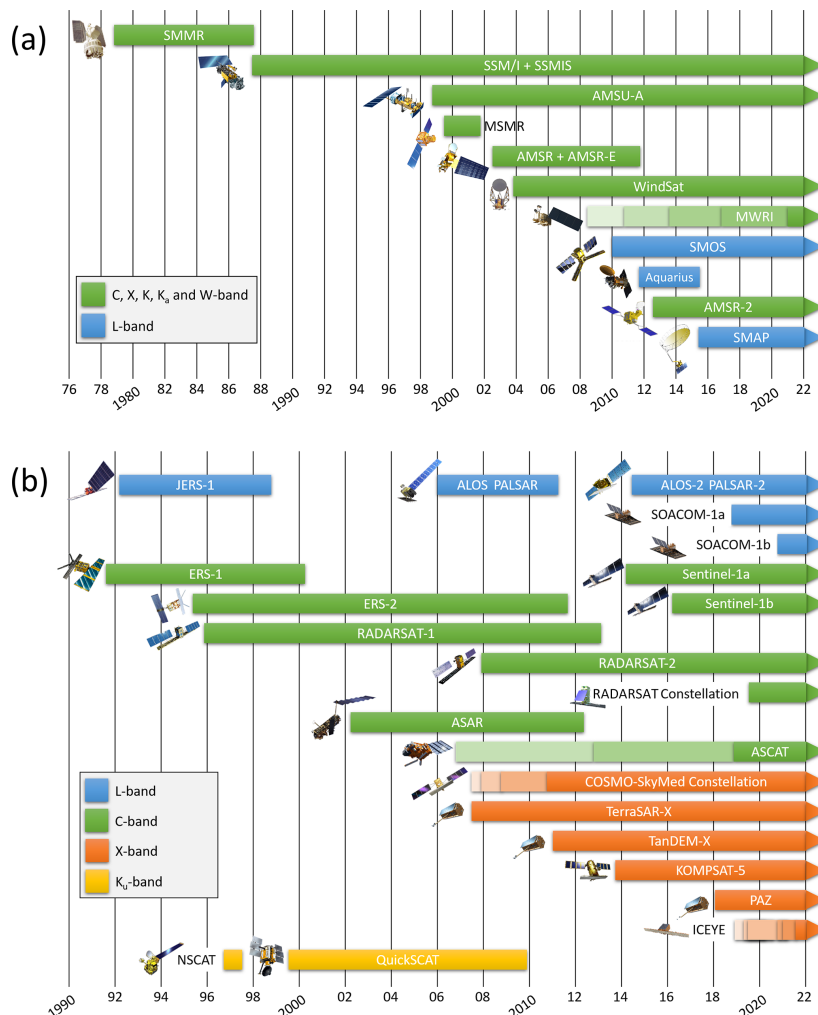


**Figure 3.** (a) Temporal coverage of spaceborne passive microwave instruments (radiometers between 1–100 GHz, sun-synchronous nearly polar orbits; more details in Table A1). (b) Selected number of spaceborne radar missions (active sensors) covering the L-band (1–2 GHz), C-band (4–8 GHz), X-band (8–12 GHz) and Ku-band (12–18 GHz). More details are provided in Table A2.

perature (LST) from radiometric data (Duan et al., 2020). Retrieval of LST from microwave remote sensing is technically more challenging and results in lower precision than similar products from thermal infrared remote sensing, 1–5 K for microwave LST vs. 0.2–2 K for thermal infrared (Jiménez-Muñoz and Sobrino, 2006; Jones et al., 2010; Osińska-Skotak, 2007; Krishnan et al., 2020; Zhang and Cheng, 2020). Microwave emissivity is also more sensitive to environmental changes (e.g., liquid water content) than thermal infrared emissivity. Although infrared LST is more precise than microwave LST, there are instances where microwave LST may be important. Specifically, microwave LST can support gap filling when thermal infrared LST is unavailable because of extended periods of cloud cover or when fine tem-

poral resolution is required. Microwave can be used to sense soil temperature up to a few centimeters deep because of its soil penetration depth. It is an important advantage over thermal infrared remote sensing, which can only detect LST and is subject to significant atmospheric contamination (Jones et al., 2007). Some studies have also shown the potential to use microwave observations to retrieve soil temperature under the snow (Kohn and Royer, 2010; Marchand et al., 2018).

Although several studies have obtained LST from microwave data, no operational microwave LST product is operationally available. Microwave LST algorithms typically achieve a precision of 2–5 K using data from AMSR-E/AMSR2 (Jones et al., 2010; Zhang and Cheng, 2020) and SMM/I and SMMR (Pulliainen et al., 1997; Ba-

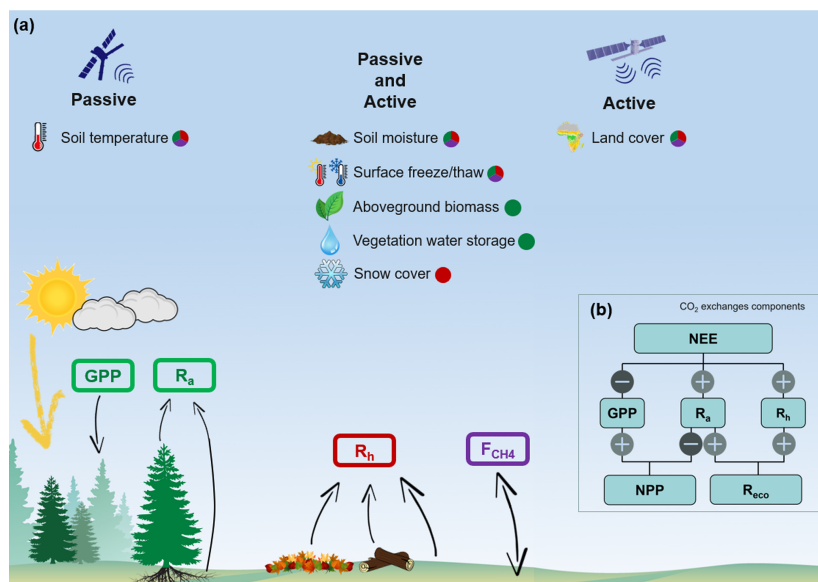


**Figure 4.** (a) Carbon dioxide and methane fluxes between the land surface and the atmosphere including gross primary production (GPP), heterotrophic respiration ( $R_h$ ), autotrophic respiration ( $R_a$ ) and net methane fluxes ( $F_{CH_4}$ ) (units:  $gC\ m^{-2}\ yr^{-1}$ ). The fluxes are color-coded (green: GPP and  $R_a$ ; red:  $R_h$ ; purple:  $F_{CH_4}$ ) to match relevant key variables important for  $CO_2$  and  $CH_4$  fluxes and derivable with microwave remote sensing. (b) Relationships of net primary productivity and net ecosystem productivity (NEP: negative net ecosystem exchange, NEE) and their component fluxes with ecosystem respiration ( $ER = R_a + R_h$ ).

sist et al., 1998; Fily et al., 2003; Mialon et al., 2007; Royer and Poirier, 2010). Other studies have used machine learning approaches, obtaining precision around 1–3 K with AMSR2 data (Aires et al., 2001; Mao et al., 2018).

### 3.3 Surface freeze–thaw state

During the short growing season in ABRs, photosynthetic  $CO_2$  uptake exceeds the respiratory  $CO_2$  losses; thus ABRs generally act as net growing season  $CO_2$  sinks (Ciais et al., 2019; Virkkala et al., 2021). However, in winter, plants become dormant and photosynthesis and  $R_a$  cease (gross primary productivity,  $GPP = 0$ ;  $R_a \approx 0$ ) owing to the cold temperatures and highly reduced photoperiod (Kimbball et al., 2004b; Rafat et al., 2021). Although  $R_h$  may continue in frozen soil, it decreases substantially (Natali et al., 2019). Modeling annual NEP in areas undergoing seasonal surface freeze–thaw cycles requires the ability to estimate the length and timing of the growing season (Seiler et al., 2022; El-Amine et al., 2022). The growing season length has a direct impact on annual GPP and thus NEP, but there is also a strong relationship between surface freeze–thaw timing and photosynthetic  $CO_2$  uptake (Frolking et al., 1996; McDonald et al., 2004; Kim et al., 2012; Fu et al., 2017; Pierrat et al., 2021). Changes in the timing of spring thaw can create a shift in growing conditions when photosynthesis is initiated (Jarvis and Linder, 2000; Tanja et al., 2003; Kimball et al.,

2004a; Piao et al., 2008; Kim et al., 2012; El-Amine et al., 2022). The timing of the start of the growing season has been shown to be more important to annual GPP than the timing of the end because of the superior light and water availability during the spring period (Tanja et al., 2003; El-Amine et al., 2022). The surface freeze–thaw state is a useful proxy for the timing and thus duration of photosynthetic activity (Harrison et al., 2020) and can potentially be used to track  $CH_4$  emissions in ABRs (Tenkanen et al., 2021).

Satellite detection of the surface freeze–thaw state is based on the dielectric contrast between water and ice at microwave frequencies. Therefore, soil emissivity is highly sensitive to phase state changes in its liquid content. When water freezes,  $\varepsilon_{soil}$  drops drastically as liquid water changes to ice because of the crystalline structure of frozen water. The rapid decrease in  $\varepsilon_{soil}$  in freezing soils translates into a much higher microwave emission and backscattering from the surface. This allows for surface freeze–thaw state retrieval from passive and active microwave measurements using temporal change detection algorithms (Mortain et al., 2012; Rautiainen et al., 2012; Roy et al., 2015; Chen et al., 2019) and threshold-based methods (Kim et al., 2012, 2017; Derksen et al., 2017). Furthermore, for oblique incidence angles, horizontal polarization is more affected than its vertical counterpart during the surface freeze–thaw transition, which favors the use of a polarization ratio as an effective tool for deter-

**Table 1.** Presently available soil moisture products from spaceborne microwave remote sensing.

	WindSat <sup>a</sup>	SMOS <sup>b</sup>	Aquarius <sup>c</sup>	AMSR-E/ AMSR2 <sup>d</sup>	SMAP <sup>e</sup>	ERS-1/2 <sup>f</sup>	ASCAT <sup>g</sup>	RADARSAT- 2 <sup>h</sup>	Sentinel-1A/B <sup>i</sup>	Climate Change Initiative <sup>j</sup>
Sensor type	Passive	Passive	Passive	Passive	Passive	Active	Active	Active	Active	Passive and active
Spatial resolution	25 km	25 km	36 km	25 km	9 km	25 km	25 km	18 m	1 km	25 km
Temporal coverage	2003–2012	2010–	2011–2015	2002–	2015–	1996–2011	2007–	2007–	2015–	1978–
Reference	Parinussa et al. (2012)	Al Bitar et al. (2017)	Bindlish et al. (2015)	Du et al. (2017)	Chan et al. (2016, 2018)	Naeimi et al. (2009), Das et al. (2017)	Wagner et al. (2013)	Merzouki et al. (2011)	EI Hajj et al. (2017)	Gruber et al. (2019)

<sup>a</sup> WindSat/Coriolis surface soil moisture (LPRM) L3 1 day 25 km × 25 km daytime V001. <sup>b</sup> SMOS L1 and L2 Science data. <sup>c</sup> Aquarius L3 Weekly Polar-Gridded Sea Surface Salinity, Version 5 (AO3\_SSS). <sup>d</sup> AMSR-E/AMSR2 Unified L2B Half-Orbit 25 km EASE-Grid Surface Soil Moisture, Version 1 (AU\_Land). <sup>e</sup> SMAP L4 Global 3-hourly 9 km EASE-Grid Surface and Root Zone Soil Moisture Geophysical Data, Version 6 (SPL4SMGP). <sup>f</sup> ERS-2 SCATTEROMETER Surface Soil Moisture Time Series and Orbit product in High and Nominal Resolution. <sup>g</sup> ASCAT Soil Moisture at 25 km Swath Grid in NRT – Metop. <sup>h</sup> RADARSAT-2 Surface Soil Moisture. <sup>i</sup> 1 km SSM (surface soil moisture) Version 1 product (SSM1km). <sup>j</sup> ESA CCI SM.

mining the surface freeze–thaw state (Rautiainen et al., 2016; Roy et al., 2017a, b).

The use of passive and active microwave remote sensing for surface freeze–thaw state detection has been widely studied, improving quickly and steadily in the last decade and resulting in various publicly available products (Table 2). As for soil moisture studies, lower microwave frequencies such as the L-band, have been the most exploited because of the prominent water phase dielectric contrast and reduced attenuation from aboveground vegetation and snow (Rautiainen et al., 2016). Surface freeze–thaw state products offer the opportunity to constrain the vegetation growing season timing and photosynthetic CO<sub>2</sub> uptake in terrestrial biosphere models.

### 3.4 Aboveground biomass

Although not a direct control on C-cycle processes, aboveground biomass (AGB) can be used to estimate aboveground C stocks. The annual net gain or loss of C by vegetation (NPP) leads to a proportional increase or decrease in AGB, respectively (Turner et al., 2004; Gough, 2011). Therefore, C storage in aboveground vegetation over a defined period can be inferred from AGB estimates from either terrestrial, aerial or spaceborne techniques (Das et al., 2021). However, using AGB only provides average C exchanges between two data acquisitions and provides no understanding of the underlying ecophysiological and biogeochemical processes. It should be noted that AGB is a minor component of the C stocks in ABRs, where most of the C is stored belowground (Houghton, 2005; Pappas et al., 2020; Walker et al., 2020). Information on AGB allows for initialization, parameterization and evaluation of terrestrial biosphere models and helps to understand, for example, the impact of discrete disturbances such as wildfire and insect outbreaks (Chirici et al., 2016).

Microwave remote sensing can provide information on AGB since microwave wavelengths typically penetrate and interact with moderately dense vegetation cover, depending on the microwave length (Liu et al., 2011a, b). Vegetation attenuation of microwaves is characterized by the vegetation optical depth (VOD;  $\gamma = e^{-VOD/\cos\theta}$ ), which is proportional to vegetation density (i.e., biomass) and water content. Vegetation optical depth is frequency-dependent and affected by the geometry (e.g., canopy structure) of the vegetation (Ulaby et al., 1990). The impact of vegetation geometry on attenuation is challenging to parametrize because of the complexity of forest canopies; therefore it is typically accounted for through vegetation type-dependent, empirically determined parameters introduced in the relationship between VOD, vegetation water content and biomass (Jackson and Schmugge, 1991; Konings et al., 2019). Microwave VOD is better suited to directly monitoring vegetation compared to spectral vegetation indices obtained using visible and infrared wavelengths such as NDVI that saturate

**Table 2.** Available surface freeze–thaw state products from spaceborne microwave remote sensing.

MEaSUREs program <sup>a</sup>	Aquarius <sup>b</sup>	SMOS <sup>c</sup>	SMAP <sup>d</sup>	NSCAT	QuickSCAT	PALSAR	ASCAT <sup>e</sup>
Sensor type	Passive	Passive	Passive	Passive	Active	Active	Active
Spatial resolution	25 km (6 km starting in 2002)	36 km	25 km	9 km	25 km	25 km	25 km
Temporal coverage	1979–2020	2011–2015	2010–ongoing	2015–ongoing	1996–1997	1999–2009	2006–2011
Reference	Kawanishi et al. (2003)	Xu et al. (2016), Prince et al. (2018)	Rautianen et al. (2016)	Kim et al. (2019)	Kimball et al. (2001)	Brucker et al. (2014)	Kerr et al. (2010)
							Naeimi et al. (2012)

<sup>a</sup> Sensors: SMMR, SSMIS, AMSR-E, and AMSR2. <sup>b</sup> Aquarius L3 Weekly Polar-Gridded Landscape Freeze/Thaw Data, Version 5 (AO3\_FT). <sup>c</sup> SMOS Level 3 Freeze and Thaw (FT). <sup>d</sup> SMAP Enhanced L3 Radiometer Global and Northern Hemisphere Daily 9 km EASE-Grid Freeze/Thaw State, Version 3 (SPL3FTP\_E). <sup>e</sup> ASCAT Surface Soil Moisture/Freeze-Thaw V2 product.

at relatively low AGB of around 50–80 Mg ha<sup>-1</sup> (Rodríguez-Fernández et al., 2018; Mialon et al., 2020; Turner et al., 2004). In contrast, VOD was shown to saturate AGB of up to 350 Mg ha<sup>-1</sup> (Vittucci et al., 2019). It has also been shown that there is a significant difference in what phenological aspects of the growing season are captured by vegetation indices such as NDVI vs. microwave VOD (Mialon et al., 2020). VOD seems to correspond better to key physiological processes such as sap flow and vegetation water storage than vegetation indices such as NDVI, which better capture dynamics of canopy phenology (Lawrence et al., 2014; Cui et al., 2015; Tian et al., 2016; Holtzman et al., 2021; Wigneron et al., 2021).

There is clear potential to improve C-cycle science in boreal forests using VOD-derived AGB (Rodríguez-Fernández et al., 2018). Several recent studies have also shown good correlations between VOD and GPP (Teubner et al., 2018, 2019). The L-band spaceborne radiometer record goes back to 2010 with SMOS, while higher-frequency VOD estimates extend back to the early 1980s. Table 3 presents several VOD products available. Santoro and Cartus (2018) counted 221 studies on SAR data applied to AGB retrieval from 1987 to 2017 using frequencies from 30 MHz up to 12 GHz. AGB investigations using active sensors can achieve a much finer spatial resolution than their passive counterparts, down to the 10 m scale. Also, recent promising advances in SAR interferometry (InSAR), polarimetric InSAR (PolInSAR) and SAR tomography (TomoSAR) techniques provide new opportunities for AGB estimates by surveying the 3D structure of vegetation (Neumann et al., 2012; Tebaldini et al., 2019). InSAR can be used to measure the vertical motion in peatlands, which is a direct indicator of the mass gain or loss by those ecosystems, which constitute a major global C pool (Alshammari et al., 2019; Zhou et al., 2019; Loisel et al., 2021). Some global biomass surveys have also exploited the multi-frequency synergy of data products in the microwave, visible and infrared wavelengths and lidar technologies (e.g., GlobBiomass: Santoro et al., 2018; Mialon et al., 2020). Although the low AGB of the Arctic tundra is challenging to monitor from microwave observations, studies have shown that it is possible to estimate the upper soil organic C (up to 30 cm from the soil–atmosphere interface) using active and passive microwave observations (Bartsch et al., 2016; Yi et al., 2022).

### 3.5 Vegetation water storage

Water availability is considered an important environmental limitation on photosynthetic processes in ABRs (Ruiz-Pérez and Vico, 2020). In terrestrial biosphere models, a lack of water availability is an environmental stress reducing the photosynthetic capacity (i.e., NPP) (Mu et al., 2007). Water stored in vegetation is critical for stomatal regulation; therefore it is strongly correlated to vegetation growth (Köcher et al., 2013; Matheny et al., 2015). In addition, vegetation water

**Table 3.** Available products for vegetation optical depth from spaceborne microwave remote sensing.

	AMSR-E/AMSR2 <sup>a</sup>	SMOS <sup>b</sup>	SMAP <sup>c</sup>	221 SAR studies	ASCAT <sup>d</sup>
Sensor type	Passive	Passive	Passive	Active	Active
Spatial resolution	25 km	25 km	36 km	≥ 10 m	25 km
Temporal coverage	2002–2020	2010–ongoing	2015–ongoing	1987–2017	2015–2019
Reference	Jones et al. (2011), Du et al. (2017)	Wigneron et al. (2021)	X. Li et al. (2022)	Santoro and Cartus (2018)	X. Liu et al. (2021)

<sup>a</sup> Daily Global Land Parameters Derived from AMSR-E and AMSR2, Version 3 (NSIDC-0451). <sup>b</sup> L3 SMOS-IC v2. <sup>c</sup> SMAP-IB L-VOD. <sup>d</sup> ASCAT IB VOD.

storage can act as a buffer for the daily demands of transpiration (Matheny et al., 2015). However, soil moisture and/or precipitation are generally used to estimate water availability since vegetation water storage estimates are rarely available (Zhang et al., 2015; Stocker et al., 2018).

Since vegetation water storage strongly affects microwave VOD because of the high absorption of microwave by water (Konings et al., 2019), microwave attenuation holds potential for estimating vegetation water storage, which can be used to evaluate vegetation water stress (Holtzman et al., 2021). To the best of our knowledge, no large-scale vegetation water storage product yet exists, but efforts toward this goal are underway (Y. Liu et al., 2021). The microwave VOD sensitivity to both AGB and the vegetation water status complicates its interpretation, although the study of the temporal and spatial trends of VOD can allow for disentangling AGB vs. the vegetation water content (Dou et al., 2023). At short timescales (i.e., diurnal), biomass variation is small and VOD trends can largely be attributed to vegetation water status. At longer timescales (i.e., annual), VOD trends come mostly from biomass dynamics (Mialon et al., 2020). Another method to distinguish water storage and biomass-related VOD changes is to use periods with similar water stress levels for VOD comparison (Konings et al., 2019).

### 3.6 Land cover

Regional and global studies on C exchanges require information on land cover (Gasser et al., 2020). Repeated satellite-based image classification provides large-scale monitoring of land cover evolution (Wang et al., 2019). Land cover and wetland classifications based on SAR imagery have been developed with the same supervised or unsupervised classification algorithms used for classifying imagery obtained with visible and infrared remote sensing (van Zyl, 1989; Pierce et al., 1994; Dobson et al., 1995; Ranson and Sun, 2000; Bartsch et al., 2007; Whitcomb et al., 2009; Lönnqvist et al., 2010; Merchant et al., 2017, 2022). Recent studies have explored the use of machine learning for land cover classification based

on SAR data (Merchant et al., 2019). SAR land cover classifications are enhanced when benefiting from multi-frequency instruments (Saatchi and Rignot, 1997) and multiple polarizations (Lee et al., 2001). The complementarity of SAR and visible/infrared imagery has already been exploited to reinforce spatial and temporal coverage and improve precision of land cover classifications (Töyrä et al., 2001; Ullmann et al., 2014; Merchant et al., 2019). SAR imagery has shown to be especially useful for delineating inundated areas (Bowling et al., 2003) or wet and moist tundra (Morrissey et al., 1996; Merchant et al., 2022), which has a strong impact on CH<sub>4</sub> emission (Watts et al., 2014). Microwave observations can also be used to monitor freshwater (FW) waterbody extent dynamics (Murfitt and Duguay, 2021). FW can act as important CH<sub>4</sub> emissions sources, especially during ice melt, but aquatic carbon cycle processes are very different than terrestrial carbon processes and were not within of the scope of this review (Matthews et al., 2020).

### 3.7 Snow cover

Unlike photosynthesis and  $R_a$ ,  $R_h$  can continue through winter in the cold regions. The insulating properties of snow cover have an important indirect impact on C fluxes, keeping the ground warmer than the air during winter, thereby maintaining microbial activity and therefore  $R_h$  (Brooks et al., 1997; Brooks and Williams, 1999; Welker et al., 2000; Elberling et al., 2007; Ravn et al., 2020). Through modeling the land surface energy exchanges, the impact of snow on the soil thermal regime can be estimated (Melton et al., 2020). Several studies have demonstrated a correlation between C fluxes and snow depth due to the insulating properties of snow (Björkman et al., 2010; Rogers et al., 2010; Natali et al., 2019). Furthermore, snow density is the main factor controlling snow thermal conductivity (Sturm et al., 1997), which should consequently influence soil temperature, winter CO<sub>2</sub> and CH<sub>4</sub> fluxes.

Estimating snow accumulation in ABRs represents a challenge for microwave remote sensing. Microwaves are par-

**Table 4.** Available snow water equivalent (SWE) products from spaceborne microwave remote sensing.

	GlobSnow <sup>a</sup>	AMSR-E/AMSR2 <sup>b</sup>
Sensor type	Passive	Passive
Spatial resolution	25 km	25 km
Temporal coverage	1980–2018	2002–ongoing
Reference	Luoju et al. (2021)	Tedesco and Jeyaratnam (2016)

<sup>a</sup> GlobSnow v3.0 NH SWE; sensors: SMMR, SSM/I, SSMIS. <sup>b</sup> AMSR-E/AMSR2 Unified L3 Global Daily 25 km EASE-Grid Snow Water Equivalent, Version 1 (AU\_DySno).

tially absorbed and scattered by snow cover, with an additional challenge in the boreal forest because of snow interception by the forest canopy (Li et al., 2019). Active and passive microwaves can retrieve information about the snowpack status based on microwave interaction with the snow microstructure (Picard et al., 2018). Because multiple snowpack characteristics influence microwaves in many ways (i.e., height, density, microstructure, layering, liquid water content), retrieving snowpack characteristics often leads to an underdetermined equation system (i.e., fewer equations than unknowns). During springtime and winter rain-on-snow (ROS) events, wet snow becomes a major limitation for microwave remote sensing. Liquid water absorbs microwave radiation, reducing microwave penetration depth in wet snow and preventing acquisition of information about either the snow or the underlying ground conditions. This is especially problematic for the retrieval of the surface freeze–thaw state during the spring thaw (Rautiainen et al., 2016). However, snowmelt is easily detected (Forster et al., 2001) and can serve as a proxy for the beginning of the growing season and the resulting initiation of C uptake (Pulliainen et al., 2017).

Estimating the snow water equivalent (SWE; i.e., the product of snow depth and density) is widely used to monitor bulk snow cover using microwaves (Chang et al., 1982; Pulliainen, 2006; Shi et al., 2016; Pulliainen et al., 2020; Saberi et al., 2020; Table 4). It should be noted that uncertainties are higher in the presence of vegetation because of the ensuing microwave attenuation (Mortimer et al., 2020) and for deep snow conditions (SWE > 150 mm: Larue et al., 2017).

#### 4 Assimilating microwave data in terrestrial biosphere models in Arctic–boreal regions

Microwave remote sensing has the potential to greatly improve predictions of C fluxes in terrestrial biosphere models. However, the use of key variables obtained from microwave remote sensing to inform terrestrial biosphere models is still limited (Lees et al., 2018). A recent effort assimilates a microwave remote sensing soil moisture data product into a

simple C-cycle model to compute the SMAP L4 global daily 9 km EASE-Grid Carbon Net Ecosystem Exchange product (SPL4CMDL; Jones et al., 2017; Fig. 5). The SPL4CMDL product provides daily NEE, GPP,  $R_h$ , soil organic C and environmental constraints for eight plant functional types at 9 km spatial resolution. The product is publicly available with data starting in 2015. The L4C carbon exchange model estimates GPP using a light-use efficiency model, where  $R_a$  is defined as a fraction of GPP and  $R_h$  is estimated using a soil decomposition model with cascading soil organic C. The GEOS-5 atmospheric model is used for the meteorological inputs, and MODIS visible/infrared products are used for land cover and photosynthetically active radiation. There is ongoing work to improve L4C estimates by integrating surface freeze–thaw state information from microwave remote sensing. The SMAP L4C product is currently the only operational C-exchange model using satellite microwave information, which provides direct information for studying seasonal cycles and long-term trends in ecosystem C exchange. SMOS soil moisture data have similarly been used in terrestrial biosphere models but for a shorter period (2010–2015; Wu et al., 2020). Lastly, the terrestrial C-flux (TCF; Kimball et al., 2009) model used AMSR-E soil moisture and temperature information to provide environmental constraints on  $R_h$  in Arctic–boreal regions (Balocchi et al., 2001; Pastorello et al., 2020). Although limited so far, those examples show the potential of integrating microwave products in terrestrial biosphere models.

#### 5 Challenges and opportunities in microwave remote sensing for supporting carbon cycle science

Although microwave remote sensing data processing is reaching a certain maturity after decades of development, challenges remain in the advancement of microwave data and their assimilation into terrestrial biosphere models (Jones et al., 2017).

##### 5.1 Disentangling the integrated microwave signal

Disentangling the integrated microwave signal originating from varying mixtures of soil, vegetation and snow remains challenging for all microwave remote sensing applications (Kerr et al., 2012; Roy et al., 2012, 2014). Recent advances have been made for both passive and active data to decouple the signal in boreal forests by exploiting multi-polarization, multi-angular and multi-frequency measurements (Larue et al., 2018; Cohen et al., 2019; Konings et al., 2019; Roy et al., 2020). Even in the Arctic biome, where AGB is relatively low, the plot-scale heterogeneity in vegetation composition and structure can pose a challenge since repeated field estimates of vegetation distribution are limited (Myers-Smith et al., 2011; J. Du et al., 2019). Furthermore, the low C fluxes of ABRs can be more challenging to estimate, and vegetation

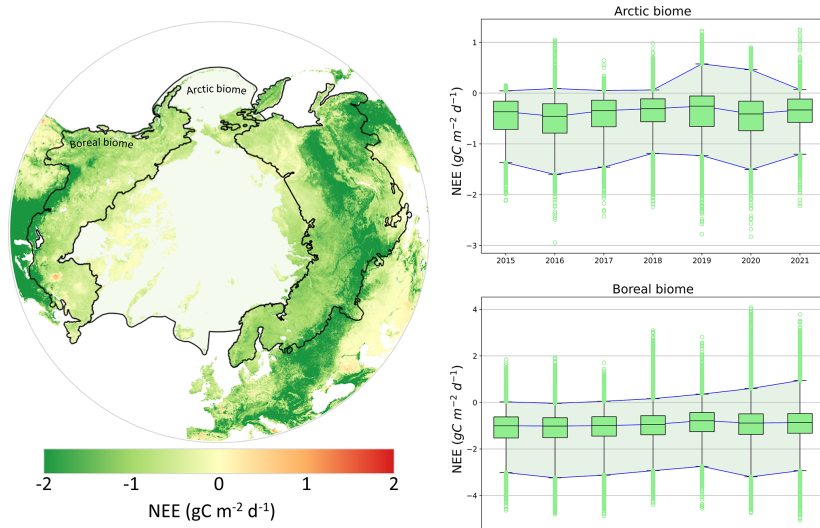


**Figure 5.** Mean monthly net ecosystem exchange (NEE) from the SPL4CMDL for July and August (i.e., peak growing season) between 2015 and 2021. The Arctic biome is delimited following the Conservation of Arctic Flora and Fauna (CAFF) working group of the Arctic Council, and the boreal biome is delineated following Potapov et al. (2008). The yearly mean NEE for the Arctic ( $N_{\text{pixel}} = 282\,288$ ) and boreal regions ( $N_{\text{pixel}} = 187\,003$ ) is presented as boxplots for the 25th–75th percentiles (box) and the 1st–99th percentiles (bracket). SMAP L4C reference: Kimball et al. (2017).

production trends can be lost in interannual variability fluctuations (i.e., low signal-to-noise ratio). The decoupling challenge can be exemplified clearly with the respective effects of soil and vegetation on surface freeze–thaw state detection since soil and vegetation might not freeze or thaw concurrently with implications for detection of surface freeze–thaw events (Roy et al., 2020). Microwave data processing must account for the high density of shallow waterbodies in ABRs, and recent efforts have sought to remove their effect on passive microwave observations in mixed pixels (Touati et al., 2019). These challenges highlight the importance of continued efforts to improve radiative transfer modeling in a way that will allow for the decoupling of the contribution of different components to the microwave signal.

## 5.2 Intra-pixel variability

Due to the coarse spatial resolution of passive microwave data products, intra-pixel variability and downscaling are important considerations. For example, a recent study from Prince et al. (2019) upholds that the time span of the surface freeze–thaw signal transition in passive microwave measurements might be related to the spatial variability of the soil state (frozen or thawed) through this transition (i.e., patchy frozen soil). Intra-pixel variability also includes the partial presence of snow during transition seasons, vegetation type mixing and snow depth distribution (Meloche et al., 2022). A recent study from Du et al. (2022) showed promising results in downscaling soil moisture to 3 m spatial resolution using

machine learning with microwave spaceborne data. Although challenging for subregional studies, the typical passive microwave remote sensing spatial resolution is well suited for regional and global climate studies. Still, most of the terrestrial biosphere model performance evaluation is done using eddy covariance data which are the most trusted and widely used reference for C-flux measurements at large scales. However, the sparsity of the measurement network in ABRs reduces our capacity to represent ABR heterogeneity in the terrestrial biosphere model (Fig. 1; Fisher et al., 2018). However, the scale mismatch between measurements is important to keep in mind; tower-based measurements of C exchanges represent footprints of approximately 1 km or less, which is a much smaller scale than many spaceborne microwave remote sensing data products.

## 5.3 Potential and upcoming spaceborne microwave remote sensing missions

Upcoming spaceborne microwave remote sensing missions will provide new microwave sensors with additional frequencies and generally improved radiometric and spatial resolution (Table 5). These upcoming missions will increase remote sensing capabilities and extend the continuous microwave coverage over the next decade. The technical and scientific advances made through these missions should be seen as an additional motivation to actively identify ways to integrate microwave data products in C-cycle science. Furthermore, the novel approach of the opportunistic use of

**Table 5.** Overview of selected future microwave satellite missions with a polar or nearly polar orbit.

Mission	SMOS-HR	CIMR	Biomass	NISAR	Tandem-L	ROSE-L
Space agency	CNES	ESA (Copernicus program)	ESA	NASA and ISRO	DLR	ESA (Copernicus program)
Frequency (GHz)	L-band	1.4, 6.9, 10.65, 18.7 and 36.5	P-band	L- and P-band	X-band	L-band
Sensor type	Radiometer	Radiometer	SAR	SAR	SAR constellation	SAR
Spatial resolution expected	10 km	5–55 km	200 m	3–10 m	7–100 m	5–10 m
Revisit coverage expected (days)	NA	NA	25–45	12	16	3–6
Main objective	SMOS continuity	AMSR continuity	Biomass	Land elevation (in- cluding biomass)	Biomass, soil mois- ture and permafrost	SWE, soil moisture and permafrost
Expected launch	Development phase	Development phase	2022	2022	2022	Development phase
References	Rodríguez- Fernández et al. (2019a, b)	Kilic et al. (2018)	Le Toan et al. (2011), Schlund et al. (2018), Quegan et al. (2019)	Alvarez-Salazar et al. (2014), Rosen et al. (2015, 2016), Kim et al. (2017)	Bachmann et al. (2016), Huber et al. (2016), Krieger et al. (2016), Moreira et al. (2018)	Pierdicca et al. (2019)

NA – not available.

spaceborne reflectometry of the global navigation satellite system (GNSS) (W. Li et al., 2022; Yu et al., 2022) already showed promising results in evaluating soil moisture (Edokossi et al., 2020), the soil freeze–thaw state (Rautiainen et al., 2022) and snow water equivalent (Royer et al., 2021).

## 6 Conclusions

Microwave remote sensing is an efficient tool for monitoring soil, seasonal snow and vegetation properties affecting water and C-cycle processes and thus has great potential to enhance our understanding of rapidly changing Arctic–boreal regions. Understanding C-cycle processes in Arctic–boreal regions will greatly benefit from an increased use of microwave data, which can only result from expanded collaboration between the microwave remote sensing and C-cycle science communities. The potential applications of satellite-based microwave remote sensing in support of C-cycle science have not been fully realized. We propose four key aspects where increased use of microwave remote sensing could support advances in C-cycle science and monitoring: (1) improve radiative transfer model skills and capabilities and the understanding of microwave signals asso-

ciated with different surface material; (2) improve assimilation approaches of microwave products in terrestrial biosphere models to overcome the challenges associated with remote cold regions where ground observations are spatially and temporally sparse; (3) develop and maintain long-term, spatially distributed, land-based measurement networks in Arctic–boreal regions to improve microwave-based products; and (4) keep a long-term perspective and coherency between space agencies to maintain the historical trends of microwave observations.

## Appendix A

**Table A1.** Microwave radiometers in the 1–100 GHz frequency range on sun-synchronous nearly polar orbits. Instrument specifications from Das and Paul (2015) and specific references.

Mission	SMMR	SSM/I SSMIS	AMSU-A	MSMR	AMSR AMSR-E	WindSat	MWRI	SMOS	Aquarius	AMSR2	SMAP
Temporal coverage	1978 (Oct)– 1987 (Aug)	1987 (Jul)– ongoing	1998 (Aug)– ongoing	1999 (May)– 2001 (Oct)	2002 (Jun)– 2011 (Oct)	2003 (Feb)– ongoing	2008 (May)– ongoing	2010 (Jan)– ongoing	2011 (Aug)– 2015 (June)	2012 (Jul)– ongoing	2015 (Apr)– ongoing
Frequency (GHz)	6.6, 10.7, 18.0, 21.0 and 87.0	19.3, 22.2, 37.0 and 85.5	23.8, 31.4 and 89.0	6.6, 10.65, 18.0 and 21.0	6.925, 10.65, 18.7, 23.8, and 37.0	6.8, 10.7, 18.7, 23.8, and 37.0	10.65, 18.7, 23.8, 36.5 and 89.0	1.4	1.413 (3 of them)	6.925, 10.65, 18.7, 23.8, 36.5 and 89.0	1.41
IFOV (km)	148 × 95 91 × 59 55 × 41 46 × 30 27 × 18	69 × 43 60 × 40 37 × 28 15 × 13	48 × 48	150 × 144 75 × 72 50 × 36 50 × 36	75 × 43 51 × 29 27 × 16 32 × 18	60 × 40 38 × 25 27 × 16 20 × 12	51 × 85 30 × 50 27 × 45 18 × 30	43 × 43 30 × 50 27 × 45 20 × 12	94 × 76 120 × 84 156 × 97	62 × 35 42 × 24 22 × 14	36 × 47
Revisit coverage (days)	2	1	1–29	2	2	8	1	3	7	2	3
Swath width (km)	822	1400	2200	1360	1445	950	1400	1000	390	1450	1000
Platform	Nimbus 7	Defense Meteoro-logical Satellite Program	NOAA-15 to 19; Aqua; MetOp-A, B and C	Oceansat-1 ADEOS II and Aqua (AMSR-E)	Coriolis constella-tion	Feng Yun-3	SMOS	SAC-D	GCOM-W1	SMAP	
Reference	Gloersen and Barath (1977)	Hollinger et al. (1990)	Yang et al. (2013)	Misra et al. (2002)	Kawanishi et al. (2003)	Gaiser et al. (2004)	Xian et al. (2021)	Kerr et al. (2010)	Brucker et al. (2014)	Maeda et al. (2016)	Entekhabi et al. (2010)

**Table A2.** Microwave radar missions.

Mission	Launch date	Mission end	Frequency (GHz)	Band	Spatial resolution (m)	Repeat cycle (days)
JERS-1	1992 (Feb)	1998 (Oct)	1.275	L	18	44
ALOS PALSAR	2006 (Jan)	2011 (May)	1.270	L	10–100	46
ALOS-2 PALSAR-2	2014 (May)	Ongoing	1.270	L	10–100	46
SOACOM-1A	2018 (Oct)	Ongoing	1.275	L	7–100	16
SOACOM-1B	2020 (Oct)	Ongoing	1.275	L	7–100	16
ERS-1	1991 (Jul)	2000 (Mar)	5.3	C	25–100	35
ERS-2	1995 (Apr)	2011 (Jul)	5.3	C	25–100	35
Sentinel-1A	2014 (Apr)	Ongoing	5.405	C	5–40	12
Sentinel-1B	2016 (Apr)	Ongoing	5.405	C	5–40	12
RADARSAT-1	1995 (Nov)	2013 (Mar)	5.3	C	8–100	24
RADARSAT-2	2007 (Dec)	Ongoing	5.405	C	3–100	24
RADARSAT constellation	2019 (Jun)	Ongoing	5.405	C	3–100	12
ASAR Envisat	2002 (Mar)	2012 (May)	5.331	C	30–1000	35
ASCAT constellation	2006 (Oct)	Ongoing	5.255	C	12.5–25 km	29
MetOp-A	2012 (Sep)					
MetOp-B	2018 (Nov)					
MetOp-C						
COSMO-SkyMed constellation	2007 (Jun) 2007 (Dec) 2008 (Oct) 2010 (Nov)	Ongoing	9.6	X	1–100	16
TerraSAR-X	2007 (Jun)	Ongoing	9.65	X	0.5–40	11
TanDEM-X	2010 (Jun)	Ongoing	9.65	X	0.5–40	11
KOMPSAT-5	2018 (Aug)	Ongoing	9.66	X	1–20	28
PAZ	2018 (Feb)	Ongoing	9.65	X	1–15	11
ICEYE constellation	2018 (Dec; 2) 2019 (May; 1) 2019 (Jul; 2) 2020 (Sep; 2) 2021 (Jan; 3) 2021 (Jul; 4)	Ongoing	9.65	X	3	22
NSCAT ADEOS	1996 (Aug)	1997 (Jun)	13.995	$K_u$	25–50 km	41
QuickSCAT	1999 (Jun)	2009 (Nov)	13.46	$K_u$	12.5–25 km	4

### Appendix B: Acronyms and abbreviations

ASAR	Advanced Synthetic Aperture Radar
ASCAT	Advanced SCATterometer
AGB	Aboveground biomass
AMSR	Advanced Microwave Scanning Radiometer
AMSR-E	AMSR for Earth Observing System
CARDAMOM	Carbon data model framework
CCI	Climate Change Initiative
CIMR	Copernicus Imaging Microwave Radiometer
CNES	Centre National d'Études Spatiales
CO <sub>2</sub>	Carbon dioxide
CH <sub>4</sub>	Methane
DLR	German Aerospace Center
<i>e</i>	Soil emissivity
ERS	European Remote Sensing satellites
ESA	European Space Agency
FAO	Food and Agriculture Organization of the United Nations
FW	Freshwater
GEOS-5	Goddard Earth Observing System, Version 5
GNSS	Global navigation satellite system
GPP	Gross primary production
H <sub>2</sub> O	Water
IFOV	Instantaneous field of view
InSAR	SAR interferometry
ISRO	Indian Space Research Organisation
LAI	Leaf area index
Lidar	Light detection and ranging
LST	Land surface temperature
MEaSURES	Making Earth System Data Records for Use in Research Environments
MODIS	Moderate Resolution Imaging Spectroradiometer
MWRI	Micro-Wave Radiation Imager
NASA	National Aeronautics and Space Administration
NDVI	Normalized difference vegetation index
NEE	Net ecosystem exchange
NEP	Net ecosystem production
NISAR	NASA-ISRO SAR mission
NPP	Net primary production
NSCAT	NASA Scatterometer
PALSAR	Phased Array type L-band SAR
PolInSAR	Polarimetric InSAR
QuickSCAT	Quick Scatterometer
<i>R</i> <sub>a</sub>	Autotrophic respiration
<i>R</i> <sub>eco</sub>	Ecosystem respiration
<i>R</i> <sub>h</sub>	Heterotrophic respiration
REP	Red-edge position
ROS	Rain-on-snow events
ROSE-L	Radar Observing System for Europe – L-Band
SAR	Synthetic-aperture radar
SMAP	Soil Moisture Active Passive
SMAP L4C	SMAP Level-4 carbon product
SMMR	Scanning Multichannel Microwave Radiometer
SMOS	Soil Moisture and Ocean Salinity
SMOS-HR	SMOS High-Resolution

SWE	Snow water equivalent
SSM/I	Special Sensor Microwave/Imager
SSMIS	Special Sensor Microwave Imager/Sounder
$T_B$	Brightness temperature
TCF	Terrestrial carbon flux
TomoSAR	SAR tomography
VOD	Vegetation optical depth
$\gamma$	Vegetation attenuation
$\eta$	Light conversion efficiency
$\eta_{\max}$	Light conversion efficiency maximum in optimal conditions
$\varepsilon$	Relative permittivity
$\theta$	Incident angle
$\sigma$	Backscattering coefficient
$\tau$	Optical depth
$\Omega$	Vegetation single-scattering albedo

*Data availability.* The SMAP L4C product used to generate Fig. 5 is available at <https://gmao.gsfc.nasa.gov/pubs/docs/Kimball852.pdf> (Kimball et al., 2017).

*Author contributions.* AM, OS and AR conceptualized the manuscript goal and objectives. AM prepared the manuscript with contributions from all co-authors.

*Competing interests.* The contact author has declared that none of the authors has any competing interests.

*Disclaimer.* Publisher's note: Copernicus Publications remains neutral with regard to jurisdictional claims in published maps and institutional affiliations.

*Acknowledgements.* This work was made possible thanks to a PhD scholarship obtained from the Natural Sciences and Engineering Research Council of Canada (NSERC) and funding obtained from the Fonds Québécois de la Recherche sur la Nature et les Technologies (FQRNT) and the Canadian Space Agency (CSA).

*Financial support.* This research has been supported by the Natural Sciences and Engineering Research Council of Canada (grant no. BESD3-546985-2020) and the Fonds Québécois de la Recherche sur la Nature et les Technologies (grant no. 273500).

*Review statement.* This paper was edited by Kirsten Thonicke and reviewed by two anonymous referees.

## References

- Adams, J., McNairn, H., Berg, A., and Champagne, C.: Evaluation of near-surface soil moisture data from an AAFC monitoring network in Manitoba, Canada: implications for L-band satellite validation, *J. Hydrol.*, 521, 582–592, <https://doi.org/10.1016/j.jhydrol.2014.10.024>, 2015.
- Aires, F., Prigent, C., Rossow, W., and Rothstein, M.: A new neural network approach including first guess for retrieval of atmospheric water vapor, cloud liquid water path, surface temperature, and emissivities over land from satellite microwave observations, *J. Geophys. Res.-Atmos.*, 106, 14887–14907, <https://doi.org/10.1029/2001JD900085>, 2001.
- Al Bitar, A., Mialon, A., Kerr, Y. H., Cabot, F., Richaume, P., Jacquette, E., Quesney, A., Mahmoodi, A., Tarot, S., Parrens, M., Al-Yaari, A., Pellarin, T., Rodriguez-Fernandez, N., and Wigneron, J.-P.: The global SMOS Level 3 daily soil moisture and brightness temperature maps, *Earth Syst. Sci. Data*, 9, 293–315, <https://doi.org/10.5194/essd-9-293-2017>, 2017.
- Alshammari, L., Boyd, D., Sowter, A., Marshall, C., Anderson, R., Gilbert, P., Marsh, S., and Large, D.: Use of Surface Motion Characteristics Determined by InSAR to Assess Peatland Condition, *J. Geophys. Res.-Biogeo.*, 125, 293–315, <https://doi.org/10.1029/2018JG004953>, 2019.
- Alvarez-Salazar, O., Hatch, S., Rocca, J., Rosen, P., Shaffer, S., Shen, Y., Sweetser, T., and Xayapraseuth, P.: Mission design for NISAR repeat-pass Interferometric SAR. Sensors, Systems, and Next-Generation Satellites XVIII, 92410C, 11 November 2014, Amsterdam, the Netherlands, 2014.
- Andresen, C. G., Lawrence, D. M., Wilson, C. J., McGuire, A. D., Koven, C., Schaefer, K., Jafarov, E., Peng, S., Chen, X., Gouttevin, I., Burke, E., Chadburn, S., Ji, D., Chen, G., Hayes, D., and Zhang, W.: Soil moisture and hydrology projections of the permafrost region – a model intercomparison, *The Cryosphere*, 14, 445–459, <https://doi.org/10.5194/tc-14-445-2020>, 2020.
- Angert, A., Biraud, S., Bonfils, C., Henning, C., Buermann, W., Pinzon, J., Tucker, C., and Fung, I.: Drier summers cancel out the CO<sub>2</sub> uptake enhancement induced by warmer springs, *P. Natl. Acad. Sci. USA*, 102, 10823–10827, <https://doi.org/10.1073/pnas.0501647102>, 2005.
- Arslan, A., Mattila, O.-P., Markkanen, T., Böttcher, K., Susiluoto, J., Törmä, M., Lemmetyinen, J., Metsämäki, S., Aurela,

- M., Kervinen, M., Takala, M., Härmä, P., Aalto, T., Laurila, T., and Pulliaisen, J.: SNOWCARBO: Monitoring and assessment of carbon balance related phenomena in Finland and northern Eurasia, 2011 IEEE International Geoscience and Remote Sensing Symposium, Vancouver, BC, Canada, 3206–3209, <https://doi.org/10.1109/IGARSS.2011.6049901>, 2011.
- Attema, E. and Ulaby, F.: Vegetation modeled as a water cloud, *Radio Sci.*, 13, 357–364, <https://doi.org/10.1029/RS013i002p00357>, 1978.
- Bachmann, M., Borla Tridon, D., De Zan, F., Krieger, G., and Zink, M.: Tandem-L observation concept – An acquisition scenario for the global scientific mapping machine, Proceedings of EUSAR 2016: 11th European Conference on Synthetic Aperture Radar, 6–9 June 2016, Hamburg, Germany, 1–5, 2016.
- Baldocchi, D., Falge, E., Gu, L., Olson, R., Hollinger, D., Running, S., Anthoni, P., Bernhofer, C., Davis, K., Evans, R., Fuentes, J., Goldstein, A., Katul, G., Law, B., Lee, X., Malhi, Y., Meyers, T., Munger, W., Oechel, W., Paw U, K., Pilegaard, K., Schmid, H., Valentini, R., Verma, S., Vesala, T., Wilson, K., and Wofsy, S.: FLUXNET: A New Tool to Study the Temporal and Spatial Variability of Ecosystem-Scale Carbon Dioxide, Water Vapor, and Energy Flux Densities, *B. Am. Meteorol. Soc.*, 82, 2415–2434, [https://doi.org/10.1175/1520-0477\(2001\)082<2415:fants>2.3.co;2](https://doi.org/10.1175/1520-0477(2001)082<2415:fants>2.3.co;2), 2001.
- Bamler, R.: Principles of Synthetic Aperture Radar, *Surv. Geophys.*, 21, 147–157, <https://doi.org/10.1023/A:1006790026612>, 2000.
- Bartsch, A., Kidd, R., Pathe, C., Scipal, K., and Wagner, W.: Satellite radar imagery for monitoring inland wetlands in boreal and sub-arctic environments, *Aquat. Conserv.*, 17, 305–317, <https://doi.org/10.1002/aqc.836>, 2007.
- Bartsch, A., Widhalm, B., Kuhr, P., Hugelius, G., Palmtag, J., and Siewert, M. B.: Can C-band synthetic aperture radar be used to estimate soil organic carbon storage in tundra?, *Biogeosciences*, 13, 5453–5470, <https://doi.org/10.5194/bg-13-5453-2016>, 2016.
- Basisit, A., Grody, N., Peterson, T., and Williams, C.: Using the special sensor microwave/imager to monitor land surface temperatures, wetness, and snow cover, *J. Appl. Meteorol. Clim.*, 37, 888–911, [https://doi.org/10.1175/1520-0450\(1998\)037<0888:UTSSMI>2.0.CO;2](https://doi.org/10.1175/1520-0450(1998)037<0888:UTSSMI>2.0.CO;2), 1998.
- Bindlish, R., Jackson, T., Cosh, M., Zhao, T., and O'Neill, P.: Global soil moisture from the Aquarius/SAC-D satellite: description and initial assessment, *IEEE T. Geosci. Remote Sens.*, 12, 923–927, <https://doi.org/10.1109/LGRS.2014.2364151>, 2015.
- Bircher, S., Demontoux, F., Razafindratisima, S., Zakharova, E., Drusch, M., Wigneron, J.-P., and Kerr, Y.: L-Band Relative Permittivity of Organic Soil Surface Layers – A New Dataset of Resonant Cavity Measurements and Model Evaluation, *Remote Sens.*, 8, 1024, <https://doi.org/10.3390/rs8121024>, 2016.
- Björkman, M., Morgner, E., Cooper, E., Elberling, B., Klemedtsdotter, L., and Björk, R.: Winter carbon dioxide effluxes from Arctic ecosystems : An overview and comparison of methodologies, *Glob. Biogeochem. Cy.*, 24, GB3010, <https://doi.org/10.1029/2009GB003667>, 2010.
- Bokhorst, S., Pedersen, S., Brucker, L., Anisimov, O., Bjerke, J., Brown, R., Ehrlich, D., Essery, R., Heilig, A., Ingvander, S., Johansson, C., Johansson, M., Jónsdóttir, I. S., Inga, N., Luojus, K., Macelloni, G., Mariash, H., McLennan, D., Rosqvist, G., Sato, A., Savela, H., Schneebeli, M., Sokolov, A., Sokratov, S., Terzaghi, S., Vikhamar-Schuler, D., Williamson, S., Qiu, Y., and Callaghan, T.: Changing Arctic snow cover: A review of recent developments and assessment of future needs for observations, modeling, and impacts, *Ambio*, 45, 516–537, <https://doi.org/10.1007/s13280-016-0770-0>, 2016.
- Bowling, L., Kane, D., Gieck, R., Hinzman, L., and Lettenmaier, D.: The role of surface storage in a low-gradient Arctic watershed, *Water Resour. Res.*, 39, 1087, <https://doi.org/10.1029/2002WR001466>, 2003.
- Box, J., Colgan, W., Christensen, T. R., Schmidt, N. M., Lund, M., Parmentier, F.-J., Brown, R., Bhatt, U., Euskirchen, E., and Romanovsky, V.: Key indicators of Arctic climate change: 1971–2017, *Environ. Res. Lett.*, 14, 045010, <https://doi.org/10.1088/1748-9326/aaafc1b>, 2019.
- Brooks, P. and Williams, M.: Snowpack controls on nitrogen cycling and export in seasonally snow-covered catchments, *Hydrolog. Process.*, 13, 2177–2190, [https://doi.org/10.1002/\(SICI\)1099-1085\(199910\)13:14/15<2177::AID-HYP850>3.0.CO;2-V](https://doi.org/10.1002/(SICI)1099-1085(199910)13:14/15<2177::AID-HYP850>3.0.CO;2-V), 1999.
- Brooks, P., Schmidt, S., and Williams, M.: Winter production of CO<sub>2</sub> and N<sub>2</sub>O from alpine tundra: Environmental controls and relationship to inter-system C and N fluxes, *Oecologia*, 110, 403–413, <https://doi.org/10.1007/PL00008814>, 1997.
- Brown, J., Ferrians, O., Heginbottom, J., and Melnikov, E.: Circum-Arctic Map of Permafrost and Ground-Ice Conditions, Version 2. Boulder, Colorado USA, NSIDC, National Snow and Ice Data Center [data set], <https://doi.org/10.7265/skbg-kf16>, 2002.
- Brucker, L., Dinnat, E. P., and Koenig, L. S.: Weekly gridded Aquarius L-band radiometer/scatterometer observations and salinity retrievals over the polar regions – Part 1: Product description, *The Cryosphere*, 8, 905–913, <https://doi.org/10.5194/tc-8-905-2014>, 2014.
- Buchwitz, M., Schneising, O., Burrows, J. P., Bovensmann, H., Reuter, M., and Notholt, J.: First direct observation of the atmospheric CO<sub>2</sub> year-to-year increase from space, *Atmos. Chem. Phys.*, 7, 4249–4256, <https://doi.org/10.5194/acp-7-4249-2007>, 2007.
- Callaghan, T., Johannsson, M., Brown, R., Groisman, P., Labba, N., Radionov, V., Bradley, R., Blangy, S., Bulygina, O., Christensen, T., Colman, J., Essery, R., Forbes, B., Forchhammer, M., Golubev, V., Honrath, R., Juday, G., Meshcherskaya, A., Phoenix, G., Pomeroy, J., Rautio, A., Robinson, D., Schmidt, N., Serreze, M., Shevchenko, V., Shiklomanov, A., Shmakin, A., Sköld, P., Sturm, M., Woo, M., Woodruff, E.: Multiple effects of changes in Arctic snow cover, *Ambio*, 40, 32–45, <https://doi.org/10.1007/s13280-011-0213-x>, 2011.
- Carreira, J., Quegan, S., Le Toan, T., Ho Tong Minh, D., Saatchi, S., Carvalhais, N., Reichstein, M., and Scipal, K.: Coverage of high biomass forests by the ESA BIOMASS mission under defense restrictions, *Remote Sens. Environ.*, 196, 154–162, <https://doi.org/10.1016/j.rse.2017.05.003>, 2017.
- Chan, S., Bindlish, R., O'Neill, P., Njoku, E., Jackson, T., Collander, A., Chen, F., Burgin, M., Dunbar, S., Piepmeier, J., Yueh, S., Entekhabi, D., Cosh, M., Caldwell, T., Walker, J., Berg, A., Rowlandson, T., Pacheco, A., McNairn, H., Thibeault, M., Martinez-Fernández, J., González-Zamora, A., Bosch, D., Starks, P., Goodrich, D., Prueger, J., Palecki, M., Small, E., Zreda, M., Calvet, J., Crow, W., and Kerr, Y.: Assessment of the SMAP passive soil moisture product, *IEEE T. Geosci. Remote*, 54, 4994–5007, <https://doi.org/10.1109/TGRS.2016.2561938>, 2016.

- Chan, S., Bindlish, R., O'Neill, P., Jackson, T., Njoku, E., Dunbar, S., Chaubell, J., Piepmeier, J., Yueh, S., Entekhabi, D., Colliander, A., Chen, F., Cosh, M., Caldwell, T., Walker, J., Berg, A., McNairn, H., Thibeault, M., Martinez- Fernández, J., Uldall, F., Seyfried, M., Bosch, D., Starks, P., Collins, C., Prueger, J., Van der Velde, R., Asanuma, J., Palecki, M., Small, E., Zreda, M., Calvet, J., Crow, W., and Kerr, Y.: Development and assessment of the SMAP enhanced passive soil moisture product. *Remote Sens. Environ.*, 204, 931–941, <https://doi.org/10.1016/j.rse.2017.08.025>, 2018.
- Chang, A., Foster, J., Hall, D., Rango, A., and Hartline, B.: Snow water equivalent estimation by microwave radiometry, *Cold Reg. Sci. Technol.*, 5, 259–267, <https://doi.org/10.1016/j.coldregions.2011.10.014>, 1982.
- Chapin III, F., Woodwell, G., Randerson, J., Rastetter, E., Lovett, G., Baldocchi, D., Clark, D., Harmon, M., Schimel, D., Valentini, R., Wirth, C., Aber, J., Cole, J., Goulden, M., Harden, J., Heimann, M., Howarth, R., Matson, P., McGuire, A., Melillo, J., Mooney, H., Neff, J., Houghton, R., Pace, M., Ryan, M., Running, S., Sala, O., Schlesinger, W., and Schulze, E.-D.: Reconciling carbon-cycle concepts, terminology, and methods, *Ecosystems*, 9, 1041–1050, <https://doi.org/10.1007/s10021-005-0105-7>, 2006.
- Chen, X., Liu, L., and Bartsch, A.: Detecting soil freeze/thaw onsets in Alaska using SMAP and ASCAT data, *Remote Sens. Environ.*, 220, 59–70, <https://doi.org/10.1016/j.rse.2018.10.010>, 2019.
- Chirici, G., Chiesi, M., Corona, P., Salvati, R., Papale, D., Fibbi, L., Sirca, C., Spano, D., Duce, P., Marras, S., Matteucci, G., Cescatti, A., and Maselli, F.: Estimating daily forest carbon fluxes using a combination of ground and remotely sensed data, *J. Geophys. Res.-Biogeosci.*, 121, 266–279, <https://doi.org/10.1002/2015JG003019>, 2016.
- Ciais, P., Tan, J., Wang, X., Roedenbeck, C., Chevallier, F., Piao, S.-L., Moriarty, R., Broquet, G., Le Quéré, C., Canadell, J., Peng, S., Poulter, B., Liu, Z., and Tans, P.: Five decades of northern land carbon uptake revealed by the interhemispheric CO<sub>2</sub> gradient, *Nature*, 568, 221–225, <https://doi.org/10.1038/s41586-019-1078-6>, 2019.
- Cohen, J., Rautiainen, K., Ikonen, J., Lemmetyinen, J., Smolander, T., Vehviläinen, J., and Pulliainen, J.: A modeling-based approach for soil frost detection in the northern boreal forest region with C-Band SAR, *IEEE T. Geosci. Remote*, 57, 1069–1083, <https://doi.org/10.1109/TGRS.2018.2864635>, 2019.
- Colliander, A., Jackson, T., Bindlish, R., Chan, S., Das, N., Kim, S., Cosh, M., Dunbar, R., Dang, L., Pashaian, L., Asanuma, J., Aida, K., Berg, A., Rowlandson, T., Bosch, D., Caldwell, T., Taylor, K., Goodrich, D., Al Jassar, H., Lopez-Baeza, E., Martínez Fernández, J., González-Zamora, A., Livingston, S., McNairn, H., Pacheco, A., Moghaddam, M., Montzka, C., Notarnicola, C., Niedrist, G., Pellarin, T., Prueger, J., Pulliainen, J., Rautiainen, K., Ramos, J., Seyfried, M., Starks, P., Su, Z., Zeng, Y., van der Velde, R., Thibeault, M., Dorigo, W., Vreugdenhil, M., Walker, J., P., Wu, X., Monerris, A., O'Neill, P. E., Entekhabi, D., Njoku, E. G., Yueh, S.: Validation of SMAP surface soil moisture products with core validation sites, *Remote Sens. Environ.*, 191, 215–231, <https://doi.org/10.1016/j.rse.2017.01.021>, 2017.
- Colliander, A., Reichle, R., Crow, W., Cosh, M., Chen, F., Chan, S., Das, N., Bindlish, R., Chaubell, J., Kim, S., Liu, Q., O'Neill, P., Dunbar, R. S., Dang, L., Kimball, J., Jackson, T., Al-Jassar, H., Asanuma, J., Bhattacharya, B., Berg, A., Bosch, D., Bourgeau-Chevez, L., Caldwell, T., Calvert, J.-C., Collins, C. H., Jenson, K., Livingston, S., Lopez-Baeza, E., Martínez-Fernández, J., McNairn, H., Moghaddam, M., Montzka, C., Notarnicola, C., Pellarin, T., Greimeister-Pfeil, I., Pulliainen, J., Gpe, J., Hernández, R., Seyfried, M., Starks, P., Su, Z., van der Velde, R., Zeng, Y., Thibeault, M., Vreugdenhil, M., Walker, J., Zribi, M., Entekhabi, D., and Yueh, S.: Validation of soil moisture data products from the NASA SMAP mission, *IEEE J. Sel. Top. Appl.*, 15, 364–392, <https://doi.org/10.1109/JSTARS.2021.3124743>, 2022.
- Cui, Q., Shi, J., Du, J., Zhao, T., and Xiong, C.: An approach for monitoring global vegetation based on multiangular observations from SMOS, *IEEE J. Sel. Top. Appl.*, 8, 604–616, <https://doi.org/10.1109/JSTARS.2015.2388698>, 2015.
- Das, B., Bordoloi, R., Deka, S., Paul, A., Pandey, P. K., Singha, L. B., Tripathi, O. P., Mishra, B. P., and Mishra, M.: Above ground biomass carbon assessment using field, satellite data and model based integrated approach to predict the carbon sequestration potential of major land use sector of Arunachal Himalaya, India, *Carbon Manag.*, 12, 201–214, <https://doi.org/10.1080/17583004.2021.1899753>, 2021.
- Das, K., and Paul, P.: Present status of soil moisture estimation by microwave, *Remote Sens.*, *Cogent Geoscience*, 1, 1084669, <https://doi.org/10.1080/23312041.2015.1084669>, 2015.
- Das, N., Entekhabi, D., Kim, S., Yueh, S., Dunbar, R. S., and Colliander, A.: SMAP/Sentinel-1 L2 Radiometer/Radar 30-Second Scene 3 km EASE-Grid Soil Moisture, Version 1. Boulder, Colorado USA, NASA National Snow and Ice Data Center Distributed Active Archive Center [data set], <https://doi.org/10.5067/9UWR1WTHW1WN>, 2017.
- Derkens, C., Xu, X., Scott Dunbar, R., Colliander, A., Kim, Y., Kimball, J. S., Black, T. A., Euskirchen, E., Langlois, A., Loranty, M. M., Marsh, P., Rautiainen, K., Roy, A., Royer, A., and Stephens, J.: Retrieving landscape freeze/thaw state from Soil Moisture Active Passive (SMAP) radar and radiometer measurements, *Remote Sens. Environ.*, 194, 48–62, <https://doi.org/10.1016/j.rse.2017.03.007>, 2017.
- Derkens, C., Burgess, D., Duguay, C., Howell, S., Mudryk, L., Smith, S., Thackeray, C., and Kirchmeier-Young, M.: Changes in snow, ice, and permafrost across Canada. Canada's Changing Climate Report – Chap. 5, Government of Canada, Ottawa, Ontario, Canada, 194–260, 2019.
- Dimitrov, D. D., Lafleur, P., Sonnenntag, O., Talbot, J., and Quinton, W. L.: Hydrology of peat estimated from near-surface water contents, *Hydrolog. Sci. J.*, 67, 1702–1721, 2022.
- Dobson, M., Ulaby, F., Hallikainen, M., and El-Rayes, M.: Microwave dielectric behavior of wet soil – Part II: Dielectric mixing models, *IEEE T. Geosci. Remote Sens.*, 23, 35–46, <https://doi.org/10.1109/TGRS.1985.289498>, 1985.
- Dobson, M., Ulaby, F., and Pierce, L.: Land-cover classification and estimation of terrain attributes using synthetic aperture radar, *Remote Sens. Environ.*, 51, 199–214, [https://doi.org/10.1016/0034-4257\(94\)00075-X](https://doi.org/10.1016/0034-4257(94)00075-X), 1995.
- Dolant, C., Langlois, A., Brucker, L., Royer, A., Roy, A., and Montpetit, B. L.: Meteorological inventory of rain-on-snow events in the Canadian Arctic Archipelago and satellite detection assessment using passive microwave data, *Phys. Geogr.*, 39, 428–444, <https://doi.org/10.1080/02723646.2017.1400339>, 2018.

- Dou, Y., Tian, F., Wigneron, J. P., Tagesson, T., Du, J., Brandt, M., Liu, Y., Zou, L., Kimball, J. S., and Fensholt, R.: Reliability of using vegetation optical depth for estimating decadal and inter-annual carbon dynamics, *Remote Sens. Environ.*, 285, 113390, <https://doi.org/10.1016/j.rse.2022.113390>, 2023.
- Du, J., Kimball, J. S., Jones, L. A., Kim, Y., Glassy, J., and Watts, J. D.: A global satellite environmental data record derived from AMSR-E and AMSR2 microwave Earth observations, *Earth Syst. Sci. Data*, 9, 791–808, <https://doi.org/10.5194/essd-9-791-2017>, 2017.
- Du, J., Watts, J., Jiang, L., Lu, H., Cheng, X., Duguay, C., Farina, M., Qiu, Y., Kim, Y., Kimball, J., and Tarolli, P.: Remote sensing of environmental changes in cold regions: methods, achievements and challenges, *Remote Sens.*, 11, 1952, <https://doi.org/10.3390/rs11161952>, 2019.
- Du, J., Kimball, J. S., Bindlish, R., Walker, J. P., and Watts, J. D.: Local Scale (3-m) Soil Moisture Mapping Using SMAP and Planet SuperDove, *Remote Sens.*, 14, 3812, <https://doi.org/10.3390/rs14153812>, 2022.
- Du, S., Liu, L., Liu, X., Guo, J., Hu, J., Wang, S., and Zhang, Y.: SIFSpec: Measuring solar-induced chlorophyll fluorescence observations for remote sensing of photosynthesis, *Sensors*, 19, 3009, <https://doi.org/10.3390/s19133009>, 2019.
- Dubock, D., Spoto, F., Simpson, J., Spencer, D., Schutte, E., and Sontag, H.: The Envisat satellite and its integration, *ESA Bull.*, 106, 26–45, 2001.
- Duan, S.-B., Han, X.-J., Huang, C., Li, Z.-L., Wu, H., Qian, Y., Gao, M., Leng, P.: Land surface temperature retrieval from passive microwave satellite observations: state-of-the-art and future directions, *Remote Sens.*, 12, 2573, <https://doi.org/10.3390/rs12162573>, 2020.
- Edokossi, K., Calabia, A., Jin, S., and Molina, I.: GNSS-Reflectometry and Remote Sensing of Soil Moisture: A Review of Measurement Techniques, Methods, and Applications, *Remote Sens.*, 12, 614, <https://doi.org/10.3390/rs12040614>, 2020.
- El-Amine, M., Roy, A., Koebisch, F., Baltzer, J., Barr, A., Black, A., Ikawa, H., Iwata, H., Kobayashi, H., Ueyama, M., and Sonnenntag, O.: What explains the year-to-year variation in the start and end of the photosynthetic growing season of boreal black spruceforests?, *Agr. Forest Meteorol.*, 324, 109113, <https://doi.org/10.1016/j.agrformet.2022.109113>, 2022.
- Elberling, B.: Annual soil CO<sub>2</sub> effluxes in the High Arctic: The role of snow thickness and vegetation type, *Soil Biol. Biochem.*, 39, 646–654, <https://doi.org/10.1016/j.soilbio.2006.09.017>, 2007.
- El Hajj, M., Baghdadi, N., Zribi, M., and Bazzi, H.: Synergic Use of Sentinel-1 and Sentinel-2 Images for operational soil moisture mapping at high spatial resolution over agricultural areas, *Remote Sens.*, 9, 1292, <https://doi.org/10.3390/rs9121292>, 2017.
- El-Rayes, M. and Ulaby, F.: Microwave dielectric spectrum of vegetation-Part I: Experimental observations, *IEEE T. Geosci. Remote.*, 25, 541–549, <https://doi.org/10.1109/TGRS.1987.289832>, 1987.
- Engman, E.: Applications of microwave remote sensing of soil moisture for water resources and agriculture, *Remote Sens. Environ.*, 35, 213-2-26, [https://doi.org/10.1016/0034-4257\(91\)90013-V](https://doi.org/10.1016/0034-4257(91)90013-V), 1991.
- Entekhabi, D., Njoku, E., O’Neill, P., Kellogg, K., Crow, W., Edelstein, W., Entin, J., Goodman, S., Jackson, T., Jackson, J., Kimball, J., Piepmeyer, J., Koster, R., Martin, N., McDonald, K., Moghaddam, M., Moran, S., Reichle, R., Shi, J., Spencer, M., Thurman, S., Tsang, L., and Van Zyl, J.: The Soil Moisture Active Passive (SMAP) mission, *P. IEEE*, 98, 704–716, <https://doi.org/10.1109/JPROC.2010.2043918>, 2010.
- Euskirchen, E., McGuire, A., Kicklighter, D., Zhuang, Q., Clein, J., Dargaville, R., Dye, D., Kimball, J., McDonald, K., Melilli, J., Romanovsky, V., and Smith, N.: Importance of recent shifts in soil thermal dynamics on growing season length, productivity, and carbon sequestration in terrestrial high-latitude ecosystems, *Glob. Change Biol.*, 12, 731–750, <https://doi.org/10.1111/j.1365-2486.2006.01113.x>, 2006.
- Fahnstock, J., Jones, M., Brooks, P., Walker, D., and Welker, J.: Winter and early spring CO<sub>2</sub> efflux from tundra communities of northern Alaska, *J. Geophys. Res.*, 103, 29023–29027, <https://doi.org/10.1029/98JD00805>, 1998.
- Fahnstock, J., Jones, M., and Welker, J.: Wintertime CO<sub>2</sub> efflux from arctic soils: implications for annual carbon budgets, *Glob. Biogeochem. Cy.*, 13, 775–779, <https://doi.org/10.1029/1999gb900006>, 1999.
- FAO – Food and Agriculture Organization of the United Nations: Global forest resources assessment 2000: main report, FAO Forestry Paper 140, United Nations, Rome, Italy, 479 pp., <https://www.fao.org/3/Y1997E/Y1997E00.htm> (last access: 16 July 2023), 2001.
- Figa-Saldafia, J., Wilson, J., Attema, E., Gelsthorpe, R., Drinkwater, M., and Stoffelen, A.: The advanced scatterometer (ASCAT) on the meteorological operational (MetOp) platform: A follow on for European wind scatterometers, *Can. J. Remote Sens.*, 28, 404–412, <https://doi.org/10.5589/m02-035>, 2002.
- Fily, M., Royer, A., Goita, K., and Prigent, C.: A simple retrieval method for land surface temperature and fraction of water surface determination from satellite microwave brightness temperatures in sub-arctic areas, *Remote Sens. Environ.*, 85, 328–338, [https://doi.org/10.1016/S0034-4257\(03\)00011-7](https://doi.org/10.1016/S0034-4257(03)00011-7), 2003.
- Fisher, J., Hayes, D., Schwalm, C., Huntzinger, D., Stofferahn, E., Schaefer, K., Luo, Y., Wullschleger, S., Goetz, S., Miller, C., Griffith, P., Chadburn, S., Chatterjee, A., Ciais, P., Douglas, T., Genet, H., Ito, A., Neigh, C., Poultre, B., Rogers, B., Sonnenntag, O., Tian, H., Wang, W., Xue, Y., Yang, Z.-L., Zeng, N., and Zhang, Z.: Missing pieces to modeling the Arctic-Boreal puzzle, *Environ. Res. Lett.*, 13, 020202, <https://doi.org/10.1088/1748-9326/aa9d9a>, 2018.
- Forster, R., Long, D., Jezel, K., Brobot, S., and Anderson, M.: The onset of Arctic sea-ice snowmelt as detected with passive- and active-microwave, *Ann. Glaciol.*, 33, 85–93, <https://doi.org/10.3189/172756401781818428>, 2001.
- Foster, A. C., Shuman, J. K., Rogers, B. M., Walker, X. J., Mack, M. C., Bourgeau-Chavez, L. L., Veraverbeke, S., and Goetz, S. J.: Bottom-up drivers of future fire regimes in western boreal North America, *Environ. Res. Lett.*, 17, 025006, <https://doi.org/10.1088/1748-9326/ac4c1e>, 2022.
- Frolking, S., Goulden, M., Wofsy, S., Fan, S.-M., Sutton, D., Munger, J., Bazzaz, A., Daube, B., Crill, P., Aber, J., Band, L., Wang, X., Savage, K., Moore, T., and Harriss, R.: Modeling temporal variability in the carbon balance of a spruce/moss boreal forest, *Glob. Change Biol.*, 2, 343–366, <https://doi.org/10.1111/j.1365-2486.1996.tb00086.x>, 1996.
- Fu, Z., Stoy, P., Luo, Y., Chen, J., Sun, J., Montagnani, L., Wohlfahrt, G., Rahman, A., Rambal, S., Bernhofer, C., Wang,

- J., Shirkey, G., and Niu, S.: Climate controls over the net carbon uptake period and amplitude of net ecosystem production in temperate and boreal ecosystems., *Agr. Forest Meteorol.*, 243, 9–18, <https://doi.org/10.1016/j.agrformet.2017.05.009>, 2017.
- Gaiser, P., St. Germain, K., Twarog, E., Poe, G., Purdy, W., Richardson, D., Grossman, W., Jones, W., L., Spencer, D., Golba, G., Cleveland, J., Choy, L., Bevilacqua, R., and Chang, P.: The WindSat spaceborne polarimetric microwave radiometer: sensor description and early orbit performance, *IEEE T. Geosci. Remote Sens.*, 42, 2347–2361, <https://doi.org/10.1109/TGRS.2004.836867>, 2004.
- Gasser, T., Crepin, L., Quilcaille, Y., Houghton, R. A., Ciais, P., and Obersteiner, M.: Historical CO<sub>2</sub> emissions from land use and land cover change and their uncertainty, *Biogeosciences*, 17, 4075–4101, <https://doi.org/10.5194/bg-17-4075-2020>, 2020.
- Gauthier, S., Bernier, P., Kuuluvainen, T., Shvidenko, A., and Schepaschenko, D.: Boreal forest health and global change, *Science*, 349, 819–822, <https://doi.org/10.1126/science.aaa9092>, 2015.
- Gloersen, P. and Barath, F.: A scanning multichannel microwave radiometer for Nimbus-G and SeaSat-A, *IEEE J. Ocean. Eng.*, 2, 172–178, <https://doi.org/10.1109/JOE.1977.1145331>, 1977.
- Gough, C. M.: Terrestrial primary production: Fuel for life, *Nat. Educ. Knowl.*, 3, p. 28, 2011.
- Grasso, M., Renga, A., Fasano, G., Graziano, M., Grassi, M., and Moccia, A.: Design of an end-to-end demonstration mission of a Formation-Flying Synthetic Aperture Radar (FF-SAR) based on microsatellites, *Adv. Space Res.*, 67, 3909–3923, <https://doi.org/10.1016/j.asr.2020.05.051>, 2021.
- Grosse, G., Harden, J., Turetsky, M., McGuire, D., Camill, P., Tarnocai, C., Frolking, S., Schuur, E., Jorgenson, T., Marchenko, S., Romanovsky, V., Wickland, K., French, N., Waldrop, M., Bourgeau-Chavez, L., and Striegl, R.: Vulnerability of high-latitude soil organic carbon in North America to disturbance, *J. Geophys. Res.*, 116, G00K06, <https://doi.org/10.1029/2010JG001507>, 2011.
- Gruber, A., Scanlon, T., van der Schalie, R., Wagner, W., and Dorigo, W.: Evolution of the ESA CCI Soil Moisture climate data records and their underlying merging methodology, *Earth Syst. Sci. Data*, 11, 717–739, <https://doi.org/10.5194/essd-11-717-2019>, 2019.
- Harrison, J., Sanders-DeMott, R., Reinmann, A., Sorensen, P., Phillips, N., and Templer, P.: Growing-season warming and winter soil freeze/thaw cycles increase transpiration in a northern hardwood forest, *Ecology*, 101, e03173, <https://doi.org/10.1002/ecy.3173>, 2020.
- Hayes, J., McGuire, A., Kicklighter, D., Gurney, K., Burnside, T., and Melillo, J.: Is the northern high-latitude land-based CO<sub>2</sub> sink weakening?, *Glob. Biogeochem. Cy.*, 25, GB3018, <https://doi.org/10.1029/2010GB003813>, 2011.
- Hollinger, J., Pearce, J., and Poe, G.: SSM/I instrument evaluation, *IEEE T. Geosci. Remote Sens.*, 28, 781–790, <https://doi.org/10.1109/36.58964>, 1990.
- Holtzman, N. M., Anderegg, L. D. L., Kraatz, S., Mavrovic, A., Sonnentag, O., Pappas, C., Cosh, M. H., Langlois, A., Lakhankar, T., Tesser, D., Steiner, N., Colliander, A., Roy, A., and Konings, A. G.: L-band vegetation optical depth as an indicator of plant water potential in a temperate deciduous forest stand, *Biogeosciences*, 18, 739–753, <https://doi.org/10.5194/bg-18-739-2021>, 2021.
- Hori, M., Sugiura, K., Kobayashi, K., Aoki, T., Tanikawa, T., Kuchiki, K., Niwano, M., and Enomoto, H.: A 38-year (1978–2015) Northern Hemisphere daily snow cover extent product derived using consistent objective criteria from satellite-borne optical sensors, *Remote Sens. Environ.*, 191, 402–418, <https://doi.org/10.1016/j.rse.2017.01.023>, 2017.
- Houghton, R.: Aboveground Forest Biomass and the Global Carbon Balance, *Glob. Change Biol.*, 11, 945–958, <https://doi.org/10.1111/j.1365-2486.2005.00955.x>, 2005.
- Huang, H., Tsang, L., Njoku, E., Colliander, A., Liao, T.-H., and Ding, K.-H.: Propagation and Scattering by a Layer of Randomly Distributed Dielectric Cylinders Using Monte Carlo Simulations of 3D Maxwell Equations With Applications in Microwave Interactions With Vegetation, *IEEE Access*, 5, 11985–12003, <https://doi.org/10.1109/ACCESS.2017.2714620>, 2017.
- Huber, S., Villano, M., Younis, M., Krieger, G., Moreira, A., Grafmueller, B., and Wolters, R.: Tandem-L: Design Concepts for a Next-Generation Spaceborne SAR System, in: *Proceedings of the EUSAR 2016: 11th European Conference on Synthetic Aperture Radar*, 6–9 June 2016, Hamburg, Germany, 1–5, 2016.
- Huntzinger, D., Schaefter, K., Schwalm, C., Fisher, J., Hayes, D., Stofferahn, E., Carey, J., Michalak, A., Wei, Y., Jain, A., Kolus, H., Mao, J., Poulter, B., Shi, X., Tang, J., and Tian, H.: Evaluation of simulated soil carbon dynamics in Arctic-Boreal ecosystems, *Environ. Res. Lett.*, 15, 025005, <https://doi.org/10.1088/1748-9326/ab6784>, 2020.
- IPCC (Intergovernmental Panel on Climate Change): Special Report on the Ocean and Cryosphere in a Changing Climate, edited by: Pörtner, H.-O. Roberts, D., Masson Delmotte, V., Zhai, P., Tignor, M., Poloczanska, E., Mintenbeck, K., Alegría, A., Nicolai, M., Okem, A., Petzold, J., Rama, B., and Weyer, N., Cambridge University Press, Cambridge, UK and New York, NY, USA, 755 pp., <https://doi.org/10.1017/9781009157964>, 2019.
- Jackson, T. and Schmugge, T.: Vegetation effects on the microwave emission of soils, *Remote Sens. Environ.*, 36, 203–212, [https://doi.org/10.1016/0034-4257\(91\)90057-D](https://doi.org/10.1016/0034-4257(91)90057-D), 1991.
- Jarvis, P. and Linder, S.: Constraints to growth of boreal forests, *Nature*, 405, 904–905, <https://doi.org/10.1038/35016154>, 2000.
- Jenson, J.: *Remote sensing of the Environment: An Earth Resource Perspective*, 2nd Edn., Pearson Prentice Hall, Upper Saddle River, New Jersey, United States, 656 pp., ISBN 978-1-29202-170-6, 2006.
- Jiménez-Muñoz, G. and Sobrino, J.: Error sources on the land surface temperature retrieved from thermal infrared single channel remote sensing data, *Int. J. Remote Sens.*, 27, 999–1014, <https://doi.org/10.1080/01431160500075907>, 2006.
- Jones, L., Kimball, J., McDonald, K., Chan, S., Njoku, E., and Oechel, W.: Satellite microwave remote sensing of boreal and Arctic soil temperatures from AMSR-E, *IEEE T. Geosci. Remote Sens.*, 45, 2004–2018, <https://doi.org/10.1109/TGRS.2007.898436>, 2007.
- Jones, L., Kimball, J., Reichle, R., Madani, N., Glassy, J., Ardizzone, J., Colliander, A., Cleverly, J., Desai, A., Eamus, D., Euksirchen, E., Hutley, L., Macfarlane, C., and Scott, R.: The SMAP Level 4 Carbon Product for Monitoring Ecosystem Land-Atmosphere CO<sub>2</sub> Exchange, *IEEE T. Geosci. Remote Sens.*, 55, 6517–6532, <https://doi.org/10.1109/TGRS.2017.2729343>, 2017.

- Jones, L. A., Ferguson, C. R., Kimball, J. S., Zhang, K., Chan, S. T. K., McDonald, K. C., Njoku, E. G., and Wood, E. F.: Satellite Microwave Remote Sensing of Daily Land Surface Air Temperature Minima and Maxima From AMSR-E, *IEEE J. Sel. Top. Appl.*, 3, 111–123, <https://doi.org/10.1109/jstars.2010.2041530>, 2010.
- Jones, M., Jones, L., Kimball, J., and McDonald, K.: Satellite passive microwave remote sensing for monitoring global land surface phenology, *Remote Sens. Environ.*, 115, 1102–1114, <https://doi.org/10.1016/j.rse.2010.12.015>, 2011.
- Kawanishi, T., Sezai, T., Ito, Y., Imaoka, K., Takashima, T., Ishido, Y., Shibata, A., Miura, M., Inahata, H., and Spencer, R.: The advanced scanning microwave radiometer for the Earth Observing System (AMSR-E): NASDA's contribution to the EOS for global energy and water cycle studies, *IEEE T. Geosci. Remote Sens.*, 41, 184–194, <https://doi.org/10.1109/TGRS.2002.808331>, 2003.
- Kerr, Y., Waldteufel, P., Wigneron, J.-P., Delwart, S., Cabot, F., Boutin, J., Escorihuela, M., Font, J., Reul, N., Gruhier, C., and Juglea, S.: The SMOS mission: New tool for monitoring key elements of the global water cycle, *IEEE T. Geosci. Remote*, 98, 666–687, <https://doi.org/10.1109/JPROC.2010.2043032>, 2010.
- Kerr, Y., Waldteufel, P., Richaume, P., Wigneron, J., Ferrazzoli, P., Mahmoodi, A., Al Bitar, A., Cabot, F., Gruhier, C., Juglea, S., Leroux, D., Mialon, A., and Delwart, S.: The SMOS soil moisture retrieval algorithm, *IEEE T. Geosci. Remote. Sens.*, 50, 1384–1403, <https://doi.org/10.1109/TGRS.2012.2184548>, 2012.
- Kilic, L., Prigent, C., Aires, F., Boutin, J., Heygster, G., Tonboe, R., Roquet, H., Jimenez, C., and Donlon, C.: Expected Performances of the Copernicus Imaging Microwave Radiometer (CIMR) for an All-Weather and High Spatial Resolution Estimation of Ocean and Sea Ice Parameters, *J. Geophys. Res.-Oceans*, 123, 7564–7580, <https://doi.org/10.1029/2018JC014408>, 2018.
- Kim, S.-B., van Zyl, J., Johnson, J., Moghaddam, M., Tsang, L., Colliander, A., Dunbar, R., Jackson, T., Jaruwananadilok, S., West, R., Berg, A., Caldwell, T., Cosh, M., Goodrich, D., Livingston, S., López-Baeza, E., Rowlandson, T., Thibeault, M., Walker, J., Entekhabi, D., Njoku, E., O'Neill, P., and Yueh, S.: Surface Soil Moisture Retrieval Using the L-Band Synthetic Aperture Radar Onboard the Soil Moisture Active-Passive Satellite and Evaluation at Core Validation Sites, *IEEE T. Geosci. Remote Sens.*, 55, 1897–1914, <https://doi.org/10.1109/TGRS.2016.2631126>, 2017.
- Kim, Y., Kimball, J., Zhang, K., and McDonald, K.: Satellite detection of increasing Northern Hemisphere non-frozen seasons from 1979 to 2008: Implications for regional vegetation growth, *Remote Sens. Environ.*, 121, 472–487, <https://doi.org/10.1016/j.rse.2012.02.014>, 2012.
- Kim, Y., Kimball, J., Xu, X., Dunbar, S., Colliander, A., and Derksen, C.: Global Assessment of the SMAP Freeze/Thaw Data Record and Regional Applications for Detecting Spring Onset and Frost Events, *Remote Sens.*, 11, 1317, <https://doi.org/10.3390/rs11111317>, 2019.
- Kimball, J., McDonald, K., Keyser, A. R., Frolking, S., and Running, S.: Application of the NASA Scatterometer (NSCAT) for determining the Daily Frozen and Nonfrozen Landscape of Alaska, *Remote Sens. Environ.*, 75, 113–126, [https://doi.org/10.1016/S0034-4257\(00\)00160-7](https://doi.org/10.1016/S0034-4257(00)00160-7), 2001.
- Kimball, J., Zhao, M., McDonald, K., Heinsch, F. A., and Running, S.: Satellite observations of annual variability in terrestrial carbon cycles and seasonal growing seasons at high northern latitudes, *Proc. Spie, Microwave Remote Sensing of the Atmosphere and Environment IV*, 5654, <https://doi.org/10.1117/12.578815>, 2004a.
- Kimball, J., McDonald, K., Running, S., and Frolking, S.: Satellite radar Remote sensing of seasonal growing seasons for boreal and subalpine evergreen forests, *Remote Sens. Environ.*, 90, 243–258, <https://doi.org/10.1016/j.rse.2004.01.002>, 2004b.
- Kimball, J., Jones, L., Zhang, K., Heinsch, F. A., McDonald, K., and Oechel, W.: A Satellite Approach to Estimate Land-Atmosphere CO<sub>2</sub> Exchange for Boreal and Arctic Biomes Using MODIS and AMSR-E, *IEEE T. Geosci. Remote Sens.*, 47, 569–587, <https://doi.org/10.1109/TGRS.2008.2003248>, 2009.
- Kimball, J., Jones, L., Glassy, J., Stavros, N., Madani, N., Reichle, R., Jackson, T., and Colliander, A.: Soil Moisture Active Passive Mission L4\_C Data Product Assessment (Version 2 Validated Release), MAO Office Note No. 13 (Version 1.0), NASA Goddard Space Flight Center, Greenbelt, Maryland, United States, 37 pp., <https://gmao.gsfc.nasa.gov/pubs/docs/Kimball852.pdf> (last access: 19 July 2023), 2017.
- Köcher, P., Horna, V., and Leuschner, C.: Stem water storage in five coexisting temperate broad-leaved tree species: significance, temporal dynamics and dependence on tree functional traits, *Tree Physiol.*, 33, 817–832, <https://doi.org/10.1093/treephys/tpt055>, 2013.
- Kohn, J. and Royer, A.: AMSR-E data inversion for soil temperature estimation under snow cover, *Remote Sens. Environ.*, 114, 2951–2961, <https://doi.org/10.1016/j.rse.2010.08.002>, 2010.
- Konings, A., Piles, M., Das, N., and Entekhabi, D.: L-band vegetation visible depth and effective scattering albedo estimation from SMAP, *Remote Sens. Environ.*, 198, 460–470, <https://doi.org/10.1016/j.rse.2017.06.037>, 2017.
- Konings, A., Rao, K., and Steele-Dunne, S.: Macro to micro: microwave Remote sensing of plant water content for physiology and ecology, *New Phytol.*, 223, 1166–1172, <https://doi.org/10.1111/nph.15808>, 2019.
- Krieger, G., Moreira, A., Zink, M., Hajnsek, I., Huber, S., Villano, M., Papathanassiou, K., Younis, M., Lopez Dekker, P., Pardini, M., Schulze, D., Bachmann, M., Borla Tridon, D., Reimann, J., Bräutigam, B., Steinbrecher, U., Tiendra, C., Sanjuan Ferrier, M., Zonno, M., Eineder, M., De Zan, F., Parizzi, A., Fritz, T., Diedrich, E., Maurer, E., Münnemannayer, R., Grafmüller, B., Wolters, R., te Henneppe, F., Ernst, R., and Bewick, C.: Tandem-L: Main results of the phase a feasibility study," 2016 IEEE International Geoscience and Remote Sensing Symposium (IGARSS), 10–15 July 2016, Beijing, China, 2116–2119, <https://doi.org/10.1109/IGARSS.2016.7729546>, 2016.
- Krishnan, P., Meyers, T., Hook, S., Heuer, M., Senn, D., and Dumas, E.: Intercomparison of In Situ Sensors for Ground-Based Land Surface Temperature Measurements, *Sensors*, 20, 5268, <https://doi.org/10.3390/s20185268>, 2020.
- Lai, D.: Methane Dynamics in Northern Peatlands: A Review, *Pedosphere*, 19, 409–421, [https://doi.org/10.1016/S1002-0160\(09\)00003-4](https://doi.org/10.1016/S1002-0160(09)00003-4), 2009.
- Lakhankar, T., Krakauer, N., and Khanbilvardi, R.: Applications of microwave Remote sensing of soil moisture for agricultural applications, *Int. J. Terraspace Sci. Eng.*, 2, 81–91, 2009.
- Larue, F., Royer, A., De Sève, D., Langlois, A., Roy, A., and Brucker, L.: Validation of GlobSnow-2 snow water equivalent

- over Eastern Canada, *Remote Sens. Environ.*, 194, 264–277, <https://doi.org/10.1016/j.rse.2017.03.027>, 2017.
- Larue, F., Royer, A., De Sève, D., Roy, A., and Cosme, E.: Assimilation of passive microwave AMSR-2 satellite observations in a snowpack evolution model over northeastern Canada, *Hydrol. Earth Syst. Sci.*, 22, 5711–5734, <https://doi.org/10.5194/hess-22-5711-2018>, 2018.
- Lawrence, H., Wigneron, J.-P., Richaume, P., Novello, N., Grant, J., Mialon, A., Al Bitar, A., Merlin, O., Guyon, D., Leroux, D., Bircher, S., and Kerr, Y.: Comparison between SMOS Vegetation Visible Depth products and MODIS vegetation indices over crop zones of the USA, *Remote Sens. Environ.*, 140, 396–406, <https://doi.org/10.1016/j.rse.2013.07.021>, 2014.
- Leanza, A., Manzoni, M., Monti-Guarnieri, A., and di Clemente, M.: LEO to GEO-SAR Interferences: Modelling and performance evaluation, *Remote Sens.*, 11, 1720, <https://doi.org/10.3390/rs11141720>, 2019.
- Lee, J.-S., Grunes, M., and Pottier, E.: Quantitative comparison of classification capability: fully polarimetric versus dual and single-polarization SAR, *IEEE T. Geosci. Remote Sens.*, 39, 2343–2351, <https://doi.org/10.1109/36.964970>, 2001.
- Lees, K., Quaife, T., Artz, R., Khomik, M., and Clarl, J.: Potential for using remote sensing to estimate carbon fluxes across northern peatlands – A review, *Sci. Total Environ.*, 615, 857–874, <https://doi.org/10.1016/j.scitotenv.2017.09.103>, 2018.
- Le Toan, T., Quegan, S., Davidson, M., Balzter, H., Paillou, P., Papathanassiou, K., Plummer, S., Rocca, F., Saatchi, S., Shugart, H., and Ilander, L.: The BIOMASS mission: Mapping global forest biomass to better understand the terrestrial carbon cycle, *Remote Sens. Environ.*, 115, 2850–2860, <https://doi.org/10.1016/j.rse.2011.03.020>, 2011.
- Li, Q., Kelly, R., Leppanen, L., Vehvilainen, J., Kontu, A., Lemmettyinen, J., and Pulliainen, J.: The influence of thermal properties and canopy-intercepted snow on passive microwave transmissivity of a scots pine, *IEEE T. Geosci. Remote Sens.*, 57, 5424–5433, <https://doi.org/10.1109/TGRS.2019.2899345>, 2019.
- Li, W., Cardellach, E., Ribó, S., Oliveras, S., and Rius, A.: Exploration of Multi-Mission Spaceborne GNSS-R Raw IF Data Sets: Processing, Data Products and Potential Applications, *Remote Sens.*, 14, 1344, <https://doi.org/10.3390/rs14061344>, 2022.
- Li, X., Wigneron, J. P., Fan, L., Frappart, F., Simon, H., Colliander, A., Ebtehaj, A., Gao, L., Fernandez-Moran, R., Liu, X. Z., Wang, M. J., Ma, H. L., Moisy, C., and Ciais, P.: A new SMAP soil moisture and vegetation optical depth product (SMAP-IB): Algorithm, assessment and inter-comparison, *Remote Sens. Environ.*, 271, 112921, <https://doi.org/10.1016/j.rse.2022.112921>, 2022.
- Lieffers, V. and Rothwell, R.: Rooting of peatland black spruce and tamarack in relation to depth of water table, *Can. J. Bot.*, 65, 817–821, <https://doi.org/10.1139/b87-111>, 1987.
- Lievens, H., Demuzere, M., Marshall, H.-P., Reichle, R., Brucker, L., Brangers, I., de Rosnay, P., Dumont, M., Giroto, M., Immerzeel, W., Jonas, T., Kim, E., Koch, I., Marty, C., Saloranta, T., Schöberl, J., and De Lannoy, G.: Snow depth variability in the Northern Hemisphere mountains observed from space, *Nat. Commun.*, 10, 4629, <https://doi.org/10.1038/s41467-019-12566-y>, 2019.
- Liljedahl, A., Boike, J., Daanen, R., Fedorov, A., Frost, G., Grosse, G., Hinzman, L., Iijima, Y., Jorgenson, J., Matveyeva, N., Necsoiu, M., Raynolds, M., Romanovsky, V., Schulla, J., Tape, K., Walker, D., Wilson, C., Yabuki, H., and Zona, D.: Pan-Arctic ice-wedge degradation in warming permafrost and its influence on tundra hydrology, *Nat. Geosci.*, 9, 312–318, <https://doi.org/10.1038/ngeo2674>, 2016.
- Liu, X., Wigneron, J.-P., Fan, L., Frappart, F., Ciais, P., Baghdadi, N., Zribi, M., Jaghuber, T., Li, X., Wang, M., Bai, X., and Moisy, C.: ASCAT IB: A radar-based vegetation optical depth retrieved from the ASCAT scatterometer satellite, *Remote Sens. Environ.*, 264, 112587, <https://doi.org/10.1016/j.rse.2021.112587>, 2021.
- Liu, Y., van Dijk, A., de Jeu, R., Canadell, J., McCabe, M., Evans, J., and Wang, G.: Recent reversal in loss of global terrestrial biomass, *Nat. Clim. Change*, 5, 470–474, <https://doi.org/10.1038/nclimate2581>, 2011a.
- Liu, Y. A., de Jeu, R. J., McCabe, M., Evans, J., and van Dijk, A.: Global long-term passive microwave satellite-based retrievals of vegetation visible depth, *Geophys. Res. Lett.*, 38, L18402, <https://doi.org/10.1029/2011GL048684>, 2011b.
- Liu, Y., Holtzman, N. M., and Konings, A. G.: Global ecosystem-scale plant hydraulic traits retrieved using model–data fusion, *Hydrol. Earth Syst. Sci.*, 25, 2399–2417, <https://doi.org/10.5194/hess-25-2399-2021>, 2021.
- Loisel, J., Gallego-Sala, A. V., Amesbury, M. J., Magnan, G., Anshari, G., Beilman, D. W., Benavides, J. C., Blewett, J., Camill, P., Charman, D. J., Chawchai, S., Hedgpeth, A., Kleinen, T., Korhola, A., Large, D., Mansilla, C. A., Müller, J., van Bellen, S., West, J. B., Yu, Z., Bubier, J. L., Garneau, M., Moore, T., Sanne, A. B. K., Page, S., Välijanta, M., Bechtold, M., Brovkin, V., Cole, L. E. S., Chanton, J. P., Christensen, T. R., Davies, M. A., De Vleeschouwer, F., Finkelstein, S. A., Froliking, S., Galka, M., Gandois, L., Girkin, N., Harris, L. I., Heinemeyer, A., Hoyt, A. M., Jones, M. C., Joos, F., Juutinen, S., Kaiser, K., Lacourse, T., Lamantowicz, M., Larmola, T., Leifeld, J., Lohila, A., Milner, A. M., Minkkinen, K., Moss, P., Naafs, B. D. A., Nichols, J., O’Donnel, J., Payne, R., Philben, M., Piilo, S., Quillet, A., Ratnayake, A. S., Roland, T. P., Sjögersten, S., Sonnentag, O., Swindles, G. T., Swinnen, W., Talbot, J., Treat, C., Valach, A. C., and Wu, J.: Expert assessment of future vulnerability of the global peatland carbon sink, *Nat. Clim. Change*, 11, 70–77, 2021.
- Lönnqvist, A., Rauste, Y., Molinier, M., and Häme, T.: Polarimetric SAR Data in Land Cover Mapping in Boreal Zone, *IEEE T. Geosci. Remote Sens.*, 48, 3652–3662, <https://doi.org/10.1109/TGRS.2010.2048115>, 2010.
- Lorente, A., Borsdorff, T., Butz, A., Hasekamp, O., aan de Brugh, J., Schneider, A., Wu, L., Hase, F., Kivi, R., Wunch, D., Pollard, D. F., Shiomi, K., Deutscher, N. M., Velazco, V. A., Roehl, C. M., Wennberg, P. O., Warneke, T., and Landgraf, J.: Methane retrieved from TROPOMI: improvement of the data product and validation of the first 2 years of measurements, *Atmos. Meas. Tech.*, 14, 665–684, <https://doi.org/10.5194/amt-14-665-2021>, 2021.
- Luojuus, K., Pulliainen, J., Takala, M., Lemmettyinen, J., Mortimer, C., Derksen, C., Mudryk, L., Moisander, M., Hiltunen, M., Smolander, T., Ikonen, J., Cohen, J., Salminen, M., Norberg, J., Veijola, K., and Venäläinen, P.: GlobSnow v3.0 Northern Hemisphere snow water equivalent dataset, *Sci. Data*, 8, 163, <https://doi.org/10.1038/s41597-021-00939-2>, 2021.
- Maeda, T., Taniguchi, Y., and Imaoka, K.: GCOM-W1 AMSR2 Level 1R Product: Dataset of brightness temperature modified using the antenna pattern matching

- technique, *IEEE T. Geosci. Remote Sens.*, 54, 770–782, <https://doi.org/10.1109/TGRS.2015.2465170>, 2016.
- Magney, T., Bowling, D., Logan, B., Grossmann, K., Stutz, J., Blanken, P., Burns, S., Cheng, R., Garcia, M., Köhler, P., Lopez, S., Parazoo, N., Racza, B., Schimel, D., and Frankenberg, C.: Mechanistic evidence for tracking the seasonality of photosynthesis with solar-induced fluorescence, *P. Natl. Acad. Sci. USA*, 116, 11640–11645, <https://doi.org/10.1073/pnas.1900278116>, 2019.
- Mao, J., Ribes, A., Yan, B., Shi, X., Thornton, P., Séférian, R., Ciais, P., Myneni, R., Douville, H., Piao, S., Zhu, Z., Dickinson, R., Dai, Y., Ricciuto, D., Jin, M., Hoffman, F., Wang, B., Huang, M., and Lian, X.: Human-induced greening of the northern extratropical land surface, *Nat. Clim. Change*, 6, 959–963, <https://doi.org/10.1038/nclimate3056>, 2016.
- Mao, K., Zuo, Z., Shen, X., Xu, T., Gao, C., and Liu, G.: Retrieval of land-surface temperature from AMSR2 data using a deep dynamic learning neural network, *Chinese Geogr. Sci.*, 28, 1–11, <https://doi.org/10.1007/s11769-018-0930-1>, 2018.
- Marchand, N., Royer, A., Krinner, G., Roy, A., Langlois, A., and Vargel, C.: Snow-covered soil temperature retrieval in Canadian Arctic permafrost areas, using a land surface scheme informed with satellite remote sensing data, *Remote Sens.*, 10, 1703, <https://doi.org/10.3390/rs10111703>, 2018.
- Marghany, M.: Principle theories of synthetic aperture radar. Synthetic aperture radar imaging mechanism for oil spills, 127–150, Gulf Professional Publishing, United States, 322 pp., ISBN 9780128181119, 2019.
- Matheny, A., Bohrer, G., Garrity, S., Morin, T., Howard, C., and Vogel, C.: Observations of stem water storage in trees of opposing hydraulic strategies, *Ecosphere*, 6, 1–13, <https://doi.org/10.1890/ES15-00170.1>, 2015.
- Matthews, E., Johnson, M. S., Genovese, V., Du, J., and Bastviken, D.: Methane emission from high latitude lakes: methane-centric lake classification and satellite-driven annual cycle of emissions, *Sci. Rep.*, 10, 12465, <https://doi.org/10.1038/s41598-020-68246-1>, 2020.
- McDonald, K., Kimball, J., Njoku, E., Zimmermann, R., and Zhao, M.: Variability in Springtime Thaw in the Terrestrial High Latitudes: Monitoring a Major Control on the Biospheric Assimilation of Atmospheric CO<sub>2</sub> with Spaceborne Microwave Remote Sensing, *Earth Interact.*, 8, 1–23, [https://doi.org/10.1175/1087-3562\(2004\)8<1:VISTIT>2.0.CO;2](https://doi.org/10.1175/1087-3562(2004)8<1:VISTIT>2.0.CO;2), 2004.
- McMahon, S., Parker, G., and Miller, D.: Evidence for a recent increase in forest growth, *P. Natl. Acad. Sci. USA*, 107, 3611–3615, <https://doi.org/10.1073/pnas.0912376107>, 2010.
- Meloche, J., Langlois, A., Rutter, N., Royer, A., King, J., Walker, B., Marsh, P., and Wilcox, E. J.: Characterizing tundra snow sub-pixel variability to improve brightness temperature estimation in satellite SWE retrievals, *The Cryosphere*, 16, 87–101, <https://doi.org/10.5194/tc-16-87-2022>, 2022.
- Melton, J. R., Arora, V. K., Wisernig-Cojoc, E., Seiler, C., Fortier, M., Chan, E., and Teckentrup, L.: CLASSIC v1.0: the open-source community successor to the Canadian Land Surface Scheme (CLASS) and the Canadian Terrestrial Ecosystem Model (CTEM) – Part 1: Model framework and site-level performance, *Geosci. Model Dev.*, 13, 2825–2850, <https://doi.org/10.5194/gmd-13-2825-2020>, 2020.
- Merchant, M., Adams, J., Berg, A., Baltzer, J., Quinton, W., and Chasmer, L.: Contributions of C-Band SAR data and polarimetric decompositions to subarctic boreal peatland mapping, *IEEE J. Sel. Top. Appl.*, 10, 1467–1482, <https://doi.org/10.1109/JSTARS.2016.2621043>, 2017.
- Merchant, M., Warren, R., Edwards, R., and Kenyon, J.: An object-based assessment of multi-wavelength SAR, optical imagery and topographical datasets for operational wetland mapping in boreal Yukon, Canada, *Can. J. Remote Sens.*, 45, 308–332, <https://doi.org/10.1080/07038992.2019.1605500>, 2019.
- Merchant, M., Obadia, M., Brisco, B., DeVries, B., and Berg, A.: Applying machine learning and time-series analysis on Sentinel-1A SAR/InSAR for characterizing arctic tundra hydro-ecological condition, *Remote Sens.*, 14, 1123, <https://doi.org/10.3390/rs14051123>, 2022.
- Merzouki, A., McNairn, H., and Pacheco, A.: Mapping soil moisture using RADARSAT-2 data and local autocorrelation statistics, *IEEE J. Sel. Top. Appl.*, 4, 128–137, <https://doi.org/10.1109/JSTARS.2011.2116769>, 2011.
- Mialon, A., Royer, A., Fily, M., and Picard, G.: Daily microwave-derived surface temperature over Canada/Alaska, *J. Appl. Meteorol. Clim.*, 46, 591–604, <https://doi.org/10.1175/JAM2485.1>, 2007.
- Mialon, A., Rodríguez-Fernández, N., Santoro, M., Saatchi, S., Mermoz, S., Bousquet, E., and Kerr, Y.: Evaluation of the sensitivity of SMOS L-VOD to forest above-ground biomass at global scale, *Remote Sens.*, 12, 1450, <https://doi.org/10.3390/rs12091450>, 2020.
- Mikan, C., Schimel, J., and Doyle, A.: Temperature controls of microbial respiration above and below freezing in Arctic tundra soils, *Soil Biol. Biochem.*, 34, 1785–1795, <https://doi.org/10.3390/rs12091450>, 2002.
- Miner, K. R., Turesky, M. R., Malina, E., Bartsch, A., Tamminen, J., McGuire, A. D., Fix, A., Sweeney, C., Elder, C. D., and Miller, C. E.: Permafrost carbon emissions in a changing Arctic, *Nat. Rev. Earth Environ.*, 3, 55–67, <https://doi.org/10.1038/s43017-021-00230-3>, 2022.
- Mironov, V. and Savin, I.: A temperature-dependent multi-relaxation spectroscopic dielectric model for thawed and frozen organic soil at 0.05–15 GHz, *Phys. Chem. Earth*, 83–84, 57–64, <https://doi.org/10.1016/j.pce.2015.02.011>, 2015.
- Misra, T., Jha, A., Putrevu, D., Rao, J., Dave, D., and Rana, S.: Ground calibration of multifrequency ScanningMicrowave radiometer (MSMR), *IEEE T. Geosci. Remote Sens.*, 40, 504–508, <https://doi.org/10.1109/36.992823>, 2002.
- Mo, T., Choudhury, B., Schmugge, T., Wang, J., and Jackson, T.: A model for microwave emission from vegetation-covered fields, *J. Geophys. Res.*, 87, 11229–11237, <https://doi.org/10.1029/JC087iC13p11229>, 1982.
- Moreira, A., Bachmann, M., Balzer, W., Tridon, D., Diedrich, E., Fritz, T., Grigorov, C., Kahle, R., Krieger, G., Hajnsek, I., Huber, S., Jörg, H., Klenk, P., Lachaise, M., Maier, M., Maurer, E., Papathanassiou, K., Parizzi, A., Prats, P., Reimann, J., Rodriguez, M., Schättler, B., Schwinger, M., Schulze, D., Steinbrecher, U., Villano, M., Younis, M., De Zan, F., Zink, M., and Zonno, M.: Tandem-L: Project Status and Main Findings of the Phase B1 Study, *IGARSS 2018 – 2018 IEEE International Geoscience and Remote sensing*

- Symposium, 22–27 July 2018, Valencia, Spain, 8667–8670, <https://doi.org/10.1109/IGARSS.2018.8518591>, 2018.
- Morrissey, L., Durden, S., Livingston, G., Steam, J., and Guild, L.: Differentiating methane source areas in Arctic environments with multitemporal ERS-1 SAR data, *IEEE T. Geosci. Remote Sens.*, 34, 667–673, <https://doi.org/10.1109/36.499746>, 1996.
- Mortimer, C., Mudryk, L., Derksen, C., Luoju, K., Brown, R., Kelly, R., and Tedesco, M.: Evaluation of long-term Northern Hemisphere snow water equivalent products, *The Cryosphere*, 14, 1579–1594, <https://doi.org/10.5194/tc-14-1579-2020>, 2020.
- Martin, J., Schröder, T., Walløe Hansen, A., Holt, B., and McDonald, K.: Mapping of seasonal freeze-thaw transitions across the pan-Arctic land and sea ice domains with satellite radar, *J. Geophys. Res.–Oceans*, 117, C08004, <https://doi.org/10.1029/2012JC008001>, 2012.
- Mu, Q., Zhao, M., Heinsch, F. A., Liu, M., Tian, H., and Running, S.: Evaluating water stress controls on primary production in biogeochemical and remote sensing based models, *J. Geophys. Res.–Biogeosci.*, 112, G01012, <https://doi.org/10.1029/2006JG000179>, 2007.
- Murfitt, J. and Duguay, C.: 50 years of lake ice research from active microwave remote sensing: Progress and prospects, *Remote Sens. Environ.*, 264, 112616, <https://doi.org/10.1016/j.rse.2021.112616>, 2021.
- Myers-Smith, I. H., Forbes, B., Wilmking, M., Hallinger, M., Lantz, T., Blok, D., Tape, K., Macias-Fauria, M., Sass-Klaassen, U., Lévesque, E., Boudreau, S., Ropars, P., Hermanutz, L., Trant, A., Collier, L., Weijers, S., Rozema, J., Rayback, S., Schmidt, N., Schaepman-Strub, G., Wipf, S., Rixen, C., Ménard, C., Venn, S., Goetz, S., Andreu-Hayles, L., Elmondorf, S., Ravolainen, V., Welker, J., Grogan, P., Epstein, H., and Hik, D.: Shrub expansion in tundra ecosystems: dynamics, impacts and research priorities, *Environ. Res. Lett.*, 6, 045509, <https://doi.org/10.1088/1748-9326/6/4/045509>, 2011.
- Myers-Smith, I. H., Kerby, J., Phoenix, G., Bjerke, J., Epstein, H., Assmann, J., John, C., Andreu-Hayles, L., Angers-Blondin, S., Beck, P., Berner, L., Bhatt, U., Bjorkman, A., Blok, C., Bryn, A., Christiansen, C., Cornelissen, J. H. C., Cunliffe, A., Elmondorf, S., Forbes, B., Goetz, S., Hollister, R., de Jong, R., Loranty, M., Macias-Fauria, M., Maseyk, K., Normand, S., Olofsson, J., Parker, T., Parmentier, F.-J., Post, E., Schaepman-Strub, G., Stordal, F., Sullivan, P., Thomas, H., Tömmervik, H., Treharne, R., Tweedie, C., Walker, D., Wilmking, M., and Wipf, S.: Complexity revealed in the greening of the Arctic, *Nat. Clim. Change*, 10, 106–117, <https://doi.org/10.1038/s41558-019-0688-1>, 2020.
- Naeimi, V., Scipal, K., Bartalis, Z., Hasenauer, S., and Wagner, W.: An Improved Soil Moisture Retrieval Algorithm for ERS and METOP Scatterometer Observations, *IEEE T. Geosci. Remote Sens.*, 47, 1999–2013, <https://doi.org/10.1109/TGRS.2008.2011617>, 2009.
- Naeimi, V., Paulik, C., Bartsch, A., Wagner, W., Kidd, R., Park, S.-E., Elger, K., and Boike, J.: ASCAT Surface State Flag (SSF): Extracting Information on Surface Freeze/Thaw Conditions From Backscatter Data Using an Empirical Threshold-Analysis Algorithm, *IEEE T. Geosci. Remote Sens.*, 50, 2566–2582, <https://doi.org/10.1109/TGRS.2011.2177667>, 2012.
- Nagler, T. and Rott, H.: Retrieval of wet snow by means of multi-temporal SAR data, *IEEE T. Geosci. Remote Sens.*, 38, 754–765, <https://doi.org/10.1109/36.842004>, 2000.
- Natali, S., Watts, J., Rogers, B., Potter, S., Ludwig, S., Selbmann, A.-K., Sullivan, P., Abbott, B., Arndt, K., Birch, L., Björkman, M., Bloom, A., Celis, G., Christensen, T., Christiansen, C., Commane, R., Cooper, E., Crill, P., Czimczik, C., Davydov, S., Du, J., Egan, J., Elberling, B., Euskirchen, E., Friberg, T., Genet, H., Göckede, M., Goodrich, J., Grogan, P., Helbig, M., Jafarov, E., Jastrow, J., Kalhor, A., Kim, Y., Kimball, J., Kutzbach, L., Lara, M., Larsen, K., Lee, B.-Y., Liu, Z., Loranty, M., Lund, M., Lupascu, M., Madani, N., Malhotra, A., Matamala, R., McFarland, J., McGuire, A., Michelsen, A., Minions, C., Oechel, W., Olefeldt, D., Parmentier, F.-J., Pirk, N., Poulter, B., Quinton, W., Rezanezhad, F., Risk, D., Sachs, T., Schaefer, K., Schmidt, N., Schuur, E., Semenchuk, P., Shaver, G., Sonnentag, O., Starr, G., Treat, C., Waldrop, M., Wang, Y., Welker, J., Wille, C., Xu, X., Zhang, Z., Zhuang, Q., and Zona, D.: Large loss of CO<sub>2</sub> in winter observed across the northern permafrost region, *Nat. Clim. Change*, 9, 852–857, <https://doi.org/10.1038/s41558-019-0592-8>, 2019.
- Neumann, M., Saatchi, S., Ulander, L., and Fransson, J.: Assessing performance of L- and P-Band polarimetric interferometric SAR data in estimating boreal forest aboveground biomass, *IEEE T. Geosci. Remote.*, 50, 714–726, <https://doi.org/10.1109/TGRS.2011.2176133>, 2012.
- Osińska-Skotak, K.: Studies of soil temperature on the basis of satellite data, *Int. Agrophys.*, 21, 275–284, 2007.
- Pallandt, M. M. T. A., Kumar, J., Mauritz, M., Schuur, E. A. G., Virkkala, A.-M., Celis, G., Hoffman, F. M., and Göckede, M.: Representativeness assessment of the pan-Arctic eddy covariance site network and optimized future enhancements, *Biogeosciences*, 19, 559–583, <https://doi.org/10.5194/bg-19-559-2022>, 2022.
- Pan, Y., Birdsey, R., Fang, J., Houghton, R., Kauppi, P., Kurz, W., Phillips, O., Shvidenko, A., Lewis, S., Canadell, J., Ciais, P., Jackson, R., Pacala, S., McGuire, A., Piao, S., Rautiainen, A., Sitch, S., and Hayes, D.: A large and persistent carbon sink in the world's forests, *Science*, 333, 988–993, <https://doi.org/10.1126/science.1201609>, 2011.
- Pan, Y., Birdsey, R., Phillips, O., and Jackson, R.: The structure, distribution, and biomass of the world's forests, *Annu. Rev. Ecol. Syst.*, 44, 593–622, <https://doi.org/10.1146/annurev-ecolsys-110512-135914>, 2013.
- Panikov, N., Flanagan, P., Oechel, W., Masteponov, M., and Christensen, T.: Microbial activity in soils frozen to below –39 °C, *Soil Biol. Biochem.*, 38, 785–794, <https://doi.org/10.1016/j.soilbio.2005.07.004>, 2006.
- Pappas, C., Maillet, J., Rakowski, S., Baltzer, J., Barr, A., Black, A., Faticchi, S., Laroque, C., Matheny, A., Roy, A., Sonnentag, O., and Zha, T.: Aboveground tree growth is a minor and decoupled fraction of boreal forest carbon input, *Agr. Forest Meteorol.*, 290, 108030, <https://doi.org/10.1016/j.agrformet.2020.108030>, 2020.
- Parinussa, R., Holmes, T., and de Jeu, R.: Soil moisture retrievals from the WindSat spaceborne polarimetric microwave radiometer, *IEEE T. Geosci. Remote Sens.*, 50, 2683–2694, <https://doi.org/10.1109/TGRS.2011.2174643>, 2012.
- Pastorello, G., Trotta, C., Canfora, E., et al.: The FLUXNET2015 dataset and the ONEFlux processing pipeline for eddy covari-

- ance data, *Sci. Data.*, 7, 225, <https://doi.org/10.1038/s41597-020-0534-3>, 2020.
- Peng, C., Ma, Z., Lei, X., Zhu, Q., Chen, H., Wang, W., Liu, S., Li, W., Fang, X., and Zhou, X.: A drought-induced pervasive increase in tree mortality across Canada's boreal forests, *Nat. Clim. Change.*, 1, 467–471, <https://doi.org/10.1038/nclimate1293>, 2011.
- Piao, S., Ciais, P., Friedlingstein, P., Peylin, P., Reichstein, M., Luyssaert, S., Margolis, H., Fang, J., Barr, A., Chen, A., Grelle, A., Hollinger, D., Laurila, T., Lindroth, A., Richardson, A., and Vesala, T.: Net carbon dioxide losses of northern ecosystems in response to autumn warming, *Nature*, 451, 49–52, <https://doi.org/10.1038/nature06444>, 2008.
- Picard, G., Sandells, M., and Löwe, H.: SMRT: an active–passive microwave radiative transfer model for snow with multiple microstructure and scattering formulations (v1.0), *Geosci. Model Dev.*, 11, 2763–2788, <https://doi.org/10.5194/gmd-11-2763-2018>, 2018.
- Pierce, L., Ulaby, F., Sarabandi, K., and Dobson, M.: Knowledge-based classification of polarimetric SAR images, *IEEE T. Geosci. Remote Sens.*, 31, 1081–1086, <https://doi.org/10.1109/36.312896>, 1994.
- Pierdicca, N., Davidson, M., Chini, M., Dierking, W., Djavidnia, S., Haarpaintner, J., Hajduch, G., Laurin, G., Lavalle, M., López-Martínez, C., Nagler, T., and Su, B.: The Copernicus L-band SAR mission ROSE-L (Radar Observing System for Europe, Proc. Spie, Microwave Remote sensing for Environmental Monitoring III, 111540E, <https://doi.org/10.1117/12.2534743>, 2019.
- Pierrat, Z., Nehemy, M. F., Roy, A., Magney, T., Parazoo, N., Laroque, C., Pappas, C., Sonnentang, O., Grossman, K., Bowling, D. R., Seibt, U., Ramirez, A., Johnson, B., Helgason, W., Barr, A., and Stutz, J.: Tower-based Remote sensing reveals mechanisms behind a two-phased spring transition in a mixed species boreal forest, *J. Geophys. Res.-Biogeosci.*, 126, e2020JG006191, <https://doi.org/10.1029/2020JG006191>, 2021.
- Potapov, P., Hansen, M., Stehman, S., Loveland, T., and Pittman, K.: Combining MODIS and Landsat imagery to estimate and map boreal forest cover loss, *Remote Sens. Environ.*, 112, 3708–3719, <https://doi.org/10.1016/j.rse.2008.05.006>, 2008.
- Prince, M., Roy, A., Brucker, L., Royer, A., Kim, Y., and Zhao, T.: Northern Hemisphere surface freeze–thaw product from Aquarius L-band radiometers, *Earth Syst. Sci. Data*, 10, 2055–2067, <https://doi.org/10.5194/essd-10-2055-2018>, 2018.
- Prince, M., Roy, A., Royer, A., and Langlois, A.: Timing and spatial variability of fall soil freezing in boreal forest and its effect on SMAP L-band radiometer measurements, *Remote Sens. Environ.*, 231, 111230, <https://doi.org/10.1016/j.rse.2019.111230>, 2019.
- Pulliainen, J., Grandell, J., and Hallikainen, M.: Retrieval of surface temperature in boreal forest zone from SS-M/I data, *IEEE T. Geosci. Remote Sens.*, 35, 1188–1200, <https://doi.org/10.1109/36.628786>, 1997.
- Pulliainen, J.: Mapping of snow water equivalent and snow depth in boreal and sub-arctic zones by assimilating space-borne microwave radiometer data and ground-based observations, *Remote Sens. Environ.*, 101, 257–269, <https://doi.org/10.1016/j.rse.2006.01.002>, 2006.
- Pulliainen, J., Aurela, M., Laurila, T., Aalto, T., Takala, M., Salminen, M., Kulmala, M., Barr, A., Heimann, M., Lindroth, A., Laaksonen, A., Derksen, C., Mäkelä, A., Markkanen, T., Lemmettyinen, J., Susiluoto, J., Dengel, S., Mammarella, I., Tuovinen, J.-P., and Vesala, T.: Early snowmelt significantly enhances boreal springtime carbon uptake, *P. Natl. Acad. Sci. USA*, 114, 11081–11086, <https://doi.org/10.1073/pnas.1707889114>, 2017.
- Pulliainen, J., Luojus, K., Derksen, C., Mudryk, L., Lemmettyinen, J., Salminen, M., Ikonen, J., Takala, M., Cohen, J., Smolander, T., and Norberg, J.: Patterns and trends of Northern Hemisphere snow mass from 1980 to 2018, *Nature*, 581, 294–298, <https://doi.org/10.1038/s41586-020-2258-0>, 2020.
- Quegan, S., Le Toan, T., Chave, J., Dall, J., Extrayat, J.-F., Minh, D., Lomas, M., Mariotti D'Alessandro, M., Paillo, P., Papathanassiou, K., Rocca, F., Saatchi, S., Scipal, K., Shugart, H., Smallman, L., Soja, M., Tebaldini, S., Ulander, L., Villard, L., and Williams, M.: The European Space Agency BIOMASS mission: Measuring forest above-ground biomass from space, *Remote Sens. Environ.*, 227, 44–60, <https://doi.org/10.1016/j.rse.2019.03.032>, 2019.
- Rafat, A., Rezanezhad, F., Quinton, W. L., Humphreys, E. R., Webster, K., and Van Cappellen, P.: Non-growing season carbon emissions in a northern peatland are projected to increase under global warming, *Commun. Earth Environ.*, 2, 111, <https://doi.org/10.1038/s43247-021-00184-w>, 2021.
- Ranson, K. and Sun, G.: Effects of environmental conditions on boreal forest classification and biomass estimates with SAR, *IEEE T. Geosci. Remote Sens.*, 38, 1242–1252, <https://doi.org/10.1109/36.843016>, 2000.
- Rantanen, M., Karpechko, A. Y., Lipponen, A., Nordling, K., Hyvärinen, O., Ruosteenoja, K., Vihma, T., and Laaksonen, A.: The Arctic has warmed nearly four times faster than the globe since 1979, *Commun. Earth Environ.*, 3, 168, <https://doi.org/10.1038/s43247-022-00498-3>, 2022.
- Rautiainen, K., Lemmettyinen, J., Pulliainen, J., Vehviläinen, J., Drusch, M., Kontu, A., Kainulainen, J., and Seppänen, J.: L-band radiometer observations of soil processes at boreal and sub-Arctic environments, *IEEE T. Geosci. Remote Sens.*, 50, 1483–1497, <https://doi.org/10.1109/TGRS.2011.2167755>, 2012.
- Rautiainen, K., Parkkinen, T., Lemmettyinen, J., Schwank, M., Wiesmann, A., Ikonen, J., Derksen, C., Davydov, S., Davydova, A., Boike, J., and Langer, M.: SMOS prototype algorithm for detecting autumn soil freezing, *Remote Sens. Environ.*, 180, 346–360, <https://doi.org/10.1016/j.rse.2016.01.012>, 2016.
- Rautiainen, K., Comite, D., Cohen, J., Cardellach, E., Unwin, M., and Pierdicca, N.: Freeze–Thaw Detection Over High-Latitude Regions by Means of GNSS-R Data, *IEEE T. Geosci. Remote Sens.*, 60, 4302713, <https://doi.org/10.1109/TGRS.2021.3125315>, 2022.
- Ravn, N., Elberling, B., and Michelsen, A.: Arctic soil carbon turnover controlled by experimental snow addition, summer warming and shrub removal, *Soil Biol. Biochem.*, 142, 107698, <https://doi.org/10.1016/j.soilbio.2019.107698>, 2020.
- Rodríguez-Fernández, N. J., Mialon, A., Mermoz, S., Bouvet, A., Richaume, P., Al Bitar, A., Al-Yaari, A., Brandt, M., Kaminski, T., Le Toan, T., Kerr, Y. H., and Wigneron, J.-P.: An evaluation of SMOS L-band vegetation optical depth (L-VOD) data sets: high sensitivity of L-VOD to above-ground biomass in Africa, *Biogeosciences*, 15, 4627–4645, <https://doi.org/10.5194/bg-15-4627-2018>, 2018.

- Rodríguez-Fernández, N., Al Bitar, A., Colliander, A., and Zhao, T.: Soil moisture remote sensing across scales, *Remote Sens.*, 11, 190, <https://doi.org/10.3390/rs11020190>, 2019a.
- Rodríguez-Fernández, N., Mialon, A., Merlin, O., Suere, C., Cabot, F., Khazaal, A., Costeraste, J., Palacin, B., Rodriguez-Suquet, R., Tournier, T., Decoopman, T., Colom, M., Morel, J.-M., and Kerr, Y.: SMOS-HR: A high resolution L-Band passive radiometer for earth science and applications, *IGARSS 2019 – 2019 IEEE International Geoscience and Remote sensing Symposium*, 28 July–2 August 2019, Yokohama, Japan, 8392–8395, <https://doi.org/10.1109/IGARSS.2019.8897815>, 2019b.
- Rogers, M., Sullivan, P., and Welker, J.: Evidence of nonlinearity in the response of net ecosystem CO<sub>2</sub> exchange to increasing levels of winter snow depth in the high Arctic of Northwest Greenland, *Arct. Antarct. Alp. Res.*, 43, 95–106, <https://doi.org/10.1657/1938-4246-43.1.95>, 2010.
- Rosen, P., Hensley, S., Shaffer, S., Veilleux, L., Chakraborty, M., Misra, T., Bhan, R., Sagi, R., and Satish, R.: The NASA-ISRO SAR mission – An international space partnership for science and societal benefit, *2015 IEEE Radar Conference (RadarCon)*, 10–15 May 2015, Arlington, United States, 1610–1613, <https://doi.org/10.1109/RADAR.2015.7131255>, 2015.
- Rosen, P., Hensley, S., Shaffer, S., Edelstein, W., Kim, Y., Kumar, R., Misra, T., Bhan, R., Satish, R., and Sagi, R.: An update on the NASA-ISRO dual-frequency DBF SAR (NISAR) mission, *2016 IEEE International Geoscience and Remote sensing Symposium (IGARSS)*, 10–15 July 2016, Beijing, China, 2106–2108, <https://doi.org/10.1109/IGARSS.2016.7729543>, 2016.
- Roy, A., Royer, A., Wigneron, J.-P., Langlois, A., Bergeron, J., and Cliche, P.: A simple parameterization for a boreal forest radiative transfer model at microwave frequencies, *Remote Sens. Environ.*, 124, 371–383, <https://doi.org/10.1016/j.rse.2012.05.020>, 2012.
- Roy, A., Royer, A., and Hall, R.: Relationship between forest microwave transmissivity and structural parameters for the Canadian boreal forest, *IEEE Geosci. Remote Sens.*, 11, 1802–1806, <https://doi.org/10.1109/LGRS.2014.2309941>, 2014.
- Roy, A., Royer, A., DerkSEN, C., Brucker, L., Langlois, A., Mialon, A., and Kerr, Y.: Evaluation of spaceborne L-Band radiometer measurements for terrestrial freeze/thaw retrievals in Canada, *IEEE J. Sel. Top. Appl.*, 8, 4442–4459, <https://doi.org/10.1109/JSTARS.2015.2476358>, 2015.
- Roy, A., Toose, P., Williamson, M., Rowlandson, T., Derksen, C., Royer, A., Berg, A., Lemmettyinen, J., and Arnold, L.: Response of L-Band brightness temperatures to freeze/thaw and snow dynamics in a prairie environment from ground-based radiometer measurements, *Remote Sens. Environ.*, 191, 67–80, <https://doi.org/10.1016/j.rse.2017.01.017>, 2017a.
- Roy, A., Toose, P., Derksen, C., Rowlandson, T., Berg, A., Lemmettyinen, J., Royer, A., Tetlock, E., Helgason, W., and Sonnentag, O.: Spatial Variability of L-Band Brightness Temperature during Freeze/Thaw Events over a Prairie Environment, *Remote Sens.*, 9, 894, <https://doi.org/10.3390/rs9090894>, 2017b.
- Roy, A., Toose, P., Mavrovic, A., Pappas, C., Royer, C., Derksen, C., Berg, A., Rowlandson, T., El-Amine, M., Barr, A., Black, A., Langlois, A., and Sonnentag, O.: L-Band response to freeze/thaw in a boreal forest stand from ground- and tower-based radiometer observations, *Remote Sens. Environ.*, 237, 111542, <https://doi.org/10.1016/j.rse.2019.111542>, 2020.
- Royer, A. and Poirier, S.: Surface temperature spatial and temporal variations in North America from homogenized satellite SMMR-SSMI microwave measurements and reanalysis for 1979–2008, *J. Geophys. Res.*, 115, D08110, <https://doi.org/10.1029/2009JD012760>, 2010.
- Royer, A., Roy, A., Jutras, S., and Langlois, A.: Review article: Performance assessment of radiation-based field sensors for monitoring the water equivalent of snow cover (SWE), *Cryosphere*, 15, 5079–5098, <https://doi.org/10.5194/tc-15-5079-2021>, 2021.
- Ruiz-Pérez, G. and Vico, G.: Effects of Temperature and Water Availability on Northern European Boreal Forests, *Front. For. Glob. Change*, 3, 34, <https://doi.org/10.3389/ffgc.2020.00034>, 2020.
- Saatchi, S. and Rignot, E.: Classification of boreal forest cover types using SAR images, *Remote Sens. Environ.*, 60, 270–281, [https://doi.org/10.1016/S0034-4257\(96\)00181-2](https://doi.org/10.1016/S0034-4257(96)00181-2), 1997.
- Saberi, N., Kelly, R., Flemming, M., and Li, Q.: Review of snow water equivalent retrieval methods using spaceborne passive microwave radiometry, *Int. J. Remote Sens.*, 41, 996–1018, <https://doi.org/10.1080/01431161.2019.1654144>, 2020.
- Santoro, M. and Cartus, O.: Research pathways of forest aboveground biomass estimation based on SAR backscatter and interferometric SAR observations, *Remote Sens.*, 10, 608, <https://doi.org/10.3390/rs10040608>, 2018.
- Santoro, M., Cartus, O., Mermoz, S., Bouvet, A., Le Toan, T., Carvalhais, N., Rozendaal, D., Herold, M., Avitabile, V., Shaun, Q., Carreiras, J., Rauste, Y., Balzter, H., Schmullius, C., and Seifert, F.: A detailed portrait of the forest aboveground biomass pool for the year 2010 obtained from multiple Remote sensing observations, *Geophys. Res. Abstr.*, EGU2018-18932, EGU General Assembly 2018, Vienna, Austria, 2018.
- Schär, C., Fuhrer, O., Arteaga, A., Ban, N., Charpiloz, C., Di Girolamo, S., Hentgen, L., Hoefler, T., Lapillonne, X., Leutwyler, D., Osterried, K., Panosetti, D., Rüdisühl, S., Schlemmer, L., Schulthess, T., Sprenger, M., Ubbiali, S., and Wernli, H.: Kilometer-scale climate models: prospects and challenges, *B. Am. Meteorol. Soc.*, 101, E567–E587, <https://doi.org/10.1175/BAMS-D-18-0167.1>, 2020.
- Schädel, C., Bader, M., Schuur, E., Biasi, C., Bracho, R., Čapek, P., De Baets, S., Diáková, K., Ernakovich, J., Estop-Aragones, C., Graham, D., Hartley, I., Iversen, C., Kane, E., Knoblauch, C., Lupascu, M., Martikainen, P., Natali, S., Norby, R., O'Donnell, J., Chowdhury, T., Šantrúčková, H., Shaver, G., Sloan, V., Treat, C., Turetsky, M., Waldrop, M., and Wickland, K.: Potential carbon emissions dominated by carbon dioxide from thawed permafrost soils, *Nat. Clim. Change*, 6, 950–953, <https://doi.org/10.1038/nclimate3054>, 2016.
- Schlund, M., Scipal, K., and Quegan, S.: Assessment of a power law relationship between P-band SAR backscatter and aboveground biomass and its implications for BIOMASS mission performance, *IEEE J. Sel. Top. Appl.*, 11, 3538–3547, <https://doi.org/10.1109/JSTARS.2018.2866868>, 2018.
- Schuur, E., McGuire, A., Schädel, C., Grosse, G., Harden, J., Hayes, D., Hugelius, G., Koven, C., Kuhr, P., Lawrence, D., Natali, S., Olefeldt, D., Romanovsky, V., Schaefer, K., Turetsky, M., Treat, C., and Vonk, J.: Climate change and the permafrost carbon feedback, *Nature*, 520, 171–179, <https://doi.org/10.1038/nature14338>, 2015.

- Seiler, C., Melton, J., Arora, V., Sitch, S., Friedlingstein, P., Anthony, P., Goll, D., Jain, A., Joetzjer, E., Lienert, S., Lombardozzi, D., Luyssaert, S., Nabel, J., Tian, H., Vuichard, N., Walker, A., Yuan, W., and Zaehle, S.: Are terrestrial biosphere models fit for simulating the global land carbon sink?, *J. Adv. Model Earth Sy.*, 14, e2021MS002946, <https://doi.org/10.1029/2021MS002946>, 2022.
- Shi, J., Xiong, C., and Jiang, L.: Review of snow water equivalent microwave remote Sensing, *Sci. China Earth Sci.*, 59, 731–745, <https://doi.org/10.1007/s11430-015-5225-0>, 2016.
- Sitch, S., McGuire, D., Kimball, J., Gedney, N., Gamon, J., Engstrom, R., Wolf, A., Zhuang, Q., Clein, J., and McDonald, K.: Assessing the carbon balance of circumpolar Arctic tundra using Remote sensing and process modelling, *Ecol. Appl.*, 17, 213–234, [https://doi.org/10.1890/1051-0761\(2007\)017\[0213:ATCBOC\]2.0.CO;2](https://doi.org/10.1890/1051-0761(2007)017[0213:ATCBOC]2.0.CO;2), 2007.
- Sniderhan, A., Mamet, S., and Baltzer, J.: Non-uniform growth dynamics of a dominant boreal tree species (*Picea mariana*) in the face of rapid climate change, *Can. J. Forest Res.*, 51, 565–572, <https://doi.org/10.1139/cjfr-2020-0188>, 2021.
- Stefan, V.-G., Indrio, G., Escorihuela, M.-J., Quintana-Sehù, P., and Villar, J., M.: High-resolution SMAP-derived root-zone soil moisture using an exponential filter model calibrated per land cover type, *Remote Sens.*, 13, 1112, <https://doi.org/10.3390/rs13061112>, 2021.
- Stocke, B., Zscheischler, J., Keenan, T., Prentice, C., Peñuelas, J., and Seneviratne, S.: Quantifying soil moisture impacts on light use efficiency across biomes, *New Phytol.*, 218, 1430–1449, <https://doi.org/10.1111/nph.15123>, 2018.
- Sturm, M., Holmgren, J., König, M., and Morris, K.: The thermal conductivity of seasonal snow, *J. Glaciol.*, 43, 26–41, <https://doi.org/10.3189/s0022143200002781>, 1997.
- Sturm, M., Schimel, J., Michaelson, G., Welker, J., Oberbauer, S., Liston, G., Fahnestock, J., and Romanovsky, V.: Winter biological processes could help convert arctic tundra to shrubland, *Bioscience*, 55, 17–26, [https://doi.org/10.1641/0006-3568\(2005\)055\[0017:WBCHC\]2.0.CO;2](https://doi.org/10.1641/0006-3568(2005)055[0017:WBCHC]2.0.CO;2), 2005.
- Sulla-Menashe, D., Woodcock, C., and Friedl, M.: Canadian boreal forest greening and browning trends: an analysis of biogeographic patterns and the relative roles of disturbance versus climate drivers, *Environ. Res. Lett.*, 13, 014007, <https://doi.org/10.1088/1748-9326/aa9b88>, 2018.
- Takala, M., Luojus, K., Pulliaiainen, J., Derksen, C., Lemmettynen, J., Kärnä, J.-P., Koskinen, J., and Bojkov, B.: Estimating northern hemisphere snow water equivalent for climate research through assimilation of space-borne radiometer data and ground-based measurements, *Remote Sens. Environ.*, 115, 3517–3529, <https://doi.org/10.1016/j.rse.2011.08.014>, 2011.
- Tanja, S., Berninger, F., Vesala, T., Markkanen, T., Hari, P., Mäkelä, A., Ilvesniemi, H., Hänninen, H., Nikinmaa, E., Huttula, T., Laurila, T., Aurela, M., Grelle, A., Lindroth, A., Arneth, A., Shibushtova, O., and Lloyd, J.: Air temperature triggers the commencement of evergreen boreal forest photosynthesis in spring, *Glob. Change Biol.*, 9, 1410–1426, <https://doi.org/10.1046/j.1365-2486.2003.00597.x>, 2003.
- Tarnocai, C., Canadell, J., Schuur, E., Kuhry, P., Mazhitova, G., and Zimov, S.: Soil organic carbon pools in the northern circumpolar permafrost region, *Gobal Biogeochem. Cy.*, 23, GB2023, <https://doi.org/10.1029/2008GB003327>, 2009.
- Tebaldini, S., Ho Tong Minh, D., Mariotti d'Alessandro, M., Vilillard, L., Le Toan, T., and Chave, J.: The status of technologies to measure forest biomass and structural properties: state of the art in SAR tomography of tropical forests, *Surv. Geophys.*, 40, 779–801, <https://doi.org/10.1007/s10712-019-09539-7>, 2019.
- Tedesco, M. and Jeyaratnam, J.: A new operational snow retrieval algorithm applied to historical AMSR-E brightness temperatures, *Remote Sens.*, 8, 1037, <https://doi.org/10.3390/rs8121037>, 2016.
- Tei, S. and Sugimoto, A.: Excessive positive response of model-simulated land net primary production to climate changes over circumboreal forests, *Plant-Environment Interactions*, 1, 102–121, <https://doi.org/10.1002/pei3.10025>, 2020.
- Tenenan, M., Tsuruta, A., Rautiainen, K., Kangasaho, V., Ellul, R., and Aalto, T.: Utilizing earth observations of soil freeze/thaw data and atmospheric concentrations to estimate cold season methane emissions in the Northern high latitudes, *Remote Sens.*, 13, 5059, <https://doi.org/10.3390/rs13245059>, 2021.
- Teubner, I., Forkel, M., Jung, M., Liu, Y., Miralles, D., Parinussa, R., van der Schalie, R., Vreugdenhil, M., Schwalm, C., Tramontana, G., Camps-Valls, G., and Drigo, W.: Assessing the relationship between microwave vegetation visible depth and gross primary production, *Int. J. Appl. Earth Obs.*, 65, 79–91, <https://doi.org/10.1016/j.jag.2017.10.006>, 2018.
- Teubner, I., Forkel, M., Camps-Valls, G., Jung, M., Miralles, D., Tramontana, G., van der Schalie, R., Vreugdenhil, Mösinger, L., and Drigo, W.: A carbon sink-driven approach to estimate gross primary production from microwave satellite observations, *Remote Sens. Environ.*, 229, 100–113, <https://doi.org/10.1016/j.rse.2019.04.022>, 2019.
- Tian, F., Brandt, M., Liu, Y., Verger, A., Tagesson, T., Diouf, A., Rasmussen, K., Mbow, C., Wang, Y., and Fensholt, R.: Remote sensing of vegetation dynamics in drylands: Evaluating vegetation visible depth (VOD) using AVHRR NDVI and in situ green biomass data over West African Sahel, *Remote Sens. Environ.*, 177, 265–276, <https://doi.org/10.1016/j.rse.2016.02.056>, 2016.
- Tomiyasu, K.: Tutorial Review of Synthetic-Aperture Radar (SAR) with Applications to Imaging of Ocean Surface, P. IEEE, 66, 563–583, <https://doi.org/10.1109/PROC.1978.10961>, 1978.
- Touati, C., Ratsimbazafy, T., Ludwig, R., and Bernier, M.: New approaches for removing the effect of water damping on SMAP freeze/thaw mapping, *Can. J. Remote Sens.*, 45, 405–422, <https://doi.org/10.1080/07038992.2019.1638236>, 2019.
- Töyrä, J., Pietroniro, A., and Martz, L.: Multisensor hydrologic assessment of a freshwater wetland, *Remote Sens. Environ.*, 75, 162–173, [https://doi.org/10.1016/s0034-4257\(00\)00164-4](https://doi.org/10.1016/s0034-4257(00)00164-4), 2001.
- Tu, Q., Hase, F., Blumenstock, T., Kivi, R., Heikkinen, P., Sha, M. K., Raffalski, U., Landgraf, J., Lorente, A., Borsdorff, T., Chen, H., Dietrich, F., and Chen, J.: Intercomparison of atmospheric CO<sub>2</sub> and CH<sub>4</sub> abundances on regional scales in boreal areas using Copernicus Atmosphere Monitoring Service (CAMS) analysis, Collaborative Carbon Column Observing Network (COCCON) spectrometers, and Sentinel-5 Precursor satellite observations, *Atmos. Meas. Tech.*, 13, 4751–4771, <https://doi.org/10.5194/amt-13-4751-2020>, 2020.
- Tucker, C. J.: Red and photographic infrared linear combinations for monitoring vegetation, *Remote Sens. Environ.*, 8, 127–150, [https://doi.org/10.1016/0034-4257\(79\)90013-0](https://doi.org/10.1016/0034-4257(79)90013-0), 1979.

- Turner, D., Ollinger, S., and Kimball, J.: Integrating remote sensing and ecosystem process models for landscape-to regional-scale analysis of the carbon cycle, *Bioscience*, 54, 573–584, [https://doi.org/10.1641/0006-3568\(2004\)054\[0573:IRSAEP\]2.0.CO;2](https://doi.org/10.1641/0006-3568(2004)054[0573:IRSAEP]2.0.CO;2), 2004.
- Ulaby, F., Moore, R., and Fung, A.: *Microwave Remote Sens.-Basel: Active and Passive*. Vol. II – Radar remote sensing and surface scattering and emission theory, Addison-Wesley Publishing Company, Advanced Book Program/World Science Division, Norwood, Massachusetts, United-States, ISBN 9780201107609, 1982.
- Ulaby, F., Allen, C., and Fung, A.: Method for Retrieving the True Backscattering Coefficient from Measurements with a Real Antenna, *IEEE T. Geosci. Remote Sens.*, GE-21, 308–313, <https://doi.org/10.1109/TGRS.1983.350558>, 1983.
- Ulaby, F., Moore, R., and Fung, A.: *Microwave Remote Sens.- Active and Passive. Vol. III. From theory to applications*, Artech House Publishers, Norwood, Massachusetts, United-States, <https://doi.org/10.1017/S0016756800015831>, 1986.
- Ulaby, F., Sarabandi, K., McDonald, K., Whitt, M., and Dobson, M. C.: Michigan microwave canopy scattering model, *Int. J. Remote Sens.*, 11, 1223–1253, <https://doi.org/10.1080/01431169008955090>, 1990.
- Ullmann, T., Schmitt, A., Roth, A., Duffe, J., Dech, S., Hubberten, H.-W., and Baumhauer, R.: Land cover characterization and classification of arctic tundra environments by means of polarized synthetic aperture X- and C-Band radar (PolSAR) and Landsat 8 multispectral imagery – Richards Island, Canada, *Remote Sens.*, 6, 8565–8593, <https://doi.org/10.3390/rs6098565>, 2014.
- van Huissteden, J. and Dolman, A.: Soil carbon in the Arctic and the permafrost carbon feedback, *Curr. Opin. Env. Sust.*, 4, 545–551, <https://doi.org/10.1016/j.cosust.2012.09.008>, 2012.
- Virkkala, A.-M., Aalto, J., Rogers, B., Tagesson, T., Treat, C., Natali, S., Watts, J., Potter, S., Lehtonen, A., Mauritz, M., Schuur, E., Kochendorfer, J., Zona, D., Oechel, W., Kobayashi, H., Humphreys, E., Goeckede, M., Iwata, H., Lafleur, P., Euskirchen, E., Bokhorst, S., Marushchak, M., Martikainen, P., Elberling, B., Voigt, C., Biasi, C., Sonnentag, O., Parmentier, F.-J., Ueyama, M., Celis, G., St.Louis, V., Emmertton, C., Peichl, M., Chi, J., Järveoja, J., Nilsson, M., Oberbauer, S., Torn, M., Park, S.-J., Dolman, H., Mammarella, I., Chae, N., Poyatos, R., López-Blanco, E., Christensen, T., Kwon, M., Sachs, T., Holl, D., and Luoto, M.: Statistical upscaling of ecosystem CO<sub>2</sub> fluxes across the terrestrial tundra and boreal domain: Regional patterns and uncertainties, *Glob. Change Biol.*, 27, 4040–4059, <https://doi.org/10.1111/gcb.15659>, 2021.
- Vittucci, C., Vaglio Laurin, G., Tramontana, G., Ferrazzoli, P., Guerriero, L., and Papale, D.: Vegetation visible depth at L-band and above ground biomass in the tropical range: Evaluating their relationships at continental and regional scales, *Int. J. Appl. Earth Obs.*, 77, 151–161, <https://doi.org/10.1016/j.jag.2019.01.006>, 2019.
- Wagner, W., Hahn, S., Kidd, R., Melzer, T., Bartalis, Z., Hassenauer, S., Figa-Saldaña, J., de Rosnay, P., Jann, A., Schneider, S., Komma, J., Kubu, G., Brugger, K., Aubrecht, C., Züger, J., Gangkofner, U., Kienberger, S., Brocca, L., Wang, Y., Blöschl, G., Eitzinger, J., and Steinocher, K.: The ASCAT soil moisture product: A review of its specifications, validation results, and emerging applications, *Meteorol. Z.*, 22, 5–33, <https://doi.org/10.1127/0941-2948/2013/0399>, 2013.
- Walker, X. and Johnstone, J.: Widespread negative correlations between black spruce growth and temperature across topographic moisture gradients in the boreal forest, *Environ. Res. Lett.*, 9, 064016, <https://doi.org/10.1088/1748-9326/9/6/064016>, 2014.
- Walker, X., Rogers, B., Veraverbeke, S., Johnstone, J., Baltzer, J., Barrett, K., Bourgeau-Chavez, L., Day, N., de Groot, W., Dieleman, C., Goetz, S., Hoy, E., Jenkins, L., Kane, E., Parisien, M.-A., Potter, S., Schuur, E., Turetsky, M., Whitman, E., and Mack, M.: Fuel availability not fire weather controls boreal wildfire severity and carbon emissions, *Nat. Clim. Change*, 10, 1130–1136, <https://doi.org/10.1038/s41558-020-00920-8>, 2020.
- Wang, J., Sulla-Menashe, D., Woodcock, C., Sonnentag, O., Keeling, R., and Friedl, M.: Extensive land cover change across Arctic–Boreal Northwestern North America from disturbance and climate forcing, *Glob. Change Biol.*, 26, 807–822, <https://doi.org/10.1111/gcb.14804>, 2019.
- Wang, J., Sulla-Menashe, D., Woodcock, C., Sonnentag, O., Keeling, R., and Friedl, M.: Extensive land cover change across Arctic–Boreal Northwestern North America from disturbance and climate forcing, *Glob. Change Biol.*, 26, 807–822, <https://doi.org/10.1111/gcb.14804>, 2020.
- Washington, W., Buja, L., and Craig, A.: The computational future for climate and Earth system models: on the path to petaflop and beyond, *Philos. T. R. Soc. A.*, 367, 833–846, <https://doi.org/10.1098/rsta.2008.0219>, 2009.
- Watts, J., Kimball, J., Bartsch, A., and McDonald, K.: Surface water inundation in the boreal-Arctic: potential impacts on regional methane emissions, *Environ. Res. Lett.*, 9, 075001, <https://doi.org/10.1088/1748-9326/9/7/075001>, 2014.
- Webb, E., Schuur, E., Natali, S., Oken, K., Bracho, R., Krapek, J., Risk, D., and Nickerson, N.: Increased wintertime CO<sub>2</sub> loss as a result of sustained tundra warming, *J. Geophys. Res.-Biogeo.*, 121, 249–265, <https://doi.org/10.1002/2014JG002795>, 2016.
- Welker, J., Fahnestock, J., and Jones, M.: Annual CO<sub>2</sub> flux in dry and moist Arctic tundra: field responses to increases in summer temperatures and winter snow depth, *Climatic Change*, 44, 139–150, <https://doi.org/10.1023/A:1005555012742>, 2000.
- Whitcomb, J., Moghaddam, M., McDonald, K., Kellndorfer, J., and Podest, E.: Mapping vegetated wetlands of Alaska using L-band radar satellite imagery, *Can. J. Remote Sens.*, 35, 54–72, <https://doi.org/10.5589/m08-080>, 2009.
- Wigneron, J.-P., Kerr, Y., Waldteufel, P., Saleh, K., Escorihuela, M.-J., Richaume, P., Ferrazzoli, P., de Rosnay, P., Gurney, R., Calvet, J.-C., Grant, J., Guglielmetti, M., Hornbuckle, B., Mätzler, C., Pellarin, T., and Schwank, M.: L-band Microwave Emission of the Biosphere (L-MEB) Model: Description and calibration against experimental data sets over crop fields, *Remote Sens. Environ.*, 107, 639–655, <https://doi.org/10.1016/j.rse.2006.10.014>, 2007.
- Wigneron, J.-P., Li, X., Frappart, F., Fan, L., Al-Yaari, A., De Lannoy, G., Liu, X., Wang, M., Le Masson, E., and Moisy, C.: Overview of the SMOS-IC data record of soil moisture and L-VOD: Historic development, applications and perspectives, *Remote Sens. Environ.*, 254, 112238, <https://doi.org/10.1016/j.rse.2020.112238>, 2021.
- Wohlfahrt, G., Gerdel, K., Migliavacca, M., Rotenberg, E., Tatarnov, F., Müller, J., Hammerle, A., Julitta, T., Spielmann, F.,

- and Yakir, D.: Sun-induced fluorescence and gross primary productivity during a heat wave, *Sci. Rep.-UK*, 8, 14169, <https://doi.org/10.1038/s41598-018-32602-z>, 2018.
- Wu, M., Scholze, M., Kaminski, T., Voßbeck, M., and Tagesson, T.: Using SMOS soil moisture data combining CO<sub>2</sub> flask samples to constrain carbon fluxes during 2010–2015 within a Carbon Cycle Data Assimilation System (CCDAS), *Remote Sens. Environ.*, 240, 111719, <https://doi.org/10.1016/j.rse.2020.111719>, 2020.
- Xian, D., Zhang, P., Gao, L., Sun, R., Zhang, H., and Jia, X.: Fengyun Meteorological Satellite Products for Earth System Science Applications, *Adv. Atmos. Sci.*, 38, 1267–1284, <https://doi.org/10.1007/s00376-021-0425-3>, 2021.
- Xiao, J., Chevallier, F., Gomez, C., Guanter, L., Hicke, J., Huete, A., Ichii, K., Nih, W., Pang, Y., Rahman, A., Sun, G., Yuan, W., Zhang, L., and Zhang, X.: Remote sensing of the terrestrial carbon cycle: A review of advances over 50 years, *Remote Sens. Environ.*, 233, 111383, <https://doi.org/10.1016/j.rse.2019.111383>, 2019.
- Xu, X., Derksen, C., Yueh, S., Dunbar, R., and Colliander, A.: Freeze/thaw detection and validation using Aquarius' L-Band backscattering data, *IEEE J. Sel. Top. Appl.*, 9, 1370–1381, <https://doi.org/10.1109/JSTARS.2016.2519347>, 2016.
- Yang, W., Meng, H., Ferraro, R., Moradi, I., and Devaraj, C.: Cross-Scan asymmetry of AMSU-A window channels: characterization, correction, and verification, *IEEE T. Geosci. Remote*, 51, 1514–1530, <https://doi.org/10.1109/TGRS.2012.2211884>, 2013.
- Yi, Y., Kimball, J., Jones, L., Reichle, R., Nemani, R., and Margolis, H.: Recent climate and fire disturbance impacts on boreal and arctic ecosystem productivity estimated using a satellite-based terrestrial carbon flux model, *J. Geophys. Res.-Biogeog.*, 118, 606–622, <https://doi.org/10.1002/jgrg.20053>, 2013.
- Yi, Y., Chen, R., Kimball, J., Moghaddam, M., Xu, X., Euskrichchen, E., Das, N., and Miller, C.: Potential satellite monitoring of surface organic soil properties in arctic tundra from SMAP, *Water Resour. Res.*, 58, e2021WR030957, <https://doi.org/10.1029/2021WR030957>, 2022.
- Yu, K., Han, S., Bu, J., An, Y., Zhou, Z., Wang, C., Tabibi, S., and Cheong, J. W.: Spaceborne GNSS Reflectometry, *Remote Sens.*, 14, 1605, <https://doi.org/10.3390/rs14071605>, 2022.
- Zhang, Q. and Cheng, J.: An empirical algorithm for retrieving land surface temperature from AMSR-E data considering the comprehensive effects of environmental variables, *Earth Space Sci.*, 7, e2019EA001006, <https://doi.org/10.1029/2019EA001006>, 2020.
- Zhang, Y., Song, C., Sun, G., Band, L., Noormets, A., and Zhang, Q.: Understanding moisture stress on light use efficiency across terrestrial ecosystems based on global flux and remote-sensing data, *J. Geophys. Res.-Biogeog.*, 120, 2053–2066, <https://doi.org/10.1002/2015JG003023>, 2015.
- Zhou, Z., Li, Z., Waldron, S., and Tanaka, A.: InSAR time series analysis of L-Band data for understanding tropical peatland degradation and restoration, *Remote Sens.*, 11, 2592, <https://doi.org/10.3390/rs11212592>, 2019.
- Zona, D., Gioli, B., Commane, R., and Oechel, W. C.: Cold season emissions dominate the Arctic tundra methane budget, *P. Natl. Acad. Sci. USA*, 113, 40–45, <https://doi.org/10.1073/pnas.1516017113>, 2015.
- van Zyl, J.: Unsupervised classification of scattering behavior using radar polarimetry data, *IEEE T. Geosci. Remote Sens.*, 27, 36–45, <https://doi.org/10.1109/36.20273>, 1989.

# Chapitre 7 : Validation du produit SMAP L4C en hiver

## 7.1 Introduction

La modélisation du cycle du carbone en régions arctiques et boréales est essentielle pour pallier à la faible couverture spatiale et temporelle de données *in situ* dans ces vastes étendues difficilement accessibles (Pallandt *et al.*, 2022). La disponibilité limitée des données de flux de carbone, particulièrement en hiver, représente également un défi pour la validation et la paramétrisation des modèles écosystémiques. La mesure des échanges de carbone par covariance des turbulences (Eddy Covariance ; EC) est la méthode la plus répandue pour valider et paramétriser les modèles écosystémiques dûs à leur haute résolution temporelle (voir annexe B.1). Cependant, les interruptions de données sont courantes en hiver dans les régions arctiques et boréales, car les équipements de mesure d'EC sont énergivores, susceptibles de tomber en panne à basse température, incapable de produire des données fiables lorsqu'engivrés et les systèmes d'alimentation solaire sont limités par le faible ensoleillement en hiver (Kittler *et al.*, 2017; Jentzsch *et al.*, 2021, Pallandt *et al.*, 2022).

La télédétection satellitaire micro-onde a le potentiel d'améliorer considérablement les prédictions de flux de carbone des modèles écosystémiques (Mavrovic *et al.*, 2023b). Cependant, l'utilisation de données de télédétection micro-onde pour informer les modèles écosystémiques est encore limitée (Lees *et al.*, 2018). Quelques études ont intégré des données d'humidité du sol du satellite SMOS dans des modèles écosystémiques sur une période restreinte (2010-2015 ; Wu *et al.*, 2020). Aussi, le modèle de flux de carbone terrestre Terrestrial Carbon Flux (TCF ; Kimball *et al.*, 2009) a utilisé des informations sur l'humidité et la température du sol issues du capteur satellitaire AMSR-E pour fournir des contraintes environnementales sur  $R_h$  dans les régions arctiques et boréales (Baldocchi *et al.*, 2001 ; Pastorello *et al.*, 2020). Bien que limités jusqu'à présent, ces exemples démontrent le potentiel d'intégration des produits micro-onde satellitaire dans les modèles écosystémiques. Le modèle L4C de l'équipe du satellite SMAP (Soil Moisture Active Passive) est le seul modèle opérationnel intégrant des données micro-onde satellitaire afin de modéliser le cycle du carbone (Jones *et al.*, 2017; Fig. 7.1). Le produit L4C fourni quotidiennement NEE, GPP,  $R_h$ , carbone organique contenu dans le sol et contraintes environnementales pour huit types fonctionnels de plantes (Plant Functionnal Type : PFT) à une résolution spatiale de 9 km à l'échelle globale depuis 2015 sur une projection EASE-Grid.

Les données d'échanges de  $CO_2$  présentées dans l'article Mavrovic *et al.* (2023b) (Sect. 3) offrent l'opportunité de comparer des données *in situ* hivernales avec les estimations de NEE du modèle L4C. Notre comparaison porte sur 5 sites d'étude provenant d'environnements arctiques et boréaux bien distincts. Le but de notre étude est de déterminer le niveau de correspondance et les biais systématiques entre les NEE de L4C et les mesures *in situ* de flux de  $CO_2$  hivernaux par gradient de diffusion dans la neige.

## 7.2 Modèle L4C

Le modèle d'échange de carbone L4C estime le NEE à partir d'un sous-modèle pour le GPP,  $R_a$  et  $R_h$  (Fig. 7.1a). Le GPP est estimé à partir d'un modèle d'efficacité d'utilisation de la lumière (Fig. 7.1b) tel que décrit par le modèle générique de la Sect. 2.2.1. Le  $R_a$  est défini comme une fraction de la GPP (voir Sect. 2.2.2). Le  $R_h$  est estimé en utilisant un modèle de dégradation en cascade de la matière organique comprise dans le sol tel que décrit par le modèle générique de la Sect. 2.2.3. Les paramètres des sous-modèles de L4C sont évalués par PFT. Les PFT de chaque pixel de  $9x9\ km$  de L4C sont déterminés à partir du produit statique de couverture du sol de MODIS à  $1x1\ km$  (Terra/Aqua Moderate resolution Imaging Spectroradiometer ; produit MOD12Q1/MDY12Q1 ; Tableau 7.1).

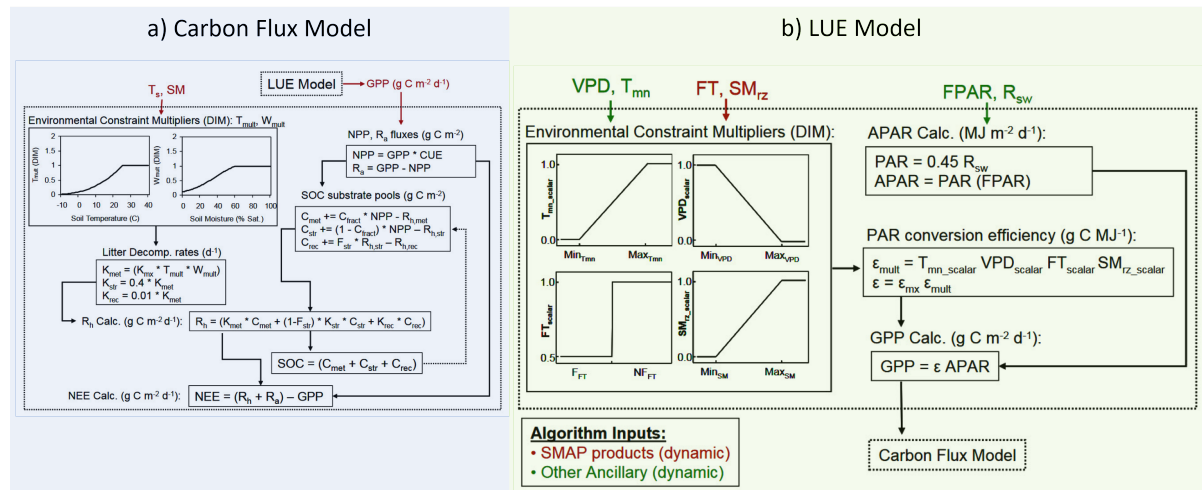


FIGURE 7.1 – Schématisation du modèle L4C. (a) Modèle simulant les flux de carbone pour chaque Plant Functionnal Type (PFT). (b) Modèle simulant la production primaire brute (Gross Primary Production : GPP) pour chaque PFT : Light use efficiency (LUE). Source : [https://nsidc.org/sites/default/files/documents/user-guide/spl4cmdl-v007-userguide\\_0.pdf](https://nsidc.org/sites/default/files/documents/user-guide/spl4cmdl-v007-userguide_0.pdf)

Le produit L4C est accessible sans restriction. L'algorithme de L4C intègre des données d'humidité du sol obtenu par télédétection micro-onde à partir du satellite SMAP, mais seulement lors de la période de dégel. Le modèle atmosphérique GEOS-5 est utilisé pour les entrées météorologiques et les produits visibles/infrarouges MODIS sont utilisés pour l'occupation du sol et le PAR.

TABLEAU 7.1 – Description des Plant Functional Type (PFT) utilisées par le modèle L4C (en vert). Ces PFT sont tirés du produit MODIS (Terra/Aqua MODerate resolution Imaging Spectroradiometer) d'occupation du sol statique (MOD12Q1/MDY12Q1). Source : <https://nsidc.org/sites/default/files/documents/technical-reference/ref-endsley-et-al-2022-l4c-psd-v22-final.pdf>

PFT Class label	PFT code	PFT Description	PFT Class used in L4_C
Water	0	For all ocean and perennial inland water bodies	No
Evergreen needleleaf	1	Evergreen needle-leaf trees (mostly conifers)	Yes
Evergreen broadleaf	2	Evergreen broadleaf trees	Yes
Deciduous needleleaf	3	Deciduous needle-leaf trees	Yes
Deciduous broadleaf	4	Deciduous broad-leaf trees	Yes
Shrub	5	Shrub (woody perennial)	Yes
Grass	6	Grasses (native Graminoids)	Yes
Cereal crop	7	Cereal cropland (domesticated agricultural crops such as wheat, oats, barley, rye )	Yes
Broadleaf crop	8	Broadleaf crop (domesticated agricultural)	Yes
Urban and Built-up	9	Urban and built-up (cities, towns, highways, etc)	No
Snow and ice	10	Snow and ice (may or may not be perennial)	No
Barren (rock) or sparsely vegetated	11	Barren, rock, or very sparsely vegetated land	No
Unclassified	254	Areas otherwise not classified as per above	No

### 7.3 Résultats et discussion

La figure 7.2 présente une comparaison des NEE simulés par le modèle L4C versus des données *in situ* obtenues hors de la saison de croissance à l'aide de la méthode du gradient de diffusion à travers le couvert neigeux ( $F_{CO_2}$  snowpack diffusion ; Mavrovic *et al.*, 2023b). Les écarts entre les résultats du modèle L4C et les données *in situ* sont importants, représentant de 100% à 642% de la valeur moyenne de  $F_{CO_2}$  pour les différents sites d'études (Tableau 7.2). Un biais systématique de surestimation du NEE par L4C est observé pour tous les sites, sauf pour CB où une sous-estimation systématique est observée (Fig. 7.3).

Les mesures de  $F_{CO_2}$  snowpack diffusion correspondent à la respiration du sol ( $R_{soil} = R_h + R_a[belowground]$ ). Le produit de L4C ne fournit pas d'estimation de  $R_{soil}$  puisqu'il ne distingue pas entre la  $R_a$  provenant d'au-dessus et en-dessous du sol. Dans les régions arctiques et boréales, la végétation est typiquement en dormance au cours de la saison hivernale et son activité est minimale (i.e., GPP négligeable ; Webb *et al.*, 2016). Ce postulat est corroboré par le modèle L4C pour les sites de CB et TVC où le GPP et  $R_a$  sont nuls et pour le site de HPC où le GPP et le Ra sont négligeables. Pour ces sites, il est justifié d'utiliser  $NEE = R_{soil}$  et de conclure que la comparaison directe entre NEE L4C et  $F_{CO_2}$  snowpack diffusion est valable. Pour les sites de MM et SOD, le modèle L4C estime que le GPP n'est pas négligeable et qu'il réduit d'environ un tiers les émissions par respiration ( $R_{eco}$ ). Comme le modèle L4C ne fournit pas d'estimation de  $R_{soil}$ , la comparaison de la Fig. 7.2 est effectuée avec le NNE. Il est important de noter

que si le GPP de ces sites n'est bel et bien pas négligeable en hiver, la  $R_{soil}$  est donc plus grand que le NEE utilisé pour la comparaison. Ainsi, il est possible que le modèle L4C surestime davantage la  $R_{soil}$  que les résultats présentés pour les sites de MM et SOD.

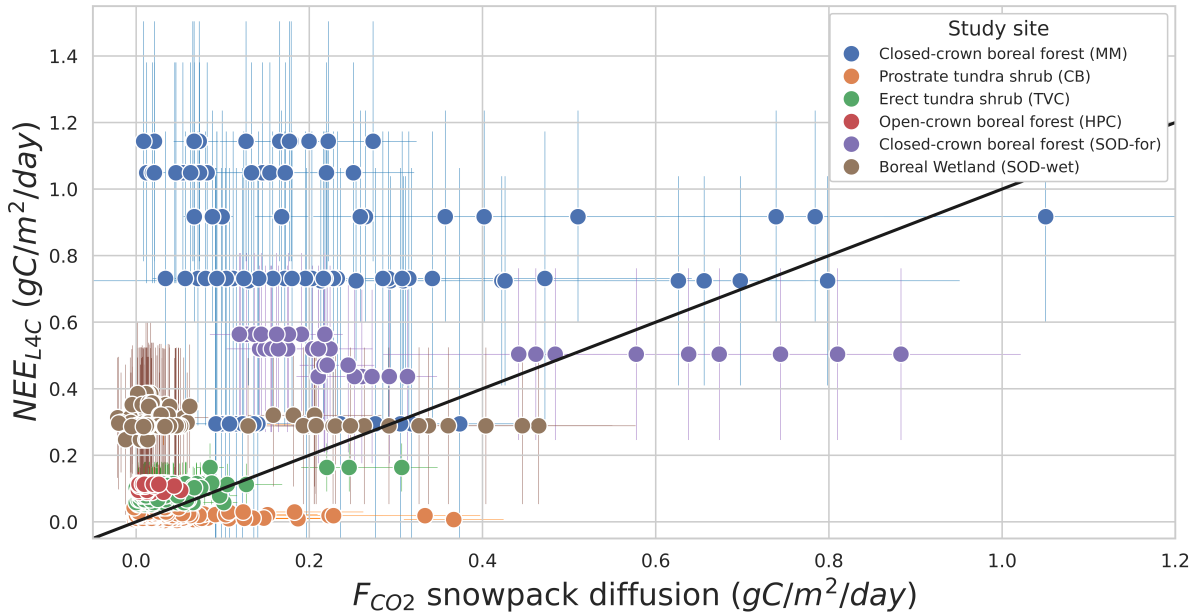


FIGURE 7.2 – Comparaison des échanges nets des écosystèmes (Net Ecosystem Exchange) estimés par le modèle L4C (NEE L4C) versus les données *in situ* obtenues en hiver à l'aide de la méthode du gradient de diffusion à travers le couvert neigeux ( $F_{CO_2}$  snowpack diffusion). La ligne diagonale noire représente la correspondance parfaite. L'incertitude des NEE L4C est fournie avec le produit SMAP L4C. Le calcul de l'incertitude des données de  $F_{CO_2}$  snowpack diffusion est détaillée dans Mavrovic *et al.*, 2023b (Sect. 3). La racine de l'erreur quadratique moyenne et les biais systématiques entre NEE L4C et  $F_{CO_2}$  snowpack diffusion peuvent être retrouvés au Tableau 7.2.

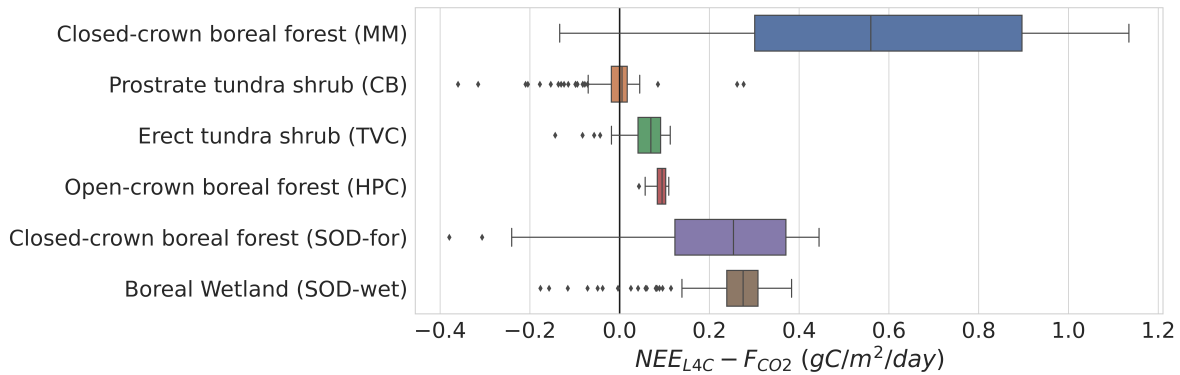


FIGURE 7.3 – Biais entre les échanges nets des écosystèmes (Net Ecosystem Exchange) estimés par le modèle L4C ( $NEE_{L4C}$ ) et les données *in situ* obtenues en hiver à l'aide de la méthode du gradient de diffusion à travers le couvert neigeux ( $F_{CO_2}$ ). Les valeurs aberrantes ont été définies comme  $> Q3 + 1.5 IQR$  où  $Q3$  est le troisième quartile et  $IQR$  l'intervalle interquartile.

TABLEAU 7.2 – Comparaison des échanges nets des écosystèmes (Net Ecosystem Exchange) simulés par le modèle L4C (NEE L4C) versus les données *in situ* obtenues en hiver à l'aide de la méthode du gradient de diffusion à travers le couvert neigeux ( $F_{CO_2}$  snowpack diffusion) pour chaque type de PFT (Plant Function Type). La racine de l'erreur quadratique moyenne (Root Mean Square Error : RMSE) est exprimée en pourcentage du  $F_{CO_2}$  moyen entre parenthèses.

Site	Ecosystem	Plant function type L4C (PFT)	PFT fraction	L4C vs $F_{CO_2}$ RMSE [gC/m <sup>2</sup> /day]	L4C vs $F_{CO_2}$ bias [gC/m <sup>2</sup> /day]	NEE decrease caused by GGP	<i>In situ</i> $F_{CO_2}$ survey area
Cambridge Bay	Prostrate tundra shrubs	Shrub Grass	72 % 7 %	0.284 (174 %)	-0.007	0 %	4x4 km
Trail Valley Creek	Erect tundra shrubs	Shrub Grass	67 % 7 %	0.072 (250 %)	+0.062	0 %	4x4 km
Havikpak Creek	Open-crown coniferous boreal forest	Shrub Grass	59 % 19 %	0.092 (642 %)	+0.090	0.9 %	250x250 m
Montmorency Forest	Closed-crown coniferous boreal forest	Deciduous needleleaf	100 %	0.666 (301 %)	+0.573	27.2 %	750x750 m
Sodankylä	Closed-crown coniferous boreal forest	Deciduous needleleaf	36 %	0.301 (100 %)	+0.205	38.7 %	700x700 m
Sodankylä	Boreal wetland	Grass	63 %	0.263 (395 %)	+0.236	30.6 %	2x2 km

Pour chaque site d'étude, les résultats présentés correspondent au PFT représentant le mieux l'échantillonnage de  $F_{CO_2}$  *in situ* (Tableau 7.2). Pour les sites de TVC, MM, SOD-for et SOD-wet, la classification de PFT de L4C représente adéquatement les observations sur le terrain. Pour le site de CB, la présence d'arbuste est minimale (< 10%), mais L4C utilise une couverture du sol dominé par l'arbuste (72%). La plus grande discordance se trouve au site HPC se situant au milieu d'une forêt boréale ouverte d'épinette noire, mais la couverture du sol de L4C est un mélange d'arbustes (59%) et de graminées (19%). Les discordances entre la couverture du sol de L4C et les observations terrains contribuent vraisemblable au grand RMSE et biais observés entre les NEE L4C et les  $F_{CO_2}$  snowpack diffusion puisque les paramètres du modèle L4C sont spécifiques à chaque type de PFT.

Il est à noter que l'échantillonnage de  $F_{CO_2}$  snowpack diffusion a été effectué sur une superficie inférieure à la taille des pixels de 9x9 km de L4C et que l'aire d'étude de chaque site était comprise dans un seul pixel de L4C (Tableau 7.2). L'échantillonnage de  $F_{CO_2}$  snowpack diffusion a été réalisé de sorte à couvrir l'ensemble des conditions de végétation, de neige et de régime thermique du sol. Conséquemment, l'étendu de la plage de  $F_{CO_2}$  snowpack diffusion est représentative de l'étendu de la variabilité intrapixel, mais la moyenne et la distribution des valeurs ne sont représentatives de la pondération de chaque type d'environnement présent dans un pixel. Un échantillonnage à l'échelle d'un pixel de L4C permettrait une comparaison multi-échelle complète.

## 7.4 Conclusion

Le produit de NEE du modèle L4C surestime majoritairement les émissions de  $CO_2$  hors de la saison de croissance en régions boréales et arctiques par rapport aux mesures *in situ*. Les raisons de cet écart systématique sont probablement multiples, mais l'évaluation de la couverture du sol (PFT) semble un facteur limitant l'habileté du modèle à estimer adéquatement le NEE hors de la saison de croissance des régions boréales et arctiques. Afin d'amener l'analyse plus loin et déterminer les raisons expliquant l'écart entre modélisation et données *in situ*, il serait pertinent de comparer les données météorologiques utilisées par le modèle L4C et celles mesurées directement sur les sites d'études afin de déterminer si les prédictions du modèle L4C sont améliorées par l'intégration de données terrain. Un tel exercice permettrait de déterminer plus précisément quelle portion de l'écart entre modélisation et données *in situ* provient des données d'entrées du modèle versus le modèle lui-même.

## Chapitre 8 : Conclusion et perspectives futures

La recherche présentée dans cette thèse représente une avancée dans la compréhension du cycle du carbone hivernal en régions arctiques et boréales. L'importance de la contribution des flux hivernaux de carbone sur le bilan annuel net a été démontré, représentant jusqu'à 42 % du bilan annuel. Cette contribution non négligeable de l'hiver doit être correctement estimée dans les modèles écosystémiques et climatiques afin de produire des prédictions fiables de l'évolution future potentielle des échanges de gaz à effet de serre en régions arctiques et boréales.

Cette étude a permis de mettre en évidence deux régimes distincts d'émissions de  $CO_2$  en hiver. Un premier régime, ayant déjà été observé par d'autres études, où le sol est complètement gelé et la totalité de l'eau se trouve sous forme de glace. C'est alors la température du sol qui est le principal contrôle environnemental des flux de  $CO_2$ . Le second régime, étudié pour la première fois dans le cadre de cette thèse, où la température du sol est près du point de congélation et qu'il y a présence d'eau liquide dans le sol (i.e., régime période zéro). C'est alors la teneur en eau liquide du sol qui devient le principal contrôle environnemental sur les flux de  $CO_2$ . Il est attendu dans un climat en réchauffement que la température du sol augmente en hiver et que la quantité d'énergie supplémentaire associée augmente également la teneur en eau liquide dans le sol. Au regard des deux régimes identifiés dans le cadre de la présente thèse, il est attendu que les émissions de  $CO_2$  augmentent en hiver dans le futur (Fig. 8.1). Dans le cas du régime période zéro, il est possible que la tendance s'inverse si les sols s'assèchent suffisamment pour que la teneur en eau liquide en hiver ne soit plus limitée par la fraction d'eau sous forme de glace, mais plutôt par la quantité totale d'eau dans le sol. Dans un tel cas, il est attendu que les émissions hivernales de  $CO_2$  diminuent. Des changements dans les régimes de précipitation pourraient également affecter l'isolation du sol en hiver par le couvert neigeux, la période la plus critique étant celle des premiers gels où la présence/absence de neige peut dicter le régime de température du sol, et ainsi l'émission de  $CO_2$ , pour le reste de l'hiver.

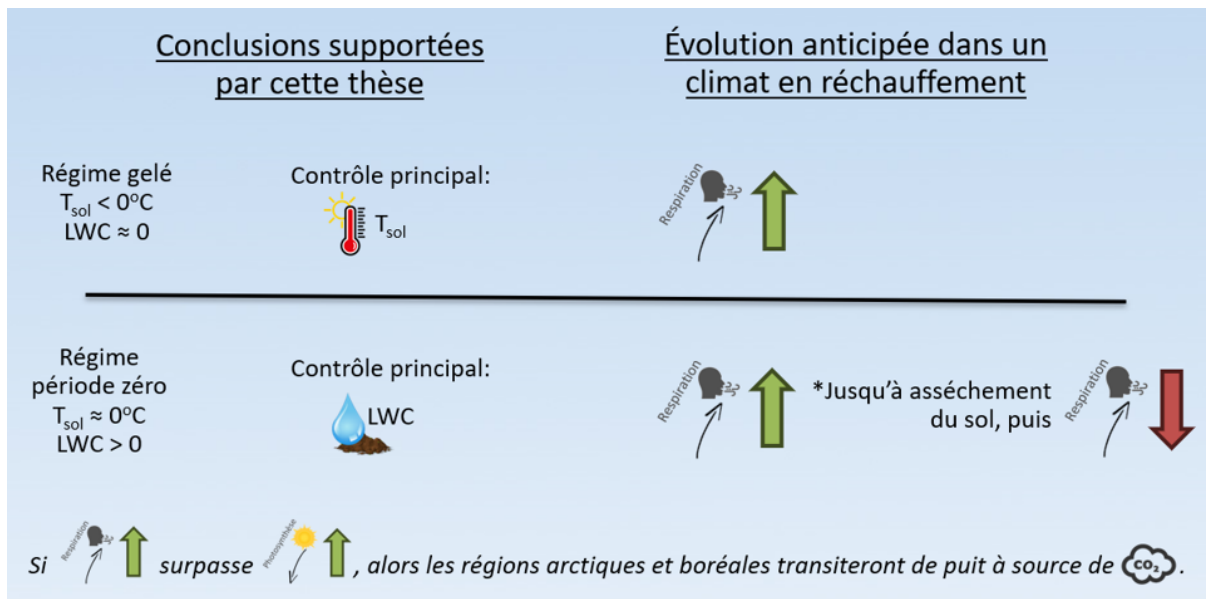


FIGURE 8.1 – Évolution anticipée des échanges de  $CO_2$  en régions arctiques et boréales au cours de l'hiver en lien avec les changements climatiques.

Une grande incertitude persiste à savoir si les régions arctiques et boréales agiront globalement comme des sources ou des puits de carbone dans le futur. Le dégel du pergélisol rend des stocks de carbone nouvellement accessible pour la décomposition stimulant les échanges de  $CO_2$  et de  $CH_4$ . Le verdissement des régions nordiques, induit par une saison de croissance rallongée et des températures moyennes plus élevées, indique une croissance de la végétation retirant davantage de  $CO_2$  de l'atmosphère. Cependant, l'augmentation des températures moyennes du sol devrait quant à elle pousser vers une augmentation des flux hivernaux de  $CO_2$  à travers les régions arctiques et boréales. La question critique demeure donc de déterminer si l'augmentation de la séquestration du  $CO_2$  par photosynthèse sera supplanté par les émissions hivernales due à la respiration hétérotrophe et, conséquemment, si les régions arctiques et boréales passeront de faibles puits de  $CO_2$  à des sources de  $CO_2$ .

Cette étude a également permis de mettre en évidence qu'en hiver, les milieux humides continuent d'émettre d'importante quantité de  $CH_4$ , tout comme au cours de la saison de croissance. À l'inverse, les sols bien drainés de la forêt boréale absorbent du  $CH_4$  en hiver. Cette étude a démontré que la teneur en eau liquide du sol est le principal contrôle environnemental de l'absorption de  $CH_4$  atmosphérique par les sols bien drainés de la forêt boréale. Puisqu'il est attendu que dans un climat en réchauffement la teneur en eau liquide dans le sol augmente, les sols bien drainés de la forêt boréale devraient absorber davantage de  $CH_4$  (Fig. 8.2). Néanmoins, cette tendance s'inversera si les conditions dans le sol deviennent anoxiques. Dans un tel cas, les sols émettront du  $CH_4$  plutôt que de l'absorber. Il est aussi important de mentionner que le dégel du pergélisol risque de modifier le paysage nordique de façon permanente, rendant certains environnements

plus propices à l'émergence de milieux humides et d'autres, plus secs (Helbig *et al.*, 2016). L'occupation du sol influence grandement les régimes d'échanges de  $CH_4$ . Alors que les sols bien-drainés absorbent généralement du  $CH_4$  atmosphérique, les milieux humides représentant d'importantes sources de  $CH_4$  vers l'atmosphère.

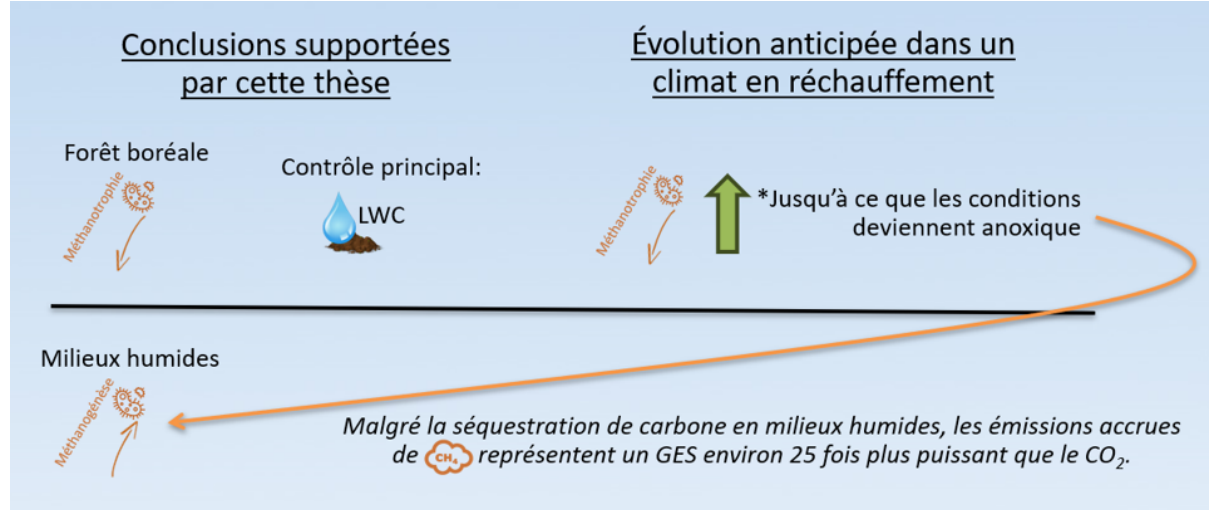


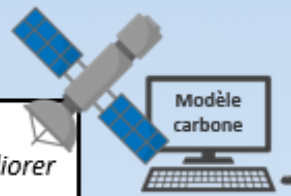
FIGURE 8.2 – Évolution anticipée des échanges de  $CH_4$  en régions arctiques et boréales au cours de l'hiver en lien avec les changements climatiques.

Cette thèse expose l'importance critique de la modélisation du cycle du carbone et de la télédétection afin d'extrapoler à l'échelle des régions arctiques et boréales les conclusions faites à partir de données *in situ*, et ainsi produire des prédictions et estimations d'échanges de  $CO_2$  et de  $CH_4$  à l'échelle globale. Notamment, il est important de réitérer le potentiel inexploité de la télédétection micro-onde afin de supporter la science du cycle du carbone en régions arctiques et boréales. Le modèle écosystémique terrestre SMAP L4C, utilisant des données de télédétection micro-onde, testé dans le cadre de cette thèse démontre une importante surestimation systématique des flux de  $CO_2$  hivernaux, illustrant que la rareté des données de flux hivernaux en régions arctiques et boréales a limité la paramétrisation et la validation des modèles écosystémiques. À ce titre, la base de données collectées dans le cadre de cette thèse possède un grand potentiel puisqu'elle représente la plus vaste base de données actuellement disponible sur la variabilité spatiale des échanges de gaz à effet de serre en hiver dans les régions arctiques et boréales.

La suite de cette thèse s'orchestra autour de trois axes : 1) La modélisation du cycle du carbone informée par télédétection, 2) L'étude détaillée de la variabilité spatiale des flux de carbone en milieux humides boréaux, et 3) L'étude de l'oxyde nitreux (Fig. 8.3). Le premier axe représente la suite directe de l'article du Chap. 6 (Mavrovic *et al.*, 2023a). Il consiste en l'intégration de données de télédétection satellitaire micro-onde pour améliorer les estimations des flux de carbone à travers le modèle SMAP L4C. L'objectif est de déterminer si l'intégration de données de télédétection satellitaire micro-

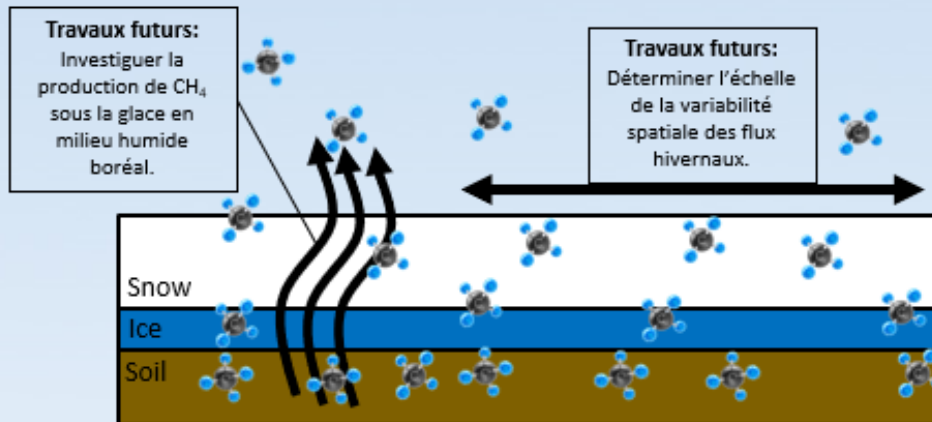
onde, principalement en bande L, permettra d'améliorer les prédictions du modèle lorsque comparé avec des données *in situ*. Ce travail touchera à la fois les flux de  $CO_2$  hivernaux et estivaux. Le second axe consiste en une étude détaillée sur la quantification de la variabilité spatiale des flux de  $CH_4$  en milieux humides boréaux. Le premier objectif de cet axe est de déterminer la taille d'un échantillon représentatif de la variabilité spatiale des flux de  $CH_4$  en milieux humides boréaux. Pour ce faire, un transect d'un kilomètre avec des mesures de flux de  $CH_4$  au 2.5m a été réalisé au site de Sodankylä (Finlande) en avril 2024. Ces données permettront de déterminer la distance à parcourir avant que la moyenne et la variance des mesures ne convergent vers une valeur stable. Ces données permettront également de déterminer si les fluctuations de flux de  $CH_4$  sont corrélés avec les variations de types de végétation et de topographie. Le deuxième objectif de cet axe est d'investiguer la production de  $CH_4$  sous l'épaisse couche de glace résultant du gel de surface du milieu humide inondé. Bien qu'une portion du  $CH_4$  parvient à se frayer un chemin jusqu'à la surface, ce qui est prouvé par les flux observés à travers le couvert de neige, une quantité importante de  $CH_4$  s'accumule sous la glace en hiver, ce qui a été prouvé par des mesures de très grandes concentrations de  $CH_4$  sous la glace. Afin d'investiguer ce phénomène, des mesures de concentrations de  $CH_4$  s'échappant de trous préalablement percés dans la glace ont été effectuées, des échantillons d'eau sous la glace ont été collectés afin de déterminer la quantité de  $CH_4$  dissous dans l'eau sous la glace et des mesures en continu ont été collectées par covariance des turbulences afin de confirmer que ce  $CH_4$  accumulé sous la glace est libéré lors de la fonte printanière. L'objectif ultime est de mettre au point une méthode robuste pour estimer la quantité de  $CH_4$  produit et emmagasiné sous la glace en hiver. La somme de cette production et du  $CH_4$  émis vers l'atmosphère à travers la glace et la neige permettra d'estimer la production totale de  $CH_4$  dans les sols des milieux humides. Le troisième axe consiste à étudier les échanges d'un gaz à effet de serre gagnant en intérêt à travers la communauté scientifique, l'oxyde nitreux ( $N_2O$ ). Le potentiel de réchauffement global du  $N_2O$  est environ 300 fois supérieur au  $CO_2$  et environ 12 fois supérieur au  $CH_4$ . La production de  $N_2O$  est intimement reliée au cycle de l'azote. De récentes études se sont penchées sur l'état actuel et l'évolution potentielle des échanges de  $N_2O$  en régions arctiques et boréales au cours de la saison de croissance (Voigt *et al.*, 2020), mais aucune données ne semblent actuellement disponibles sur les échanges de  $N_2O$  en hiver. La méthodologie développée dans le cadre de cette thèse pour collecter des mesures hivernales d'échanges de  $CO_2$  et de  $CH_4$  sera appliquée au  $N_2O$ . Les flux de  $N_2O$  étant inférieurs aux flux de  $CO_2$  et de  $CH_4$ , il est possible que des adaptations à la méthode soient requises afin de réduire le taux minimal de détection. Si la méthode est adaptée avec succès, nous collecterons la première base de données sur les flux de  $N_2O$  hivernaux en régions arctiques et boréales où peu de choses sont connus sur cycle de l'azote en hiver.

1) Intégration de données de télédétection satellitaire micro-onde pour améliorer les estimations des flux de carbone.



Thèse en cours de Rémi Madelon,  
*Utilisation de données satellitaires micro-onde bande L pour améliorer la modélisation des flux de carbone dans les régions Arctiques*

2) Étude détaillée des flux de CH<sub>4</sub> des milieux humides.



3) Étude des flux de N<sub>2</sub>O (cycle de l'azote), un GES environ 300 fois plus puissant que le CO<sub>2</sub>.

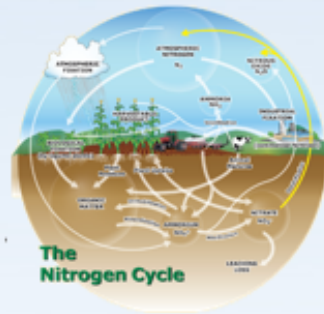


FIGURE 8.3 – Projets futurs et en cours découlant de cette thèse.

## **Financement**

Cette thèse a été financée par le Conseil de recherche en sciences naturelles et en génie du Canada (CRSNG ; Bourses Alexander-Graham-Bell et Michael-Smith), le Fonds de recherche du Québec – Nature et technologies (FRQNT ; Bourse B2X et Subvention DIALOGUE), Savoir Polaire Canada (POLAIRE), la bourse Universalis Causa de l’UQTR, le Programme de formation scientifique dans le Nord (PFSN) et le Programme de collaboration France-Québec.

## Bibliographie complémentaire aux articles

Arora, V., Boer, G. : Fire as an interactive component of dynamic vegetation models. *Biogeosciences*, 110(G2), G02008, doi : 10.1038/nclimate2318, 2005.

Arora, V., Boer, G. : Uncertainties in the 20th century carbon budget associated with land use change. *Global Change Biology*, 16, 3327–3348, doi : 10.1111/j.1365-2486.2010.02202.x, 2010.

Arora, V., Melton, J. R., Plummer, D. : An assessment of natural methane fluxes simulated by the CLASS-CTEM model. *Biogeosciences*, 15, 4683–4809, doi : 10.5194/bg-15-4683-2018, 2018.

Bayer, A., Fuchs, R., Mey, R., Krause, A., Verburg, P., Anthoni, P. : Diverging land-use projections cause large variability in their impacts on ecosystems and related indicators for ecosystem services. *Earth System Dynamics*, 12(1), 327–351, doi : 10.5194/esd-12-327-2021, 2021.

Björkman, M., Morgner, E., Cooper, E., Elberling, B., Klemedtsson, L., Björk, R. : Winter carbon dioxide effluxes from Arctic ecosystems : An overview and comparison of methodologies. *Gobal Biogeochemical Cycles*, 24, GB3010, doi : 10.1029/2009GB003667, 2010a.

Björkman, M., Morgner, E., Björk, R., Cooper, E., Elberling, B., Klemedtsson, L. : A comparison of annual and seasonal carbon dioxide effluxes between sub-Arctic Sweden and High-Arctic Svalbard. *Polar Research*, 9(1), 75-84, doi : 10.1111/j.1751-8369.2010.00150.x, 2010b.

Boucher, O., Friedlingstein, P., Collins, B., Shine, K. : The indirect global warming potential and global temperature change potential due to methane oxidation. *Environmental Research Letters*, 4(4), 044007, doi : 10.1088/1748-9326/4/4/044007, 2009.

Burba, G. : Eddy Covariance Method for Scientific, Industrial, Agricultural, and Regulatory Applications. LI-COR Biosciences, Lincoln, Nebraska, États-Unis, 331 pages, 2013.

Burba, G., Anderson, T., Komissarov, A. : Accounting for spectroscopic effects in laser-based open-path eddy covariance flux measurements. *Global Change Biology*, 25(6), 2189-2202, doi : 10.1111/gcb.14614, 2019.

Christensen, T., Ekberg, A., Strom, L., Mastepanov, M., Panikov, N., Oquist, M., Svensson, B., Nykanen, H., Martikainen, P., Oskarsson, H. : Factors controlling large scale variations in methane emissions from wetlands. *Geophysical Research Letters*, 30(7), 1414, doi : 10.1029/2002GL016848, 2003.

Curry, C. L. : Modeling the soil consumption of atmospheric methane at the global scale. *Global Biogeochemical Cycles*, 21(4), GB4012, doi : 10.1029/2006GB002818, 2007.

Derrien, D., Barré, P., Basile-Doelsch, I., Cécillon, L., Chabbi, A., Crème, A., Fontaine, S., Henneron, L., Janot, N., Lashermes, G., Quénéa, K., Rees, F., Dignac, M.-F. : Current controversies on mechanisms controlling soil carbon storage : implications for interactions with practitioners and policy-makers. A review. *Agronomy for Sustainable Development*, 43(21), GB4012, doi : 10.1007/s13593-023-00876-x, 2023.

Gedney, N., Cox, P., Huntingford, C. : Climate feedback from wetland methane emissions. *Geophysical Research Letters*, 31(9), L20503, doi : 10.1029/2004GL020919, 2004.

GOFC-GOLD : A sourcebook of methods and procedures for monitoring and reporting anthropogenic greenhouse gas emissions and removals associated with deforestation, gains and losses of carbon stocks in forests remaining forests, and forestation.GOFC-GOLD : Report version COP22-1. GOFC-GOLD Land Cover Project Office, Wageningen University, Netherlands, 2016.

Harvey, L. D. D. : A guide to global warming potentials (GWP). *Energy Policy*, 21(1), 24-34, doi : 10.1016/0301-4215(93)90205-T, 1993.

Huemmrich, K., Gamon, J., Tweedie, C., Oberbauer, S., Kinoshita, G., Houston, S., Ku-chy, A., Hollister, R., Kwon, H., Mano, M., Harazono, Y., Webber, P., Oechel, W. : Remote sensing of tundra gross ecosystem productivity and light use efficiency under varying temperature and moisture conditions. *Remote Sensing of Environment*, 114(3), 481-489, doi : 10.1016/j.rse.2009.10.003, 2010.

Kittler, F., Eugster, W., Foken, T., Heimann, M., Kolle, O., Göckede, M. : High-quality eddy-covariance  $CO_2$  budgets under cold climate conditions. *Biogeosciences*, 122(8), 2064-2084, doi : 10.1002/2017JG003830, 2017.

Kleinen, T., Mikolajewicz, U., Brovkin, V. : Terrestrial methane emissions from the Last Glacial Maximum to the preindustrial period. *Climate of the Past*, 16(2), 575–595, doi : 10.5194/cp-16-575-2020, 2020.

Lamarque, L., Félix-Faure, J., Deschamps, L., Lévesque, E., Cusson, P.-O., Fortier, D., Giacomazzo, M., Guillemette, F., Paillassa, J., Tremblay, M., Maire, V. : Footprint prediction of scalar fluxes using a Markovian analysis. *Ecosystems*, 26, 1238–1259, doi : 10.1007/s10021-023-00829-1, 2023.

Leclerc, M., Thurtell, G. : Footprint prediction of scalar fluxes using a Markovian analysis. *Boundary-Layer Meteorology*, 52(3), 247-258, doi : 10.1007/BF00122089, 1990.

Liu, L., Zhuang, Q., Oh, Y., Shurpali, N., Kim, S., Poulter, B. : Uncertainty Quantification of Global Net Methane Emissions From Terrestrial Ecosystems Using a Mechanistically Based Biogeochemistry Model. *Biogeosciences*, 125(6), e2019JG005428, doi : 10.1029/2019JG005428, 2020.

Luo, G., Kiese, R., Wolf, B., Butterbach-Bahl, K. : Effects of soil temperature and moisture on methane uptake and nitrous oxide emissions across three different ecosystem types. *Biogeosciences*, 10(5), 3205-3219, doi : 10.5194/bg-10-3205-2013, 2013.

Malhi, Y., Baldocchi, D., Jarvis, P. : The carbon balance of tropical, temperate and boreal forests. *Plant, Cell & Environment*, 22(6), 715-740, doi : 10.1046/j.1365-3040.1999.00453.x, 1991.

McCarthy, N., Guyot, A., Dowdy, A., McGowan, H. : Wildfire and Weather Radar : A Review. *JGR Atmospheres*, 124(1), 266-286, doi : 10.1029/2018JD029285, 2019.

Moffat, A., Papale D., Reichstein, M., Hollinger, D., Richardson, A., Barr, A., Beckstein, C., Braswell, B., Churkina, G., Desai, A., Falge, E., Gove, J., Heimann, M., Hui, D., Jarvis, A., Kattge, J., Noormets, A., Stauch, V. : Comprehensive comparison of gap-filling techniques for eddy covariance net carbon fluxes. *Agricultural and Forest Meteorology*, 147(3-4), 209-232, doi : 10.1016/j.agrformet.2007.08.011, 2007.

Monteith, J. : Solar Radiation and Productivity in Tropical Ecosystems. *Journal of Applied Ecology*, 9(3), 747-766, doi : 10.2307/2401901, 1972.

Novick, K., Walker, J., Chan, W., Schmidt, A., Sobek, C., Vose, J. : Eddy covariance measurements with a new fast-response, enclosed-path analyzer : Spectral characteristics and cross-system comparisons. *Agricultural and Forest Meterology*, 181, 17-32, doi : 10.1016/j.agrformet.2013.06.020, 2013.

Olefeldt, D., Hovemyr, M., Kuhn, M., Bastviken, D., Bohn, T., Connolly, J., Crill, P., Euskirchen, E., Finkelstein, S., Genet, H., Grosse, G., Harris, L., Heffernan, L., Helbig, M., Hugelius, G., Hutchins, R., Juutinen, S., Lara, M., Malhotra, A., Manies, K., McGuire, A. D., Natali, S., O'Donnell, J., Parmentier, F.-J., Räsänen, A., Schädel, C., Sonnentag, O., Strack, M., Tank, S., Treat, C., Varner, R., Virtanen, T., Warren, R., Watts, J. : The Boreal–Arctic Wetland and Lake Dataset (BAWLD). *Earth System Science Data*, 13(11), 5127–5149, doi : 10.5194/essd-13-5127-2021, 2021.

Papale, D., Reichstein, M., Aubinet, M., Canfora, E., Bernhofer, C., Kutsch, W., Longdoz, B., Rambal, S., Valentini, R., Vesala, T., Yakir, D. : Towards a standardized processing of Net Ecosystem Exchange measured with eddy covariance technique : algorithms and uncertainty estimation. *Biogeosciences*, 3, 571–583, doi : 10.5194/bg-3-571-2006, 2006.

Raynolds, M., Walker, D., Balser, A., Bay, C., Campbell, M., Cherosov, M., Daniëls, F., Eidesen, P., Ermokhina, K., Frost, G., Jedrzejek, B., Jorgenson, M., Kennedy, B., Khodol, S., Lavrinenko, I., Lavrinenko, O., Magnússon, B., Matveyeva, N., Metúsalemsson, S., Nilseno, L., Olthofp, I., Pospelovh, I., Pospelovah, E., Pouliotp, D., Razzhivinm, V., Schaepman-Strubq, G., Šibíkr, J., Telyatnikov, M. Y., Troeva, E. : A raster version of the Circumpolar Arctic Vegetation Map (CAVM). *Remote Sensing of Environment*, 232, 111297, doi : 10.1016/j.rse.2019.111297, 2019.

Saunois, M., Bousquet, P., Poulter, B., Peregon, A., Ciais, P., Canadell, J. G., Dlugokencky, E. J., Etiope, G., Bastviken, D., Houweling, S., Janssens-Maenhout, G., Tubiello, F. N., Castaldi, S., Jackson, R. B., Alexe, M., Arora, V. K., Beerling, D. J., Bergamaschi, P., Blake, D. R., Brailsford, G., Brovkin, V., Bruhwiler, L., Crevoisier, C., Crill, P., Covey, K., Curry, C., Frankenber, C., Gedney, N., Höglund-Isaksson, L., Ishizawa, M., Ito, A., Joos, F., Kim, H.-S., Kleinen, T., Krummel, P., Lamarque, J.-F., Langenfelds, R., Locatelli, R., Machida, T., Maksyutov, S., McDonald, K. C., Marshall, J., Melton, J. R., Morino, I., Naik, V., O'Doherty, S., Parmentier, F.-J. W., Patra, P. K., Peng, C., Peng, S., Peters, G. P., Pison, I., Prigent, C., Prinn, R., Ramonet, M., Riley, W. J., Saito, M., Santini, M., Schroeder, R., Simpson, I. J., Spahni, R., Steele, P., Takizawa, A., Thornton, B. F., Tian, H., Tohjima, Y., Viovy, N., Voulgarakis, A., van Weele, M., van der Werf, G. R., Weiss, R., Wiedinmyer, C., Wilton, D. J., Wiltshire, A., Worthy, D., Wunch, D., Xu, X., Yoshida, Y., Zhang, B., Zhang, Z., Zhu, Q. : The global methane budget 2000–2012. *Earth System Science Data*, 8(2), 697–751, doi : 10.5194/essd-8-697-2016, 2016.

Schuepp, P., Leclerc, M., MacPherson, J., Desjardins, R. : Footprint prediction of scalar fluxes from analytical solutions of the diffusion equation. *Boundary-Layer Meteorology*,

50(1-4), 355-373, doi : 10.1007/BF00120530, 1990.

Seidl, R., Schelhaas, M.-J., Rammer, W., Verkerk, P. : Increasing forest disturbances in Europe and their impact on carbon storage. *Nature Climate Change*, 4, 806-810, doi : 10.1038/nclimate2318, 2014.

Senf., C., Seidl, R., Hostert, P. : Remote sensing of forest insect disturbances : Current state and future directions. *International Journal of Applied Earth Observation and Geoinformation*, 60, 49-60, doi : 10.1016/j.jag.2017.04.004, 2017.

Shu, S., Jain, A. K., Kheshgi, H. S. : Investigating wetland and nonwetland soil methane emission and sinks across the contiguous United States using a land surface model. *Global Biogeochemical Cycles*, 34(7), e2019GB006251, doi 10.1029/2019GB006251, 2020.

Soloway, A., Amiro, B., Dunn, A., Wofsy, S. : Carbon neutral or a sink ? Uncertainty caused by gap-filling long-term flux measurements for an old-growth boreal black spruce forest. *Agricultural and Forest Meteorology*, 233, 110-121, doi : 10.1016/j.agrformet.2016.11.005, 2017.

Torn, S., Chapin III, F. : Environmental and biotic controls over methane flux from Arctic tundra. *Chemosphere*, 26(1-4), 357-368, doi : 10.1016/0045-6535(93)90431-4, 1993.

Turner, D., Ollinger, S., Kimball, J. : Integrating Remote Sensing and Ecosystem Process Models for Landscape- to Regional-Scale Analysis of the Carbon Cycle. *BioScience*, 54(6), 573-584, doi : 10.1641/0006-3568(2004)054[0573 :IRSAEP]2.0.CO ;2, 2004.

Voigt, C., Marushchak, M., Abbott, B., Biasi, C., Elberling, B., Siciliano, S., Sonnentag, O., Stewart, K., Yang, Y., Martikainen, P. : Nitrous oxide emissions from permafrost-affected soils. *Nature Reviews Earth & Environment*, 1, 420–434, doi : 10.1038/s43017-020-0063-9, 2020.

Walter, B. P., Heimann, M. : A process-based, climate-sensitive model to derive methane emissions from natural wetlands : Application to five wetland sites, sensitivity to model parameters, and climate. *Global Biogeochemical Cycles*, 14(3), 745–765, doi : 10.1029/1999GB001204, 2000.

Wu, H., Cui, H., Fu, C., Li, R., Qi, F., Liu, Z., Yang, G., Xiao, K., Qiao, M. : Unveiling the crucial role of soil microorganisms in carbon cycling : A review. *Science of The Total Environment*, 909, 168627, doi : 10.1016/j.scitotenv.2023.168627, 2024.

## **Annexe A - Protocole concentration de gaz**

### **A.1 Introduction**

Un protocole a été développé et déployé dans le cadre de cette thèse afin de déterminer la concentration de gaz ( $CO_2$  ou  $CH_4$ ) dans le couvert neigeux à différente profondeur, et ce, afin de déterminer les flux par gradient de diffusion à travers le couvert de neige. Le protocole a été divisé en 4 étapes : (1) Collecte du gaz à travers le couvert neigeux, (2) Transfert des échantillons de gaz collectés dans des fioles pour l'entreposage long terme, (3) Traitement des échantillons de gaz avec un analyseur de gaz, et (4) Calcul de la concentration des échantillons de gaz. Au cours des saisons hivernales 2021-2022 et 2022-2023, des équipes de mesures terrain à Cambridge Bay (hiver 2021-2022 ; Polar Canada, Canadian High Arctic Research Station et Viventem), Sodankylä (hivers 2021-2022 et 2022-2023 ; Finnish Meteorological Institute) et Trail Valley Creek (hiver 2021-2022 ; Future Skills Centre) ont reçu le protocole présenté ci-dessous afin d'effectuer des campagnes de mesures autonomes (étapes 1 et 2). Les échantillons ainsi collectés ont ensuite été transférés à l'UQTR pour déterminer leur concentration (étapes 3 et 4).

### **A.2 Collecte d'échantillons de gaz**

L'objectif de cette étape est de collecter des échantillons de gaz provenant de différentes profondeurs à travers le couvert de neige (Fig. 3.3.2). La collecte est effectuée en tentant de minimiser les perturbations du couvert de neige afin de ne pas altérer le gradient naturel de concentration de gaz présent à travers le couvert de neige. Pour se faire, une mince tige creuse est utilisée pour aspirer le gaz présent dans les porosités du manteau neigeux. La tige est insérée verticalement à partir de l'interface neige/atmosphère et poussée progressivement vers le sol alors que des échantillons de gaz sont aspirés aux diverses profondeurs pré-déterminées. Un minimum de deux échantillons à des profondeurs différentes est nécessaire afin d'estimer une valeur de flux. Néanmoins, il est recommandé d'en collecter davantage afin de minimiser l'incertitude sur les valeurs de flux et d'éviter d'être incapable d'estimer un flux dû à un échantillon perdu ou contaminé. Un profil vertical comprenant cinq échantillons de gaz (incluant l'air ambiant) s'est avéré un bon compromis entre incertitude et temps d'échantillonnage, le protocole présenté ici est donc basé sur un profil vertical à cinq échantillons. La quantité de gaz collectée par échantillon est dépendante de ce qui est requis par la méthode de détermination de la concentration de ce gaz. La méthode développée à l'UQTR requiert une collecte d'environ  $60\ ml$  de gaz par échantillon. Il est possible d'estimer une valeur de flux peu importe la distance

verticale entre les échantillons, mais il est recommandé de suivre les deux recommandations suivantes : (1) Un espace minimal de  $5 - 7.5\text{ cm}$  devrait être conservé entre deux échantillonnage afin d'éviter que les volumes d'échantillonnage se recoupe, cet espace est basé sur un échantillonnage de  $60\text{ ml}$  de gaz et une densité de la neige entre  $100$  et  $650\text{ kg m}^{-3}$ , et (2) Le gaz provenant du bas de couvert de neige est moins à risque d'être affecté par le vent et ainsi l'estimation des flux est moins à risque d'être biaisé. Avec cinq échantillons, une distribution à peu près uniformément répartie le long du profil vertical s'est avérée adéquate et est présentée dans le protocole ci-dessous. Suite à la collecte des échantillons de gaz, il est important de mesurer les paramètres du couvert de neige afin de permettre l'estimation des valeurs de flux, principalement la densité et température de la neige. Des vidéos expliquant le protocole de collecte du gaz à travers le couvert de neige ont été produites pour nos partenaires collectant les échantillons de gaz sur le terrain :

Collecte d'échantillon de gaz (français) : <https://youtu.be/BFDUbZyNlQ>

Collecte d'échantillon de gaz (anglais) : <https://youtu.be/072OqZ1I-YM>

Mesure des propriétés de la neige (anglais) : <https://youtu.be/l6gsE3qjEgw>

### A.2.1 Procédure

- 1) Déterminer la localisation de la prise de mesure
- 2) Évaluer la hauteur de neige ( $h_{snow}$ ) approximative du couvert de neige environnant avec la tige d'échantillonnage.
- 4) Déterminer la profondeur des échantillons de gaz à collecter à partir de  $h_{snow}$ . Pour un profil à cinq échantillons, il est recommandé d'utiliser l'air ambiant,  $3/4 h_{snow}$ ,  $1/2 h_{snow}$ ,  $1/4 h_{snow}$  et l'interface sol/neige.
- 3) Collecter l'échantillon d'air ambiant : activer le piston de la seringue quelques fois pour évacuer le gaz latent, puis aspirer environ  $55\text{ ml}$  d'air ambiant  $5\text{ cm}$  au-dessus de l'interface neige/atmosphère.
- 5) Insérer la tige d'échantillonnage à la profondeur désirée.
- 6) Connecter une seringue à la tige d'échantillonnage.

- 7) Évacuer le gaz latent dans la tige d'échantillonnage et la seringue : aspirer 3 – 5  $ml$  de gaz du couvert de neige (Fig. A.1a), puis l'évacuer vers l'atmosphère (Fig. A.1b).
- 8) Aspirer environ 55  $ml$  de gaz provenant du couvert de neige (un peu moins pour des  $T_{air} < -15^{\circ}C$ ) (Fig. A.1a).
- 9) Fermer la valve de sortie de la seringue.
- 10) Déconnecter la seringue de la tige d'échantillonnage.
- 11) Noter la profondeur de l'échantillon collecté.
- 12) Pousser la tige d'échantillonnage à la profondeur suivante souhaitée pour le prochain échantillon de gaz et répéter les étapes 6 à 11 jusqu'à l'obtention de tous les échantillons de gaz du profil vertical.
- 13) Creuser un puit à neige et mesurer les propriétés de la neige (densité, température, etc.)

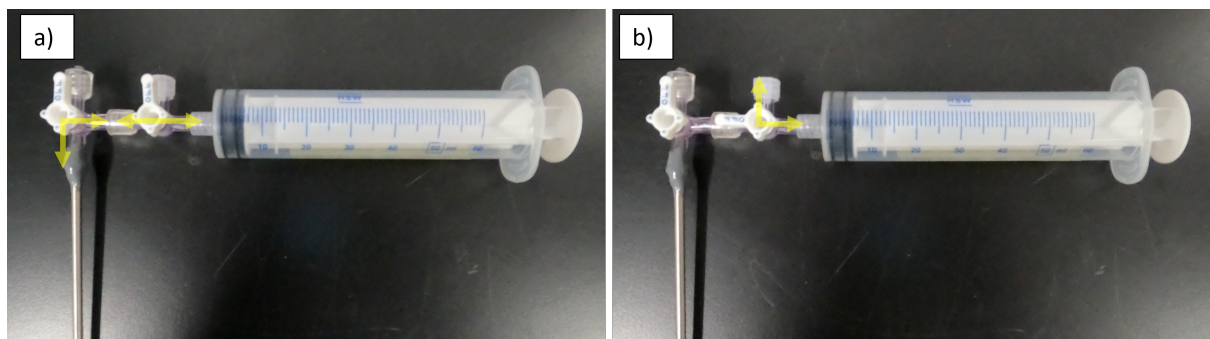


FIGURE A.1 – Positionnement des valves à trois voix. (a) Circulation du gaz entre la tige d'échantillonnage et la seringue. (b) Circulation du gaz entre la seringue et l'atmosphère.

### A.2.2 Liste du matériel nécessaire

- Tige d'échantillonnage d'une longueur suffisante pour le couvert de neige attendu : au moins 2 tiges si possible
- Disque d'arrêt en caoutchouc : 1 par tige d'échantillonnage plus quelques-uns de remplacement
- Tube de transport pour les tiges d'échantillonnage : 1
- Seringue munie d'une valve à trois voix ( $\geq 60 ml$ ) : suffisamment pour l'échantillonnage prévu
- Sonde avalanche graduée : 1

- Cahier de notes
- Crayon
- Équipement de mesure des propriétés du couvert de neige

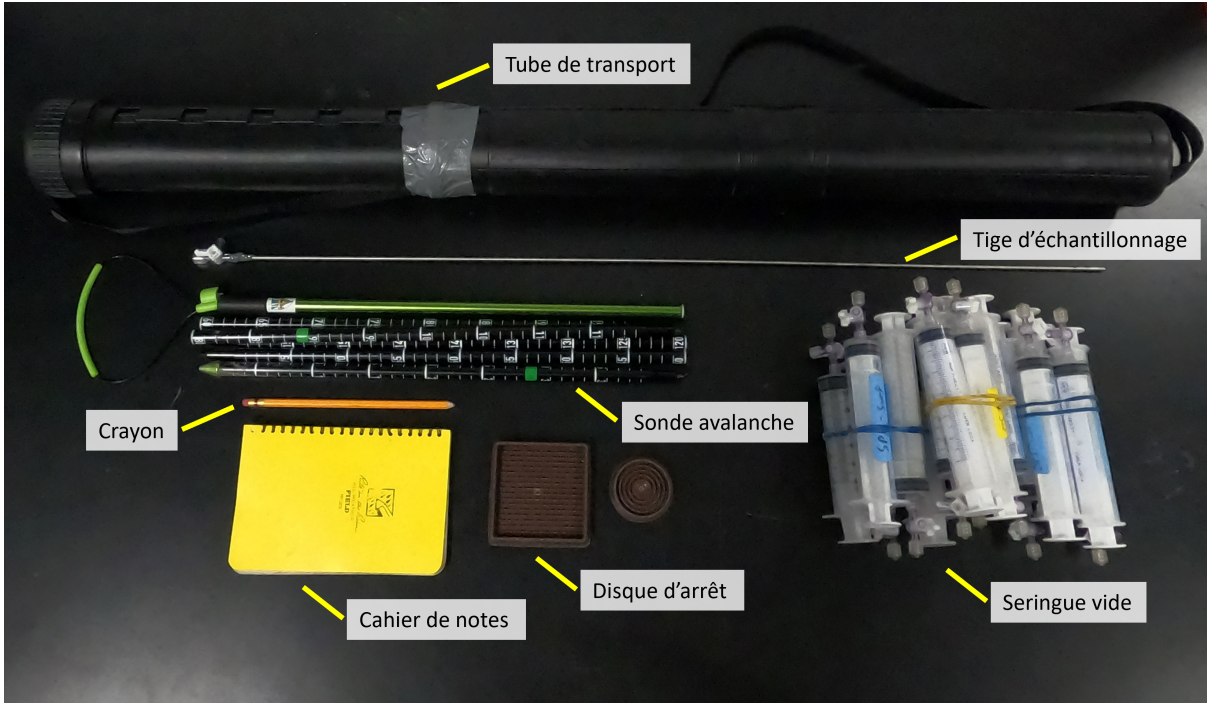


FIGURE A.2 – Liste du matériel nécessaire pour la collecte d'échantillons de gaz.

### A.3 Transfert d'échantillons de gaz

La collecte des échantillons de gaz sur le terrain se fait à l'aide de seringues. Les seringues ne sont pas des récipients fiables pour conserver du gaz au-delà d'environ 24 h. S'il est impossible de traiter rapidement les échantillons de gaz avec un analyseur de gaz après la collecte, il est essentiel de transférer les échantillons de gaz dans des fioles permettant le transport et l'entreposage à long terme. Les fioles *Labco Exetainer® 12 ml* (Labco Ltd., Lampeter, UK) s'avèrent une solution fiable et testée pour le transport et l'entreposage des échantillons de gaz pour au moins 6 mois (Mavrovic *et al.*, 2023b). Une vidéo expliquant le protocole de transfert des échantillons de gaz a été produite pour nos partenaires collectant les échantillons de gaz sur le terrain :

Transfert d'échantillon de gaz (anglais) : [https://youtu.be/\\_7V8SWBSevQ](https://youtu.be/_7V8SWBSevQ)

#### A.3.1 Procédure

1) Mettre en place le montage : placer le tube de transfert de façon à ce que la sortie sans aiguille soit complètement submergée dans un récipient d'eau et la sortie avec aiguille

soit à l'air libre (Fig. A.3).

- 2) Identifier une fiole vide avec l'identifiant de site, date, numéro de profile et profondeur d'échantillonnage de la seringue sélectionnée.
- 3) Connecter l'aiguille du tube de transfert à la fiole en perçant le septum.
- 4) Connecter une aiguille à la valve de la seringue.
- 5) Connecter la seringue à la fiole en perçant le septum.
- 6) Appliquer une pression constante sur le gaz de la seringue en appuyant sur son piston.
- 7) Ouvrir la valve de la seringue pour laisser le gaz circuler entre la seringue et la fiole (s'assurer que la sortie vers l'air ambiant soit fermée) : des bulles d'air devraient remonter à la surface du récipient d'eau.
- 8) Retirer l'aiguille du tube de transfert du septum de la fiole lorsqu'il reste entre 30 et 35 *ml* de gaz dans la seringue.
- 9) Continuer d'appliquer une pression sur le gaz de la seringue jusqu'à ce que la seringue soit vide.
- 10) Retirer l'aiguille de la seringue du septum de la fiole.

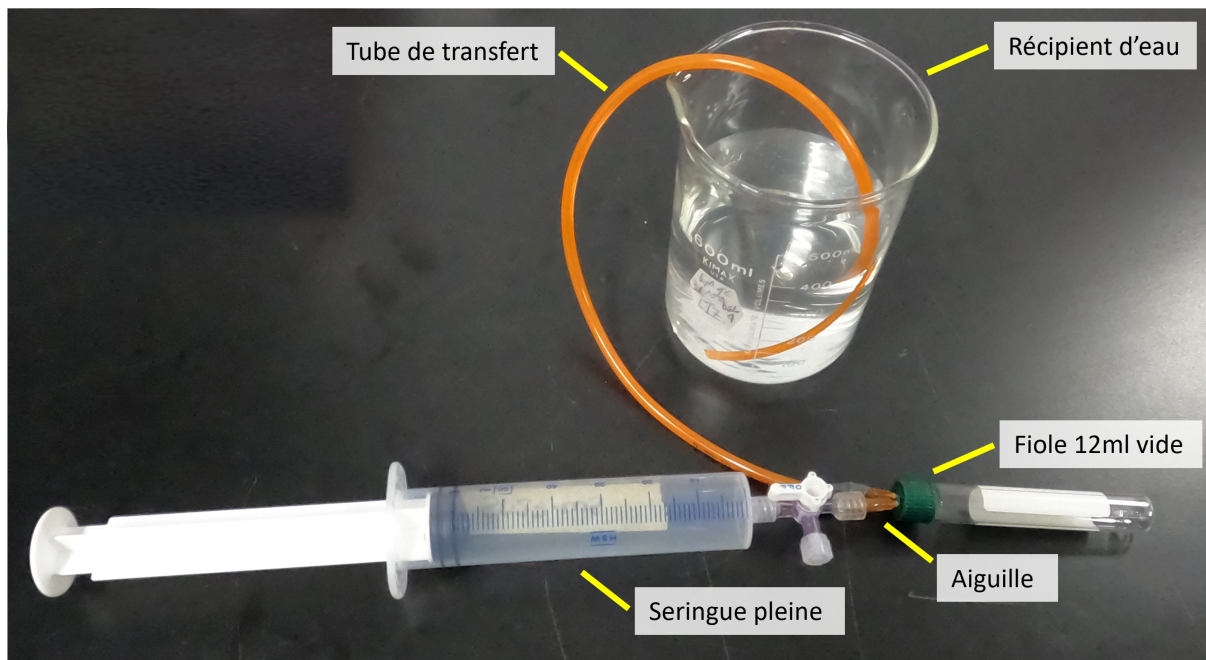


FIGURE A.3 – Montage pour le transfert d'échantillons de gaz tel qu'il devrait être après l'étape 5 de la procédure.

### A.3.2 Liste du matériel nécessaire

- Fioles *Labco Exetainer® 12 ml* (Labco Ltd., Lampeter, UK) : suffisamment pour la quantité d'échantillons de gaz à transférer
- Seringue pleine d'un échantillon de gaz
- Tube de transfert avec aiguille : quelques-uns
- Récipient d'eau
- Aiguilles : une douzaine
- Crayon

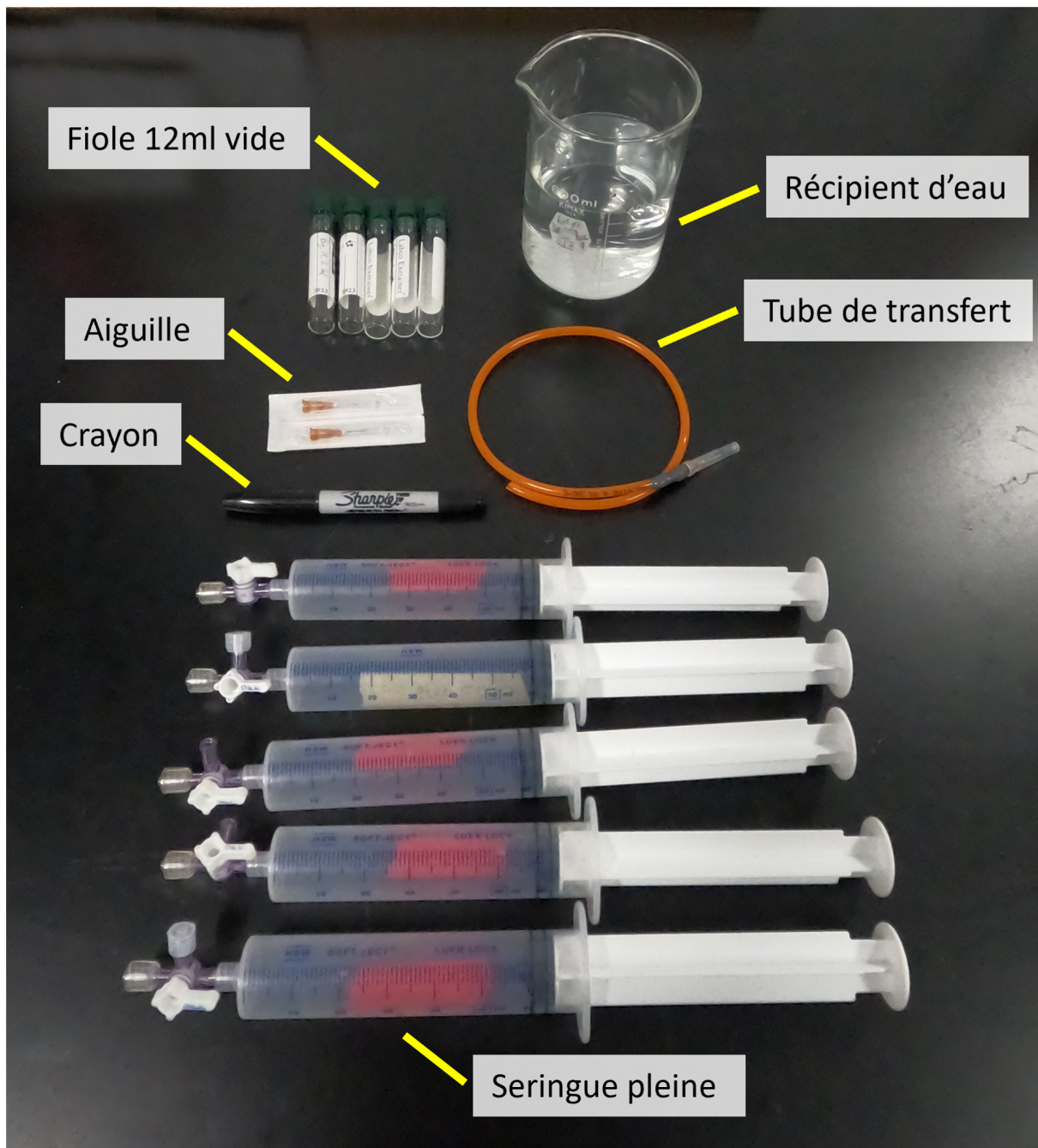


FIGURE A.4 – Matériel nécessaire pour le transfert d'échantillons de gaz.

#### A.4 Concentration des échantillons de gaz

Une fois collectés, les échantillons de gaz doivent être transportés vers un analyseur de gaz afin de déterminer leur concentration. Il existe plusieurs analyseurs de gaz et méthodes variant largement en précision. Le protocole présenté ici utilise un analyseur de gaz *Licor LI-7810 CH<sub>4</sub>/CO<sub>2</sub>/H<sub>2</sub> Trace Gas Analyzer* (LI-COR Biosciences, Lincoln, Nebraska) et est inspiré du protocole à circuit ouvert mis en place par *Licor* pour les échantillons de gaz à petit volume

(<https://www.licor.com/documents/xst0ld9j0zfby78bmpdq19i7rmjjjmng>). Cette méthode re-

quiert d'utiliser des gaz d'étalonnages à concentration connue et un gaz de référence circulant en continu dans l'analyseur de gaz. Il est recommandé que le gaz de référence ait une valeur loin de la valeur typique des échantillons de gaz, nous avons utilisé 200 ppm  $CO_2$  / 1.1 ppm  $CH_4$ . Un minimum de deux gaz d'étalonnage est requis afin d'obtenir une courbe d'étalonnage. Nous en avons utilisé trois à des fins de contre-vérification tout en moyenne sur une dizaine d'échantillons de chaque gaz d'étalonnage. Les gaz d'étalonnage utilisés sont 0 ppm  $CO_2$  / 0 ppm  $CH_4$ , 400 ppm  $CO_2$  / 1.8 ppm  $CH_4$  et 1000 ppm  $CO_2$  / 10 ppm  $CH_4$ . La méthode ainsi développée a été comparée aux résultats obtenus par deux autres équipes avec deux autres analyseurs de gaz et méthodes. Aucune différence significative n'a été constatée en comparant les résultats obtenus sur les mêmes sites d'études avec les différents analyseurs de gaz (Sect. 3.3.6).

#### A.4.1 Procédure

- 1) Mettre en place le montage en circuit ouvert présenté à la Fig. A.5.
- 2) Démarrer l'analyseur de gaz et attendre qu'il atteigne sa température d'opération (environ 30-40 minutes).
- 3) Ajuster le débit du gaz de référence circulant en continu à environ 4 L/min.
- 4) Si les échantillons de gaz proviennent de fioles : Connecter une seringue vide équipée d'une valve à deux voix à la fiole contenant l'échantillon de gaz en perçant le septum, puis ouvrir la valve pour aspirer la totalité de l'échantillon de gaz en créant une sous-pression en tirant le piston de la seringue avant de fermer la valve.
- 5) Évaluer le volume de l'échantillon de gaz à partir de la gradation de la seringue.
- 6) Noter l'heure telle qu'indiqué par l'analyseur de gaz quelques secondes avant de transférer l'échantillon de gaz dans l'analyseur de gaz.
- 7) Connecter une seringue contenant l'échantillon de gaz à la connexion à trois voix juste avant l'entrée de l'analyseur de gaz.
- 8) Ouvrir la valve à deux voix.
- 9) Appliquer une pression constante sur le piston de la seringue afin de transférer la totalité de son contenu dans l'analyseur de gaz. La pression appliquée devrait être suffisamment faible pour ne pas saturer la lecture de l'analyseur de gaz (figure A.6).

- 10) Noter l'heure telle qu'indiquée par l'analyseur de gaz une fois que la mesure de concentration s'est stabilisée à la valeur du gaz de référence circulant en continu.
- 11) Répéter les étapes 4 à 9 pour chaque gaz d'étalonnage et chaque échantillon à analyser.

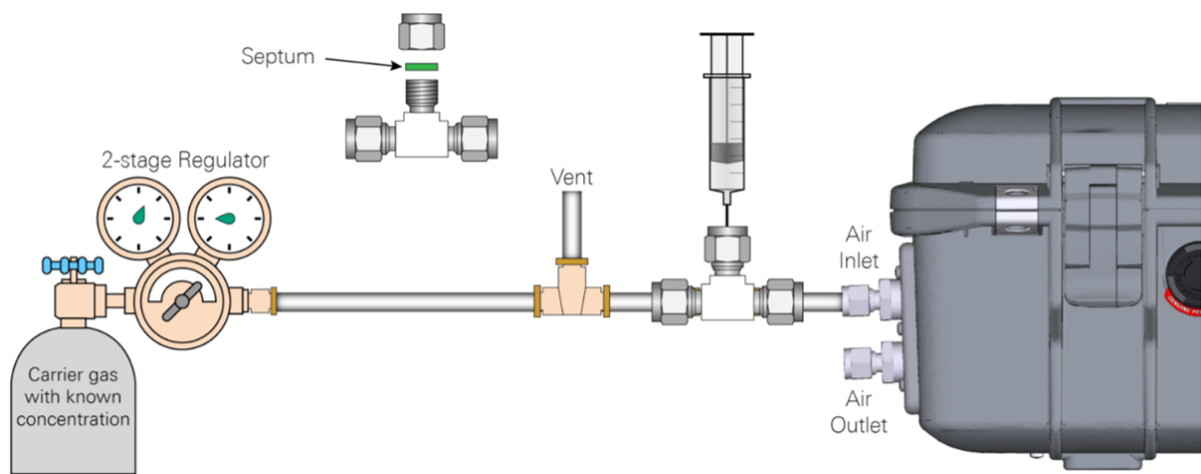


**FIGURE A.5 –** Montage pour analyse d'échantillon de gaz de faible volume à partir d'un analyseur de gaz *Licor LI-7810 CH<sub>4</sub>/CO<sub>2</sub>/H<sub>2</sub>*) *Trace Gas Analyzer*. L'ajout d'un débitmètre entre le régulateur et la connexion à trois voix pour la ventilation est utile afin de réguler le flux de gaz entrant dans l'analyseur de gaz et ainsi éviter de surcharger la pompe de l'analyseur de gaz. Source : <https://www.licor.com/documents/xst0ld9j0zfb78bmpdqi9i7rmjjjjmg>

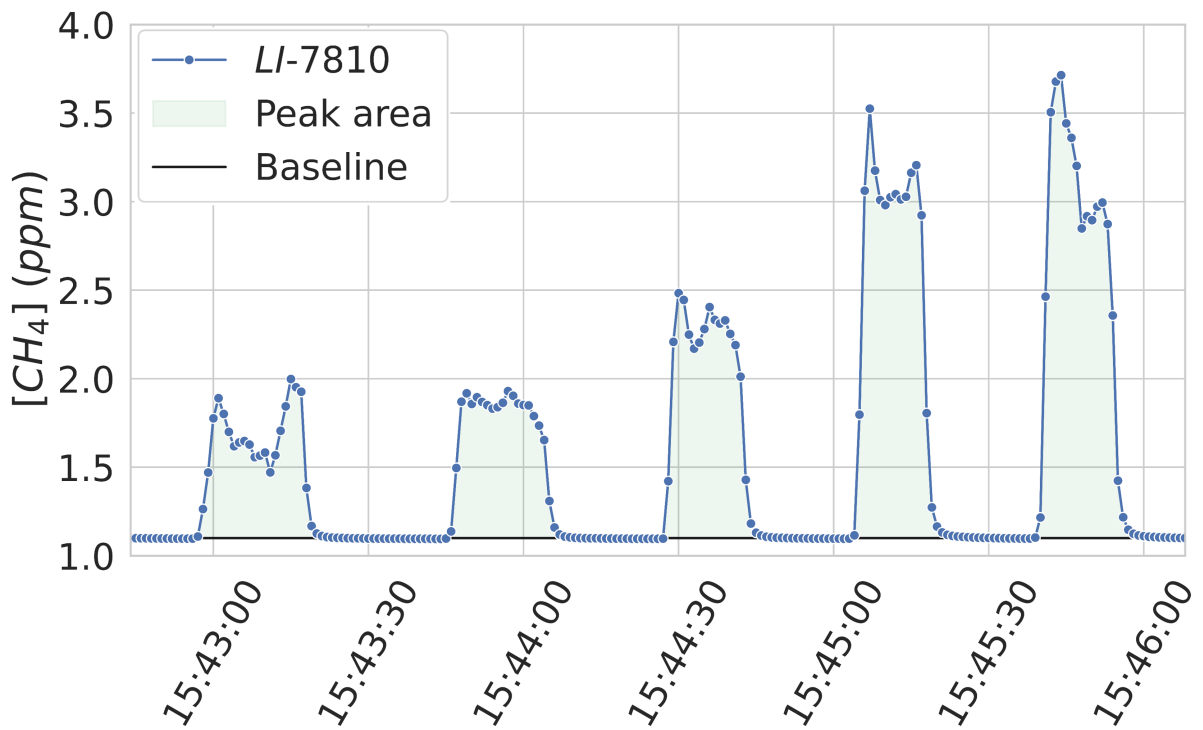


FIGURE A.6 – Concentration de  $CH_4$  en fonction du temps tel que mesurée par l'analyseur de gaz *Licor LI-7810 CH<sub>4</sub>/CO<sub>2</sub>/H<sub>2</sub> Trace Gas Analyzer* pour un profil de cinq échantillons de gaz provenant de Sodankylä. Chaque pic représente un échantillon de gaz et la baseline représente le gaz de référence circulant en continu dans l'analyseur de gaz.

#### A.4.2 Liste du matériel nécessaire

- Analyseur de gaz *Licor LI-7810 CH<sub>4</sub>/CO<sub>2</sub>/H<sub>2</sub> Trace Gas Analyzer* (LI-COR Biosciences, Lincoln, Nebraska)
- Gaz de référence : au moins 2
- Régulateur de pression
- Débitmètre
- Tube en polyéthylène 1/8" : environ 2 mètres
- Raccord à trois voix
- Raccord à trois voix avec septum
- Seringue vide ( $\geq 40\ ml$ )
- Aiguille : une vingtaine
- Clés (40mm et 9/16")

## A.5 Traitement des données

La méthode du calcul de la concentration des échantillons de gaz à faible volume (<https://www.licor.com/documents/xst0ld9j0zfb78bmpdq9i7rmjjjmg>) nécessite d'étalonner le rapport de l'aire des pics de concentration de gaz (*Peak area*) sur le volume de gaz ( $V_{cal}$  ou  $V_{sample}$ ) en fonction de la différence entre la concentration du gaz échantillonné ( $[CH_4]_{cal}$  ou  $[CH_4]_{sample}$ ) et la concentration du gaz circulant en continu dans l'analyseur de gaz ( $[CH_4]_{base}$ ) (Eq. A.3). Le  $CH_4$  est utilisé ici à titre d'exemple, il en va de même pour le  $CO_2$ . Une fois l'étalonnage terminé, il est possible de calculer la concentration des échantillons de gaz (Sect. A.5.2). La précision de cette méthode est inférieure à 1 %, ce qui en fait une source d'incertitude négligeable par rapport à d'autres paramètres plus incertains à considérer dans l'évaluation de l'incertitude des flux de carbone (Mavrovic *et al.*, 2023b).

### A.5.1 Étalonnage

L'étalonnage de l'analyseur permet de trouver la relation entre *Peak area* /  $V_{cal}$  et la concentration de l'échantillon de gaz d'étalonnage via le paramètre  $\alpha$  :

$$\frac{\text{Peak area}}{V_{cal}} = \alpha \cdot ([CH_4]_{cal} - [CH_4]_{base}) \quad (\text{A.3})$$

Pour déterminer l'aire sous les pics de concentration de gaz d'étalonnage, il faut d'abord isoler chaque pic de gaz d'étalonnage à partir des temps notés aux étapes 6 et 10 de la Sect. A.4.1 (Fig. A.6). Le calcul de *Peak area* est effectué entre les mesures de l'analyseur de gaz *Licor LI-7810* et la concentration moyenne de  $[CH_4]_{base}$  telle que mesurée par l'analyseur de gaz. L'implémentation de ce calcul a été effectuée avec la fonction *integrate.trapezoid* de la librairie *SciPy* utilisant la méthode des trapèzes (*Python 3.10.6*).

Le rapport entre *Peak area* et  $V_{cal}$  est théoriquement constant. Néanmoins, à des volumes de gaz inférieurs à 30 ml, ce rapport s'écarte de la moyenne (Fig. A.7). Lorsque le volume de gaz des échantillons est inférieur à 30 ml, il est recommandé de déterminer une calibration spécifique à chaque  $V_{sample}$  à partir d'une régression telle que celle présentée à la Fig. A.7.

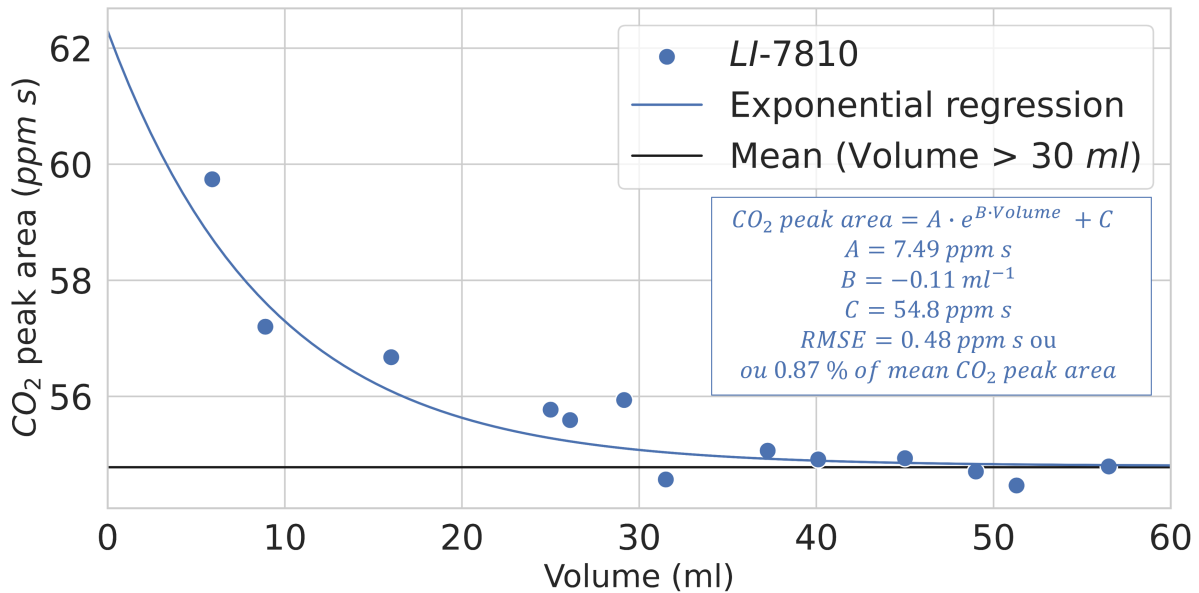


FIGURE A.7 – Aire sous la courbe des pics de concentration de  $CO_2$  en fonction du volume de l'échantillon de gaz d'étalonnage utilisé. La ligne noire représente la moyenne des aires sous la courbe pour les échantillons de gaz d'étalonnage avec un volume supérieur à 30 ml. Cette moyenne est égale à  $54.78 \text{ ppm s ml}^{-1}$  avec un écart-type de  $0.17 \text{ ppm s ml}^{-1}$  ( $0.31\%$  de la moyenne). Les données proviennent d'une procédure d'étalonnage effectué à l'UQTR avec un analyseur de gaz *Licor LI-7810 CH<sub>4</sub>/CO<sub>2</sub>/H<sub>2</sub> Trace Gas Analyzer* le 2021-09-24.

L'étalonnage de l'analyseur de gaz est obtenu à partir de la relation entre  $Peak area/V_{cal}$  et  $[CH_4]_{cal} - [CH_4]_{base}$  (Fig. A.8). En plus des gaz d'étalonnage, la valeur théorique de  $Peak area/V_{cal} = 0$  lorsque  $[CH_4]_{cal} = [CH_4]_{base}$  est utilisé pour l'étalonnage. Le coefficient de corrélation de l'étalonnage est typiquement supérieur à 0.999, permettant une détermination précise de la concentration des échantillons de gaz à partir du paramètre  $\alpha$ .

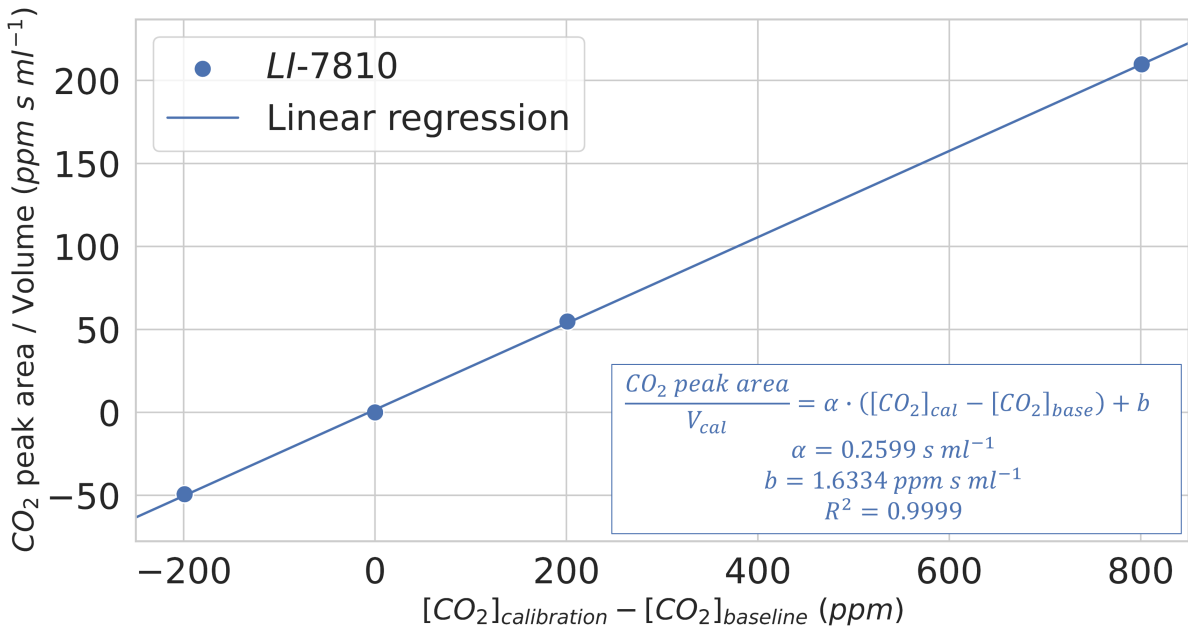


FIGURE A.8 – Étalonnage de l’analyseur de gaz pour les échantillons de gaz à faible volume. Rapport entre l’aire sous la courbe des pics de concentration de  $CO_2$  et le volume de gaz d’étalonnage en fonction de la différence entre la concentration du gaz d’étalonnage et le gaz circulant en continu dans l’analyseur de gaz. Les données proviennent d’une procédure d’étalonnage effectué à l’UQTR avec un analyseur de gaz *Licor LI-7810 CH<sub>4</sub>/CO<sub>2</sub>/H<sub>2</sub> Trace Gas Analyzer* le 2021-09-24.

### A.5.2 Calcul concentration

Une fois l’étalonnage terminé, l’Éq. A.3 peut être adaptée afin de déterminer la  $[CH_4]_{sample}$  :

$$[CH_4]_{sample} = \alpha \cdot \frac{Peak\ area}{V_{sample}} + [CH_4]_{base} \quad (\text{A.4})$$

La valeur de  $\alpha$  est celle trouvée à la section A.5.1 et *Peak area* est déterminé de la même façon qu’à la section A.5.1.

## Annexe B - Méthodes de mesure des flux de carbone

La collecte de données de flux de carbone en hiver dans les régions arctiques et boréales se heurte à plusieurs défis techniques reliés aux conditions hivernales difficiles et à l'étendue de ces vastes régions éloignées (Natali *et al.*, 2019 ; Virkkala *et al.*, 2022). Les méthodes disponibles pour mesurer les flux de carbone en hiver comprennent : 1) la covariance turbulente (Sect. B.1), 2) les mesures en chambre sous ou au-dessus du couvert neigeux (Sect. B.2) et 3) la méthode du gradient de diffusion à travers le couvert neigeux (Sect. 3 et 4). Chacune de ces méthodes présente ses avantages et ses limites (figure B.1), tel que décrit aux sous-sections suivantes.

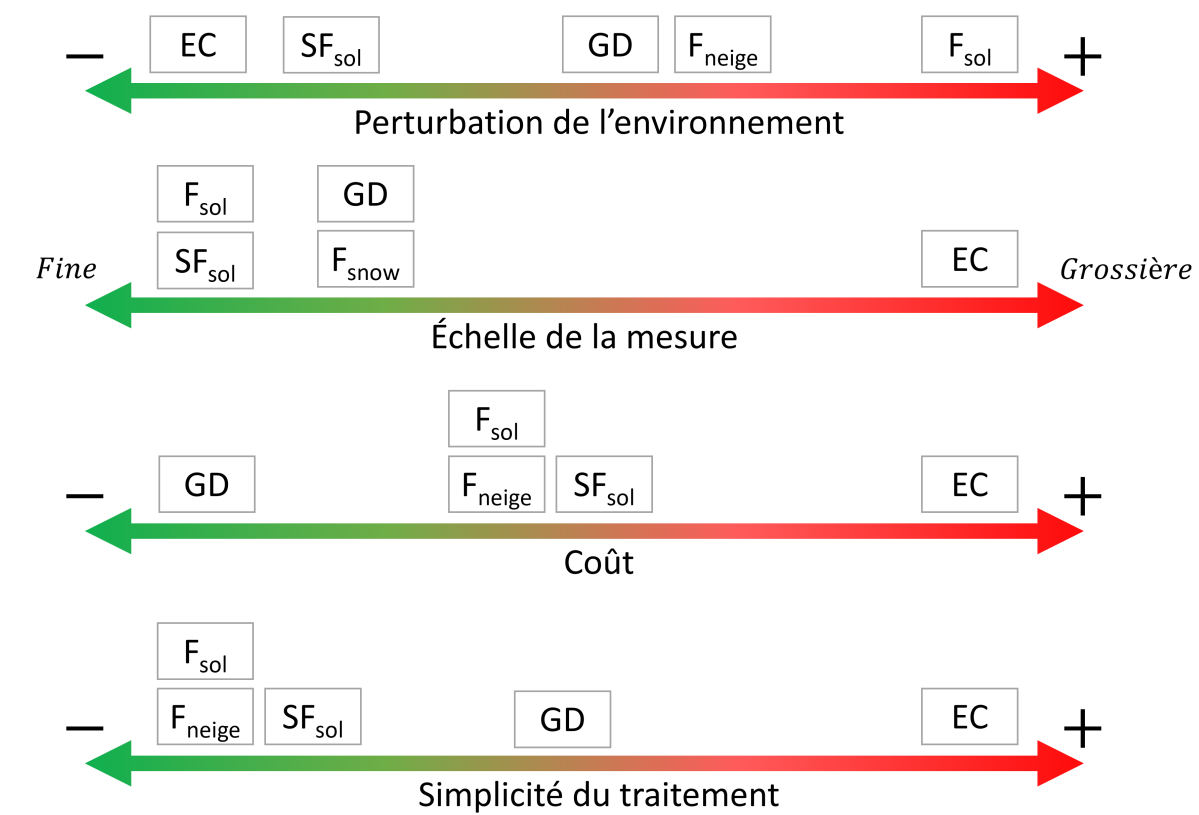


FIGURE B.1 – Comparaison des méthodes de mesure des flux de carbone : covariance des turbulences (EC), gradient de diffusion (GD), chambre dynamique ou statique placée sur la neige ( $F_{neige}$ ), au sol ( $F_{sol}$ ) et au sol en permanence ( $SF_{sol}$ ).

### B.1 Covariance des turbulences

La technique des covariances des turbulences (EC) exploite les turbulences présentes dans l'atmosphère afin d'estimer les flux nets de carbone entre la surface terrestre et l'atmosphère à haute résolution temporelle et en minimisant les perturbations environnementales (Baldocchi *et al.*, 2001 ; Pastorello *et al.*, 2020). Le flux d'air de la couche inférieure de l'atmosphère peut être simplifié comme un flux horizontal entraînant de nom-

breux tourbillons en rotation appelé turbulence (figure B.2). Ces turbulences possèdent une composante horizontale et une composante verticale. La méthode des covariances des turbulences (Eddy Covarianc : EC) est une technique permettant de calculer les flux turbulents vitaux à partir de la composante verticale des turbulences (Balocchi, 2003). Les turbulences atmosphériques fluctuant très rapidement, la mesure d'EC reposent donc sur une fréquence de mesure très rapide, typiquement entre 10 et 20 hertz. Deux types de mesure sont requis : la composante verticale de la vitesse des turbulences mesurée à partir d'un anémomètre acoustique et la concentration de  $CO_2$  et/ou de  $CH_4$  mesuré à partir d'un analyseur de gaz (figure B.3). L'anémomètre acoustique est constitué de 6 capteurs acoustiques appariés (i.e., trois axes de mesures) permettant de mesurer la direction et la vitesse du vent en trois dimensions. L'analyseur de gaz typique présenté à la figure B.3b mesure la concentration de  $CO_2$  de l'atmosphère par spectroscopie. Un laser infrarouge effectue un parcours ouvert (i.e., à même l'air ambiant) entre la tête et la section principale de l'analyseur de gaz. D'autres systèmes à parcours fermé aspirent l'air via une pompe dans un parcours clos où la lecture spectroscopique est effectuée (Papale *et al.*, 2006 ; Burba, 2013). Une nouvelle classe d'analyseurs de gaz à parcours encloîtré combine avantageusement les propriétés des systèmes à trajets fermés (résistance aux intempéries, correction minimale des fluctuations de la densité et température de l'air) et des systèmes à trajets ouverts (faible demande énergétique, fréquence de mesure élevée, bonne réponse spectrale, stabilité de la calibration) (Novick *et al.*, 2013 ; Burba *et al.*, 2019). Le système à parcours encloîtré est un hybride des systèmes ouvert et fermé exploitant de courts tubes d'échantillonnage afin de guider le gaz vers un compartiment interne de l'analyseur spectral.

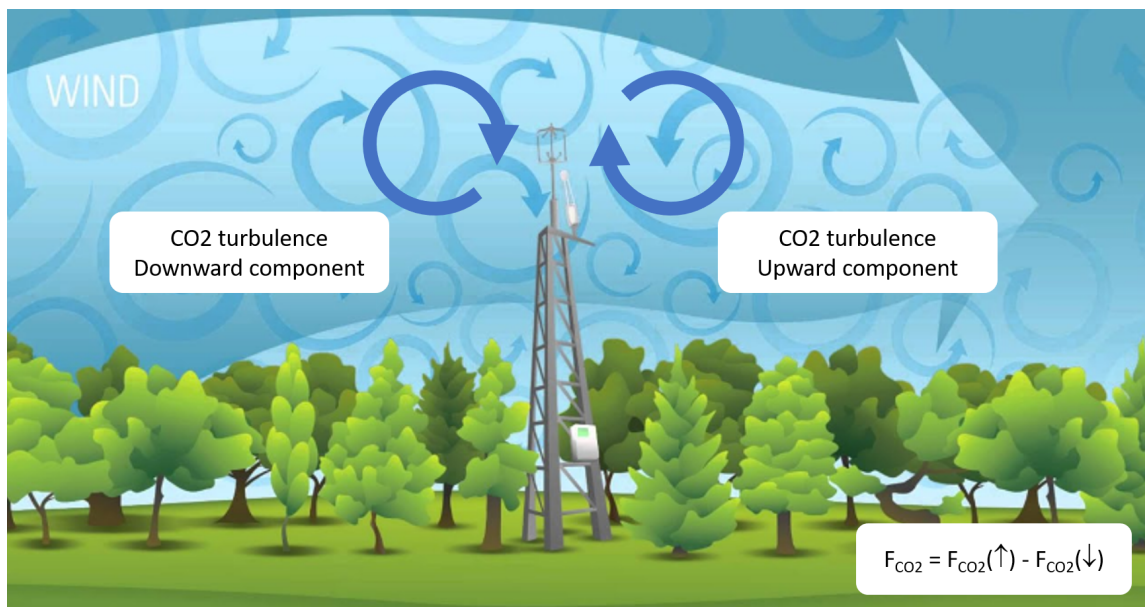


FIGURE B.2 – Principe de la mesure des flux de carbone à partir de la covariance des turbulences. Schéma inspiré de Burba (2013).

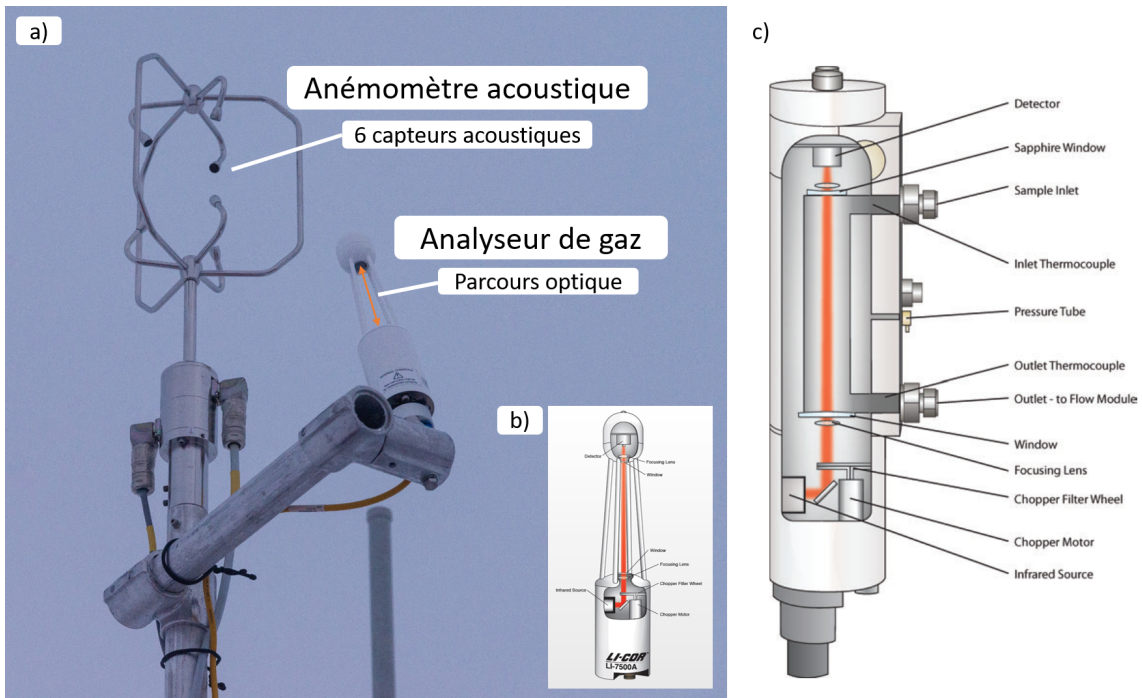


FIGURE B.3 – (a) Système de mesure des turbulences des flux installé au site L-3 de l’expédition MOSAiC. (b) Schéma d’un analyseur de gaz pour  $CO_2$  à parcours ouvert (LI-7500A de LI-COR). (c) Schéma d’un analyseur de gaz pour  $CO_2$  à parcours encloitré (LI-7200 de LI-COR). Crédit photo : (a) Thea Schneider. Crédit schéma : (b) Burba (2013), (c) Novick *et al.*, 2013.

Les systèmes de covariance des turbulences demeurent pour l’instant la seule technique permettant d’obtenir des données de flux de carbone à haute résolution temporelle (e.g., réseau global FLUXNET; Baldocchi *et al.*, 2001; Pastorello *et al.*, 2020). Cependant, c’est également la technique la plus onéreuse et elle génère un flux de données imposant et lourd à traiter dû à sa grande fréquence de mesure. L’empreinte de mesure d’EC dépend de la hauteur des mesures et fluctue selon l’orientation et la force des vents, une estimation approximative de sa taille est de 200 à 500 mètres pour une mesure effectuée de 2 à 3,5 mètres de hauteur (Leclerc et Thurtell, 1990; Schuepp *et al.*, 1990; Webb *et al.*, 2016). Il faut également mentionner que les interruptions de données dans les séries temporelles sont importantes, particulièrement en hiver, et doivent généralement être comblées en choisissant une des multiples techniques de “gap filling” existantes (Moffat, *et al.*, 2007; Soloway *et al.*, 2017). Cette problématique d’interruption des données est substantielle en Arctique puisque les instruments des systèmes EC sont énergivores et rencontre des problèmes reliés aux basses températures et aux limites d’alimentation des systèmes hors du réseau électrique (Pallandt *et al.*, 2022).

## B.2 Chambre dynamique et statique

La méthode de la chambre dynamique ou statique pour mesurer les flux de carbone est une méthode portable avec une empreinte au sol minimal ( $< 1m$ ) (McDowell *et al.*, 2000). La chambre peut être déposée à même le sol ou sur la neige. La chambre statique

(ou fermée) permet d'estimer les flux de carbone à partir de l'accumulation de gaz dans la chambre provenant de son ouverture unique vers le sol ou la neige. Les flux sont calculés à partir de la variation de concentration de gaz en fonction du temps, le volume du système, et la surface mesurée. Dans une chambre dynamique (ou ouverte), la concentration d'un gaz est évaluée à deux endroits de différentes hauteurs, nommés  $C_{in}$  et  $C_{out}$  (figure B.4a). Il est ensuite possible de calculer les flux de gaz ( $F$ ) à partir du gradient de concentration ainsi obtenue, le débit de circulation d'air ( $Q$ ) contrôlé par la pompe du système et l'empreinte au sol de la chambre ( $A$ ).

$$F = Q \frac{C_{out} - C_{in}}{A} \quad (\text{B.5})$$

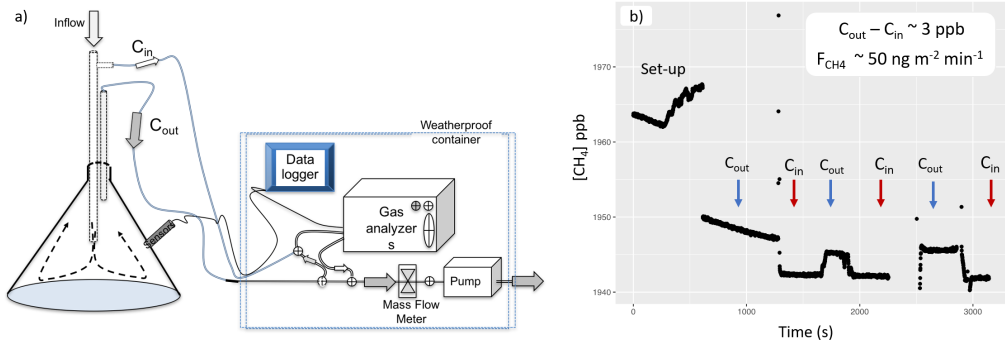


**FIGURE B.4 –** (a) Schéma d'une chambre dynamique pour la mesure des flux de carbone. (b) Données de flux de méthane au site L-3 de l'expédition MOSAiC, analyseur de gaz LICOR 7810. Ce schéma et ces données proviennent du système fait sur mesure par Steve Archer (Senior Research Scientist, Bigelow Laboratory for Ocean Sciences, East Boothbay, Maine) présenté à la figure B.5.

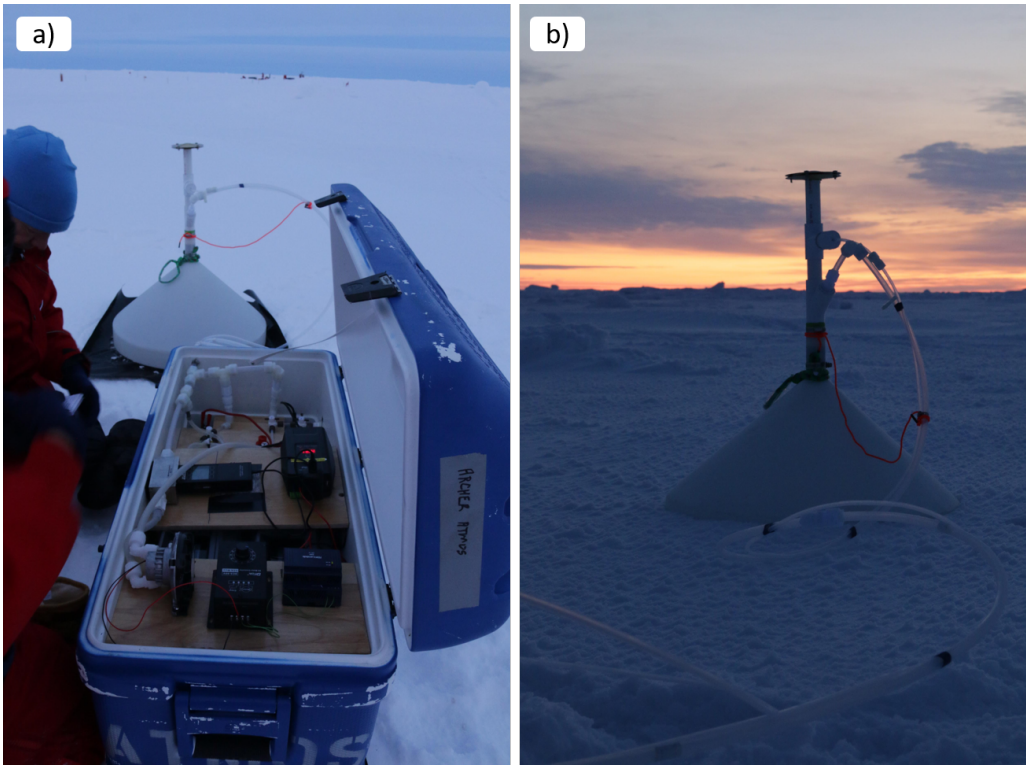


FIGURE B.5 – Chambre dynamique mobile pour mesure des concentrations et des flux de  $CO_2$ ,  $H_2O$  et  $CH_4$ . Système fait sur mesure par Steve Archer au Bigelow Laboratory, Maine, États-Unis. (a) Analyseur de gaz. (b) Chambre collectant les gaz. Crédit photo : Katie Aspen Gavenus.

La méthode de la chambre statique ou dynamique peut être déployée sur le couvert neigeux ou directement sur le sol, affectant ainsi l'interprétation des résultats. Placer la chambre sur le couvert neigeux ( $F_{neige}$ ) fournit une mesure des échanges de gaz à l'interface neige/atmosphère et non une mesure directe des flux de carbone provenant du sol en raison de la rétention et de la diffusion latérale au sein du couvert neigeux, créant généralement un biais négatif (McDowell et al., 2000; Björkman et al., 2010a; Webb et al., 2016). La chambre peut également être placée directement sur le sol ( $F_{sol}$ ) en excavant le couvert neigeux (Elberling et al., 2007), fournissant ainsi une mesure directe des flux de carbone provenant du sol qui est cependant sujette à un biais positif généré par un effet de tunnel dû à l'excavation de la neige (McDowell et al., 2000; Björkman et al., 2010). Les perturbations inévitables de la couche de neige réduisent également la possibilité de revisiter les mêmes emplacements subséquemment, car le régime thermique du sol est altéré par la perturbation du couvert de neige. Alternativement, des chambres permanentes peuvent être installées avant la première chute de neige, mais cela perturbe l'état du sol et de la couche de neige autour de la chambre (Webb et al., 2016). McDowell et al. (2000) et Björkman et al. (2010a) démontrent ce biais, tous leurs résultats indiquant une différence significative entre les mesures sur sol et sur neige ( $F_{sol} > F_{neige}$ ), alors que les mesures sur neige sont en accord avec les mesures par gradient de diffusion ( $F_{diff}$ ). Ce biais s'accroît avec la hauteur de neige.

## Annexe C - Publications à titre de premier auteur et coauteur

Dans cette annexe sont détaillées tous les articles publiés au cours de la thèse à titre de premier auteur et de co-auteur. Chaque article est suivi d'une description de la contribution à l'article.

**Mavrovic, A., Sonnentag, O., Lemmetyinen, J., Voigt, C., Aurela, M., and Roy, A. (in review)** *Winter methane fluxes over boreal and Arctic environments. Geophysical Research Letters.*

⇒ Conception et planification de l'étude. Organisation des campagnes de terrains. Implémentation de la méthode de mesure. Collecte, analyse et traitement des données. Rédaction du manuscrit.

*Gélinas, A., Filali, B., Langlois, A., Kelly, R., Mavrovic, A., Demontoux, F., and Roy, A. (in review) New wideband large aperture open-ended coaxial microwave probe for soil dielectric characterization. IEEE Transactions on Geoscience and Remote Sensing .*

⇒ Contribution à la conception de l'étude et la rédaction du manuscrit.

**Mavrovic, A., Sonnentag, O., Lemmetyinen, J., Voigt, C., Rutter, N., Mann, P., Sylvain, J.-D., and Roy, A. (2023b)** *Environmental controls of winter soil carbon dioxide fluxes in boreal and tundra environments. Biogeosciences, vol. 20, no° 24, p. 5087–5108, doi : [10.5194/bg-20-5087-2023](https://doi.org/10.5194/bg-20-5087-2023).*

⇒ Conception et planification de l'étude. Organisation des campagnes de terrains. Implémentation de la méthode de mesure. Collecte, analyse et traitement des données. Rédaction du manuscrit.

**Mavrovic, A., Sonnentag, O., Lemmetyinen, J., Baltzer, J., Kinnard, C., and Roy, A. (2023)** *Reviews and syntheses : Recent advances in microwave remote sensing in support of arctic-boreal carbon cycle science. Biogeosciences, vol. 20, no° 14, p. 2941–2970, doi : [10.5194/bg-20-2941-2023](https://doi.org/10.5194/bg-20-2941-2023).*

⇒ Conception et planification de l'étude. Rédaction du manuscrit.

**Mavrovic, A., Pardo Lara, R., Berg, A., Demontoux, F., Royer, A., and Roy, A. (2021)** *Soil dielectric characterization during freeze–thaw transitions using L-band coaxial and soil moisture probes. Hydrology and Earth System Sciences, vol. 25, p. 1117–1131, doi : [10.5194/hess-25-1117-2021](https://doi.org/10.5194/hess-25-1117-2021).*

⇒ Conception et planification de l'étude. Mesure en laboratoire. Analyse et traitement des données. Rédaction du manuscrit.

*Holtzman, N., Anderegg, L., Kraatz, S., **Mavrovic, A.**, Sonnentag, O., Pappas, C., Cosh, M., Langlois, A., Lakhankar, T., Tesser, D., Steiner, N., Colliander, A., Roy, A., and Konings, A. (2021) L-band vegetation optical depth as an indicator of plant water potential in a temperate deciduous forest stand. Biogeosciences, vol. 18, no° 2, p. 739-753, doi : [10.5194/bg-18-739-2021](https://doi.org/10.5194/bg-18-739-2021).*

⇒ Collecte et traitement des données de permittivité électrique des feuilles. Rétro-action fournie sur la rédaction du manuscrit.

***Mavrovic, A.**, Madore, J.-B., Langlois, A., and Roy, A. (2020) Snow liquid water content measurement using an open-ended coaxial probe (OECP). Cold Regions Science and Technology, vol. 171, p. 102958, doi : [10.1016/j.coldregions.2019.102958](https://doi.org/10.1016/j.coldregions.2019.102958).*

⇒ Conception et planification de l'étude. Organisation des campagnes de terrains. Implémentation de la méthode de mesure. Collecte, analyse et traitement des données. Rédaction du manuscrit.

*Roy, A., Toose, P., **Mavrovic, A.**, Pappas, C., Royer, A., Derksen, C., Berg, A., Rowlandson, T., El-Amine, M., Barr, A., Black, A., Langlois, A., and Sonnentag, O. (2020) L-Band response to freeze/thaw in a boreal forest stand from ground- and tower-based radiometer observations. Remote Sensing of Environment, vol. 237, 111542, doi : [10.1016/j.rse.2019.111542](https://doi.org/10.1016/j.rse.2019.111542).*

⇒ Organisation des campagnes de terrains. Collecte et traitement des données.